The benefits of adipocyte metabolism in bone regeneration

Inaugural – Dissertation

to obtain the academic degree

Doctor rerum naturalium (Dr. rer. nat.)

submitted to the Department of Biology, Chemistry, Pharmacy

of Freie Universität Berlin

by

Lisa-Marie Burkhardt

2022

This thesis and all implemented experiments were performed from June 2018 to June 2022 at the BIH – Julius Wolff Institute of Biomechanics and Musculoskeletal regeneration (BIH – JWI), Charité Universitätsmedizin Berlin under the guidance of PD Dr. rer. nat. Katharina Schmidt-Bleek, Dr. –Ing. Sven Geissler, Prof. Dr. –Ing. Georg N. Duda all associated at BIH – JWI and Prof. Dr. Tim J. Schulz associated at the German Institute of Human Nutrition (DifE) Potsdam-Rehbrücke.

1st reviewer: PD Dr. rer. nat. Katharina Schmidt-Bleek

2nd reviewer: Prof. Dr. –Ing. Georg N. Duda

Date of defense: 21st of March, 2023

Acknowledgement

First of all, I have to say, that I really struggle to find the words describing the last four years of my research career. I will start by saying that these years were spend with a bunch of extraordinarily good scientist from the Schmidt-Bleek lab, Geissler lab and Schulz lab. They were years full of happiness, innovative thoughts, fruitful discussions, and loving cohesiveness. To be honest, the “dark side” of these research years including overturned hypotheses, non-functional assays, struggles with defining research goals, challenging presentations and grant writings were always supported by my first supervisor Dr. rer. nat. Katharina Schmidt-Bleek. I will never forget her wording saying that ”research is not about going from A, to B, to C but it is about going from A, to G, to Z, and back to A”. With that, my intention of staying passionate and curious about my research while finding new angles as well as showing perseverance throughout facing many obstacles was strongly solidified. This will continue to accompany me during my future research career. Thanks Kate for all of that!

My special thanks go to Dr. Christian Bucher, with whom I had numerous late-night discussions and who advised me throughout the whole project. I would like to thank Sabine Stumpp, Carolin Paschke as well as Claudia Garrido Gutiérrez from the Schmidt-Bleek lab for all discussions, the support, and the kind words and for always having an open ear. Further, I would like to specifically thank some people from the Geissler lab: First of all, Dr. Ing. Sven Geissler for including me in his group and providing me with food for discussions, knowledge exchange, mental support, and a lab space where I could always feel welcomed. My thanks goes out to Nina Stelzer, Kerstin Mika, Julia Löffler and Charlotte Rinne for standing by my side and help me grow during this time. I want to give a special thanks to Dorit Jacobi for her scientific guidance, lab structure, enormous knowledge, liquor in falcons!, her music taste and her cooling pads in summer to safe me during extensive lab work.

There are so many people that shaped my way throughout my thesis and that made my time here at the Julius-Wolff Institute/BCRT become a wonderful journey. A great thanks goes to Prof. Dr. Tim Julius Schulz for being a caring project partner providing me with loads of additional knowledge, Caroline Frädrich for working together with me during the lasts steps of my research and Prof. Dr.-Ing. Georg Duda for his guidance, support, and confidence to engage me in the larger context of science, communicate my research, and have the courage to shoot higher.

Finally, and most importantly I want to give my greatest and heartwarming thanks to all my family members. Especially, my sisters Katrin and Stefanie, my brother-in-law Immanuel, my parents, my loving grandma and grandpa and my boyfriend Stephan for staying by my side for better or worse and for supporting me with all their heart and mind, giving love, understanding

and stability. I want to sincerely thank my loving friends, Tami, Laura, Susi, Jacky and Sophie, as well as Anna and Isi. Even though words cannot describe it, you know exactly how much you have stood by me and that you enrich my (research) heart and soul.

Statutory declaration

I hereby assure that I have composed the present thesis entitled

‘The benefits of adipocyte metabolism in bone regeneration’

independently and have used no other appliances than indicated. Parts being gathered from other works according to wording or meaning I have indicated in every single case by declaration of source. I hereby state furthermore, that I have produced my works according to the principles of good scientific practice. I further declare that I have not registered for any examination procedure at any other institution, and that I have not submitted the dissertation to any other faculty as a thesis in this or any other form.

Berlin, 1st of December 2022

Lisa Burkhardt

Table of content

Acknowledgement V

Statutory declaration VII

Table of content IX

Summary XIII

Zusammenfassung XV

List of abbreviations XVII

List of tables XX

List of figures XX

Preamble XXIV

1. Introduction - 1 -

1.1. Bone healing as multiphase process - 1 -

1.2. PPARG agonist as anti-diabetic drug and more? - 3 -

1.3. PPARG signaling - 5 -

1.4. Bone regeneration and its major therapeutic targets - 6 -

1.4.1. Anti-inflammation in bone regeneration - 6 -

1.4.2. Metabolic adjustments in bone regeneration - 10 -

1.4.3. Metabolic shift of the pro- and anti-inflammatory fracture milieu - 14 -

1.5. Bone marrow adipocytes and regional characteristics - 15 -

1.6. PPARG shaped adipocytes during high energetic demand - 16 -

1.7. PPARG driven features for ‘superhealing’ - 17 -

1.7.1. PPARG driven insulin signaling in bone - 17 -

1.7.2. PPARG and insulin dependent glucose signaling - 19 -

1.7.3. PPARG driven paracrine features - 19 -

1.8. Aim of this thesis - 21 -

2. Materials and methods - 23 -

2.1. In vivo experiments using a mouse fracture model - 23 -

2.1.1. Mouse femoral osteotomy model - 23 -

2.1.2. Surgical procedure and external fixation method - 23 -

2.1.3. Experimental conditions tested in the mouse femoral osteotomy model - 24 -
2.1.4. Termination and sample collection - 26 -
2.2. Ex vivo experiments using mouse samples - 27 -
2.2.1. Histological stainings determining bone and tissue composition - 27 -
2.2.2. Micro computed tomography (microCT) determining skeletal parameters - 28 -
2.2.3. Flow cytometry analysis determining immune composition - 29 -
2.2.4. Flow cytometry analysis determining the stromal cell composition - 31 -
2.2.5. Fatty acid screening determining phospholipid composition - 34 -
2.2.6. Statistical analysis - 34 -
2.3. In vitro experiments using human bone marrow derived stromal cells (hBMSCs)- 35 -
2.3.1. Characteristics and expansion of patient derived hBMSC - 35 -
2.3.2. Osteogenic differentiation of hBMSCs with/without drug supplementation - 37 -
2.3.3. Adipogenic differentiation of hBMSCs with/without drug supplementation - 41 -
2.3.4. Osteogenic differentiation of hBMSCs with adipocyte conditioned media - 42 -
2.3.5. CyQUANT proliferation assay in osteogenic and adipogenic differentiation - 44 -
2.3.6. Preparation of hBMSC samples for RNA sequencing analysis - 45 -
2.3.7. Metabolic profiling of hBMSCs during osteogenic differentiation - 46 -
2.3.8. Glucose uptake profiling of hBMSCs during osteogenic differentiation - 48 -
2.3.9. Adipokine profiling of hBMSCs during osteogenic differentiation - 48 -
2.3.10. Statistical analysis - 49 -
3. Results - 51 -
3.1. Ex vivo characterization of inflammation related effects on bone regeneration in mice - 51 -
3.1.1. TNFa/IFNg neutralization and its effects on adipocytes and $CD4^+$ T helper 2 subset polarization - 51 -
3.2. Ex vivo characterization of PPARG related effects on bone regeneration in mice- 52 -
3.2.1. PPARG driven induction of adipose tissue and lipids in bone - 53 -
3.2.2. PPARG driven beneficial skeletal parameters - 57 -
3.2.3. PPARG driven $CD4^+$ T helper 2 subset polarization - 58 -

3.3. In vitro characterization of PPARG related effects in human bone marrow MSCs (hBMSCs) - 60 -

3.3.1. PPARG as driving force of enhanced osteogenic capacity and increased matrix mineralization of hBMSCs - 60 -

3.3.2. PPARG as driving force of metabolic changes in osteogenic hBMSCs - 79 -

3.3.3. PPARG driven osteo-adipocytes trigger metabolic changes by a unique gene expression pattern - 92 -

4. Discussion - 97 -

4.1. Studying bone regeneration under explorative immune activation - 97 -

4.1.1. BMAs as connecting piece between regeneration and anti-inflammation - 97 -

4.1.2. PPARG agonist primed BMAs combine site specific pro-regenerative effects on bone - 99 -

4.2. Changing the adipocyte focus to bone - Mirroring beneficial PPARG activation in osteogenic cultures - 101 -

4.2.1. PPARG agonist driven insulin sensitization and insulin supplementation differs in osteogenic cultures - 102 -

4.2.2. PPARG agonist treatment highlights adipocyte and bone co-induction - 103 -

4.2.3. PPARG stimulated osteo-adipocytes present specific characteristics improving bone regeneration - 105 -

4.2.4. PPARG stimulates a high metabolic fitness supporting osteogenic differentiation - 110 -

4.2.5. Hyperinsulinemia: PPARG agonist treatment as rescue mechanism? - 113 -

4.2.6. And what about hyperglycemia? - 115 -

5. Limitations and outlook - 118 -

6. Conclusion - 119 -

Bibliography - 121 -

Appendix - 159 -

A. 1. Materials and methods - 159 -

A. 2. Results - 161 -

Summary

It is well known that patients suffering from disturbed fracture healing have to cope with diminished quality of life and ensue medical expenses for society. Such disorders represent the most expensive group of diagnoses in the emergency department and cause a significant health and economic impact worldwide. During bone regeneration, the interaction of immune cells and mesenchymal stromal cells by various paracrine or cell-cell driven mechanisms is indispensable to restore skeletal integrity. The osteogenic lineage formation is known to support bone regeneration, whereas the accumulation of the adipogenic lineage cells is widely thought to promote low grade inflammation and skeletal damage. Chronic low grade inflammation is largely caused by pro-inflammatory immune cells and inflamed adipose tissue, both of which are likely known causes of obesity and other metabolic disorders.

This work hypothesizes, that a beneficial metabolic and immune-modulatory power of bone marrow adipocytes can be identified to support bone regeneration. Bone marrow adipocytes are highlighted as energy and metabolite providing partakers in conditions of high energetic demand such as bone healing. A regulatory effect of adipocyte secreted factors on the local inflammatory milieu is proposed. This pro-regenerative bone marrow adipose tissue is shown to be induced by the anti-inflammatory diabetes drug rosiglitazone activating the peroxisome proliferator-activated receptor γ (PPARG).

To that end, PPARG agonist treatment, currently known as detrimental in relation to bone, was shown to induce bone marrow adipose tissue in the distal parts of the bone such as at the fracture site and at the distal growth plate. Surprisingly, the induction of adipocytes did not cause dysfunctional bone fracture healing but steered beneficial skeletal parameters during bone repair in osteotomized mice. Additionally, pro-osteogenic changes in the lipid compartment and the induction of anti-inflammatory $CD4^+$ T helper 2 immune cells were identified. The specific features of PPARG agonist treated bone marrow adipocytes in regeneration were verified using human patient derived mesenchymal stromal cells isolated from bone. In accordance with the in vivo study, PPARG agonist treatment during osteogenic differentiation resulted in an increased osteogenic potential and mineralization as well as an enhanced metabolic fitness determined by higher OCR/ECAR ratios, higher oxidative spare capacity and an upregulation of glucose uptake. Interestingly, the secretion of adiponectin as specific paracrine effect of PPARG agonist treated adipocytes during osteogenic cultures could be determined as beneficial for bone formation.

In this thesis, the possibility of using PPARG agonists, thiazolidinediones (TZDs), as short-term treatment to guide a pro-regenerative, metabolically active bone marrow adipose tissue further driving faster bone bridging was explored. PPARG driven effects were outlined as

metabolic switch in MSCs during osteogenic differentiation and were shown to induce beneficial effects by secreting high amounts of anti-inflammatory adiponectin during mineralization. Hereby, the impact of PPARG agonist induced bone marrow adipose tissue on providing the necessary metabolites to sustain osteogenic stromal cells as well as polarizing an anti-inflammatory milieu during bone regeneration was highlighted.

Zusammenfassung

Patienten, welche unter einer gestörten Frakturheilung leiden, kämpfen mit einer verminderten Lebensqualität. Solche Frakturheilungsstörungen stellen die teuerste Gruppe von Diagnosen in der Notaufnahme dar und verursachen weltweit erhebliche gesundheitliche und wirtschaftliche Auswirkungen. Während der Knochenheilung ist die Interaktion von Immunzellen und mesenchymalen Stromazellen durch verschiedene parakrine oder zellgesteuerte Mechanismen unerlässlich um die Integrität des Skeletts wiederherzustellen. Es ist bekannt, dass die Differenzierung der osteogenen Linie die Knochenregeneration unterstützt, während die Anhäufung von Zellen der adipogenen Linie als Ursache für Entzündungen und Skelettschäden gilt. Chronische Entzündungen werden hier größtenteils durch entzündungsfördernde Immunzellen und entzündetes Fettgewebe verursacht. Beide Ursachen sind ebenfalls bekannte Auslöser von Adipositas und anderen Stoffwechselstörungen.

In dieser Arbeit wird die Hypothese aufgestellt, dass ein bestimmter Subtyp von vorteilhaften metabolisch und immun-modulatorisch aktiven Knochenmarks-Adipozyten zur Unterstützung der Knochenregeneration beitragen kann. Diese Adipozyten im Knochenmark spielen eine wichtige Rolle vor allem in der Knochenheilung und verbessern das Energie-Reservoir-Angebotsgleichgewicht der mitstreitenden Zellen und decken den erhöhten Energiebedarf. Hier wird den Adipozyten und den von ihnen sezernierten Faktoren eine regulierende Wirkung auf das lokale Entzündungsmilieu im Knochen zugeschrieben. Dieses pro-regenerative Knochenmarks-Fettgewebe kann in diesem Fall durch das entzündungshemmende Diabetes-Medikament Rosiglitazone induziert werden, dessen Effekte aus der Aktivität des Peroxisom-Proliferator-aktivierten Rezeptor γ (PPARG) resultieren.

Mit der vorliegenden Arbeit wurde gezeigt, dass eine Behandlung mit PPARG-Agonisten, Fettgewebe aus dem Knochenmark in distalen Teilen des Knochens, z. B. an der Frakturstelle und der distalen Wachstumsplatte induziert. Die Induktion von Adipozyten führte nicht zu einer Beeinträchtigung der Frakturheilung, sondern verursachte eine verbesserte Knochenstruktur, welche am Prozess der Knochenregeneration in einem Maus-Osteotomie Modell getestet wurde. Darüber hinaus wurden pro-osteogene Veränderungen im Lipidkompartiment und die Induktion von entzündungshemmenden CD4+ T Helfer Typ 2 Immunzellen festgestellt. Die positiven, in-vivo Eigenschaften von PPARG-Agonist behandelten, aus dem Knochenmark stammenden Adipozyten, konnten mit Hilfe von in vitro Experimenten reproduziert werden. Dies wurde anhand von humanen, mesenchymalen Stromazellen aus dem Knochenmark überprüft. In Übereinstimmung mit der In-vivo-Studie führte die Behandlung mit PPARG-Agonisten während der osteogenen Differenzierung zu einer Steigerung des osteogenen

Potenzials und zu einer erhöhten Mineralisierungsrate. Zusätzlich konnte eine Verbesserung der metabolischen Fitness dieser Zellen festgestellt werden, welche sich durch ein höheres OCR/ECAR-Verhältnis, eine höhere oxidative Reservekapazität und eine Hochregulierung der Glukoseaufnahme bemerkbar machte. Interessanterweise erwies sich die Sekretion von Adiponektin, eines von PPARG-Agonist stimulierten Adipozyten sezernierten Peptid-Hormones, während osteogener Kulturen als vorteilhaft für die Knochenbildung.

Hiermit wurde die Möglichkeit untersucht, PPARG-Agonisten z.B. Thiazolidindione (TZDs), als Kurzzeitbehandlung einzusetzen, um ein pro-regeneratives, metabolisch aktives Knochenmarks-Fettgewebe zu induzieren und hiermit eine schnellere Knochenneubildung zu fördern. Die PPARG-gesteuerten Effekte wurden bemerkbar durch die Umstellung der metabolischen Aktivität von MSCs während der osteogenen Differenzierung. Weiterhin wurde gezeigt, dass die Mineralisierung von MSCs durch hohe Mengen an entzündungshemmendem Adiponektin unterstützt werden können. PPARG-Agonist induziertes Knochenmarks-Fettgewebe wurde hiermit erstens: Für die Bereitstellung von notwendigen Metaboliten, zweitens: Zur Aufrechterhaltung osteogener Stromazellen, sowie drittens: Der Polarisierung eines entzündungshemmenden Milieus während der Knochenregeneration hervorgehoben.

List of abbreviations

SPF specific-pathogen free

PPARG peroxisome proliferator-activated receptor gamma

BADGE bisphenol a diglycidyl ether

DMSO dimethylsulfoxid

TNFa tumor necrosis factor alpha

IFNg interferon gamma

microCT micro computed tomography

NaCl sodium chloride

PBS Phosphate-buffered saline

BAT brown adipose tissue

WAT white adipose tissue

HE hematoxylin and eosin

BMD bone mineral density

CaHA calcium hydroxyapatite

VOI volume of interest

TH T helper cells

FMO fluorescence minus one

BMAT bone marrow adipose tissue

SD standard deviation

hBMSCs human bone marrow derived stromal cells

SC stromal cells

DMEM dulbecco's modified eagle media

FCS fetal calf serum

P/S penicillin/streptomycin

ALP alkaline phosphatase

AR	alizarin red
PB	presto blue
pNPP	4-nitrophenylphosphate
OD	optical density
NR	nile red
RT	room temperature
IBMX	3-isobutyl-metylxanthine
Cebpa	CCAAT enhancer binding protein alpha
Srebf1c	sterol regulatory element binding protein 1c
Cebpb	CCAAT enhancer binding protein beta
cAMP	cyclic adenosine monophosphate
PKA	cAMP dependent protein kinase A
aCM	adipocyte conditioned media
EM	expansion control
MDC	max delbrück center for molecular medicine
BIH	berlin institute of health
Glut	glutamine
Gluc	glucose
FCCP	carbonyl cyanide-4 (trifluoromethody) phenylhydrazone
Rot/AntA	rotenone/antimycin A
ATP	adenosine triphosphate
ECAR	extracellular acidification rate
OCR	oxygen consumption rate
2DG6P	2-deoxyglucose-6-phosphate
2DG	2-deoxyglucose
BMA	bone marrow adipocytes

SCD-1	stearoyl-CoA desaturase 1
rBMAT	regulated bone marrow adipose tissue
cBMAT	constitutive bone marrow adipose tissue
MMI	moment of inertia
BS/BV	bone surface/bone volume
Tb.Th	trabecular thickness
Tb.N	trabecular number
TV	tissue volume
BV	bone volume
IL1b	interleukin 1 beta
MCP-1	monocyte chemoattractant protein 1
RBP-4	retinol binding protein 4
OXPHOS	oxidative phosphorylation

List of tables

TABLE 1: SUMMARY OF THE EXPERIMENTAL CONDITIONS, TREATMENTS AND ANALYSIS IN THE MOUSE OSTEOTOMY MODEL ..... - 24 -
TABLE 2: PROTOCOL ELUCIDATING THE HEMATOXYLIN/EOSIN STAINING (HE STAINING) ..... - 27 -
TABLE 3: ANALYSIS CHARACTERISTICS FOR THE PERFORMANCE OF ALL MICRO COMPUTED TOMOGRAPHIES (MICROCT) ..... - 28 -
TABLE 4: EXTRACELLULAR AND INTRA-NUCLEAR MARKERS DEFINING THE $CD4^+$ T HELPER SUBSET COMPOSITION ..... - 30 -
TABLE 5: SUMMARY OF THE EXTRACELLULAR MARKERS DEFINING THE MESENCHYMAL STROMAL CELL SUBSETS IN BONE MARROW ..... - 32 -
TABLE 6: COMPONENTS OF THE OSTEOGENIC DIFFERENTIATION COCKTAIL ..... - 37 -
TABLE 7: SUMMARY OF DRUG AND SOLVENT CONTROL CONCENTRATIONS IMPLEMENTED DURING IN VITRO ASSAYS ..... - 38 -
TABLE 8: PROTOCOL FOR THE ALP MEASUREMENT ..... - 39 -
TABLE 9: COMPONENTS OF THE ADIPOGENIC DIFFERENTIATION COCKTAIL ..... - 41 -
TABLE 10: SUMMARY OF RNA SAMPLES INCLUDED FOR SEQUENCING ANALYSIS ..... - 45 -
TABLE 11: CONSUMABLE MATERIALS ..... - 159 -
TABLE 12: CHEMICALS ..... - 160 -
TABLE 13: KITS ..... - 160 -
TABLE 14: SOFTWARE ..... - 161 -
TABLE 15: ANIMALS AND CELLS ..... - 161 -

List of figures

FIGURE 1: THE BONE HEALING CASCADE AND ITS PARTAKERS ADAPTED FROM [49][24][24][50] ..... - 3 -
FIGURE 2: GLUCOSE AS FUEL FOR GLYCOLYSIS AND OXPHOS ADAPTED FROM [163][161][156] ..... - 12 -
FIGURE 3: METABOLIC CHANGES IN FRACTURE RESIDING IMMUNE CELLS ADAPTED FROM [159] ..... - 14 -
FIGURE 4: METABOLIC CHANGES IN FRACTURE RESIDING MSCS ADAPTED FROM [190] ..... - 15 -
FIGURE 5: MOUSEEXFIX – MOUNTING OF FIXATOR, OSTEOTOMY AND FIXATION DEVICE USED ..... - 24 -
FIGURE 6: SUMMARY OF THE TISSUES HARVESTED FROM EACH EXPERIMENTAL CONDITION IN THE OSTEOTOMY MODEL ..... - 26 -
FIGURE 7: GATING STRATEGY FOR ANALYZING $CD4^+$ TH1, TH2 AND TH17 SUBSETS ..... - 31 -
FIGURE 8: ILLUSTRATION OF THE GATING STRATEGY FOR THE DISTINCT MESENCHYMAL STROMAL CELL SUBSET IN BONE MARROW ..... - 33 -
FIGURE 9: THREE PRE-DEFINED REGIONS ANALYZED FOR BONE MARROW ADIPOSE TISSUE (BMAT) ..... - 34 -
FIGURE 10: SUMMARY OF PATIENT SPECIFIC CHARACTERISTIC OF HBMSCS ..... - 36 -
FIGURE 11: ILLUSTRATION OF THE OSTEOGENIC DIFFERENTIATION SETUP ..... - 38 -
FIGURE 12: ILLUSTRATION OF THE OSTEOGENIC DIFFERENTIATION TIME-POINTS ..... - 39 -

FIGURE 13: FORMULA FOR THE CALCULATION OF ALKALINE PHOSPHATASE ACTIVITY (ALP) ..... - 39 -
FIGURE 14: ILLUSTRATION OF ADIPOGENIC DIFFERENTIATION TIME-POINTS ..... - 42 -
FIGURE 15: ILLUSTRATION OF THE CONDITIONING OF ADIPOGENIC MEDIA AND ITS RE-USE DURING OSTEOGENIC DIFFERENTIATION ..... - 43 -
FIGURE 16: ILLUSTRATION OF THE CONDITIONS DURING THE OSTEOGENIC DIFFERENTIATION WITH ADIPOCYTE SECRETED FACTORS ..... - 44 -
FIGURE 17: ILLUSTRATION OF RNA ISOLATION TIME-POINTS DURING OSTEOGENIC/ADIPOGENIC DIFFERENTIATION ..... - 46 -
FIGURE 18: ILLUSTRATION OF THE SEAHORSE XF CELL MITO STRESS TEST (AGILENT) ..... - 47 -
FIGURE 19: NEUTRALIZATION OF PRO-INFLAMMATORY CYTOKINES TNFA AND IFNG INDUCING ADIPOCYTE ACCUMULATION IN THE FRACTURED BONE AND SYSTEMIC $CD4^+$ TH2 POLARIZATION ..... - 51 -
FIGURE 20: PPARG AGONIST TREATMENT INDUCES ADIPOCYTE ACCUMULATION IN THE MARROW SIMULTANEOUSLY WITH STRONGER BRIDGING OF BONE ON DAY 21 OF BONE REGENERATION ..... - 53 -
FIGURE 21: PPARG AGONIST DRIVEN ADIPOCYTE ACCUMULATION IN BONE FOCUSES ON DISTAL BONE REGIONS WERE CONSTITUTIVE BMAT (CBMAT) IS LOCATED ..... - 54 -
FIGURE 22: PPARG AGONIST TREATMENT INDUCES AN INCREASED ACCUMULATION OF LARGE FAT VACUOLES IN THE DISTAL REGION AT THE GROWTH PLATE OF UNFRACTURED AND FRACTURED BONES ..... - 55 -
FIGURE 23: TREATMENT WITH PPARG AGONIST ROSIGLITAZONE INDUCES ADIPOCYTES AT THE DISTAL PART OF THE OSTEOTOMY AND INCREASES SCD-1 AND OMEGA 6 IN UNFRACTURED, CONTROL BONES ..... - 56 -
FIGURE 24: PPARG AGONIST TREATMENT DOES NOT HINDER BONE FRACTURE BRIDGING DURING HEALING .- 57 -
FIGURE 25: TREATMENT WITH PPARG AGONIST ROSIGLITAZONE HAS BENEFICIAL EFFECTS ON THE BONE STRUCTURE OF FRACTURED BONE DURING HEALING OF HEALTHY, YOUNG MICE HOUSED UNDER ENVIRONMENTAL PATHOGEN EXPOSED HOUSING ..... - 58 -
FIGURE 26: TREATMENT WITH PPARG AGONIST ROSIGLITAZONE STEERS ANTI-INFLAMMATORY $CD4^+$ T HELPER 2 SUBSET POLARIZATION IN MOUSE SPLENOCYTES AND HAS NO SYSTEMIC EFFECT ON THE PRO-INFLAMMATORY $CD4^+$ TH17 AND TH1 SUBSETS ..... - 59 -
FIGURE 27: TREATMENT WITH PPARG AGONIST ROSIGLITAZONE ENHANCES THE POTENTIAL OF HBMSCS TO DIFFERENTIATE INTO THE OSTEOGENIC LINEAGE SHOWN BY THE INCREASE OF EARLY OSTEOGENIC ALP ACTIVITY AND PNNP CONSUMPTION ..... - 61 -
FIGURE 28: TREATMENT WITH PPARG AGONIST ROSIGLITAZONE ENHANCES THE CALCIFICATION LEVELS OF HBMSCS IN LATE OSTEOGENIC STAGES ..... - 62 -
FIGURE 29: TREATMENT WITH PPARG AGONIST ROSIGLITAZONE AND SUPPLEMENTATION OF INSULIN INDUCES A DISTINCT PATTERN OF MATRIX MINERALIZATION AND SIGNIFICANTLY INCREASES THE CALCIFICATION DURING OSTEOGENIC DIFFERENTIATION ..... - 64 -
FIGURE 30: PROLIFERATIVE CAPACITY OF HBMSCS IS MARKEDLY INCREASED BY STIMULATION WITH INSULIN COMPARED TO THE TREATMENT WITH PPARG AGONIST ROSIGLITAZONE DURING OSTEOGENIC DIFFERENTIATION ..... - 65 -

FIGURE 31: INSULIN SUPPLEMENTATION IS SHOWN TO SIGNIFICANTLY UPREGULATE METABOLIC ACTIVITY AND PROLIFERATION DURING OSTEOGENIC DIFFERENTIATION WHEREAS NO EFFECTS CAN BE SHOWN IN THE PPARG AGONIST TREATED GROUP ..... - 65 -
FIGURE 32: PPARG AGONIST TREATMENT INDUCES A BILATERAL DIFFERENTIATION POTENTIAL IN HBMSCS WITH THE ACCUMULATION OF ADIPOCYTES DURING OSTEOGENIC DIFFERENTIATION ..... - 67 -
FIGURE 33: VISUALIZATION OF INDIVIDUAL, PATIENT SPECIFIC ADIPOCYTE ACCUMULATION DURING OSTEOGENIC MINERALIZATION OF HBMSCS WITH PPARG AGONIST TREATMENT ..... - 68 -
FIGURE 34: PPARG AGONIST TREATMENT INDUCES A SIGNIFICANT ACCUMULATION OF ADIPOCYTES DURING OSTEOGENIC DIFFERENTIATION VISUALIZED BY FLUORESCENCE STAINING OF LIPIDS AND DNA ..... - 69 -
FIGURE 35: PPARG AGONIST TREATMENT RESULTS IN ADIPOCYTES ACCUMULATION AND HIGHEST CALCIUM DEPOSITION INDEPENDENT OF THE INSULIN DRIVEN INCREASE IN CALCIFICATION ..... - 70 -
FIGURE 36: PPARG AGONIST TREATMENT FORMS MORPHOLOGICAL SIMILAR ADIPOCYTES DURING OSTEOGENIC DIFFERENTIATION AS COMPARED TO THE STANDARD ADIPOGENIC DIFFERENTIATION ..... - 70 -
FIGURE 37: ADIPOGENIC DIFFERENTIATION WITH AND WITHOUT PPARG AGONIST STIMULATION RESULTS IN EQUAL AMOUNTS OF ADIPOCYTES AND NO INCREASE IN ADIPOGENIC DIFFERENTIATION IS SHOWN USING PPARG AGONIST TREATMENT ..... - 71 -
FIGURE 38: PPARG AGONIST TREATMENT SIGNIFICANTLY INCREASES ADIPONECTIN SECRETION DURING OSTEOGENIC DIFFERENTIATION AND ADIPOGENIC DIFFERENTIATION ..... - 72 -
FIGURE 39: ADIPOKINES MARKEDLY INCREASED IN THE PPARG AGONIST STIMULATED OSTEO-ADIPOCYTES COMPARED TO THE PPARG AGONIST TREATED FAT FORMING ADIPOCYTES ..... - 73 -
FIGURE 40: PPARG AGONIST STIMULATED OSTEO-ADIPOCYTES HAVE A SIGNIFICANTLY DIFFERENT PARACRINE CAPACITY COMPARED TO OSTEOGENIC DIFFERENTIATED HBMSCS WITHOUT PPARG AGONIST INDUCED OSTEO-ADIPOCYTES ..... - 74 -
FIGURE 41: PPARG AGONIST TREATMENT DURING OSTEOGENIC DIFFERENTIATION RESULTS IN OPPOSING ADIPOKINE SECRETION WHEN COMPARED TO INSULIN SUPPLEMENTED OSTEOGENIC DIFFERENTIATION - 75 -
FIGURE 42: PPARG AGONIST TREATMENT OF FAT FORMING ADIPOCYTES RESULTS IN THE INCREASE OF ADIPONECTIN AND RBP4 WITHOUT INFLUENCING THE SECRETION OF PRO-INFLAMMATORY CYTOKINES SUCH AS IL1B AND MCP1 ..... - 76 -
FIGURE 43: INDIVIDUAL PATIENT SPECIFIC EFFECTS ARE PRESENTED AND SHOW A STEADY INCREASE OF MINERALIZATION IN HBMSC DIFFERENTIATED INTO THE OSTEOGENIC LINEAGE WHILE SUPPLEMENTING ADIPOGENIC MEDIA ..... - 77 -
FIGURE 44: INSULIN DRIVEN INCREASE OF OSTEOGENIC MINERALIZATION IS REDUCED BY ADDITIONAL ADIPOGENIC MEDIA BUT PPARG AGONIST PRE-CONDITIONED MEDIA SHOWS A STEADILY INCREASE OF MINERALIZATION POTENTIAL ..... - 78 -
FIGURE 45: FAT FORMING ADIPOGENIC MEDIA HAS NO SIGNIFICANT IMPACT ON THE OSTEOGENIC DIFFERENTIATION CAPACITY OF HBMSCS REGARDLESS OF PPARG AGONIST TREATMENT ..... - 79 -
FIGURE 46: HBMSC UNDERGOING OSTEOGENIC DIFFERENTIATION REPRESENT INCREASING OCR/ECAR RATIOS ON DAY 5 AND ENHANCED OXIDATIVE PHOSPHORYLATION IN EARLY STAGES OF OSTEOGENIC DIFFERENTIATION ..... - 80 -

FIGURE 47: HBMSC UNDERGOING OSTEOGENIC DIFFERENTIATION SHOW AN EARLY INCREASE OF OCR BUT NO DECREASE OF ECAR ON DAY 2 AFTER OSTEOGENIC INDUCTION ..... - 81 -
FIGURE 48: A STEADILY INCREASING OXYGEN CONSUMPTION FAVORING CELLULAR ATP DEMAND AND A HIGHER ATP PRODUCTION BY MITOCHONDRIA IS SHOWN FOR HBMSCS UNDER OSTEOGENIC DIFFERENTIATION ..... - 82 -
FIGURE 49: LATER OSTEOGENIC DIFFERENTIATION TIME-POINTS WHERE MINERALIZATION AND CALCIUM DEPOSITION STARTS ARE ACCOMPANIED BY A HIGHER OXIDATIVE SPARE CAPACITY ..... - 83 -
FIGURE 50: PPARG AGONIST TREATMENT OF HBMSCS POSITIVELY IMPACTS THE OCR/ECAR RATIO DURING OSTEOGENIC DIFFERENTIATION ..... - 84 -
FIGURE 51: PPARG AGONIST TREATMENT OF HBMSCS DURING EXPANSION RESULTS IN A SIGNIFICANT INCREASE OF THE OCR/ECAR RATIO ON DAY 10 OF EXPANSION ..... - 85 -
FIGURE 52: PPARG AGONIST TREATMENT OF EXPANDED HBMSCS SHOWS INCREASING OCR BUT NO IMPACT ON ECAR ..... - 85 -
FIGURE 53: PPARG AGONIST TREATMENT RESULTS IN A SIGNIFICANT ELEVATION OF OXIDATIVE SPARE CAPACITY AND WITH THAT A HIGHER ENERGETIC FITNESS IS SHOWN AT LATER OSTEOGENIC STAGES ..- 86 -
FIGURE 54: PPARG AGONIST TREATMENT ENABLES THE INDUCTION OF A BENEFICIAL METABOLIC OCR INCREASE IN PATIENTS WITH POOR OSTEOGENIC DIFFERENTIATION CAPACITY ..... - 87 -
FIGURE 55: INSULIN TREATMENT OF HBMSCS DURING OSTEOGENIC DIFFERENTIATION MAINTAINS THE OCR/ECAR RATIO AT A CONSTANT LEVEL, WHEREAS COMBINED PPARG AGONIST AND INSULIN TREATMENT ELEVATES THE OCR/ECAR RATIO ..... - 88 -
FIGURE 56: INSULIN AND PPARG AGONIST TREATMENT STEERS A SIGNIFICANT INCREASE OF BASAL ACTIVITY AND ATP TURNOVER ON DAY 5 BUT LEADS TO A SIGNIFICANT DOWNREGULATION OF BOTH ON DAY 10 OF OSTEOGENIC DIFFERENTIATION ..... - 89 -
FIGURE 57: OXIDATIVE SPARE CAPACITY IS UNIQUELY UPREGULATED BY PPARG AGONIST TREATMENT INDEPENDENT OF INSULIN, WHEREAS INSULIN TREATMENT STEERS A SIGNIFICANT INCREASE OF PROTON LEAK DURING OSTEOGENIC DIFFERENTIATION ..... - 91 -
FIGURE 58: PPARG AGONIST TREATMENT REMARKABLY UPREGULATES GLUCOSE UPTAKE DURING OSTEOGENIC DIFFERENTIATION ESPECIALLY IN COMBINATION WITH INSULIN TREATMENT ..... - 92 -
FIGURE 59: SPECIFIC GENES AND SIGNALING CAN BE IDENTIFIED IN PPARG AGONIST STIMULATED OSTEOGENIC HBMSCS ..... - 94 -
FIGURE 60: CHANGING THE OSTEO-ADIPOCYTE MILIEU FOR REGENERATION ..... - 120 -
FIGURE 61: THE ADIPOGENIC LINEAGE IS SLIGHTLY DECREASED BY THE TREATMENT WITH PPARG AGONIST ROSIGLITAZONE IN UNFRACTURED AND FRACTURED BONE MARROW ..... - 161 -
FIGURE 62: PPARG AGONIST TREATMENT HAS NO EFFECT ON THE OSTEOGENIC PRECURSOR CELLS BUT ENHANCES THE MULTIPOTENT PRECURSOR SUBSET IN THE BONE MARROW ..... - 162 -
FIGURE 63: OSTEOGENIC BASELINE POTENTIAL OF PATIENT HBMSCS DIFFERS IN ALP ACTIVITY AND CALCIFICATION RATE ..... - 163 -
FIGURE 64: INDIVIDUAL PATIENT SPECIFIC EFFECTS ARE SHOWN FOR PPARG AGONIST AND INSULIN STIMULATED EARLY AND LATE OSTEOGENIC DIFFERENTIATION ..... - 164 -

Preamble

This thesis consists of two parts. Part 1 summarizing the in vivo study and part 2 outlining the in-depth in vitro study. This project was done in close collaboration between the laboratory of PD Dr. rer. nat. Katharina Schmidt-Bleek, the laboratory of Dr. –Ing. Sven Geissler and the laboratory of Prof. Dr. Tim Schulz. Further this work was enriched by a collaborative work with Caroline Frädrich from the Institute of Experimental Endocrinology and was improved by the statistical analysis of Dr. Andranik Ivanov.

1. Introduction

1.1. Bone healing as multiphase process

The regeneration of bone is one of the most successful healing processes next to liver regeneration. The bones unique feature to renew and rebuild without scar formation by a complex multiphase process makes it a very special tissue and its investigation could represent a template for steering the regeneration of other tissues within the human body that usually end up in scar formation [1][2]. In addition, bone marrow is known as source of distinct cell types such as the immune and hematopoietic lineage and is described as highly metabolic environment [2]. This study suggests, that the metabolic blueprint of cells and the metabolic reprogramming during intense energetic needs of fracture healing is of high importance to restore tissue. Metabolic reprogramming provides energy to balance inflammation, induce angiogenesis, and control proliferation and differentiation of immune and mesenchymal stromal cells [3][4]. Starting from the 1940s, the close regulation of bone growth by endocrine glands as well as the influence of adipocyte secreted hormones and adipokines on bone remodeling and nutrient metabolism has been highlighted [5][6][7]. It is now known that changes in the metabolic capacity of cells, especially MSCs, can either drive or reduce bone regeneration [8][9]. In fact, identifying a metabolic fuel cocktail for beneficial tissue regeneration has become an important research goal and will be further investigated in this thesis [3][10][11]. In addition to that, a critical aspect of a positive bone healing outcome is the regulation of inflammatory phases and the immune cells involved in each stage of regeneration. After traumatic bone injury, initial healing of bone is marked by a hematoma formation and pro-inflammatory phase subsequently followed by four successive, overlapping healing stages (**Figure 1 A**): the anti-inflammatory hematoma phase, soft callus formation phase, hard callus formation phase and remodeling phase [12][2]. Initially, injury-related damaged blood vessels and inhibited nutrient supply cause a challenging environment for cells within the early pro-inflammatory hematoma at the fracture site [3][13]. This early hematoma already contains mesenchymal stromal cells as well as circulating immune cells e.g. macrophages, monocytes and lymphocytes from the periphery, which undergo an activation process. This leads to pro-inflammatory cytokine accumulation and removal of damaged tissue [14]. In addition, damaged tissue can activate immune cells by danger associated DAMP signals released from apoptotic cells, e.g. byproducts and matrix proteins which are commonly recognized via TLRs [15][16][17]. Hereby, more pro-inflammatory cytokines are secreted into the fracture milieu e.g. monocyte chemoattractant protein-1 (MCP1), IL6, CCL2 which act as amplifiers of inflammation [18]. The cytokine and chemokine cocktail attracts additional pro-inflammatory immune cells, MSCs and endothelial progenitor cells, which have a high nutrient and oxygen consumption. This results in hypoxia and HIF1a stabilization [19][20][2]. The

trauma induced influx of immune cells is accompanied by increasing levels of chemoattractants including pro-regenerative lipid mediators (leukotrienes) and protein mediators (chemokines and cytokines) that can likewise be secreted by local adipocytes [21][22][20]. Not only innate immune cells e.g. M1 macrophages, but also the activation and differentiation of pro-inflammatory CD8+ T cell subsets as well as CD4+ T helper 1 (TH1) and T helper 17 (TH17) cells is evident (**Figure 1 C**). The CD4+ T helper cell compartment will be the immunological focus of the presented work.

Following the first pro-inflammatory wave, angiogenesis and revascularization is initiated to restore the nutrient flow [13][23][24]. In order to achieve that, an important anti-inflammatory switch is described during early hematoma formation [25]. The transitioning of pro-inflammatory signaling towards anti-inflammatory signaling is shown as critical stage during healing. This is of high importance since the resolution of inflammation circumvents a compromised healing process, which is marked by failures in the complex healing process and a delay in bone regeneration [26][27][28]. By that, a restorative environment is induced [26][27]. In addition, the switch towards a restorative anti-inflammatory reaction induces osteoblast function and bone repair [29][15]. In this stage, pro-regenerative cytokines such as IL10, TGFb and IL4 (**Figure 1 B**) steer M2 macrophage and CD4+ TH2 cell polarization (**Figure 1 C**), which contribute to the anti-inflammatory milieu [3][30][31]. MSC are likewise known for their own specific inhibition of pro-inflammation by the induction of T cell inhibition via immunosuppression. In order to further downregulate pro-inflammatory triggers, MSC are able to release immunomodulatory IDO and prostaglandin E2 exerting anti-inflammatory features and regulating bone healing [32][33][34][35]. In parallel to the resolution of inflammation, the repair phase is initiated by MSCs and fibroblasts. The repair phase includes soft- and hard callus formation. Both, MSCs and fibroblasts take part in the facilitation of soft callus formation and the maturation of granulation tissue. Fibroblasts are known to form new matrix and MSCs proliferate and differentiate towards the chondrogenic- and osteogenic lineage [36][1]. The highly organized callus is formed by intramembraneous- and endochondrial ossification. This enables the necessary bridging of the fracture and mechanical stabilization of the bone fragments [37][1]. Subsequently, hypertrophic cartilage is induced, vessels re-appear and a second wave of angiogenic-osteogenic coupling is enabled for the formation of woven bone [38]. Woven bone is further modified to build the hard callus of the bone [1]. Mineralization of the surrounding tissue is enabled by osteoblasts via the activation of alkaline phosphatase [39]. Finally, a tightly correlating bone degradation and remodeling of the bone is needed to obtain the mechanical strength of the bone [38]. This remodeling phase is steered by growth hormones such as BMPs [40]. BMPs are important partakers in bone remodeling as they represent pro-osteogenic growth factors and are able to induce fibroblast-chondroblast-

osteoblast transformation [41][42]. In this way, remodeling of the woven bone is achieved by gradual replacement with lamellar bone [39]. MSC differentiation into the adipogenic lineage has likewise been studied in relation to bone regeneration and inflammation. The common view on adipocytes in regeneration and inflammation is of rather negative nature, since adipocytes have been shown to steer chronic low grade inflammation in metabolic compromised conditions as well as to impair bone healing [43][44][45][46]. However, adipocytes are predominantly highlighted in this thesis as another cell type of impact during the anti-inflammatory switch, harboring a positive influence on bone regeneration and metabolism which is not yet fully recognized [47][48].

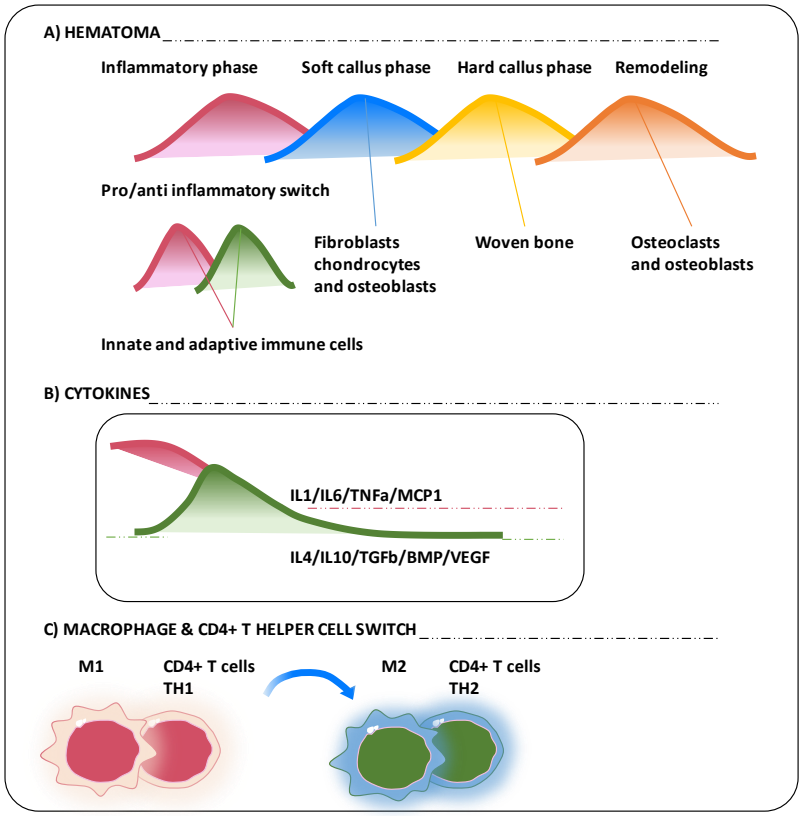

Figure 1: The bone healing cascade and its partakers adapted from [49][24][24][50]
The initial inflammatory phase consists of hematoma formation, pro-inflammation (red) and anti-inflammatory switch (green). Pro-inflammation generates a milieu of IL1/IL6/TNFa and MCP1 recruiting MSCs and activation immune cells e.g. M1 macrophages and CD4+ TH1 cells. Anti-inflammation is induced by pro-regenerative cytokines such as IL4, IL10 and TGFb, by that polarizing of M2 macrophages and CD4+ TH2 cells. Following that, bone repair is initiated and facilitates soft- and hard callus formation as well as bone remodeling

1.2. PPARG agonist as anti-diabetic drug and more?

The main features of antidiabetic drugs are the induction of a positive metabolic and anti-inflammatory change, both systemic and adipose tissue specific [51][52]. However, anti-diabetic treatment is linked to diverse side effects on bone integrity in dependence of the treatment period and drug that is used [53]. Next to standardized insulin-treatments, the most

commonly used anti-diabetic drugs to date comprise the first-line drug metformin as well as the group of insulin sensitizing thiazolidinediones (TZDs) in short glitazones [54]. TZDs such as pioglitazone and rosiglitazone represent a major therapeutic drug class for the treatment of T2DM, with both of them acting as PPARG agonist improving insulin sensitivity [55][56]. In fact, all anti-diabetic drug treatments harbor undesired side-effects e.g. hypoglycemia, weight gain, cardiovascular complications and in relation to bone increased fracture risks [55]. Underlining that, it has to be taken into consideration that metabolic disease conditions are either way associated with cardiovascular defects and atherosclerosis by the accumulation of cholesterol in macrophages forming plaques in the arterial wall [57][58][59][60]. This is why, it is important to re-evaluate the use of such drugs in certain healthy conditions as well as regarding the temporal scope of TZD therapy. In this work, I will reconsider a positive angle of TZD treatment within the scope of the already described detrimental effects. Indeed, TZDs are known to have beneficial features, which could be of interest in other critical, physiological conditions such as tissue and bone regeneration as well as general conditions associated with inflammatory processes.

In obesity and T2DM chronic, low-grade inflammation causes detrimental effects on the immune compartment, steering adipose tissue inflammation [61]. Excessive activation of leukocytes and their accumulation within adipose and other tissues represents the key driving event of insulin resistance [62]. Constant high energy intake rewires adipocytes into hypertrophic ones, secreting adipokines which further interfere with insulin signaling [62]. In addition, increased fatty acid and triacylglycerides are deposited in non-adipose tissues causing a metabolic overload [62]. Indeed, patients suffering from metabolic disease show simultaneous skeletal disorders including osteopenia, osteoporosis and increased fracture rates. All of them resulting from abnormal cytokines and adipokine production damaging the healthy bone environment. [63] PPARG agonists are known for their beneficial effects in steering anti-inflammation and metabolic re-balance. In line with that, healthy adipocytes are known regulators of whole body insulin sensitivity. Adipocyte function and maintenance is controlled by peroxisome proliferator-activated receptor g (PPARG) and its activation by PPARG agonist treatment e.g. anti-diabetic drugs leads to increased storage of fatty acids while reducing circulating ones [59][64][62]. Additionally PPARG activates the expression of adiponectin resulting in further insulin sensitivity of liver and muscle [65]. Controversially, the PPARG agonist rosiglitazone, which is used in this thesis, has been withdrawn from the market in Europe because of cardiovascular side effects [66]. In the United States this was not the case, because no evidence of these side effects has been provided and even cardiovascular benefits have been described [67][68]. A controversial view on TZDs and their common usage in combinational treatment with other drugs during metabolic disease is summarized. Potential

effects of TZDs in bone metabolism have not yet been described. However, PPARG agonist treatment is associated with de-novo differentiation of pre-adipocytes with high insulin sensitivity [69]. Of note, PPARG activation is associated with a brown-like adipocyte induction coupled to an increase of mitochondrial capacity [70]. A similar adipocyte accumulation is described within the bone marrow [71][72][73]. But, the phenotypic and functional state of adipocytes during fracture injury are described only to that extend, that they present a unique adipocyte subtype very different from the common white, brown and brown-in-white (brite) adipocytes in other niches [74]. Indeed, PPARG agonist rosiglitazone presents a valuable tool to study the sole PPARG driven effects on bone marrow adipocyte accumulation under an anti-inflammatory, pro-metabolic shield during bone regeneration.

1.3. PPARG signaling

Peroxisome proliferator-activated receptors (PPARs) are members of the nuclear hormone receptor superfamily of ligand-inducible transcription factors [75][76]. In fact, PPARs are important targets in metabolic compromised conditions, where PPAR agonists are used to improve insulin resistance and dyslipidemia [77]. Three subtypes of those fatty acid-activated nuclear receptors are known: PPARA, PPARB/D and PPARG. Those receptors play a major role in regulating adipogenesis, lipid and energy metabolism, inflammation and metabolic homeostasis [78][79]. This regulation occurs by binding of lipid ligands and the formation of heterodimers with the nuclear retinoid X receptor (RXR) [80]. Furthermore, the interaction with co-activators of transcription e.g. PPARG coactivator-1a (PGC1a) and PPARG coactivator-1b (PGC1b) as well as the binding of the whole complex to PPAR response elements within promotor target genes is necessary [81]. [82] PPARG is the main transcription factor and regulator of adipogenesis, with adipogenic MSCs and adipose tissue expressing the highest levels, whereas the expression of PPARG in other tissues/cells e.g. skeletal muscle, lung, colon, T cells and macrophages is likewise described [83][84]. Two isoforms are known: First, PPARG1, which is being expressed in various tissue/cell types. Second, PPARG2, which is commonly expressed in adipose tissue [85]. Both activating and inactivating features of PPARG are described by either agonistic ligand-dependent transactivation or antagonistic transrepression of target genes and signaling. [84] Agonistic ligands of PPARG are of variable nature e.g. endogenous ligands comprising unsaturated fatty acids and eicosanoids, as well as prostaglandins specifically 15d-PGJ2. Further, synthetic ligands are known to be used as anti-diabetic drugs e.g. the above described TZDs [86][87].

1.4. Bone regeneration and its major therapeutic targets

1.4.1. Anti-inflammation in bone regeneration

Up to now, 5-10% of fractures are known to develop failure of healing and non-unions [88]. Treatment of patients suffering from impaired bone formation, detrimental regeneration and non-union after trauma or injury is of high cost and finding new treatment strategies is under-researched [89]. The gold standard for studying in vivo bone regeneration is implementing a mouse femur osteotomy model, where an external fixator is used to stabilize the bone fracture and with that standardizing the experimental healing process [90]. Fundamental research on bone regeneration has been done using animals of specific-pathogen free housing without any environmentally priming of the immune system to achieve normalized and constant research outcomes. However, especially during regeneration of bone, the interplay of bone with the innate immune compartment e.g. macrophages as well as adaptive effector/memory subsets is of high importance [1]. The existence of the adaptive immunity is shown to strongly impact different steps of the regenerative cascade, especially the first stage of hyperinflammation [91]. This is why mice with an environmentally primed immune system have been used in our research setup [92][93][94]. Overstimulated T effector cells induce a pro-inflammatory response without a counteracting compensatory anti-inflammation, which is detrimental during bone healing. Indeed, enhanced pro-inflammatory signaling is described to inhibit osteogenic lineage differentiation especially by the secretion of INFg and TNFa [95][96]. In fact, only IFNg is identified for its direct effect on osteogenic differentiation capacity, whereas TNFa is partially essential in the initial pro-inflammatory phase, only acting deleterious at high concentrations [97][95][98]. The inhibition of TNFa driven inflammatory effects on bone can be partially prevented by anti-TNFa therapy, such as in the case of bone mineral density loss in rheumatoid arthritis [99]. However, the temporal fashion in which cytokines such as TNFa and IFNg should be targeted in therapeutic treatment of bone injury matters because the initial pro-inflammatory reaction initiating bone regeneration is indispensable [100]. In this research the neutralization of both IFNg and TNFa was used during the early course of bone healing without considering the temporal fashion of cytokine secretion. By that, marking a potential weakness for the evaluation of cytokine driven inflammation and its influence on immune cells. However, a specific evaluation could be done regarding the lineage development of human MSCs under IFNg neutralization. In fact, human osteoblast-like cells are identified with low levels of IFNg expression [101]. In line with that, IFNg signaling is described as important checkpoint in early osteogenesis, while IFNg inhibits adipogenesis via downregulation of PPARG signaling [102][103]. A delicate balance between inflammatory factors and their concentration as well as the subsequent resolution is essential for a beneficial healing outcome. However, a prolonged pro-inflammatory phase at the regeneration onset is shown to impair the pro-regenerative shift

towards the anti-inflammatory healing phase [25][104][24]. IFNg overexpression and the resulting downregulation of PPARG is known to steer pro-inflammatory CD4+ TH1 cells impairing the healing outcome of bone [105]. This establishes an inverse relationship between PPARG expression and pro-inflammatory cytokine secretion. To enable successive bone regeneration, the induction of anti-inflammatory signaling can be triggered by the activation of innate immune cells e.g. M2 macrophages as first cells infiltrating injured areas of bone and the further polarization of adaptive CD4+ TH1 towards TH2 cell subset via anti-inflammatory cytokine secretion [106][20][107]. T helper cells are positively correlated with bone repair [91]. While both, macrophages and T helper cells harbor beneficial features on the regeneration outcome when primed towards anti-inflammation by e.g. PPARG upregulation [20].

1.4.1.1. **M2 macrophages**

Macrophages are categorized into three main subtypes: undifferentiated M0, pro-inflammatory M1 and alternatively activated and anti-inflammatory M2 macrophages [31]. Macrophages of the M1 and M2 phenotype have diverse impacts on bone regeneration [108]. Pro-inflammatory M1 macrophages express TLR4 and are the first innate immune cells to be activated by DAMP signals e.g. high levels of IFNg and TNFa. Both cytokines are present in the pro-inflammatory bone environment [107][109]. In addition, low-grade systemic inflammation resulting from unbalanced cytokine release from either immune cells or adipocytes enhances the pro-inflammatory M1 activation [110]. However, not only DAMPs have the ability to induce TLR4 signaling, the activation of TLR4 is likewise induced by saturated fatty acids [111]. In contrast, PPARG agonist treatment and unsaturated fatty acids represent potent antagonists for TLR4 resolving IFNg initiated inflammation. This is not only reducing inflammation in bone but also metabolic disorders [111][112]. In bone, M2 macrophages contribute to tissue repair by enhancing the re-establishment of vasculature as well as by steering mineralization of newly formed bone [113]. Further, target cytokines of beneficial bone healing are known to be secreted by M2 macrophages e.g. IL10 and IL4. In addition, M2 macrophages produce signaling molecules such as prostaglandin E2 and bone morphogenetic protein 2 (BMP2) supporting MSC mediated bone regeneration [18][114]. More specifically, the activation of bone marrow-derived M2 macrophages can be put into correlating with PPARG activation. M2 polarization is initiated by ligand activation of PPARG, PPARD, or by steering the IL4-STAT6 signaling pathway [115][116]. The transcription of anti-inflammatory genes in M2 macrophages also depends on a program regulated by PPARG signaling [117]. **The metabolic view:** Since the ratios between M1/M2 macrophages are shown to be highly increased in obese white adipose tissue (WAT), the induction of an M2-macrophage phenotype in adipose tissue is linked to an improvement of metabolic disorders by increasing insulin sensitivity [118][119][120][117]. This induction of M2 macrophages leading to healthy WAT could be

translated to bone marrow and bone marrow associated adipocytes. In concordance, adiponectin and its positive effect on metabolic disorders is described to promote M2 macrophage proliferation via PPARG signaling further resulting in browning of adipose tissue [121][122]. With that it can be highlighted that anti-inflammatory mechanisms of M2 macrophages are strongly regulated by PPARG activity. Subsequently, M2 macrophages are able to secrete cytokines that induce TH2 immune responses and adaptive, anti-inflammatory signaling which could be of beneficial impact during bone regeneration [108].

1.4.1.2. **T helper type 2 cells**

Human memory T helper cells are known to reside within the bone marrow and become activated independently of antigen encounters. Cytokines and chemokines produced by stromal cells mediate their survival and maintenance. Effector/memory T cell subsets are associated with pro-inflammation in the same way as specific subsets of CD4+ memory helper T cells of the TH1 and TH17 type. Both cell types differentiate upon encountering different cytokine environments and by activation of specific transcription factors [123]. CD4+ memory TH1 cell differentiation is associated with the transcriptional activity of TBet [124]. With IFNg determining one of the key cytokines in TH1 responses. TH1 cells harbor a controversial impact in relation to bone pathologies with secreted IFNg as trigger for bone formation or IFNg/TNFa driven bone resorption [125][126][96]. CD4+ memory TH17 cells differentiate by engaging RORgT as transcription factor [127]. In relation to bone, TH17 cells are mainly discussed as inducers of bone resorption and negative regulators of bone regeneration [125][126][96]. The main driver for TH1 development is IFNg. However, TH17 cells are inhibited by IFNg secretion. All of these subset specific cytokines are present in the inflammatory cytokine milieu during early hematoma phase [128]. In summary, pro-inflammatory and detrimental TH1/TH17 responses in bone are associated with the induction of a cytokine named IL1b, while TH1 responses correlate with additional high MCP1 production [129][130]. Interestingly, the resolution of inflammation by IL1b inhibition can be achieved by PPARG activation [131]. Furthermore, the key cytokine IFNg interferes with PPARG agonist signaling, whereas PPARG activation results in the downregulation of IFNg levels [132][133]. With that, PPARG agonist treatment marks a possible strategy of inhibiting a prolonged IFNg response in bone, by restoring its healing capacity. Interestingly, the induction of PPARG is required for the activation and proliferation of the well-known anti-inflammatory $CD4^+$ memory TH2 cells, happening at the expense of TH1 cell development [134]. TH2 cells are associated with regulatory and anti-inflammatory features in bone repair [134]. Deletion of PPARG in $CD4^+$ T cells can cause severe overproduction of IFNg, emphasizing the impact of PPARG on the reduction of TH1 inflammatory responses [116][105]. **The metabolic view:** Treatment with the PPARG agonist rosiglitazone, a well-known anti-diabetic drug, has been shown to

downregulate TNFa and IFNg levels in chronic inflamed diabetic mice while enhancing anti-inflammatory signaling and inhibiting IL1b secretion [135]. Next to that, TH2 cells depend on a PPARG-conditioned fatty acid uptake program, by that linking PPARG activation with beneficial T cell subset induction and a distinct metabolic program during bone regeneration [134][136]. TH2 cells have the capacity to improve insulin resistance and chronic inflammation in metabolic disorders [137][138][139]. Thus, PPARG promotes the release of TH2 cytokines, thereby inhibiting pro-inflammatory responses and benefitting bone formation. [131] [116][140]. Since PPARG plays an essential role in controlling TH2 effector function, it has the potential to be a potent therapeutic target for steering bone healing.

1.4.1.3. **Bone marrow adipocytes**

The cytokine IFNg commonly steers inflammatory reactions in bone as well as in bone marrow adipocytes (BMAs) by promoting the release of pro-inflammatory IL1b and TNFa [102][104]. Within this thesis, the negative impact of pro-inflammatory IFNg and TNFa on the inflammatory milieu itself but also on the development of bone marrow adipocytes (BMAs) is proposed. It is known, that IFNg not only has deleterious effects on bone, but also inhibits the differentiation of certain cell types, such as adipocytes, by inhibiting the nuclear receptor PPARG, which is considered the most important transcription factor in adipocytes [102]. In concordance, TNFa mirrors the effect of IFNg in the inhibition of pre-adipocyte and adipocyte differentiation by either activating the nuclear corepressors or inhibiting NF-kB signaling [141][142]. In combination, TNFa and IL1 decrease PPARA and PPARG levels in liver [143]. Downregulation of PPARG in BMAs may also be associated with an increase in pro-inflammatory cues such as TNFa and IL1. In contrast, the anti-inflammatory TH2 type immune responses are shown to influence adipose tissue and its metabolic capacity in a positive way e.g. by counteracting WAT inflammation [144]. Adipocytes have the capability to change from a pro- towards an anti-inflammatory phenotype. This is accompanied by the modification of their own paracrine properties, morphology and inert immune cell composition.[48][145][50]

This thesis proposes a strong connection between the inflammatory milieu in bone and the accumulation of BMAs, whereby immune cells and adipocytes may drive each other's inflammatory phenotype. Steering a beneficial anti-inflammatory adipocyte type to improve metabolic and regenerative bone disorders is under researched. Healthy adipocytes harbor IL4, which is secreted by adipocyte residing M2 and TH2 cells. Both M2 and TH2 cells promote anti-inflammatory cytokines such as IL10 and drive anti-inflammatory PPARG dependent Tregs [146][147]. In fact, IFNg knock-out models show increased insulin sensitivity and decreased adipose tissue inflammation in dependence of PPARG activation [148]. Proteins/hormones secreted by adipocytes are known as adipokines [149]. A steady balance of pro- and anti-inflammatory adipokines secreted by adipocytes is of importance. This balance

is tightly controlled by the metabolic status, and dysregulated by infection or chronic inflammation. Adipokine balance plays a crucial role in the regulation of obesity driven adipose tissue inflammation.[150] In this thesis, we would like to draw the attention towards the impact of adipokines on not only adipose tissue- but also bone tissue inflammation. Adipokines not only regulate metabolic flexibility, but also have an impact on immune cells and can be characterized by their pro- or anti-inflammatory nature [50]. The most described adipokine is adiponectin, which indeed has the ability to activate PPARG and induce TH2 cell polarization [151].

To come back to treating unhealthy pro-inflammation in bone and adipose tissue, PPARG is a well-known target for improving metabolic diseases. This is because it combines beneficial immune cell changes via anti-inflammatory signaling and the resulting re-balance of the metabolic system.[152] Changes in bone marrow resident adipocytes are scarcely studied and the impact of adipocytes on bone regeneration by adipokines, cytokines and T cell interaction is not well elucidated. The common knowledge on adipocytes in bone is of detrimental nature. Within this thesis, the positively balanced bone marrow adipocytes and the induction of a PPARG driven pro-regenerative adipocyte type will be discussed.

1.4.2. Metabolic adjustments in bone regeneration

1.4.2.1. Oxidative phosphorylation and glycolysis

Bone regeneration requires a high amount of energy to be provided to various cell types, especially to hBMSCs able to undergo adipogenesis, as in adipocyte formation and osteogenesis, as in bone formation. Energy in form of ATP is produced by the central carbon metabolism comprising many distinct pathways under which the major glycolysis pathway is highlighted in this thesis. The carbon metabolism is tightly coupled to mitochondrial respiration/oxidative phosphorylation. Both glycolysis (using glucose and its conversion towards pyruvate) and oxidative phosphorylation (requires presence of oxygen) are the main providers of cellular ATP in mammals [153]. Starting the process of ATP generation, glucose is the fuel for the glycolysis pathway, it is converted to pyruvate, further driving ATP production within the cytoplasm of the cell (**Figure 2**). The tricarboxylic acid cycle, in short TCA cycle uses pyruvate to create reducing equivalents, which are required for the electron transport towards the mitochondrial respiratory chain also referred to as electron transport chain (ETC). The electron transport through the mitochondrial membrane achieves a mitochondrial membrane potential, which is used during the oxidative phosphorylation (OXPHOS) pathway. This process fuels the production of ATP within mitochondria [154].[155][156] In detail, electrons are transferred within the ETC at either complex I (NADH:ubiquinone oxidoreductase) or complex II (FADH2:succinate dehydrogenase) within mitochondria. Electrons from both

complexes are further transported towards complex III (coenzyme Q:cytochrome c reductase) and then to cytochrome c. The last station of passing electrons is the transfer of electrons from cytochrome c to the complex IV, where oxygen binds electrons and is reduced to H2O. While transporting electrons, a total of 10 protons are transferred from the mitochondrial matrix to the intermembrane space [157]. This is known to induce an electrochemical proton gradient, the mitochondrial membrane potential, which drives protons back into the mitochondrial matrix. This only happens when a protein channel such as the complex V (ATP synthase) is engaged. By transporting four protons through the channel, the ATP synthase enables the production of one ATP molecule.[3][157] The oxygen consumption during this process is commonly known as the mitochondrial respiration of cells [158].[157] OXPHOS is a highly efficient process of ATP generation to supply energy and enable longevity of cells [159]. This process maximizes the yield of ATP to an amount of in total 36 ATP per molecule glucose. By that, only 2 ATP from glycolysis but 34 ATP from TCA/OXPHOS are further transported into mitochondria.[160][161] However, this energy gain is only possible by functional coupling between glycolysis and OXPHOS as well as the presence of oxygen [162].

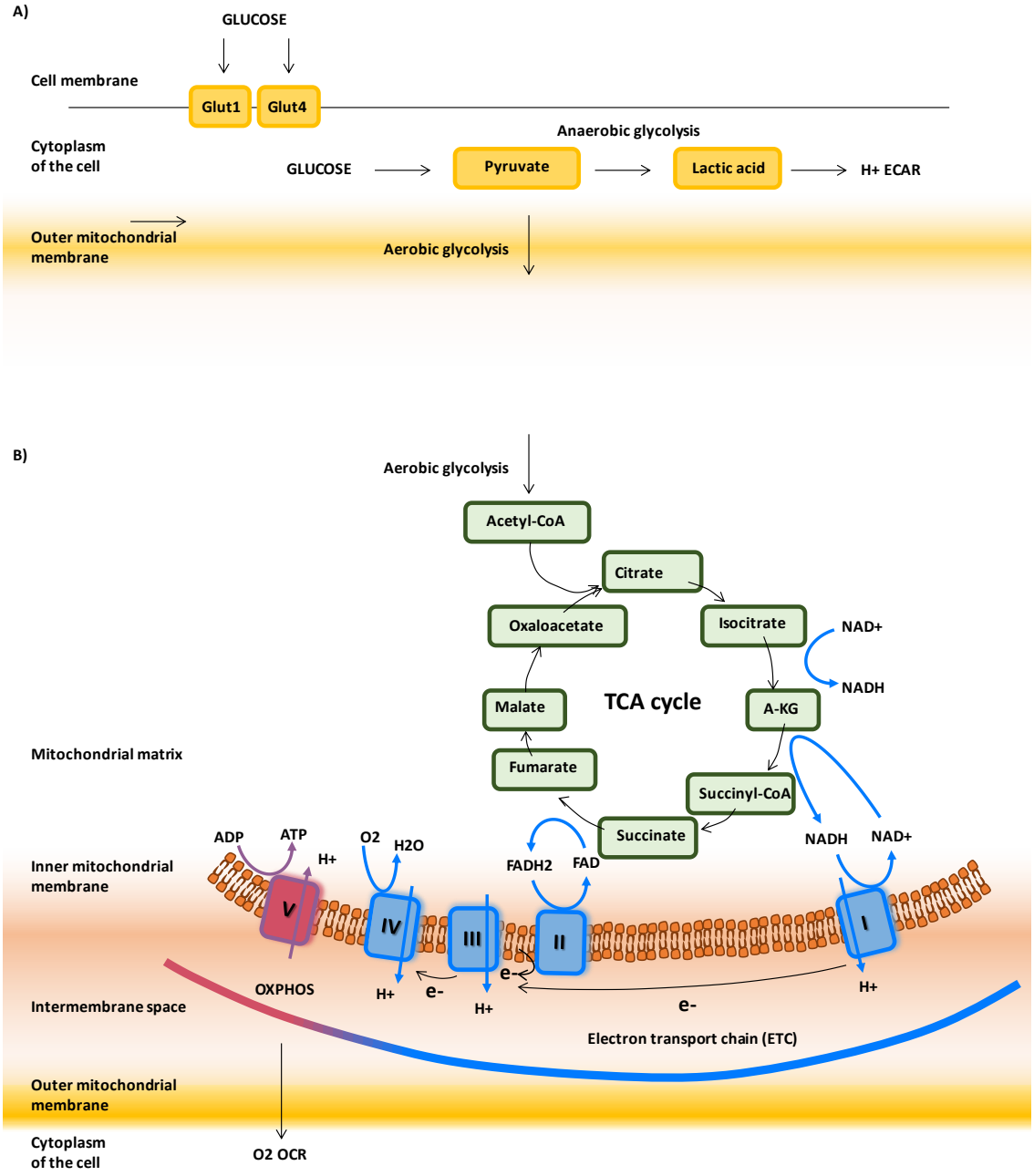

Figure 2: Glucose as fuel for glycolysis and OXPHOS adapted from [163][161][156]
Glucose is used as fuel for the generation of energy in the form of ATP. Two pathways can be triggered. A] First, glucose is transported into the cell cytoplasm by glucose transporters e.g. Glut4 and Glut1. Glucose is converted to pyruvate and lactic acid by anaerobic glycolysis generating 2 molecules of ATP **(yellow)**. ECAR is measured as extracellular acidification rate (ECAR) taking into account H+ accumulation in the cytoplasm. B] Second, aerobic glycolysis can be initiated. The tricarboxylic acid cycle (TCA) **(green)** uses glucose to generate reducing equivalents, which are further required for the electron transport chain (ETC) **(blue)**. The electron transport generates a membrane potential in the inner mitochondrial membrane, which is important for the oxidative phosphorylation pathway (OXPHOS) further leading to ATP production within the mitochondrial matrix **(red)**. OXPHOS is measured as oxidative consumption rate (OCR) taking into account the production of O2. The TCA and OXPHOS cycle yields a total of 34 ATP molecules. NAD: Nicotinamide adenine dinucleotide, NADH: Nicotinamide adenine dinucleotide hydrogen, FAD: Flavin adenine dinucleotide, FADH: Flavin adenine dinucleotide hydroquinone, ADP: Adenosine diphosphate, ATP: Adenosine triphosphate, A-KG: Alpha-ketoglutaric acid

Indeed, under a hypoxic milieu e.g. the milieu of bone, glycolysis and OXPHOS are decoupled [162]. During anaerobic glycolysis, glucose is oxidized to pyruvate, which is not introduced into

the TCA/OXPHOS pathway but is further converted to lactate, leading to extracellular acidification by the accumulation of lactic acid [161]. This process only generates a low amount of 2 ATP per molecule glucose and this amount alone is not enough fuel for cells under dramatic stress situations such as a fracture [3]. This thesis will identify a new possibility to steer higher energy generation by the activation of PPARG in order to support bone fracture healing.

1.4.2.2. **Fatty acids and mitochondrial fatty acid b-oxidation**

The utilization of fatty acids by osteoblasts is indispensable for osteogenic differentiation and bone formation [164]. The oxidation of fatty acids by osteoblasts account for 40-80% of energy yield and is exceptionally important in mature osteoblasts while mineralization [165][166]. Polyunsaturated fatty acids can act as ligands for PPARG activation either resulting in an anti- or pro-inflammatory response. Evidence accumulates that fatty acids have an essential role in bone metabolism[167].

One way to improve energy supply during fracture healing is that fatty acids can be used to initiate mitochondrial fatty acid B oxidation (FAO). Hereby, additionally recharging OXPHOS, both FAO and OXPHOS representing major and tightly linked processes to metabolize fat and glucose [168]. This mechanism is likewise described for cells under high energetic demand such as bone cells in a fracture milieu. Interestingly, fatty acid oxidation can generate high amounts of ATP e.g. over 100 ATP molecules by complete b-oxidation of one palmitate molecule, which represents a major fatty acid in mammal cells [159][169]. This high ATP generation could be useful for cells during bone regeneration, providing sufficient energy supply for the healing process. Another main point is that mitochondrial fatty acid b-oxidation metabolizes fatty acids to prevent fatty acid-induced insulin resistance and lipotoxicity [170]. Initially, fatty acids are oxidized by NAD+ and FAD, generating acetyl coenzyme A (CoA) which is further degraded to CO2 within the citric acid cycle. The recycling of NADH and FADH2 is done by the ETC in mitochondrial respiration to generate further NAD+ and FAD for the next round of fatty acid oxidation. [171] The control of fatty acid oxidation as well as generally enhanced mitochondrial respiration is associated with the activity of coactivators such as peroxisome proliferator-activated receptor-g coactivator-1b and -1a (PGC1a, PGC1b) [172]. In this thesis, the connection between PPARG agonist stimulation during bone healing is put into relation with beneficial effects on the metabolism of hBMSCs e.g. enhancing energy supply by fatty acid b-oxidation, reducing lipotoxicity of BMAs under stress conditions and by that antagonizing detrimental metabolic conditions [173]. [174][175][171]

1.4.3. Metabolic shift of the pro- and anti-inflammatory fracture milieu

1.4.3.1. Immune cells

Metabolic fitness and metabolic activity of cells is known to adapt to the energy requirements of various biological processes and underlies environmental influences [176]. The initial fracture environment underlies a physiological hypoxia and oxygen depletion. Indeed, prolonged oxygen tension and hypoxic conditions can over activated neutrophils and cause pro-inflammation which further damages the already injured tissue. Oxygen deprivation at the fracture site induces HIF1a and steers anaerobic glycolysis as well as an energetic shift towards fatty acid synthesis in M1 macrophages, resulting in enhanced production of pro-inflammatory cytokines such as TNFa and IL1b [177][178][179][180]. Within the fracture environment, pro-inflammatory CD4+ TH17 T helper cells shift their metabolic program from OXPHOS during quiescence state towards aerobic glycolysis enabling effector functions [181]. In concordance, the change of high oxygen tension towards low oxygen tension by oxygen depleting neutrophils enables the resolution of inflammation [182][183]. In addition, CD4+ T helper cells are quickly sensing and changing according to the pathological hypoxic fracture environment and are important interaction partners for MSCs in exchanging signaling mediators [180]. The pro-regenerative and anti-inflammatory change from M1 and TH1/TH17 T helper cells towards M2 and TH2 T helper cells is accompanied by metabolic changes (**Figure 3**) [184]. M2 macrophages mostly use fatty acid oxidation and oxidative glucose metabolism and downregulate glycolysis [177]. In addition, Tregs and TH2 T helper cells use ATP generated by OXPHOS and lipid and fatty acid oxidation [185].

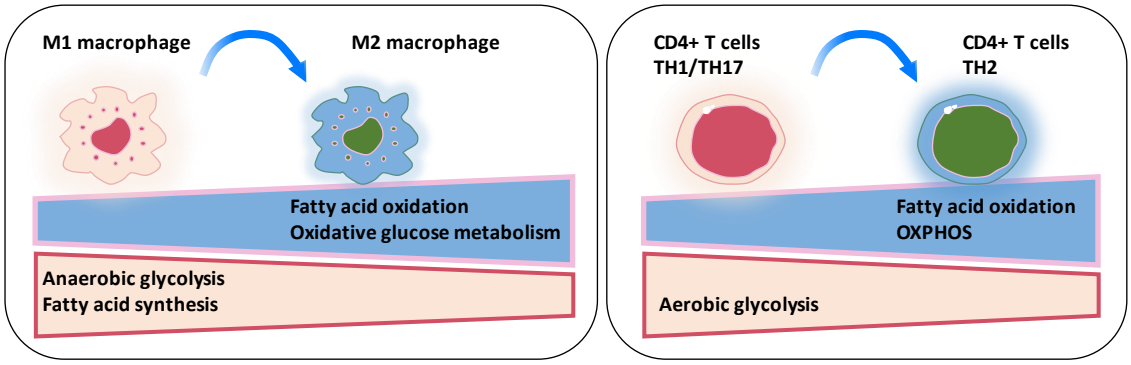

Figure 3: Metabolic changes in fracture residing immune cells adapted from [159]
M1 macrophages change their metabolic requirements from anaerobic glycolysis and fatty acid synthesis towards fatty acid oxidation and oxidative glucose metabolism when switching to the anti-inflammatory M2 phenotype **(left)**. CD4+ T helper cells change from aerobic glycolysis towards fatty acid oxidation and OXPHOS during anti-inflammatory TH2 cell induction **(right)**

1.4.3.2. Mesenchymal stromal cells

In general, the regeneration or formation of bone requires a strong fitness of human bone MSCs to cover the high energetic demand of the multiphase, well-regulated process of

complete and healthy regeneration without forming scars. Slight hypoxia and avascularity is necessary for the initiation of MSC clustering in the early healing phase.[186] MSCs commonly reside under hypoxic conditions within the bone marrow. That means that they depend on glycolysis while resting and further require ATP generated by glycolysis in early stages of osteogenic differentiation, when high rates of proliferation have to be maintained. By that, glycolysis is represented as main energetic process during the initial, pro-inflammatory fracture phase [3].

PPARG activation is shown to restore vascularization, which is important during oxygen and energy supply for osteogenic differentiation and matrix mineralization of MSCs leading to bone remodeling and formation [187][188][189]. MSCs likewise change their metabolic profile from glycolysis towards OXPHOS to obtain enough energy in form of ATP to differentiated into the osteogenic lineage and produce mineralized matrix (**Figure 4**) [3].

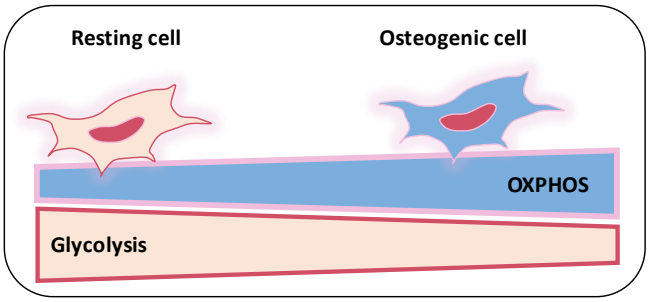

Figure 4: Metabolic changes in fracture residing MSCs adapted from [190]
MSCs change their metabolic requirements from sole glycolysis (red) towards glycolysis and OXPHOS when switching from a resting state towards osteogenic differentiation to fulfill their high energetic need (blue)

1.5. Bone marrow adipocytes and regional characteristics

Different adipose tissue types are scattered throughout the body, having an impact on healthy metabolic features and endocrine functions. Visceral and subcutaneous WAT represents an energy-rich storage body, whereas BAT is specialized in energy driven thermogenesis [191][192]. A third type of brown-in-white (brite) adipocytes is known for its dual ability to store lipids but also obtains thermogenic characteristics while transdifferentiation from a white to brown phenotype [193][194]. The transdifferentiation of this brite adipose tissue type is steered by PAPRG activation and induces enhanced mitochondrial capacity and mitochondrial oxidation in these adipocytes [195]. This thesis has its focus on the specific characterization of adipose tissue within the bone, which is termed bone marrow adipose tissue (BMAT). Only scarce evidence on the characteristics of bone marrow adipocytes (BMAs) is available but this specific and very different adipose tissue gains more and more attention [196]. Generally BMAT resembles both BAT and WAT in distinct features [196]. However, recent evidence tends to the notion that BMAT contains active brite adipocytes [197]. In comparison to the

MSCs of the major white and brown adipose tissue depots, bone marrow residing MSCs present most similarities to WAT MSCs [198]. However, their adipogenic lineage commitment is far more complicated and scarcely described. Controversially, this adipogenic lineage is described to arise from a mesenchymal-osteogenic lineage. In fact, it is known that bone marrow adipocytes differentiate from MSCs and undergo a lineage specialization process with prior decision making between osteogenic and adipogenic lineage commitment. [199][200][201] Even with some similarities, mature bone marrow adipocytes are clearly distinct from other adipocytes of brown and white adipose tissue depots within the body [74]. Bone marrow adipose tissue has a markedly different response to glucose and insulin and can be defined as specialized subtype with close ties to the skeletal and hematopoietic niches [202][71][43]. Two distinct types of bone marrow adipose tissues have been described in the literature [21]. One termed regulated BMAT (rBMAT) located in red, hematopoietic-rich proximal bone regions and being acquired during aging. The other one being defined as the constitutive, yellow BMAT (cBMAT) located in distal bone regions and formed during embryogenesis and/or early childhood [22]. Both types were determined to have inherently different developmental patterns with rBMAT of young individuals being marked with a highly plastic fate [23][203][204]. Negative effects of adipocytes in bone have been shown to originate from the accumulation of RBMAT and its high content of saturated fatty acids, which can steer rather detrimental effects during bone regeneration [26][27]. In contrast, cBMAT has been known as stable energy rich hub containing unsaturated fatty acids, inducing beneficial effects on bone and potentially serving as rescue depot [24][25]. [26][27]

This strongly questions the view on unilateral, detrimental effects of adipocytes in bone, especially when the composition of the two BMAT types might be influenced by PPARG agonist treatment. Even if the level of PPARG expression is similar in both r- and cBMAT regardless of the skeletal location, their response to PPARG activation is only scarcely described [205]. We suggest a new view on the development of beneficial BMAT types during emergency hematopoiesis such as in fractured bones. The next chapter will underline the possible features of PPARG driven adipocytes during bone regeneration.

1.6. PPARG shaped adipocytes during high energetic demand

In this thesis, bone healing is underlined as a process not only depending on the osteogenic compartment but also requiring the presence of adipocytes. In the injury setting, adipocyte accumulation is described during skeletal muscle injury and bone injury as well as during chondrocyte differentiation. Hyperplasia and de novo differentiation of small adipocytes enhance insulin sensitivity of bone marrow stromal cells when under PPARG stimulation, whereas under metabolic compromised conditions adipocytes secrete detrimental factors such as inflammatory cytokines and adipokines [206][207][208][209][210]. From the literature, we

know that adipocytes are the main regulators of energy metabolism [211][212]. However, the metabolic impact of adipogenic differentiation during bone fracture healing is not clear and strongly debated in the community.

Interestingly, during the regeneration of tissue a concurrent induction of adipogenic cells and osteogenic cells is shown. Adipogenic differentiation relies on the activation of the main nuclear transcription factor peroxisome proliferator-activated receptor γ (PPARG). But not only that, PPARG is known for its governance of cell fate during MSC differentiation. Its expression is present in both adipogenic as well as osteogenic MSCs and can induce both differentiation processes [213][214]. This is the reason why stimulation with a PPARG agonist not only presents a valuable tool to induce adipocytes in general but may also lead to an enhanced osteogenic differentiation. Indeed, the concurrent induction of adipocytes and bone cells is described for patients treated with e.g. BMP2 and IL6. This treatment is shown to result in enhanced bone fracture healing [215]. This result is of most interest, since PPARG activation is essential for both BMP2-driven adipogenesis and osteogenesis during bone repair. Apart from the crucial impact of PPARG activation on both differentiation processes, adipocytes may re-nourish the surrounding cells, which have lost their nutrient supply because of damaged vessels within the fracture gap [216]. Furthermore, PPARG activation in adipocytes is especially important because it maintains the expression of e.g. adiponectin and other lipogenic enzymes and thereby preserves insulin sensitivity and an anti-inflammatory effects in adipocytes [217][218]. We highlight that shaping adipocytes in the fracture gap towards a pro-regenerative, metabolically balanced and anti-inflammatory adipocyte type by using PPARG agonist treatment is of importance for driving regeneration. Further, we want to point out that PPARG agonist induced adipocytes may not only enhance energy supply for the surrounding cells but also steer osteogenic differentiation by PPARG activation [219]. In addition to the pro-osteogenic effects, the beneficial metabolic potential of PPARG driven adipocytes in regards to osteogenic differentiation of hBMSCs will be investigated as follows: First, by giving an insight on the insulin metabolism under PPARG agonist activation. Second, by analyzing the insulin dependent glucose metabolism and third, by screening for PPARG agonist driven adipokines of insulin sensitizing or anti-inflammatory nature.

1.7. PPARG driven features for ‘superhealing’

1.7.1. PPARG driven insulin signaling in bone

Insulin is an important hormone, which is secreted by beta-cells and has the ability to control metabolic features by stimulating the absorption of lipids, fatty acids and glucose from blood towards adipose tissue, skeletal muscle and liver [220]. Hyperinsulinemia, insulin resistance and hyperglycemia all result in a high level of blood glucose [58]. In detail, a reduced insulin

signaling is commonly shown by the limited activity e.g. phosphorylation of insulin receptor substrate (IRS). The phosphorylation of IRS is tightly linked with the activation of two signaling cascades regulating insulin driven metabolic actions: First, the phosphoinositide-3 kinase (Pi3K) and second, the protein kinase B (PKB) [221]. IRS are further involved in the activation of downstream cascades, such as mitogen-activated protein kinase (MAPK), which cooperates with Pi3K to control cell growth and differentiation [222][223]. Dysregulation of those signaling cascades results in metabolic impairment, insufficient energetic expenditure and chronic inflammation [224]. Insulin related metabolic processes and subsequent signaling cascades are thought to influence bone structure. This is why, this thesis will highlight the upregulation of signaling cascades such as Pi3K, MAPK and PKB in osteogenic hBMSCs for the characterization of insulin sensitivity and signaling efficacy. Healthy bone formation is shown to be dependent on insulin signaling. Insulin availability promotes the expression of both insulin receptor (IR) and insulin like growth factor 1 receptor (IGF-1R) in osteoblasts [222][223]. The activation of both receptors can be regulated by the available insulin concentration. Low insulin concentrations are shown to affect the highly sensitive IR, whereas high concentrations of insulin e.g. hyperinsulinemia could likewise activate, the less sensitive IGF-1R. [225][226] In this work, PPARG agonist driven insulin sensitization and subsequent signaling is compared to a control condition marked by a strong availability of insulin during osteogenic differentiation. Thus, the PPARG agonist driven insulin sensitivity refers to the lower insulin concentration and the high insulin concentration may be considered to mimic IGF-1R signaling. Of importance will be the balanced insulin/IGF-1 axis, which is essential for a beneficial bone healing outcome. To rebalance insulin signaling, PPARG activation is known to reduce circulating insulin and to enhance metabolic fitness [227][228][223][229]. In the contrary, metabolic compromise is known to induce detrimental effects on bone remodeling, leading to bone illness such as osteopenia, osteoporosis, fracture risk and impaired healing [230][231]. This is due to either impaired insulin signaling or critically elevated insulin signaling, both of which result in adverse healing and present a point of attack for improving osteogenic differentiation. [232][222][223] IRS-1, IRS-2 and IGF-1 are known to differentially impact BMSC differentiation towards the osteogenic and adipogenic lineage. On the one hand, IRS-1 signaling is associated with a reduced adipogenesis by the downregulation of PPARG within bone marrow, whereas IRS-2 is known to steer adipogenesis. [233][234]. IRS-1 and IRS-2 not only have an impact on the lineage decision of BMSCs but are likewise expressed in the adipocyte compartment of the bone. In fact, IRS-1 and IRS-2 are both expressed in BMAs and are strongly regulated by PPARG activation. [235][236] The summarized effects provide evidence on the influence of PPARG activation on insulin signaling, which could be of importance in BMAs during bone regeneration. In this thesis, we will not only investigate the PPARG agonist driven impact on BMAs during bone regeneration but also the impact of PPARG agonist driven

insulin sensitivity on the mineralization capacity of osteogenic hBMSCs. This will be then compared to the impact of high insulin concentrations. Thus, we hope to discuss the beneficial PPARG agonist induced balance of insulin metabolism during osteogenic differentiation and to specify these effects through underlying signaling cascades.

1.7.2. PPARG and insulin dependent glucose signaling

Synthetic PPARG agonists lead to enhanced whole body insulin sensitivity. PPARG activation has various points of attack downstream of insulin signaling, one of them presenting the induction of higher glucose and lipid metabolism. By that, PPARG activation can improve detrimental hypermetabolic states e.g. high levels of glucose (hyperglycemia) by reducing blood glucose levels [227]. Glucose is the main nutrient for osteoblasts and its uptake is crucial during osteogenic differentiation [237]. This work will focus on the insulin driven glucose uptake during osteogenic differentiation and mineralization of hBMSCs. It will elucidate the role of PPARG agonist stimulation in improving this process. Underlining that, literature on PPARG activation shows improvement of glucose disposal rate via Pi3K kinase activity [238]. Especially rosiglitazone as PPARG agonist is known to induce upregulation of Pi3K and Akt2. While, Pi3K kinase is an essential signaling molecule inducing insulin mediated glucose uptake, glycogen synthesis and cell differentiation. [239] In line with that, PPARG agonist treatment is shown to upregulate GLUT4 and GLUT1 promoting glucose uptake in skeletal muscle [240]. Various pathways are positively regulated by PPARG activation e.g. Pi3K in association with Wnt/b-catenin signaling, additionally helping to re-balance a dysregulated IGF-1/IR axis [227]. This work will examine how PPARG agonists enhance insulin as well as glucose metabolism to promote osteogenic differentiation.

1.7.3. PPARG driven paracrine features

BMAT is known for its unique paracrine and endocrine functions influencing the bone marrow niche and its cell compartment e.g. MSC hematopoiesis and osteogenesis [208]. The physiological input of BMAs is commonly described as detrimental, however beneficial metabolic adaptations are left largely unrecognized. This is why, the impact of PPARG driven BMAs and their paracrine features during osteogenic differentiation will be re-evaluated in this thesis. Bone marrow adipocytes as secretory and metabolic organ can communicate with other organs/cells by direct or indirect regulation [241]. This is of importance also in relation to bone healing, since a variety of cells have to interact to improve the bone regeneration outcome. The secretory profile of BMAs includes adipokines, adipocytokines, hormones and fatty acids and differs strongly in comparison to other common adipose tissue depots [242][243]. Pro-inflammatory, anti-inflammatory and senescence associated secretory phenotype factors are secreted by BMAs and have an influence on the bone micro-environment, the metabolic balance and the bone healing outcome [241][244][245][246].

1.7.3.1. **Pro-inflammatory adipokines**

It is known that the secretory profile of BMAs differs from the adipocytes within the other body cavities [243]. Still, the resulting effects of the secreted adipokines on e.g. the bone environment are suggested to be similar. This is why, the general characteristics of adipokines, which are likewise associated with the secretory profile of BMAs, are described to provide a foundation for possible effects of BMA driven adipokine secretion in bone healing. In this thesis, the secretory profile of PPARG agonist driven BMAs will be analyzed regarding pro- and anti-inflammatory adipokine secretion during high and low insulin conditions.

In general, pro-inflammatory adipokines include leptin, resistin, TNFa, IL6 and RBP4 and many more [241]. The list of pro-inflammatory adipokines grows and the pro-inflammatory **chemokine monocyte chemoattractant protein-1 (MCP1)** commonly produced by macrophages and endothelial cells has been added to the list [247]. In response to inflammation, MCP1 is needed for the recruitment of monocytes and leukocytes and its expression level is enhanced in association with metabolic stress situations e.g. insulin resistance [248][249][250][251]. In bone, decreased bone mineral density (BMD) and a prolonged detrimental inflammatory phase is associated with enhanced expression of MCP1, IL6, IL1b, TNFa and leptin [18][252]. Another prominent cytokine candidate of the pro-inflammatory type is **interleukine-1 beta (IL1b)**. Il1b is produced by adipocytes during inflammatory processes and is associated with enhanced levels of MCP1 and IL6 within the adipose tissue milieu [253][247]. By that, IL1b likewise plays a role in obesity-linked insulin resistance and diminished glucose uptake [254]. In summary, IL1b may be associated with detrimental effects in the bone environment since insulin metabolism and insulin-induced glucose transport is of high importance for osteogenic differentiation. It is currently known, that the production of IL1b in inflammatory adipocytes enhances symptoms of rheumatoid arthritis in conjunction with leptin and other inflammatory cytokines [255].

1.7.3.2. **Anti-inflammatory adipokines**

Anti-inflammatory adipokines comprise adiponectin, fibroblast growth factor 21 (FGF21), secreted frizzled-related protein 5 (SFRP5) and omentin [241]. The most prominent anti-inflammatory and anti-diabetic adipokine is the hormone **adiponectin (APN)** [256]. Interestingly, adiponectin is associated with an inverse relationship to fat mass and is predominantly produced in the bone marrow [257][258]. The pro-metabolic and anti-inflammatory nature of adiponectin makes it a prominent adipokine of BMAs to support bone regeneration. Not only could adiponectin support the metabolic and inflammatory balance but also is known for its pro-osteogenic effects on BMSCs [243]. Adiponectin has three receptors T-cadherin, AdipoR1 and AdipoR2, while the latter two can bind different forms of adiponectin e.g. globular and full length adiponectin [259]. The binding of adiponectin towards AdipoR1 is

shown to activate PPARa, AMPK and p38MAPK and is associated with the stimulation of fatty-acid oxidation (FAO) and glucose uptake [259][260]. In relation to bone, FAO and improved glucose uptake may lead to improved metabolic status of BMSCs during fracture healing. Adiponectin further upregulates insulin signaling and enhances insulin sensitivity [261]. It is well described, that adiponectin receptors AdipoR1 and AdipoR2 are expressed in osteoblasts, osteoclasts and chondrocytes [262][263]. The further workings of adiponectin are described in relation to bone, where adiponectin stimulates the proliferation, differentiation and mineralization of osteoblasts by AdipoR1 and AMP kinase signaling.[261] In this work, the effect of adipokines during osteogenic differentiation will underline the interaction between BMA and osteogenic BMSCs and may allow for the development of a new strategy to induce a positive bone marrow milieu leading to a favorable healing outcome.

1.8. Aim of this thesis

With this introduction, we intend to explain the important workings of bone fracture healing underlying a broad energy supply and the necessity of a pro- to anti-inflammatory change. This change is thought to depend on the interface between bone marrow adipocytes and osteogenic BMSCs. This interface is highlighted by the mutual influence of secreted immunoregulatory adipokines from BMAs on the bone environment. Within this thesis, the impact of PPARG activation on the dual induction of adipo- and osteogenic differentiation will be underlined, suggesting an important physiological connection of the bone and adipocyte compartment. On top, PPARG activation is presented as potential all-rounder for pro-metabolic and anti-inflammatory features. Its activation is shown to increase insulin sensitivity as well as glucose uptake in BMSCs preparing them for the high energy demand in the fracture healing process [264][265]. In addition PPARG activation may result in the improvement of oxidative stress, mitochondrial respiration and metabolic flexibility and helps to restore the metabolic balance during fracture repair [266]. All summarized beneficial effects are examined with respect to osteogenic differentiation of BMSCs. In passing, the immunoregulatory effects of PPARG agonist driven adipocytes and the induction of anti-inflammatory T cell subsets is highlighted.

2. Materials and methods

2.1. In vivo experiments using a mouse fracture model

2.1.1. Mouse femoral osteotomy model

In this research the impact of adipocyte driven metabolic changes on the immune reaction and healing outcome of bone fractures was investigated. For this purpose, a mouse osteotomy model implemented in the femur of mice has been known as the gold standard method for bone healing research and was extensively studied in the community. Therefore, the AO foundation and Research Implant Systems (RIS) developed a fixator to stabilize the fracture in bone during and after the surgery. This system was used to standardize the procedure and circumvent the need of further model development. In addition, the variety of analysis tools which have been established and have been made commercially available, represented an advantage for the use of this animal model. In this study, female C57BL/6N mice of the age of 12 weeks were investigated. Mice were commercially bought from Charles River Laboratories (Germany) and housed for 4 weeks before undergoing surgery and fracture induction. The healing was studied until three weeks (21 days) post-surgery, with the surgery marking day 0.

2.1.2. Surgical procedure and external fixation method

Before the surgery, mice were subcutaneously injected and treated with an anesthetic called buprenorphine (temgesic) at a concentration of 0.03mg/kg. Additional, the osteotomy and application of the external fixator was implemented under anesthetic isoflurane and administered 8mg/kg/body weight clindamycin as antibiosis to avoid intra-operative contamination. During the operation mice were kept at a warm temperature using a heating plate. In order to protect the eyes during surgery, mice were treated with eye ointment to prevent dehydration. The surgery included the application of the external, x-ray permeable fixator on the left femur of the mouse using four screws with 0.45 mm in diameter. To implement the fixator, a lateral, longitudinal incision was made starting at the knee and extending towards the hip joint. The muscle was bluntly prepared to reveal the femur. After that, the first pinhole was drilled proximal to the distal metaphysis and three further pinholes helped stabilize the external fixator parallel to the femoral axis. Finally, a 0.7 mm wide osteotomy was induced using a wire saw (RISystem, Davos, Switzerland) in between the two middle pins **(Figure 5)**. After the surgery, the wound was closed and all mice received tramadol until three days post-surgery via the drinking water (25mg/mL). All surgeries were performed by our team of veterinarians Dr. med. vet. Agnes Ellinghaus and Dr. med. vet. Katja Reiter as well as my mentor PD Dr. rer. nat. Katharina Schmidt-Bleek.

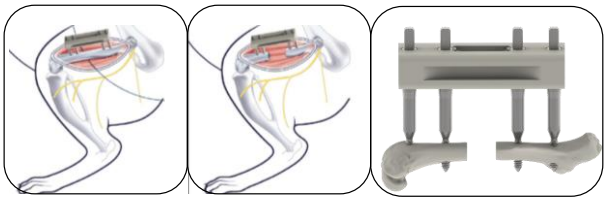

Figure 5: MouseExFix – mounting of fixator, osteotomy and fixation device used
The MouseExFix external fixator is shown on a mouse femur as stabilization for the induced 0.7 mm wide osteotomy. The osteotomy is stabilized by the four screws with 4.5 mm in diameter. The displayed figure is illustrated by RISystem. The MouseExFix is a standardized external fixator system developed by RISystem, Davos, Switzerland

2.1.3. Experimental conditions tested in the mouse femoral osteotomy model

In this research the following experimental conditions were tested to obtain an insight into the fracture healing process. For this purpose, the adipogenic differentiation in bone as well as inflammatory parameters affecting the healing outcome were modified in distinct experimental setups. In each condition a final number of six mice was analyzed, considering the exclusion of mice, whose bones were fixated in a suboptimal manner or whose bone ends were misaligned during the osteotomy. In each condition, the induced osteotomy was compared to a control bone. In this case the contralateral bone without osteotomy was harvested from the same individual mouse. The different experimental conditions have been summarized in the table below **(Table 1)**.

Table 1: Summary of the experimental conditions, treatments and analysis in the mouse osteotomy model

Four conditions are included in the experimental mouse femoral osteotomy model: environmental exposed control condition, treatment with the PPARG agonist rosiglitazone, treatment with the PPARG antagonist BADGE and the neutralization of TNFa and IFNg. All groups are analyzed for their bone/tissue pattern using histology, their bone structure using microCT, their immune cell/stromal cell composition measured by flow cytometry and metabolic groups are analyzed for their fatty acid composition. The exposed control group serves as control group for the naturally developing immune system. The rosiglitazone group is marked by the rosiglitazone diet and the induction of adipogenic stromal cells in bone. The BADGE group marks the antagonistic features to the rosiglitazone treatment by injection of the PPARG antagonist BADGE. The neutralizing antibodies against TNFa and IFNg are injected serving as reducers of pro-inflammatory immune responses during bone healing

d0 - surgery	treatment	d21 – experimental analysis
environmental exposed condition	-	histology|microCT|flow cytometry| fatty acid screening
rosiglitazone condition	rosiglitazone diet From d-3 to d21	histology|microCT|flow cytometry| fatty acid screening
BADGE condition	intraperitoneal BADGE injection from d3 to d14	histology|microCT|flow cytometry
anti-TNFa/anti-IFNg condition	Intraperitoneal antibody injection d-2|d1|d4|d7|d10	histology|microCT|flow cytometry

2.1.3.1. **Environmental exposed condition**

It is important to mention that mice of all conditions were kept in an environmental pathogen exposed housing and not in a sterile specific-pathogen free (SPF) housing, allowing the impact of a healthy adaptive immune system to be observed in the research. The environmental exposed housing started four weeks pre-surgery and was confirmed to induce a higher immune potential. Due to the environmental impact on the mice, a higher variability in the results was taken into account. Control mice were environmentally exposed for four weeks pre-surgery until 21 days post-surgery without the influence of an additional treatment. Moreover, control mice received a standard diet without γ-radiation (V1534 – ssniff).

2.1.3.2. **Rosiglitazone condition**

In the rosiglitazone condition, mice were fed a standard diet with 12mg/kg rosiglitazone (V1534 – ssniff with rosiglitazone maleate (item no. 11884 - Caymen chemical)) for a period of 24 days, starting 3 days prior surgery until 21 day post-surgery [267][268]. Rosiglitazone, a well-known anti-diabetic drug and peroxisome proliferator-activated receptor γ(PPARG) agonist was used for the activation of the main transcription factor PPARG, driving adipogenic differentiation [55][56]. The treatment with rosiglitazone was implemented to induce adipogenic differentiation within the bone, with an additional side effect of driving the immune compartment towards an anti-inflammatory milieu. The rosiglitazone diet was renewed every 2-3 days insuring the stability of the drug included in the diet. In addition, the diet pellets were weighed after each renewal to ensure the daily drug consumption during the experimental treatment.

2.1.3.3. **BADGE condition**

Bisphenol a diglycidyl ether (BADGE), known as a synthetic PPARG antagonist was used for the inhibition of PPARG driven adipogenic differentiation, steering diminishment of adipocytes in bone [269]. Mice treated with BADGE during the course of the experiment received a daily intraperitoneal (i.p.) injection of 30mg/kg BADGE diluted in 100uL phosphate-buffered saline (PBS) starting from 3 days post-surgery until day 14 [270]. For that purpose, the solid form of BADGE (D3415-250G – Sigma Aldrich) was solubilized in dimethylsulfoxid (DMSO), generating a maximal concentration of 10% DMSO in the final injection cocktail. Mice were treated with BADGE for a total of 11 days during the course of the experiment.

2.1.3.4. **Anti-TNFa/anti-IFNg condition**

The blockage of soluble tumor necrosis factor alpha (TNFa) and interferon gamma (IFNg) with neutralizing antibodies was performed to reduce the detrimental pro-inflammatory reaction driven by both cytokines during bone healing. Mice treated with neutralizing antibodies against TNFa and IFNg (BE0058-25MG, BE0312-25MG – InVivoMab) received a combined i.p. injection of 300ug of each antibody diluted to a final volume of 200uL sodium chloride (NaCl)

per injection [96]. The antibody treatment was implemented on five specific days during the course of the experiment starting 2 days prior surgery, followed by injections on day 1 post-surgery, day 4 post-surgery, day 7 post-surgery and day 10 post-surgery **(Table 1)**.

2.1.4. Termination and sample collection

Mice were terminated on day 21 post osteotomy. For that, mice received i.p. injections with ketamine (60 mg/kg/body weight) and medetomidine (0.3 mg/kg/body weight) and were kept under deep anesthesia while termination. The mice were terminated by intracardiac blood sampling and further hyperextension of the neck. All terminations were performed by Dr. med. vet. Katja Reiter, Dr. Christian Bucher and PD Dr. rer. nat. Katharina Schmidt-Bleek. Day 21 represents the analysis time point comprising the progression of all important healing phases but where bone healing was not fully concluded. Femoral bones including the osteotomized and the contralateral control bone as well as the tibial bones, spleen and different adipose tissues were harvested from the mice. Adipose tissues such as brown adipose tissue (BAT) specifically cervical BAT, white adipose tissue (WAT) subcutaneously aligned next to the femoral bones and subcutaneous abdominal WAT were extracted. Additionally, blood samples were collected to implement plasma extractions.

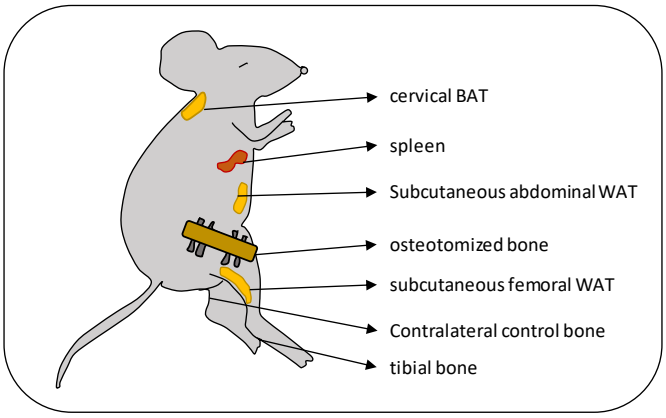

Figure 6: Summary of the tissues harvested from each experimental condition in the osteotomy model
The following tissues have been harvested for each experimental condition, cervical brown adipose tissue (BAT), spleen for immune cell analysis, subcutaneous abdominal white adipose tissue (WAT), osteotomized bone for bone structure analysis and stromal cell composition, subcutaneous femoral white adipose tissue (WAT), contralateral control bone for stromal cell analysis and the tibial bone (illustration adapted from [271])

Two experimental sample groups were collected separately. The first sample group of osteotomized/contralateral bones anticipated for histological analysis and micro computed tomography (microCT) were stored in 4% paraformaldehyde (PFA) for 24h before transferring bone samples to PBS for the structural analysis using microCT. Afterwards, bone samples were decalcified for 14 days and dehydrated before being embedded in paraffin for histological stainings.

The second experimental sample group of osteotomized/contralateral bones as well as spleen samples anticipated for flow cytometric analysis were stored in PBS before undergoing further cell isolation and staining procedure. The remaining samples such as adipose tissues, femoral bones, tibiae as well as extracted plasma samples were stored at -80°C for later analysis of fatty acids and phospholipids.

2.2. Ex vivo experiments using mouse samples

All chemicals and consumables used in the following ex vivo experiments are summarized within the appendix chapters **A.1. Materials and methods**.

2.2.1. Histological stainings determining bone and tissue composition

Paraffin embedded osteotomized as well as contralateral control bones were cut into five micrometer thick sections with a rotation microtome. Afterwards, the sections were histologically stained with hematoxylin and eosin (HE) to visualize the fracture healing progress as well as the accumulation of adipose tissue in distinct locations within the bone. The following protocol was implemented for the HE staining (**Table 2**). Important to mention is that the HE solution consisted of papanicolaous solution 1a Harris hematoxylin (1.09253; Merck) and eosin (2C140; Chroma – Waldeck), which was pre-diluted in a 1:10 ratio with distilled water and combined with glacial acetic acid, diluted in a 1:50 ratio in the final working solution. The HE solution had to be filtered to eliminate the metallic deposition before each staining.

Table 2: Protocol elucidating the Hematoxylin/Eosin staining (HE staining)
The following protocol has been used to stain bone slices with HE (protocols provided by Sabine Stumpp, Marzena Princ, Gabriela Korus). This staining visualizes the composition of bone and tissue and especially the accumulation of adipocytes within the bone marrow. For that purpose, samples are deparaffinized and transferred through ethanol solutions. Further, samples are transferred to distilled water before hematoxylin staining. After that, differentiation of the samples with HCL-alcohol and watering with tap water is implemented. In the following, the samples are stained with eosin and go through differently concentrated ethanol before being embedded with vitroclud

Hematoxylin/Eosin staining

- Deparaffinize the samples with xylol _____2x 10min
- Transfer the samples through descending ethanol solutions_____2min each [100%, 96%, 80%, 70% ethanol]
- Transfer the samples to distilled water [aqua dest.]_____2min
- Transfer the samples to hematoxylin [Harris] solution_____7min
- Transfer the samples to distilled water [aqua dest.]_____2x rinse
- Differentiate the samples with HCL-alcohol [0,25%]_____differentiate
- Transfer the samples tap water_____10min watering
- Transfer the samples to eosin solution [0,2%]_____2min
- Transfer the samples to 96% ethanol_____differentiate
- Transfer the samples to 96% ethanol_____rinse
- Transfer the samples to 100% ethanol_____2x 2min
- Transfer the samples to xylol_____2x 2min
- Cover the samples with vitroclud

Using the HE staining, nuclei and acidic mucosa were stained in blue and cytoplasm was stained in rose/red. Adipose tissue accumulation was determined by the remarkable white, empty vacuoles within bone. Adipose tissue vacuoles were analyzed, localized and counted by the implementation of a macro script, specifically generated for the purpose of automatic calculation of adipose tissue vacuoles (provided by Mario Thiele) using the program ImageJ (Fiji; version v1.52t).

2.2.2. Micro computed tomography (microCT) determining skeletal parameters

To analyze skeletal parameters, 3D x-ray microCT was implemented with the bruker skyscan 1172 high-resolution microCT (BRUKER, Kontich, Belgium). For that purpose, osteotomized bones were prepared in PBS with surrounding plastic tubes for mechanical stabilization of each bone, before removing the external fixator and the attached pins with a screwdriver. Then, the bone samples were transferred to a custom made sample revolver. Prior to each measurement, a flat field correction was performed to account for deviations in the scanner. The following analysis characteristics were used to perform the measurements (**Table 3**).

Table 3: Analysis characteristics for the performance of all micro computed tomographies (microCT)
Important parameters for the micro computed tomography describing the skeletal features of bone in each experimental setup are shown in the table. The skyscan 1172 has been used to scan the bones with a source voltage of 70kV, camera binning of 2x2, image pixel size of 8.01um and an aluminum filter of 0.5mm (parameters established by Dr. Christian Bucher)

[system]
Scanner=Skyscan1172
Instrument S/N=10K01158
Hardware version=G
Software=Version 1. 5 (build 27)
[acquisition]
Configuration: 70kV_8um_2x2_AlFilt_840ms
Source Voltage (kV)= 70
Camera binning=2x2
Image Rotation=-0.0400
Image Pixel Size (um)= 8.01
Filter=Al 0.5 mm
Image Format=TIFF
Exposure (ms)= 840
Rotation Step (deg)=0.200

In addition, bone mineral density (BMD) calibration rod pairs composed of epoxy resin with embedded fine calcium hydroxyapatite (CaHA) powder at concentrations of 0.25 and 0.75 $g.cm^{-3}$ and a diameter of 2mm were included as recommended calibration controls for mouse bone samples. Reconstruction and analysis of the bone samples was done using the skyscan NRecon software (version 1.7.0.3) and the CTAn analyzer (version 1.18.8.0). Further applications such as Gaussian smoothing with smoothing kernel=2, ring artifact correction =10, misalignment compensation, reconstruction angular range with 199.4 deg and beam hardening correction of 25% were implemented. The determined volume of interest (VOI) comprised a

range of 175 slices including the osteotomy gap in its center. Furthermore, a gray value threshold of 410 mg hydroxyapatite per cm^3 was defined to distinguish between non-mineralized and mineralized bone. This threshold was calculated according to the manufacturers protocol described in “Bone mineral density (BMD) and tissue mineral density (TMD) calibration and measurement by micro-CT using Bruker-MicroCT” relying on both calibration rod pairs and their attenuation coefficient (AC) [272]. For that, the AC of both, the minimal and the maximal CaHA concentration phantom rod, were measured and recorded by calculating the mean (total) density value of all voxels within the phantom rod VOI using attenuation as unit. Both values: Min value for BMD of 0.25 $g.cm^{-3}$ and AC= 0.0173494 as well as the maximal value for BMD of 0.75 $g.cm^{-3}$ and AC= 0.0363677 were implemented within the density range calibration. This resulted in the adjusted formula for BMD analysis.

2.2.3. Flow cytometry analysis determining immune composition

2.2.3.1. Immune cell isolation from spleen

Immune cells were isolated from the mouse spleen to characterize critical $CD4^+$ T helper subset changes between detrimental, pro-inflammatory TH1/TH17 phenotypes and beneficial, anti-inflammatory TH2 phenotypes during bone healing. The mouse spleen was processed under a constant cold temperature of 4°C, while retaining the samples on ice. The isolation started by transferring the spleen to a PBS filled 60mm tissue culture dish and by cutting the organ in smaller pieces using a scalpel. The small organ pieces were then filtered through a 40 µm mesh using PBS and by additionally pressing the spleen derived cells through the mesh using a syringe plunger. The isolated cells were centrifuged on 4°C, for seven minutes at 400g and the supernatant was removed. Further, cells were resuspended in 1X RBC lysis buffer (420301 – BioLegend), pre-diluted 1:10 in distilled water (1088811 – Ampuwa, Fresenius Kabi) and incubated for five minutes on ice. The cell suspension was filtered over a 40 µm mesh to remove free DNA parts and was centrifuged on 4°C, for seven minutes at 400g. The supernatant was removed and the final cell suspension was counted using the automated cell counter countess II FL (A25750 – Invitrogen/Invitrogen).

2.2.3.2. Extracellular and intra-nuclear staining procedure

To determine the overall composition as well as subset changes in the $CD4^+$ T helper cell compartment in the distinct mouse conditions, a 13-color flow cytometry panel was implemented, analyzing spleen resident immune cells of mice with the use of extracellular and intra-nuclear markers. The following table comprises surface CD markers and transcription factors determining the $CD4^+$ T helper cell phenotype via flow cytometry (**Table 4**).

Table 4: Extracellular and intra-nuclear markers defining the CD4$^+$ T helper subset composition
The following extracellular and intra-nuclear markers have been used to determine different CD4+ T helper subsets in the spleen of mice. Antibodies are summarized with their specific clone, the chosen fluorochrome and the laser/filter implemented while measuring (panel established by Dr. Christian Bucher)

Antibody	Laser/filter	Fluorochrome	Clone
Live/Dead	NUV450/50	UV	
CD45	V525/50	V500	30-F11
CD3e	B695/40	BB700	145-2C11
CD4	R780/60	APC-Fire750	GK1.5
CD8a	V780/60	BV785	53-6.7
TCRgd	YG780/60	BV421	GL3
CD62L	R710/50	APC-R700	MEL-14
CD44	V450/50	PE-Cy7	IM7
CD25	YG610/20	PE/Dazzle594	PC61
FoxP3	B525/50	AF488	MF23
Tbet	V660/20	BV650	O4-46
GATA3	R670/14	AF647	L50-823
RORgT	YG585/15	PE	Q31-378

For the staining of intra-nuclear markers defining CD4$^+$ T helper cell subsets such as TH1 (TBET), TH2 (GATA3), Treg (FoxP3) and Th17 (RORgT), the isolated cells were diluted to 1,5x10^6 per 100 µL PBS. First, 3 µL of the live/dead staining antibody (L23105 – Invitrogen) in a 1:10 pre-dilution with PBS was incubated for 30 minutes on ice. After that, the cell suspension was centrifuged with PBS+0,5%BSA+0,1%NaN3 on 4°C, seven minutes at 400g and the supernatant was discarded. To block unspecific binding of antibodies, 1 µL of FcX-blocking cocktail (101319 – BioLegend) was added to the cell pellet for initial 10 minutes on 4°C before the addition of extracellular staining antibodies for another 20 minutes. After the extracellular staining, the cell suspension was centrifuged as described above and 1mL of 1X TrueNuclearFix solution in a 1:4 pre-dilution with Fix/Perm dilution buffer (True-Nuclear Transcription Factor Buffer Set, 424401 – BioLegend) was added to each pellet and incubated for 60 minutes on room temperature. After fixation, the cell suspension was centrifuged two times in a row as described above using 1X permeabilization buffer pre-diluted 1:10 with ampuwa and the supernatant was discarded. The last step included the staining for intra-nuclear transcription factors for 30 minutes on room temperature. After that, the cell suspension was centrifuged with 1X permeabilization buffer on room temperature for seven minutes and at 400g, followed by a second centrifugation step with PBS+0,5%BSA+0,1%NaN3 on 4°C, for seven minutes at 400g. Before acquisition, 100 µL

PBS was added to the cell suspension. Finally, the stained cells were measured on the LSR Fortessa system (BD Bioscience).

2.2.3.3. Flow cytometric analysis and gating strategy

The investigation of CD4⁺ T helper subsets in each experimental condition was done by flow cytometric analysis using the software FlowJo (version 10.7.1 – BD Biosciences). The following gating strategy characterizing the different subsets of CD4⁺ TH1, Treg, Th2 and T17 cells in the mouse spleen was implemented, the gates were adjusted and corrected with fluorescence minus one (FMO) stainings for each antibody while analysis.

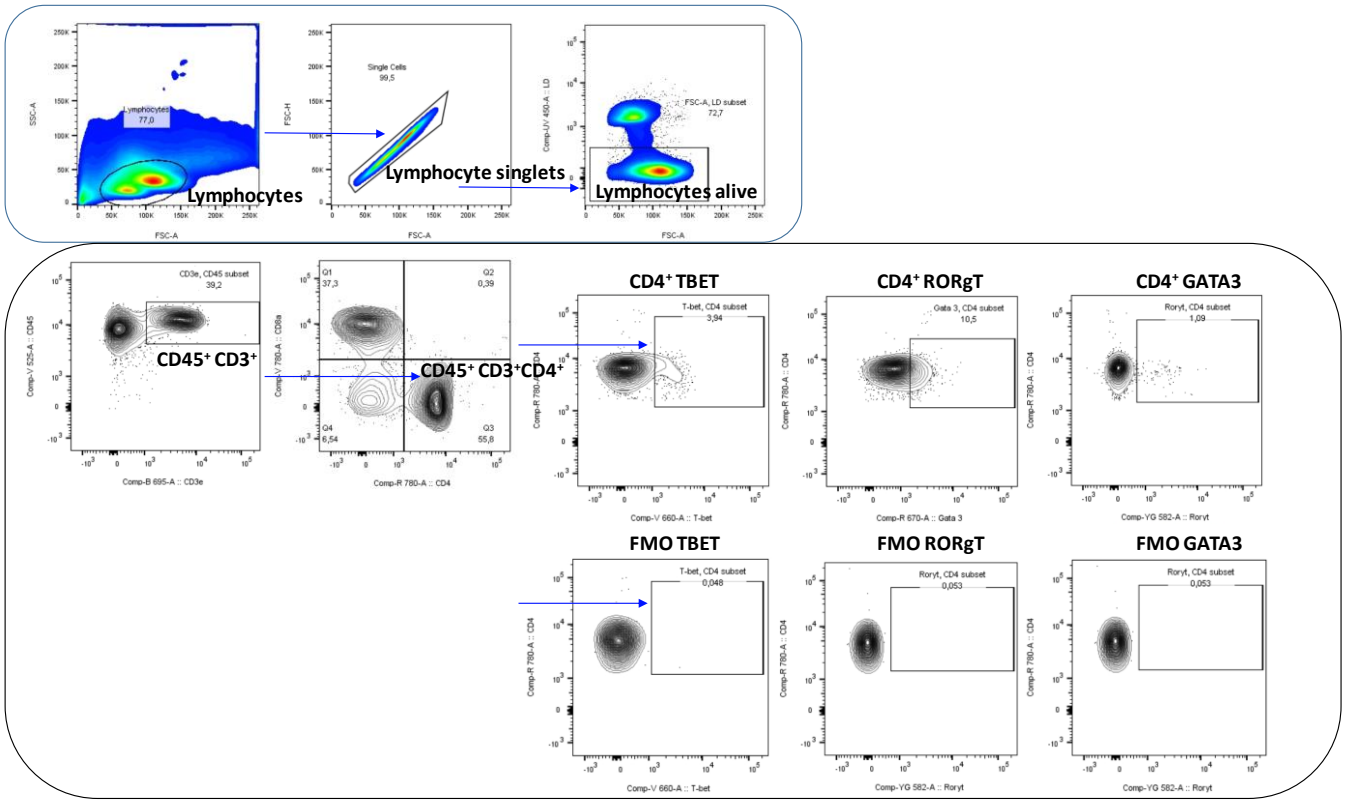

Figure 7: Gating strategy for analyzing CD4⁺ TH1, TH2 and TH17 subsets
The following gating strategy has been implemented focusing on the lymphocyte subset, further gating the singlets and alive lymphocytes prior to specifying the CD3⁺ T cell subset. Within the CD3⁺ T cells, the CD4⁺ T helper cells are specified and the distinct subsets of CD4⁺ T cells namely TH1 (gating on CD4⁺ TBET⁺ TH cells), TH2 (gating on CD4⁺ GATA3⁺ TH cells) and TH17 (gating on CD4⁺ RORgT⁺ TH cells) are quantified. The subset gates of CD4⁺ T helper cells are determined by the usage of fluorescence minus one (FMOs) to distinguish the negative and positive populations

2.2.4. Flow cytometry analysis determining the stromal cell composition

2.2.4.1. Mesenchymal stromal cell isolation from bone

Mesenchymal stromal cells were isolated from the mouse bone to characterize treatment driven effects on the adipogenic-, osteo-chondrogenic- and multipotent lineage compartment. Bones were processed under a constant cold temperature of 4°C as described for the immune cell isolation from spleen. First, the bones were transferred on a 60mm tissue culture dish and

both ends were cut using bone scissors. Following that, the bones were cut in half to harvest as much bone marrow resident cells as possible. To collect the bone stromal cell suspension, the bone marrow was flushed out with a needle until the bone changed its color from red (bone filled with marrow) to white (bone without marrow). The flushed bone marrow stromal cells were filtered using a 40 µm mesh and rinsed using cold PBS. The cell suspension was centrifuged on 4°C, for seven minutes at 400g. The supernatant was discarded and the final cell suspension was counted using the automated cell counter countess II FL (A25750 – Invitrogen/Invitrogen).

2.2.4.2. **Extracellular staining procedure**

To phenotypically characterize the changes in the mesenchymal stromal cell compartment induced by the different experimental conditions, an 11-color flow cytometry panel was established. The panel comprised lineage determining surface markers summarized in the following table (**Table 5**).

Table 5: Summary of the extracellular markers defining the mesenchymal stromal cell subsets in bone marrow

The following extracellular markers have been used to define distinct mesenchymal stromal cell subsets comprising the adipogenic-, the osteo-chondrogenic- and the multipotent lineage. The pregating includes the lineage negative subset marked by the loss of CD45 and CD31 expression. The bone marrow stromal lineage is gated by using the marker Sca1 and is varying expression defines the two main subsets. The marker CD140a defines the osteo-chondrogenic subset and the marker CD24 is used for the definition of the adipogenic stromal lineage

Antibody	Laser/filter	Fluorochrome	Clone
Live/Dead	NUV450/50	UV	
CD45	V525/40	BV510	30-F11
CD34	V450/50	BV421	RAM34
CD11b	R710/50	AF700	M1/70
CD31	YG610/20	PE/Dazzle594	390
CD29	YG780/60	PeCy7	HMB1-1
CD44	R780/60	APC-Cy7	IM7
Sca-1	V710/50	BV711	D7
CD51	YG585/15	PE	RMV-7
CD140a	R660/20	APC	APA5
CD24	B525/50	AF488	M1/69

For the extracellular staining procedure, the collected stromal cell suspension was diluted to $1x10^6$ in 100 µL PBS. Following that, the Live/dead staining agent was pre-diluted in PBS and then added to the cell suspension for an incubation of 30 minutes on ice (L23105 – Invitrogen). After that, cells were centrifuged with PBS+0,5%BSA+0,1%NaN3 on 4°C, seven minutes at 400g and the supernatant was discarded. Further, the cells were incubated with 1 µL of FcX-

blocking cocktail (101319 – BioLegend) for 10 minutes prior to the extracellular surface marker staining involving 20 minutes of staining on ice. After the staining, cells were centrifuged with PBS+0,5%BSA+0,1%NaN3 on 4°C, seven minutes at 400g and the supernatant was discarded. To ensure fixation of the stained fluorochromes, cells were incubated for further 30 minutes with 500 µL of FluoroFix staining buffer (422101 – BioLegend). Cells were centrifuged with PBS+0,5%BSA+0,1%NaN3 on 4°C, seven minutes at 400g and the supernatant was discarded. Before acquisition, 100 µL PBS was added to the cell suspension. Finally, the stained cells were measured on the LSR Fortessa system (BD Bioscience).

2.2.4.3. Flow cytometric analysis and gating strategy

Treatment derived effects on the mesenchymal stromal lineage differentiation were investigated by flow cytometric analysis in the same manner as described for the characterization of $CD4^+$ T helper subset of the spleen. The following gating strategy was used for the definition of the adipogenic-, osteogenic- and multipotent mesenchymal stromal lineage in bone marrow (**Figure 8**).

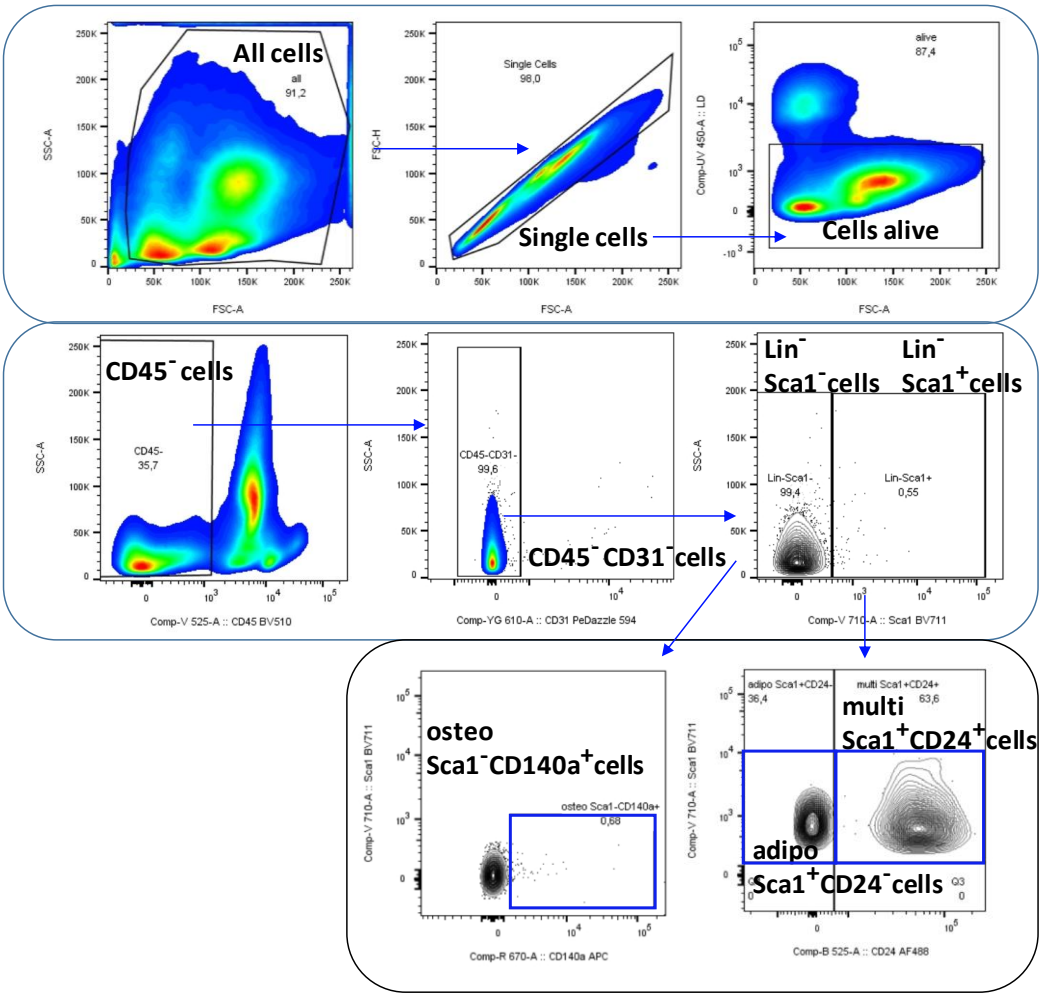

Figure 8: Illustration of the gating strategy for the distinct mesenchymal stromal cell subset in bone marrow

First, all cells are pre-gated for single, alive cells before using the lineage negative marked by the loss of CD45 and CD31 as initial step to define mesenchymal stromal cells. Further, all lineage negative cells are distinguished by Sca1 expression in Sca1- marking the osteo-chondrogenic lineage and Sca1+ marking the adipogenic lineage precursors. Further the osteo-chondrogenic subset is defined by the expression of CD140a and the adipogenic subset is defined by the loss of expression of CD24. The multipotent subset is defined by the gain of CD24 expression [43]

2.2.5. Fatty acid screening determining phospholipid composition

For the analysis of fatty acids and phospholipids the contralateral, femoral bones of mice were stored at a constant temperature of -80°C before being processed on dry ice for further analysis. The femoral bones were cut in three different parts representing three different locations of adipose tissue regions in mouse bone (**Figure 9**). Afterwards, all bone parts were crushed to powder using a mortar and dry ice. The samples were stored in 250uL PBS for further analysis and each sample was measured using a protein normalization control. The analysis of all samples was done at the German Institute of Human Nutrition (DifE – Potsdam, Rehberge).

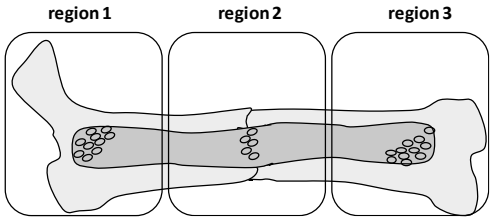

Figure 9: Three pre-defined regions analyzed for bone marrow adipose tissue (BMAT)
The two main BMAT regions are shown as region 1 describing the proximal regulated BMAT and as region 3 marking the distal constitutive BMAT, both harboring differences in fatty acid composition. A third region is proposed as region 2 distally from the locality where the fracture is set during the experimental bone regeneration in mice.

2.2.6. Statistical analysis

All data generated by the described methods such as HE stainings quantifying adipose tissue accumulation, microCT analysis characterizing bone parameters, $CD4^+$ T helper cell subset characterization and fatty acid analysis defining phospholipid changes, were analyzed and visualized using the software Prism (version 8, GraphPad). Statistical testing of *in vivo* and *ex vivo* generated sample means was done with the unpaired, parametric t-test with Welch's correction (not assuming equal standard deviations (SDs)). This test was used assuming a Gaussian distribution with no assumption of both populations having the same SD, which was suitable for the small number of animals tested in each condition. Significance was assigned for p values below 0.05. Importantly, the 3R principle of replacement, reduction and refinement has been followed throughout all *in vivo* experiments.

2.3. In vitro experiments using human bone marrow derived stromal cells (hBMSCs)

To mirror the performed in vivo experiments in the human setting, in vitro experiments using human bone marrow derived stromal cells were implemented. Since the most important effects on *in vivo* bone healing were shown by the treatment with the PPARG agonist rosiglitazone, the in vitro experiments were implemented to highlight and specify the PPARG agonistic effects. For that purpose, hBMSCs were isolated from healthy clinical patients, with the exception of one diabetic patient (Charité Center for Orthopedics and Trauma Surgery – CC9), that all underwent trauma surgery. The isolated hBMSCs were kindly provided by the Core Unit Cell Harvesting (Cell biology group – Berlin Institute of Health, BIH) with former signed consent from the patient (ethical approvement EA 099/10). The characterization of the hBMSC phenotype and multi-lineage differentiation potential towards the adipogenic, osteogenic and chondrogenic lineage was done according to the International Society for Cellular Therapy [273][274][275]. All chemicals and consumables used in the following in vitro experiments are summarized within the appendix chapters **A.1. Materials and methods**.

2.3.1. Characteristics and expansion of patient derived hBMSC

A total of seven patient derived hBMSCs were analyzed for their potency to differentiate towards the osteogenic and adipogenic lineage under specific drug supplementation of rosiglitazone as PPARG agonist and insulin. Hereby, important metabolic effects during bone formation were studied. A summary of all patients and their characteristics can be taken from the following table (**Figure 10**). A mixed pool of patient-derived hBMSCs selected by age and gender was used for all experiments performed in my research. All patient-derived hBMSCs were anonymized using specific patient (Pat) codes.

Patient	Age (years)	Gender
Pat346	57	female
Pat660	65	female
Pat784	72	male
Pat326	48	female
Pat919	73	male
Pat1626	35	male
Pat347	52	male

Figure 10: Summary of patient specific characteristic of hBMSCs
Patient hBMSCs are described with specific characteristics including age, gender, and diagnostics. All characteristics can harbor an impact on the following experiments described within this thesis and can influence the extent of patient specific effects. Patients have been selected based on the osteogenic differentiation capacity while choosing hBMSCs which harbor a poor osteogenic capacity. To include young as well as older patient derived hBMSCs, the age of patients ranged from 35 to 73 years. Mostly healthy patients have been chosen for the in vitro experiments with one exception namely Pat660 which suffered from diabetes mellitus and had been medicated with the anti-diabetic drug metformin. The goal included the identification of the effect of the PPARG agonist rosiglitazone on healthy patients and as side information describing the effects in one patient already being medicated with an insulin sensitizer metformin.

Before undergoing the different experimental purposes, $0.5x10^6$ hBMSCs from passage 1-2 were thawed in a 37°C water bath, seeded in a 300 cm^2 tissue culture flask (T300, 90301 – TPP) and media was changed after 24h post seeding to remove the remaining dimethylsulfoxid (DMSO) implemented as cryoprotectant. Cells were grown in low-glucose Dulbecco's Modified Eagle Media (DMEM) media supplemented with 10% fetal calf serum (FCS) and 1% penicillin/streptomycin (P/S) in a 37°C/5%CO_2 incubator (BINDER). The media of cells was changed every three to four days and propagation of cells was done after 7-10 days of expansion. For this purpose, cells cultured at 70-80% confluence were washed with 60mL of PBS to remove the remaining culture media and 4 mL pre-warmed trypsin was added for 2 minutes at 37°C detaching the cells from the flask. After the incubation, cells were shaken and the detachment was checked under the microscope. The trypsination was stopped by adding 16 mL of pre-warmed DMEM with 10%FCS and 1%P/S. Cells were counted using the CasyTT cell counter (Schärfe System) and re-seeded at a concentration of $0.7x10^6$ using a T300 flask. Following that, cells were cultured at 70-80% confluence for up to another 10 days until the suitable cell number was achieved. HBMSCs from passage 3-4 were used for all different experimental purposes.

2.3.2. Osteogenic differentiation of hBMSCs with/without drug supplementation

For the osteogenic differentiation, hBMSCs were re-seeded in DMEM with 10%FCS and 1%P/S at a concentration of $4.8x10^3$ on a 48 well plate format. After 24h, the induction of cells with osteogenic media was implemented. In the following table, the standard composition of osteogenic media is shown (**Table 6**).

Table 6: Components of the osteogenic differentiation cocktail
The osteogenic differentiation media consists of low glucose DMEM supplemented with FCS, glutamine, penicillin and streptomycin and the following osteogenic inducers dexamethasone steering the transcription of Runx2, l-ascorbic acid inducing collagen type-1 synthesis and b-glycerol phosphate producing hydroxyapatite minerals

Supplement	Volume	Final concentration
Dexamethasone (pre-diluted 1:100 - 10µM)	10µL	0,1µM
L-ascorbic acid (50mM)	1µL	50µM
B-glycerol phosphate (200mM)	50µL	10mM
Penicillin/Streptomycin	10µL	1%
Glutamax	10µL	1%
FCS	100µL	10%
Low glucose DMEM	819µL	

The depicted supplements are required to induce osteogenic differentiation. To that purpose, L-ascorbic acid was added to induce collagen type-1 synthesis, β-glycerol phosphate to produce hydroxyapatite minerals and dexamethasone to steer the transcription of Runx2. The plate layout for the osteogenic differentiation comprised all outer wells of the 48 well plate filled with PBS to reduce edge effects during the experimental process. Each plate contained control wells with cells cultured in DMEM with 10%FCS and 1%P/S as expansion control. Further, all conditions were conducted in triplicates to include the impact of well to well differences. To investigate the effect of PPARG agonist rosiglitazone and insulin on the osteogenic differentiation, the following concentrations of rosiglitazone and insulin were supplemented to the standard osteogenic media (**Table 7**). Lyophilized rosiglitazone was pre-diluted and aliquoted in DMSO as 1mM stock solution. Further 1:1000 dilutions of the rosiglitazone/DMSO stock solution was achieved using osteogenic media (OM) resulting in the highest concentration of rosiglitazone of 1 µM. Since DMSO can influence the differentiation process of hBMSCs, an additional solvent control was included in all experiments. The cytotoxicity effect and proliferation effect of rosiglitazone was ruled out in a separate experiment using

DMEM with 10%FCS and 1%P/S as expansion media, which is why an expansion control with rosiglitazone was not included in the differentiation experiments (section **2.3.5**).

Table 7: Summary of drug and solvent control concentrations implemented during in vitro assays
The effects of PPARG agonist rosiglitazone have been induced using a high concentration of 1 µM rosiglitazone and a low concentration of rosiglitazone while the solvent control is implemented in the highest concentration used in the assay. Insulin is supplemented in a concentration of 2mM in consistence with the insulin concentration used in the adipogenic induction cocktail and mimicking a high metabolic state of the hBMSCs

Supplement	Solvent	Concentration/mL
Rosiglitazone	DMSO	1µM
Rosiglitazone	DMSO	10nM
Insulin	HCL	2µM
Solvent control	DMSO	1µM

The following figure shows a typical plate layout used for the osteogenic differentiation with/without rosiglitazone and insulin supplementation (**Figure 11**).

OM	OM	OM	DMEM	DMEM	DMEM
OM 1µM	OM 1µM	OM 1µM	OM 10nM	OM 10nM	OM 10nM
OM DMSO	OM DMSO	OM DMSO	OM insulin+10nM	OM insulin+10nM	OM insulin+10nM
OM Insulin	OM Insulin	OM Insulin	OM insulin+1µM	OM insulin+1µM	OM insulin+1µM

Figure 11: Illustration of the osteogenic differentiation setup
The following conditions have been tested in triplicates during the osteogenic differentiation assay. OM – osteogenic differentiation control, OM 1 µM – osteogenic differentiation with 1 µM PPARG agonist rosiglitazone, OM DMSO – osteogenic differentiation with 1 µM solvent control, OM insulin – osteogenic differentiation with 2 µM insulin supplementation, DMEM – expansion control, OM 10nM – osteogenic differentiation with 10nM PPARG agonist rosiglitazone, OM insulin+10nM – osteogenic differentiation with combined insulin and 10nM PPARG agonist rosiglitazone supplementation, OM insulin+1 µM – osteogenic differentiation with combined insulin and 1 µM PPARG agonist rosiglitazone treatment

The osteogenic differentiation experiment lasted for 21 days and included early osteogenic time points measuring alkaline phosphatase (ALP) activity on day 0, day 4 and day 7 as well as late osteogenic time points measuring mineralization *via* alizarin red (AR) stainings on day 10, day 14, day 18 and day 21 (**Figure 12**). In addition, the supernatant of all conditions was harvested on each of those days using one and the same plate throughout the whole experiment. The supernatant was stored at -80°C for the follow-up assay of adipokine profiling described below. In combination with early and late osteogenic target assays, the metabolic activity of cells was measured on each day using PrestoBlue cell viability reagent (A13261 –

Invitrogen). For that purpose, the reagent PrestoBlue was prediluted 1:10 in DMEM with 10%FCS and 1%P/S and cells were incubated with a volume of 200 µL PrestoBlue solution for 1h on 37°C. The change in color from blue to red depending on the metabolic activity was measured with an excitation/emission wavelength of 560/590 nm on a plate reader (Infinite 200 PRO – TECAN).

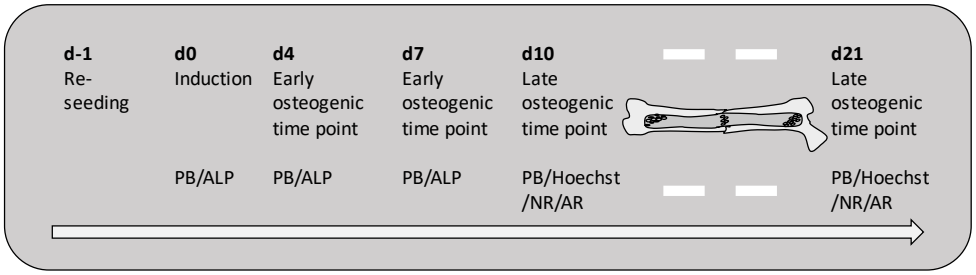

Figure 12: Illustration of the osteogenic differentiation time-points
The osteogenic differentiation assay is defined by distinct analysis time-points. The re-seeding of expanded hBMSCs is done on day -1 and after 24h of attachment the induction of osteogenic differentiation is implemented using the osteogenic induction cocktail. On this day, baseline values for PrestoBlue and ALP activity are measured. On day 4 and day 7 the early osteogenic time-points are determined by measuring PrestoBlue and ALP activity. From day 10 to day 21 specific late osteogenic time-points are identified and PrestoBlue, Hoechst (DNA staining), NileRed (NR) and AlizarinRed (AR) staining are done to quantify adipogenic co-differentiation and osteogenic mineralization. The late osteogenic time-points varied from patient to patient as a result of patient variability and differentiation potential

2.3.2.1. **Alkaline phosphatase activity**

In bone, alkaline phosphatase (ALP) is highly expressed and its activity is used as an early marker for osteogenic differentiation. To determine ALP activity, the dephosphorylation of the phosphatase substrate 4-nitrophenylphosphate (pNPP) was measured by photometry at optical density (OD) of λ=405nm. To that purpose, the following protocol was implemented (**Table 8**) and the ALP activity was calculated as followed (**Figure 13**).

$C = (E-E^0) / \varepsilon \times d$

E = adsorbance (OD)
E^0 = adsorbance blank (OD)
c = molar concentration (mol/L)
ε = molar absorbance coefficient (L x mol-1 x cm-1)
d = thickness of layer (cm)
d = 0.3294 cm for a 96 well plate filled with 100µL solution

Figure 13: Formula for the calculation of alkaline phosphatase activity (ALP)
The formula for the calculation of ALP activity consists of the following parameters: difference of adsorbance and adsorbance blank, the molar adsorbance coefficient □ and the thickness of layer of the 96 well plate with 100 µL solution

Table 8: Protocol for the ALP measurement
PrestoBlue and ALP has been measured on the same plate on each early osteogenic differentiation time-point. Prior to ALP, PrestoBlue is measured following a washing step before adding ALP buffer as washing agent.

Following that, ALP buffer and pNPP substrate is added in the same volume for 10 minutes of incubation on 37°C. The reaction is stopped by the addition of NaOH and measured with a plate reader

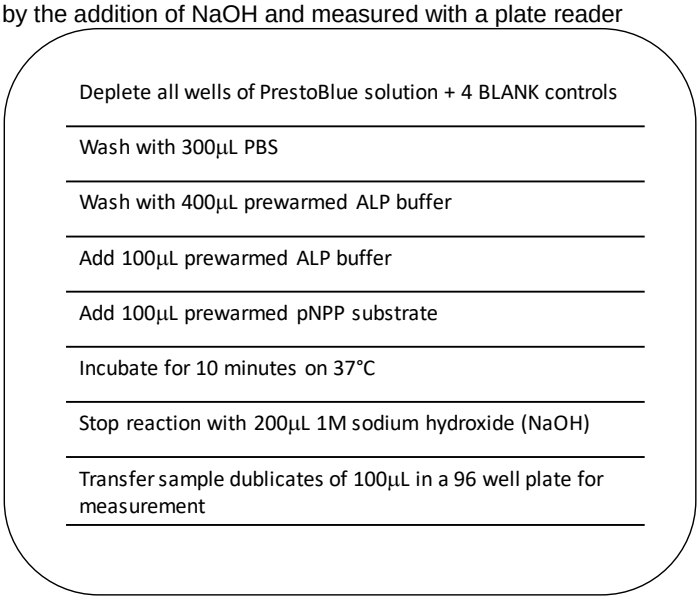

2.3.2.2. **Alizarin red staining (AR) with DNA quantification and lipid co-induction**

To determine the amount of calcium deposition of hBMSCs on late osteogenic time points, AR staining was implemented using the following protocol. In order to quantify the calcium deposition, Hoechst staining for DNA quantification was performed. To determine the co-induction of adipogenic cells and osteogenic cells during differentiation, the Hoechst DNA staining was combined with a NileRed staining (NR) for lipid droplet characterization (section **2.3.3**). Prior to staining, differentiated hBMSCs were fixed with 150 µL 4% PFA//PBS for 10 minutes in the dark and at room temperature (RT). Following that, cells were washed twice using 300 µL PBS and 150 µL of PBS without staining agents was added to implement the baseline measurement for the Hoechst/NR staining. To proceed with the DNA/lipid stainings, Hoechst and NR staining agents were diluted 1:1000 in PBS and hBMSCs were incubated with 150 µL of staining solution for 20 minutes, in the dark and at RT. The remaining staining solution was removed by washing twice using 300 µL PBS and Hoechst/NR was measured in 150 µL PBS solution. To prepare for the AR staining solution, hBMSCs were washed with 300 µL distilled water, overlaid with 150 µL 0.5% AR solution and incubated for 10 minutes at RT. The excessive staining was removed by washing three times with distilled water and the stained calcification of cells was dried and further photographed to visualize the matrix. For the quantification of matrix mineralization, the dried matrix was dissolved with 124 µL cetylpyridiniumchlorid per well for 30 to 60 minutes. 100 µL of the resulting purple solution was transferred to a 96-well plate before measuring calcification. The DNA quantification, lipid droplet accumulation and calcification of hBMSCs were finally measured on a plate reader. To that purpose, Hoechst and NR were measured with an excitation/emission wavelength of

352/421 nm and an excitation/emission wavelength of 460/535 nm respectively. Furthermore, the calcification was measured at an OD of λ=562nm (Infinite 200 PRO – TECAN).

2.3.3. Adipogenic differentiation of hBMSCs with/without drug supplementation

To compare the co-localized adipogenic cells during osteogenic differentiation with default differentiated adipogenic cells, standard adipogenic differentiation was performed for each set of patient derived hBMSCs. For the adipogenic differentiation, hBMSCs were re-seeded in DMEM with 10%FCS and 1%P/S using the same experimental conditions as for the osteogenic differentiation. Therefore, hBMSCs were seeded at a concentration of $4.8x10^3$ on a 48 well plate format. Following 24h of cell attachment, the induction of cells with adipogenic media was implemented. In the following table, the standard composition of adipogenic media is depicted (**Table 9**).

Table 9: Components of the adipogenic differentiation cocktail
The adipogenic differentiation is implemented in high glucose DMEM with FCS and Penicillin/Streptavidin supplemented with the following adipogenic inducers: Dexamethasone and indomethacin steering adipogenic gene induction such as Cebpa, Srebf1c and C/EBPb resulting in PPARG upregulation, IBMX inducing cAMP and PKA upregulation and insulin resulting in the upregulation of PPARG transcription

Supplement	Volume	Final concentration
Dexamethasone (1mM)	1µL	1µM
Insulin from bovine pancreas (335µM)	6µL	2µM
3-isobutyl-1-methylxanthine (IBMX) (500mM)	1µL	500µM
Indomethacin (50mM)	2µL	100µM
High glucose DMEM (L-glucose 4.500mg/L)	880µL	-
Filtration of adipogenic medium		
Subsequent addition of 10%FCS and 1%P/S	100µL 10µL	

It is important to mention, that the adipogenic media containing all supplements had to undergo sterile filtration since some of the supplements were prepared in a non-sterile manner. The supplement cocktail of dexamethasone, insulin, 3-isobutyl-methylxanthine (IBMX) and indomethacin combined with high-glucose Dulbecco's Modified Eagle media was used to steer adipogenic differentiation. Dexamethasone and indomethacin were added to steer adipogenic genes such as Cebpa and Srebf1c or C/EBPb with both additives driving PPARG upregulation. The addition of IBMX resulted in a combined upregulation of cAMP and PKA and insulin was

used to induce late stage adipocyte differentiation by the same effects on PPARG transcription as the above described supplements within the cocktail [276]. The adipogenic differentiation experiment lasted 14 days with one late adipogenic differentiation time point on day 14 selectively staining intracellular lipid droplets using NR staining. In the following a timeline of the adipogenic differentiation experiment is shown (**Figure 14**).

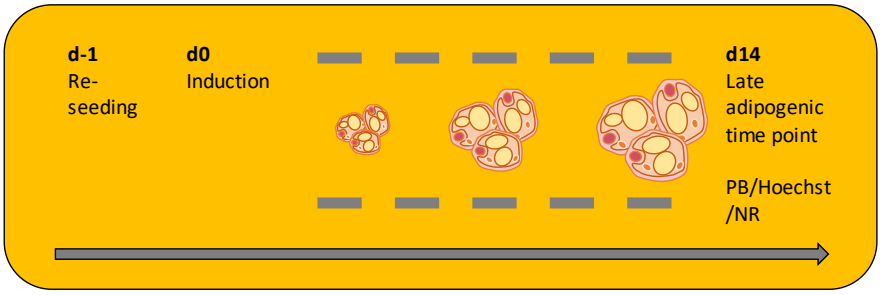

Figure 14: Illustration of adipogenic differentiation time-points
Adipogenic differentiation is implemented in the same time frame as the osteogenic differentiation starting with a re-seeding on day -1 and adipogenic induction by the adipogenic cocktail on day 0. Following that, the adipogenesis is controlled every other day until day 7 – day 10 when adipocytes start to form. The late adipogenic time-point on day 14 already comprises large amounts of adipocytes to be analyzed with PrestoBlue, Hoechst (DNA staining) and NileRed as adipocyte staining

The NR staining and Hoechst DNA quantification was implemented in the same manner as it was used during osteogenic differentiation for the staining of co-localized lipid droplets during mineralization. Prior to the DNA/lipid staining, the measurements of metabolic activity via PrestoBlue staining was performed. All three stainings were conducted as described above with the final read-out being the lipid accumulation (section **2.3.2**, **2.3.2.2**). The experimental setup and plate layout was implemented in the same manner as described above using adipogenic media as foundation implementing changes in the tested conditions. Hereby, the supplementation of two rosiglitazone concentrations as well as a solvent control was tested excluding the supplementation of additional insulin during adipogenic differentiation experiments. It is important to note, that the solvent control was particularly important during adipogenic differentiation, since DMSO had a stronger influence on adipogenic compared to the osteogenic cells.

2.3.4. Osteogenic differentiation of hBMSCs with adipocyte conditioned media

To analyze the paracrine features of adipogenic hBMSCs with and without drug supplementation, adipocyte conditioned media was generated from each set of patient derived hBMSCs.

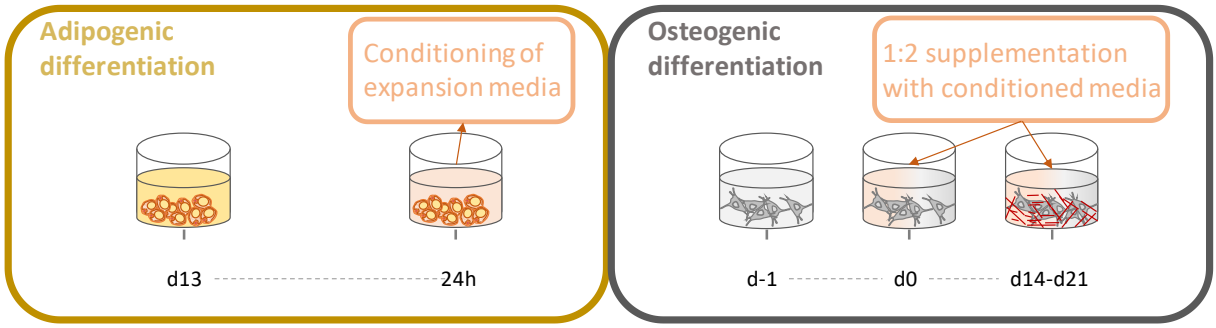

Figure 15: Illustration of the conditioning of adipogenic media and its re-use during osteogenic differentiation
To simulate the paracrine effects of adipocytes on the osteogenic differentiation process, adipogenic hBMSCs have been differentiated for 13 days prior to the conditioning of expansion media without adipogenic inducers gathering paracrine adipocyte factors for 24h. This conditioned media is further used starting from day 0 until day 14 – day 21 as a 1:2 dilution of conditioned media with 2x concentrated osteogenic inducers in standard osteogenic media. Conditioned media/osteogenic inducer cocktail was re-newed every 3 days.

For that purpose, hBMSCs were re-seeded at a concentration of $2x10^5$ on a 75 cm^2 tissue culture flask (T75, 90076 – TPP) and adipogenic differentiation was induced 24h post seeding. Adipocyte conditioned media (aCM) was gained from standard adipogenic differentiation with (aCM+1 ∝M) and without (w/o) 1 ∝M of rosiglitazone supplementation, equally concentrated solvent control (aCM+DMSO) and expansion control (EM). The adipogenic differentiation experiment lasted 14 days including a media change from adipogenic media to low-glucose DMEM with 10%FCS and 1%P/S on day 13. The adipogenic hBMSCs were cultured in low-glucose DMEM with 10%FCS and 1%P/S for the following 24h for the cells to release all paracrine factors excluding the impact of adipogenic differentiation supplements. The final 18mL of aCM were centrifuged for 5 minutes on RT and at 500g to remove remaining cell debris. The conditioned media was stored at -80°C for the follow-up osteogenic differentiation. To this aim, the aCM was implemented during standard osteogenic differentiation in a 1:2 dilution with osteogenic media containing twofold concentrated osteogenic supplements. The aCM/osteogenic media mix was changed on every early and late osteogenic time point including d0, d4, d7, d10, d14, d18 and d21. The experimental layout was implemented as followed (**Figure 16**).

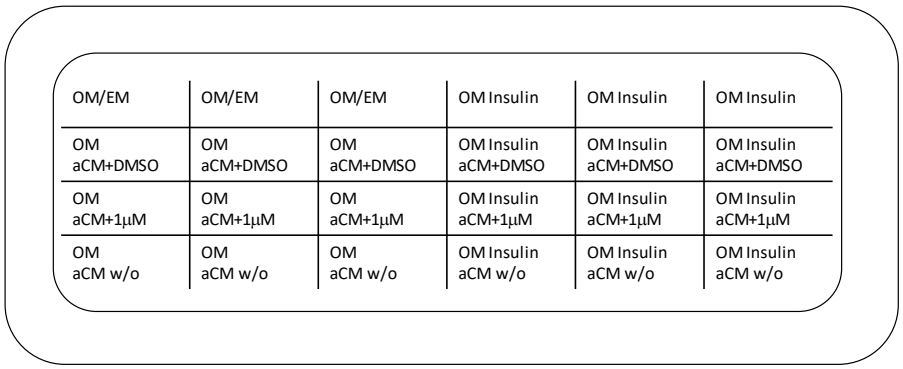

Figure 16: Illustration of the conditions during the osteogenic differentiation with adipocyte secreted factors
The following conditions have been tested as triplicates during osteogenic differentiation with adipocyte secreted factors: OM/EM – osteogenic media supplemented with conditioned media from expanded hBMSCs, OM/aCM+DMSO – osteogenic media supplemented with adipogenic conditioned media differentiated with solvent control, OM/aCM+1 µM – osteogenic media supplemented with adipogenic conditioned media differentiated with 1 µM PPARG agonist rosiglitazone, OM/aCM w/o – osteogenic media with adipogenic conditioned media differentiation without supplements, OM insulin – osteogenic differentiation with 2 µM insulin and all three above described adipogenic conditioned media with additional insulin supplementation during osteogenic differentiation

In detail, the experimental setup was implemented using the same experimental read-out as described for the standard osteogenic differentiation including PB/ALP and PB/Hoechst/NR/AR measurements for early and late osteogenic time points (**2.3.2.1, 2.3.2.2**).

2.3.5. CyQUANT proliferation assay in osteogenic and adipogenic differentiation

To analyze the proliferative effects of the drug rosiglitazone and the additional insulin supplementation during osteogenic and adipogenic differentiation, the CyQUANT Cell Proliferation Assay kit (CyQUANT, C7026 – Invitrogen) was implemented. At first, the proliferative effect was characterized in expansion media to define the baseline proliferation and cytotoxicity of the drug. To that end, the screening for proliferative effects was done on d0, d4, d7 and d10 of expansion. Following that, the proliferation assay was included while steering osteogenic and adipogenic differentiation. The proliferative effects induced during both differentiation processes were analyzed on d0, d4 and d7. For all described experimental setups, hBMSCs were re-seeded at a concentration of $1.8x10^3$ on a 48-well plate format. The cell concentration was reduced during the assay to allow proliferative effects due to increased capacity of space for cell expansion. In order to analyze cell proliferation, cells were measured for their metabolic activity by staining with PB according to the protocol described for both differentiation processes (section **2.3.2**). Afterwards, cell were washed twice with 400mL PBS, the remaining PBS was discarded and the plates were tapped on paper cloths to completely remove the liquid. The cell plates were frozen at -80°C to ensure efficient cell lysis in order to stain for DNA using CyQUANT. To analyze the proliferative capacity of cells, the plates were thawed for 30 minutes before undergoing analysis. While thawing, the CyQUANT staining

solution was prepared according to the manufacturer's protocol. Following that, cells were stained with 150 µL of CyQUANT GR dye/cell lysis buffer mix including four additional BLANK control wells without cells to identify background signals. Stained hBMSCs were incubated for five minutes on RT and measured with an excitation/emission wavelength of 485/530nm on a plate reader (Infinite 200 PRO – TECAN).

2.3.6. Preparation of hBMSC samples for RNA sequencing analysis

Three sets of patient derived hBMSCs were cultured and harvested from different experimental setups comprising standard osteogenic/adipogenic differentiation with and without drug supplementation as well as osteogenic differentiation using adipocyte conditioned media. The complete list of samples can be appreciated in the following table (**Table 10**).

Table 10: Summary of RNA samples included for sequencing analysis
Three different patient hBMSCs including Pat346, Pat784, Pat660 were selected for RNA sequencing analysis. Different cell culture conditions of each patient were harvested for further RNA sequencing analysis. Two different experimental setups were tested including samples from day 7 and samples from day 14 of osteogenic differentiation. The following conditions were analyzed for the gene expression changes in each experimental setup: Expansion control, osteogenic control differentiation, PPARG agonist treated osteogenic differentiation as well as adipogenic differentiation and the influence of the adipocyte secretome on osteogenic differentiated hBMSCs.OM=osteogenic differentiation; AM=adipogenic differentiation; aCM=adipogenic conditioned media; DMSO=solvent control; 1 µM=1 µM PPARG agonist rosiglitazone; w/o=without supplement; DMEM, short EM=expansion control

Patient	Sample name	Sample description
| Pat346 |	DMEM d7	Expansion control day 7
| Pat784 |	AM d7	Adipogenic differentiation control day 7
| Pat660 |	OM d7	Osteogenic differentiation control day 7
	OM 1µM d7	Osteogenic differentiation with 1µM PPARG agonist rosiglitazone day 7
	OM/EM d7	Osteogenic media supplemented with conditioned media from expanded hBMSCs day 7
	OM/aCM w/o d7	Osteogenic media with adipogenic conditioned media differentiation without supplements day 7
	OM/aCM+DMSO d7	Osteogenic media supplemented with adipogenic conditioned media differentiated with solvent control day 7
	OM/aCM+1µM d7	Osteogenic media supplemented with adipogenic conditioned media differentiated with 1µM PPARG agonist rosiglitazone day 7
	DMEM d14	Expansion control day 14
	AM d14	Adipogenic differentiation control day 14
	OM d14	Osteogenic differentiation control day 14
	OM 1µM d14	Osteogenic differentiation with 1µM PPARG agonist rosiglitazone day 14
	OM/EM d14	Osteogenic media supplemented with conditioned media from expanded hBMSCs day 14
	OM/aCM w/o d14	Osteogenic media with adipogenic conditioned media differentiation without supplements day 14
	OM/aCM+DMSO d14	Osteogenic media supplemented with adipogenic conditioned media differentiated with solvent control day 14
	OM/aCM+1µM d14	Osteogenic media supplemented with adipogenic conditioned media differentiated with 1µM PPARG agonist rosiglitazone day 14

Those hBMSCs were generated for a follow up RNA sequencing analysis identifying the underlying genetic patterns particularly induced by the drug treatment (RNA sequencing by Dr.

Tatiana Borodina and team, performed at the MDC genomics core facility/BIH). For that purpose, hBMSCs were re-seeded at a concentration of $6x10^4$ on a 6-well plate format. The cells were cultured according to the already described protocol for each experimental setup (**2.3.2, 2.3.3, 2.3.4**). The included experimental time points of RNA isolation for each differentiation process can be taken from the following (Figure 17).

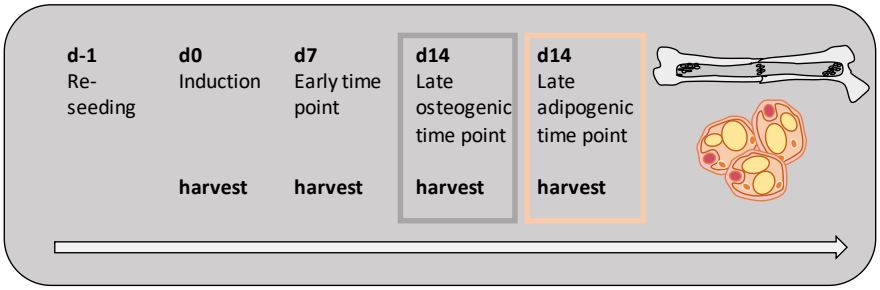

Figure 17: Illustration of RNA isolation time-points during osteogenic/adipogenic differentiation
The differentiation of hBMSCs for the RNA sequencing has been done according to the standard differentiation protocols starting with a re-seeding on day -1 and an osteogenic/adipogenic induction after 24h of attachment. On day 0 hBMSCs have been harvested as baseline control. Following that, the early differentiation time-point on day 7 and the late differentiation time-point on day 14 has been harvested for the identification of early and late regulated genes by PPARG agonist treatment

Prior to RNA isolation the cells were washed twice with 5mL of PBS and 300 µL Tryzol reagent was used to mechanically scrape the cells of the wells. HBMSCs in Tryzol solution were frozen at -80°C before isolating RNA. Isolation of RNA was achieved using the direct-zol RNA Miniprep kit (R2053 – Zymo Research) according to the manufacturer's protocol. The concentration of RNA was determined using a NanoDrop spectrophotometer (Peqlab). The results of this research regarding the RNA sequencing analysis are only focused on the main comparisons of gene expression between the osteogenic control and the PPARG agonist treated osteogenic differentiation condition on day 7 as well as on day 14. The analysis and statistical evaluation of the generated RNA sequencing data was performed by Dr. Andranik Ivanov (Beule lab, bioinformatics core facility/BIH).

2.3.7. Metabolic profiling of hBMSCs during osteogenic differentiation

Osteogenic differentiated hBMSCs under PPARG agonist rosiglitazone treatment and insulin supplementation were additionally analyzed for their metabolic profile using the Seahorse XF Cell Mito Stress test (Agilent). For that purpose, hBMSCs were re-seeded at a concentration of $2x10^4$ on a 96-well cell culture microplate and differentiated for 10 days into the osteogenic lineage with and without drug and/or insulin supplementation. The osteogenic differentiation was implemented in the same manner as described above (**2.3.2**). Cells were prepared for seahorse measurements on day 2, day 5 and day 10. A typical experimental layout for the seahorse analysis contained five replicates of each condition while determining all edge wells of the plate as BLANK controls. One day prior to the analysis, sensor cartridges were prepared

by adding 200 µL calibrant solution to each well and cartridges were pre-warmed in a non-CO_2 incubator at 37°C. On the analysis time points, cells were washed twice with 200 µL seahorse XF DMEM basal media supplemented with 2mM glutamine (Glut) and 5.5 mM glucose (Gluc). After the remaining cell culture media was removed, 175 µL seahorse media was added to each well including the BLANK wells. In the following, cell culture microplates were incubated for 1h in a non-CO_2 incubator at 37°C. While incubating the cell culture microplate, the sensor cartridge was loaded with four different inhibitor solutions including 1 µM oligomycin, 2 µM carbonyl cyanide-4 (trifluoromethody) phenylhydrazone (FCCP) and 1 µM of rotenone/antimycin A (Rot/AntA) mixture. All inhibitors were diluted in seahorse XF DMEM supplemented with 2mM Glut and 5.5mM Gluc. The inhibitor oligomycin was used as ATP synthase (complex V) inhibitor. This inhibitor is known to induce a decrease in mitochondrial respiration and crosslink this to cellular ATP production. Further, the inhibitor FCCP was implemented inducing maximal mitochondrial respiration. FCCP is shown to disrupt the mitochondrial membrane potential and points out the spare respiratory capacity also interpreted as the ability of cells to overcome increased energy demand. Lastly, the inhibitors Rot/AntA are added to inhibit complex I and complex III respectively. This inhibition is described to shut down mitochondrial respiration and enable the calculation of nonmitochondrial respiration of the cells (Seahorse XF Cell Mito Stress kit – Agilent). The analysis procedure is described in the following figure (**Figure 18**). Throughout the seahorse measurements, the oxygen consumption rate (OCR) as well as the extracellular acidification rate (ECAR) were measured using the Seahorse XFe96 analyzer (Agilent).

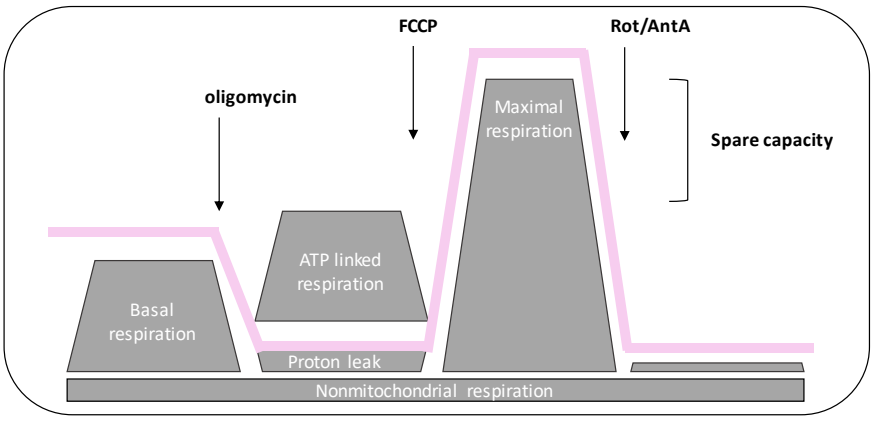

Figure 18: Illustration of the Seahorse XF Cell Mito Stress test (Agilent)
The seahorse analyzer serves as tool to analyze the metabolic profile of PPARG agonist treated hBMSCs. The assay includes the following measurements: three measurements of baseline respiration prior to oligomycin addition, three measurements of oligomycin addition and induction of ATP linked respiration by inhibition of ATP synthase complex V. Furthermore, the H+ proton leak can be measured as remaining baseline respiration not coupled to ATP production. Next, three measurements of the maximal respiration are determined by the addition of the inhibitor FCCP disrupting the mitochondrial membrane potential. From this value, the spare respiratory capacity can be determined. Lastly, three measurements of the non-mitochondrial respiration are included by adding the inhibitors rotenone and antimycin A completely shutting down the mitochondrial respiration

After the seahorse measurement, cell culture microplates were stored at -80°C for follow up analysis determining the DNA concentration of each condition using CyQUANT.

2.3.8. Glucose uptake profiling of hBMSCs during osteogenic differentiation

In addition to the metabolic profiling describing the mitochondrial respiration capacity, hBMSCs were analyzed for their glucose uptake potential using the Glucose Uptake-Glo assay (J1342 - Promega). Changes in glucose uptake by the treatment of hBMSCs with PPARG agonist rosiglitazone and insulin during osteogenic differentiation were determined on day 6 and day 11 of differentiation. For that purpose, hBMSCs were re-seeded at a concentration of $4.8x10^3$ on a 48-well plate format and differentiated according to the osteogenic differentiation protocol described above (**2.3.2**). The glucose uptake was measured by a nonradioactive, bioluminescent assay based on determining the amount of 2-deoxyglucose-6-phosphate (2DG6P) accumulation after 2-deoxyglucose (2DG) is added to the cells. For each condition a background signal was determined by using an OMIT control, where no 2DG was added as substrate and therefore no 2DG6P accumulation was achieved. On each analysis time point fresh osteogenic medium with rosiglitazone/insulin treatment was added to the cells for an incubation time of 30 minutes on 37°C. After that, all insulin treated conditions were re-stimulated with insulin at a concentration of 2 µM for 1h on 37°C to enhance the insulin driven glucose uptake. Following that, cells were washed with 300 µL PBS and incubated with 100 µL of PBS containing 1mM 2DG excluding the OMIT control condition. After 10 minutes of incubation with 2DG on RT, 50 µL of stop buffer was added and the plates were briefly shaken before transferring 75 µL of each condition to a 96-well plate format. The assay was continued according to the manufacturer's protocol by adding 25 µL of neutralization buffer. The plates were briefly shaken and 100 µL of 2DG6P detection reagent was added for an incubation period of 1h. Finally, bioluminescence was measured with one second integration on a plate reader (Infinite 200 PRO – TECAN).

2.3.9. Adipokine profiling of hBMSCs during osteogenic differentiation

The harvested supernatants generated during the osteogenic and adipogenic differentiation as well as during the osteogenic differentiation with adipocyte conditioned media were characterized regarding their adipokine profile. Thereby, the secretory changes in hBMSCs during osteogenic differentiation with and without PPARG agonist rosiglitazone and insulin supplementation were determined and adipocyte driven paracrine effects were described. For that purpose, supernatants were thawed twice at the most and were analyzed using the Legendplex Human Adipokine panel (13-plex, 740196 – BioLegend). The Legendplex was performed according to the manufacturer's protocol using the assay optimized for a V-bottom plate. It is important to note, that the sample and reagent volume was downscaled to 10 µL per sample instead of 25 µL and the incubation of capture beads with analyte was achieved

overnight ensuring efficient binding to the analyte using the downscaled reaction volume. After the assay was performed, samples were measured on the CytoFLEX S flow cytometer (Beckman Coulter).

2.3.10. Statistical analysis

Statistical analysis was implemented using the software Prism (version 8, GraphPad). The normalization of in vitro stimulated conditions of each set of patient derived hBMSCs was achieved by the remove baseline and column math tool generating a ratio of value/baseline (expansion media in all settings) format of the data. Statistical testing between control and treatment group was achieved by using a parametric, ratio-paired t test. Here, differences in control values due to patient variability but consistent effects in the treatment groups were considered. The unpaired non-parametric Mann-Whitney test comparing ranks was implemented for non-Gaussian distributions and the unpaired, parametric t test with Welch's correction was performed for data of Gaussian distribution. Statistical significance was assigned when reporting a P value <0.05.

3. Results

3.1. Ex vivo characterization of inflammation related effects on bone regeneration in mice

3.1.1. TNFa/IFNg neutralization and its effects on adipocytes and CD4⁺ T helper 2 subset polarization

The first experiment included the reduction of pro-inflammatory cytokines during bone regeneration and showed an important connection between adipose tissue accumulation and anti-inflammation. A significantly increased accumulation of adipose tissue in bone by the treatment with neutralizing antibodies against pro-inflammatory cytokines such as TNFa and IFNg was shown (**Figure 19 A, C**). Furthermore, a significant shift within the $CD4^+$ T helper cell compartment in spleen lymphocytes of mice towards anti-inflammatory T helper 2 cells was achieved by systemically blocking those pro-inflammatory cytokines (**Figure 19 B**). It is important to mention, that adipose tissue accumulation in this experimental setup had no significant effect on the healing outcome, when accumulating at the fracture site (not shown). Due to the surprisingly neutral effects on the skeletal system the focus of this thesis was drawn on primarily inducing beneficial, anti-inflammatory adipose tissue in bone at the bone fracture side, by stimulating the PPARG transcription factor without systemically targeting the pro-inflammatory response during bone regeneration.

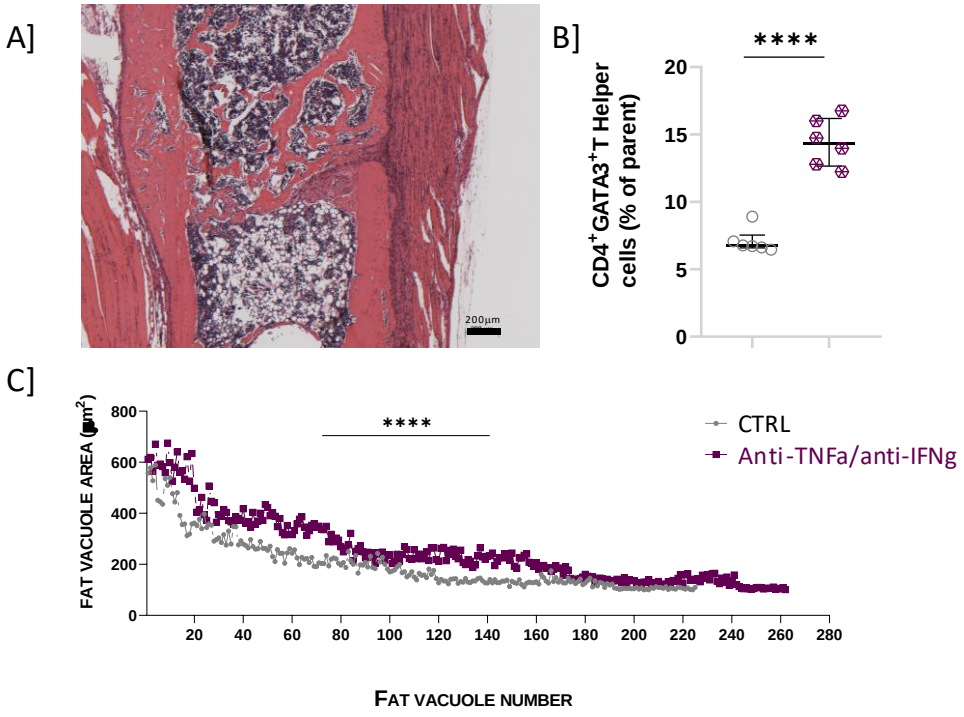

Figure 19: Neutralization of pro-inflammatory cytokines TNFa and IFNg inducing adipocyte accumulation in the fractured bone and systemic $CD4^+$ TH2 polarization

A] $CD4^+$ T helper 2 subset polarization being significantly increased by treatment with neutralizing antibodies against TNFa and IFNg (unpaired t-test with Welch's correction $p<0.0001$, n=6), relative expression of GATA3 (%) within the $CD4^+$ T cell compartment, pre-gated on $Livedead^+CD45^+CD3^+CD4^+$ T cells of murine splenocytes **B]** Histological staining of paraffin embedded fractured femoral bone of mice treated with neutralizing antibodies against TNFa/IFNg showing enhanced adipocyte accumulation distal from the fracture side (below the fracture) **C]** Quantification of adipocyte accumulation distal from the fracture side comparing fat vacuole area (μm^2) and vacuole number, significantly increased by the treatment with neutralizing antibodies against TNFa/IFNg (unpaired t-test with Welch's correction $p<0.0001$, n=4)

3.2. Ex vivo characterization of PPARG related effects on bone regeneration in mice

PPARG activation during bone regeneration was studied to specify the adipose tissue driven effects on the bone healing process. While using rosiglitazone as a specific drug acting as PPARG agonist (PPARG activator), a non-specific PPARG antagonist namely BADGE was used in the reference group [277]. Due to the partial agonistic effects of BADGE, the reference group showed high data spreading and non-significant results during the in vivo study (not shown). This is why the focus of the following results was based on the PPARG agonist treated mice in comparison to untreated control mice. PPARG agonist treatment highlighted a stronger bridging of the fractured bone (see also **3.2.2**) and higher amounts of adipocytes within the bone marrow compared to the untreated controls (**Figure 20**).

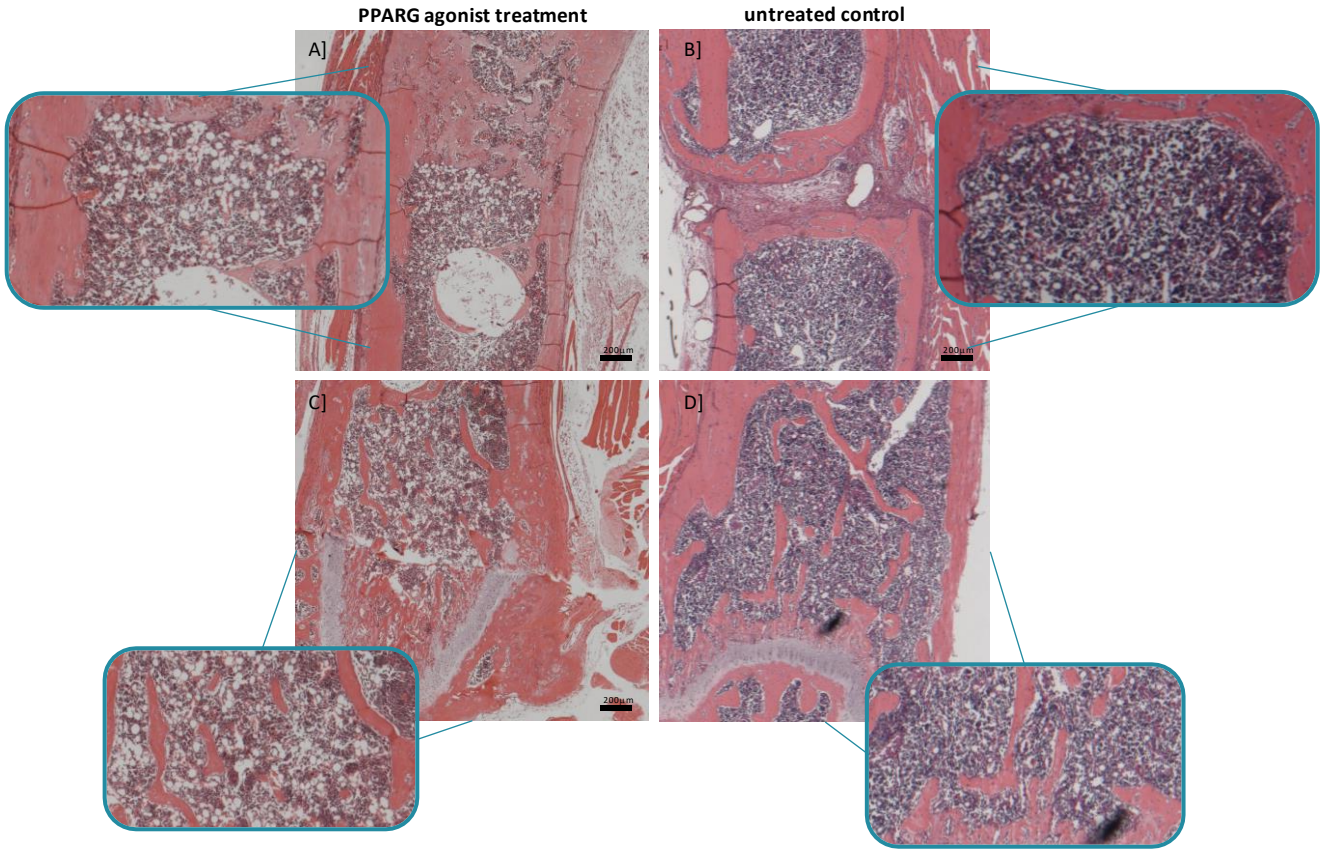

Figure 20: PPARG agonist treatment induces adipocyte accumulation in the marrow simultaneously with stronger bridging of bone on day 21 of bone regeneration
Untreated young mice represent a bone marrow harboring very low amounts of adipocytes. The osteotomized, untreated control group hereby serves as comparative group while exploring bone regeneration under PPARG agonist driven adipocyte accumulation in the bone marrow **A]** PPARG stimulation upregulates adipocyte accumulation in proximity of the fracture while improving bone bridging B] Untreated controls show less adipocyte accumulation and slower bridging of bone **C]** Adipocyte accumulation is likewise induced within the bone marrow near the growth plate by treatment with PPARG agonist rosiglitazone **D]** Less adipocytes are visualized at the growth plate of untreated controls

3.2.1. PPARG driven induction of adipose tissue and lipids in bone

The appreciated accumulation of adipose tissue next to the fracture gap and its concurrent beneficial effect on bone fracture bridging, let us to the question on how to identify specific characteristics of this pro-regenerative adipose tissue type. Current knowledge on bone marrow adipose tissue and its accumulation in specific bone regions includes the presence of proximal adipose tissue known as rBMAT and distal adipose tissue known as cBMAT. Treatment of mice with the PPARG agonist rosiglitazone resulted in an upregulation of adipocyte accumulation within the bone marrow cavity especially at the distal part of the growth plate of fractured as well as unfractured bones (**Figure 21** and **Figure 22**). Surprisingly, adipocyte accumulation was specifically found at the distal region of the fracture (mBMAT), where it has not yet been described in the literature (**Figure 21 A, D** and **Figure 23 A, B, C**). When focusing on the cell compartment within the bone, the precursors of mature adipocytes namely the $Sca1^{+}CD24^{-}$ adipogenic mesenchymal stromal lineage in the fractured and

unfractured bone were slightly decreased by PPARG agonist treatment, whereas the presence of the osteogenic Sca1^{-}CD24^{-}CD140a^{+} lineage was not changed by PPARG agonist treatment. The multipotent Sca1^{+}CD24^{+} lineage was increased in both fractured and unfractured bones by the treatment with the PPARG agonist rosiglitazone (shown in the appendix, **Figure 61** and **Figure 62**).

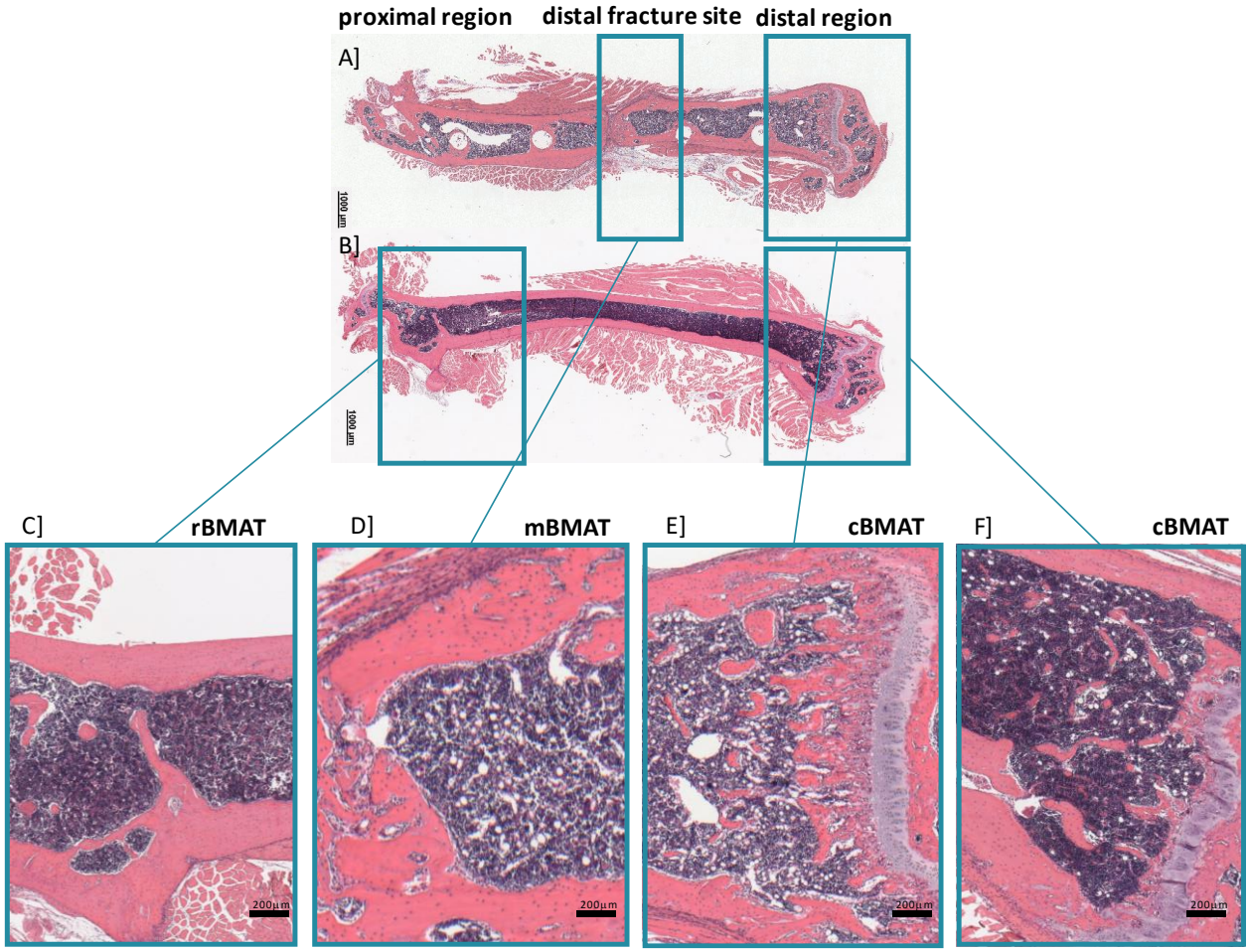

Figure 21: PPARG agonist driven adipocyte accumulation in bone focuses on distal bone regions were constitutive BMAT (cBMAT) is located
A] During fracture healing the accumulation of adipocytes is highlighted for day 21 post osteotomy in regions distal from the fracture in proximity to the fracture site and at the growth plate of the distal bone region (knee) **B]** In unfractured, contralateral bone a similar pattern is shown with adipocyte accumulating driven by PPARG stimulation. Adipocyte accumulation is displayed especially in the distal bone regions whereas no adipocyte accumulation is shown in proximal bone regions **C]** Adipocytes accumulating in the proximal regions of bone are determined regulatory bone marrow adipose tissue (rBMAT) **D]** Adipocytes accumulating in distal bone near the fracture site are referred to as pro-regenerative, mixed BMAT (mBMAT) **E] F]** Constitutive BMAT (cBMAT) are adipocyte accumulating in the distal bone region near the growth plate of the knee

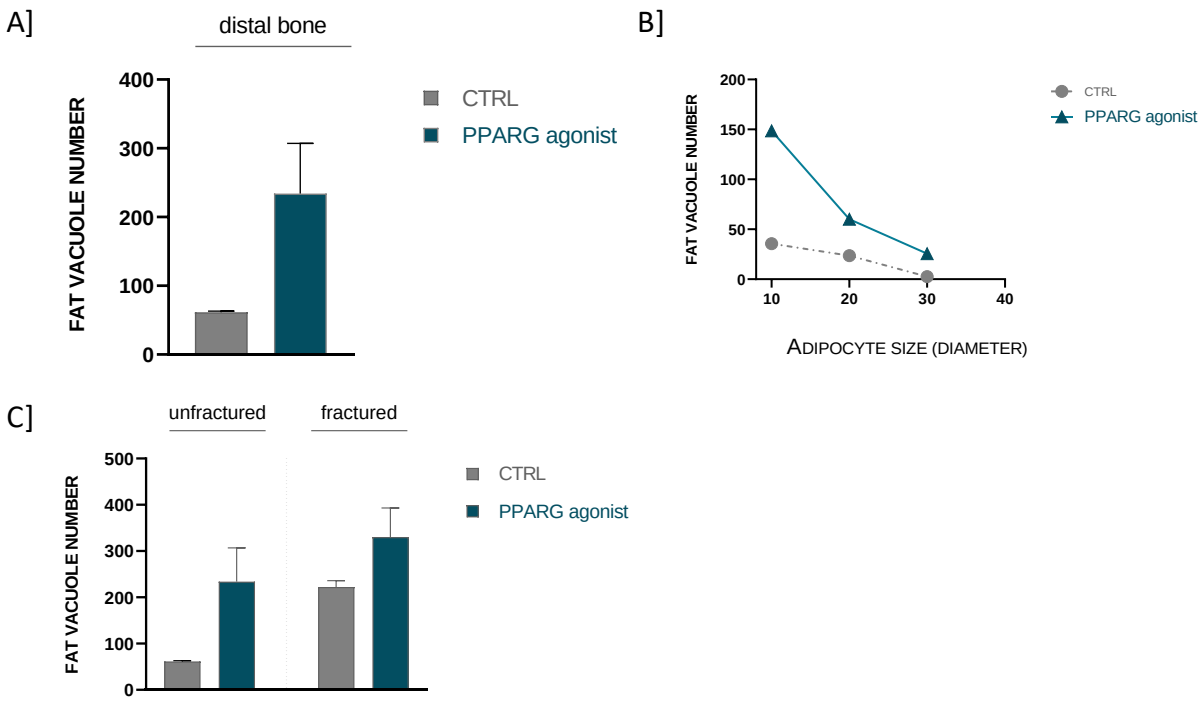

Figure 22: PPARG agonist treatment induces an increased accumulation of large fat vacuoles in the distal region at the growth plate of unfractured and fractured bones
Adipocytes in the bone marrow are quantified as number of fat vacuoles within a specific region of the bone, here the distal part near the growth plate. Total number and size are shown for unfractured and fractured PPARG agonist treated bones (cyan) compared to control bones (dark grey) **A]** The accumulation of cBMAT is shown for the unfractured control bone compared to the bone treated with PPARG agonist rosiglitazone (n=2 each) **B]** The increasing amount of cBMAT is shown in relation to the increasing adipocyte size (diameter) post PPARG agonist treatment. The control bones show a decreased cBMAT expansion and are characterized by small adipocytes (n=2 each) **C]** Unfractured bones are displayed for their increase in distal cBMAT located at the growth plate by PPARG agonist treatment. Fractured bones are shown with an even higher increase in cBMAT by PPARG agonist treatment (unfractured n=2, fractured n=4)

The induced, large, bone marrow adipocytes (BMAs) were further characterized in terms of fatty acids and phospholipids using the unfractured femoral bones of each condition. For this analysis, bones were sectioned according to previously defined BMAT regions (**Figure 9)**. PPARG agonist treated BMAs were shown to harbor increased levels of stearoyl-CoA desaturase 1 (SCD-1) in all bone localities with a significant increase of SCD-1 in the mixed bone marrow adipose tissue (mBMAT) location, reflecting the part of the bone where the fracture is set under osteotomy conditions (**Figure 23 D**). In addition to that, an increase of omega-6 phospholipids, especially in the proximal, regulated BMAT (rBMAT) of unfractured, femoral control bones was shown (**Figure 23 E**). In contrast to that, omega-3 phospholipids were rather reduced in all three BMAT localities with the strongest reduction displayed in the distal, constitutive BMAT (cBMAT) of unfractured bones (**Figure 23 F**).

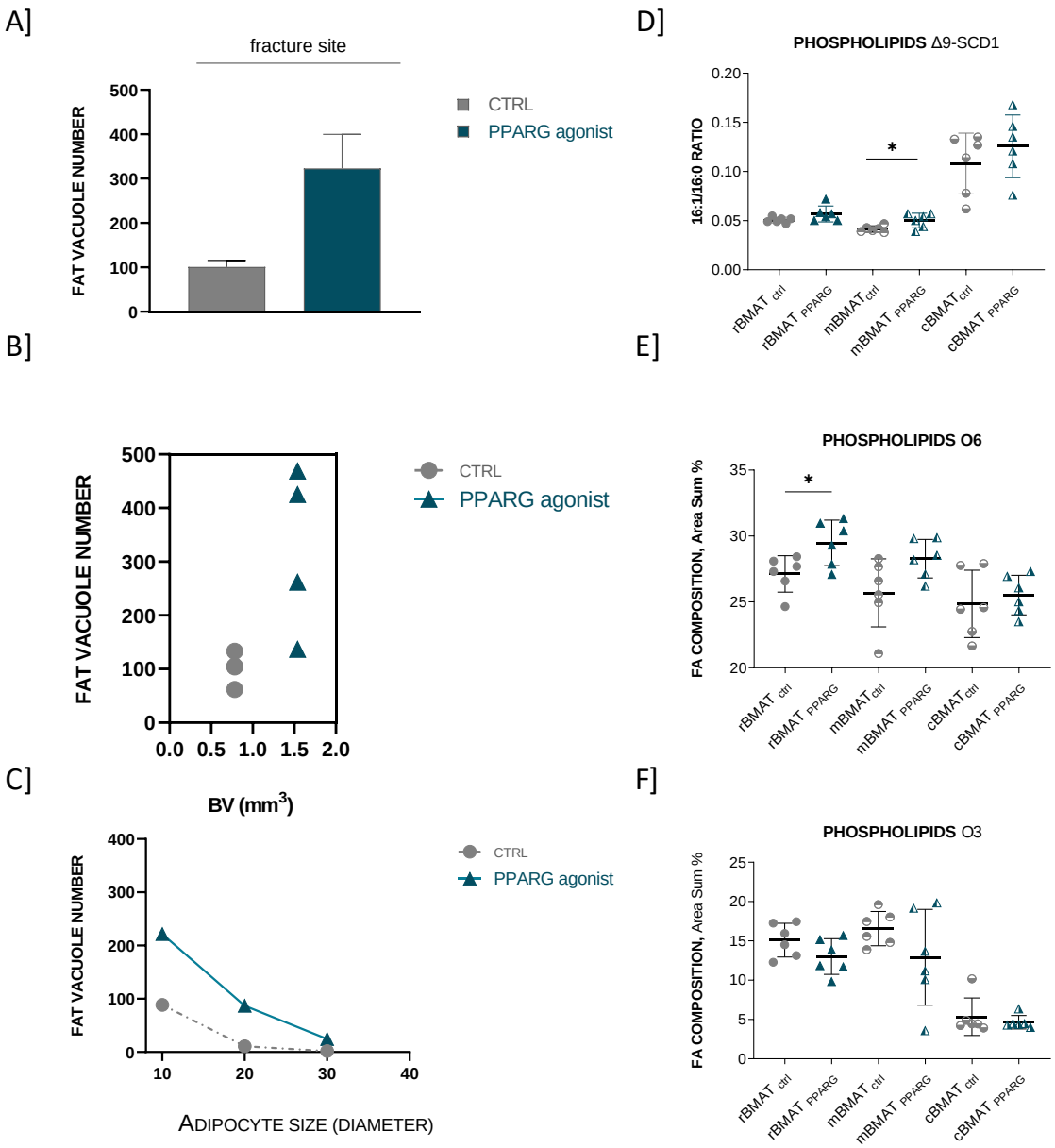

Figure 23: Treatment with PPARG agonist rosiglitazone induces adipocytes <u>at the distal part of the osteotomy</u> and increases SCD-1 and omega 6 in unfractured, control bones

Treatment with PPARG agonist rosiglitazone increases the accumulation of fat vacuoles of large size at the distal region of the fracture gap **A]** The fat vacuole number is increased at the fracture site by PPARG agonist treatment (cyan) compared to the control bones (dark grey) (unpaired t-test with Welch's correction p=0.059, n=4) **B]** The increase in adipocytes is displayed in relation to the correlating increase in bone volume (BV) (n=3-4 each) **C]** PPARG agonist treatment induces significantly lower amounts of small fat vacuoles at the distal fracture site and increases higher amounts of large fat vacuoles (unpaired t-test with Welch's correction p=0.0324 for small and p=0.058 for large fat vacuoles, n=4) Further, phospholipids and fatty acid changes measured in contralateral, non-fractured control bones of mice treated with a PPARG agonist are depicted **D]** The significant increase in phospholipid □9 SCD-1 by PPARG agonist treatment is shown by the increased ratio of palmitoleic acid to palmitic acid being most prominent in the mBMAT region. An increasing trend is likewise shown in the other bone regions (unpaired t-test with Welch's correction p=0.0341, n=6) **E]** Fatty acid composition of omega 6 phospholipids significantly increased by PPARG treatment in the rBMAT region, with the same trend being shown in the mBMAT (unpaired t-test with Welch's correction p=0.0266, n=6) **F]** No significant changes are shown in the fatty acid composition of omega 3 phospholipids during PPARG agonist treatment of mice

3.2.2. PPARG driven beneficial skeletal parameters

To verify the stronger bridging of bone fractures under PPARG agonist treatment, the quality of bone was studied by measuring various microCT parameters. While at first glance the healing outcome seems similar, an in depth characterization showed a significant difference in bone parameters of PPARG agonist treated compared to untreated controls. This is visualized in the following by micro computed tomography images of the bone fracture gap on day 21 of healing (**Figure 24**). Beneficial bone parameters were determined in the PPARG agonist treated group during bone fracture healing. In detail, a significant increase of the polar moment of inertia (MMI polar) was shown comparing the PPARG agonist treated group and the control (**Figure 25 B**). Furthermore, the bone volume on bone surface ratio (BS/BV) was significantly increased in the PPARG treated group as well as the trabecular thickness (Tb.Th) of bone (**Figure 25 A, D**). In contrast to that, the trabecular number (Tb.N) showed a decreasing trend when under PPARG stimulation (**Figure 25 C**). The tissue volume (TV) and bone volume (BV) was shown to be significantly increased in the PPARG treated group compared to the control (**Figure 25 E, F**). The significant changes in the above stated bone parameters display a strong improvement of bone regeneration during PPARG agonist treatment in comparison to the control.

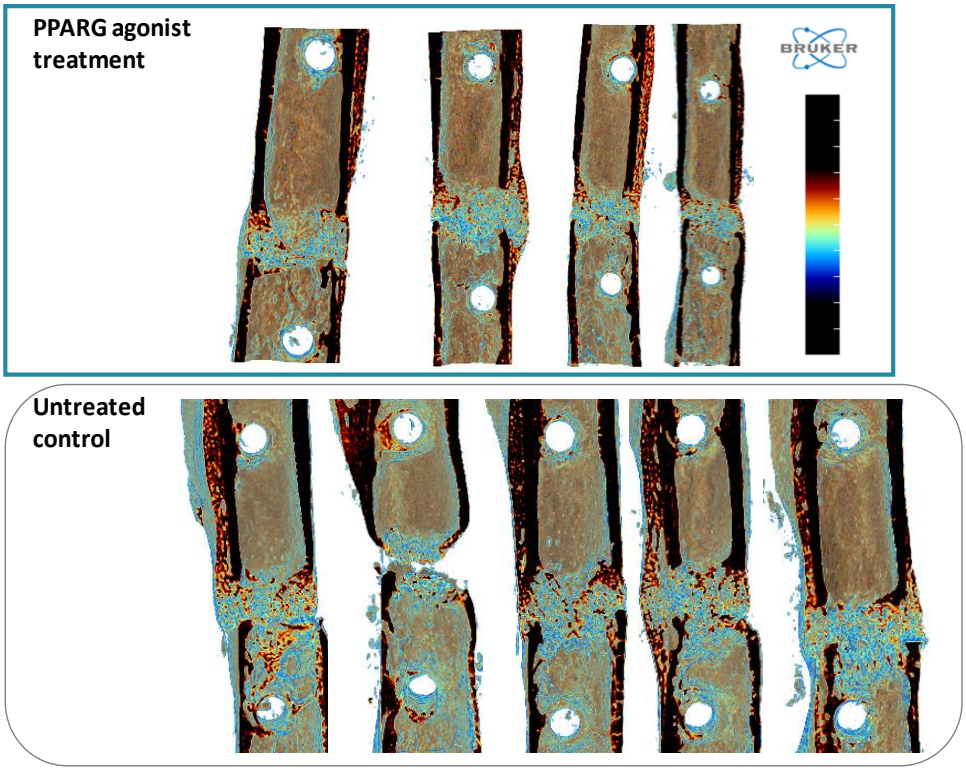

Figure 24: PPARG agonist treatment does not hinder bone fracture bridging during healing
Treatment with the PPARG agonist rosiglitazone (cyan border color) results in equal bone bridging when compared to untreated controls (grey border color) on day 21 of healing. The bone structure of treated and untreated mice is visualized by distinct colors. The color scheme is computed according to pixel intensity/density highlighting different bone compartments

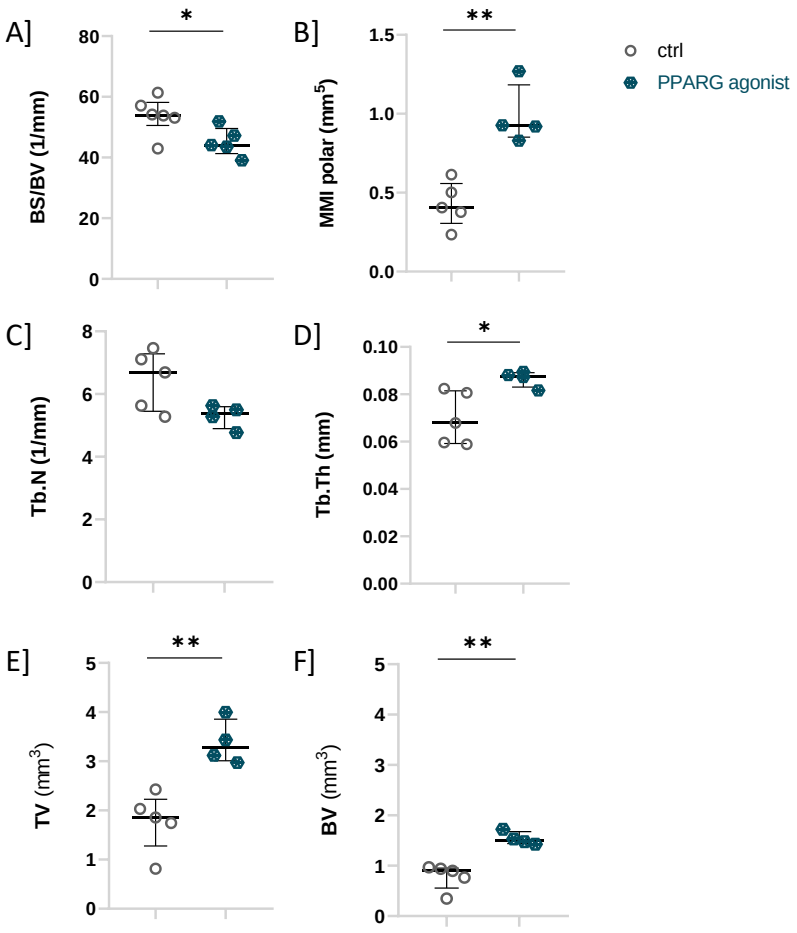

Figure 25: Treatment with PPARG agonist rosiglitazone has beneficial effects on the bone structure of fractured bone during healing of healthy, young mice housed under environmental pathogen exposed housing
A] B] PPARG treatment steers a significantly higher bone volume shown by the decrease of bone surface to bone volume ratio (unpaired t-test with Welch's correction p=0.028, n=4-5) and significantly increases the ability of bone to cope with torsional forces defined by the polar moment of inertia (MMI polar) (unpaired t-test with Welch's correction p=0.0039, n=4-5) **C] D]** The trabecular bone structure is shown to be significantly increased in terms of trabecular thickness (Tb.Th) and no significant difference is shown for the trabecular number (Tb.N) in the PPARG agonist treated bone during fracture healing (unpaired t-test with Welch's correction for Tb.Th p=0.0256, n=4-5) **E] F]** The significantly increased tissue (TV) and bone volume (BV) under PPARG agonist treatment shows further enhancement of bone stability during fracture healing (unpaired t-test with Welch's correction p=0.0025 and p=0.0011, n=4-5)

3.2.3. PPARG driven CD4⁺ T helper 2 subset polarization

Anti-inflammatory features of PPARG agonist treatment and its concurrent induction of anti-inflammatory adipose tissue in bone were identified by the characterization of the CD4⁺ T helper (TH) immune compartment. In concordance with the beneficial skeletal parameters induced by PPARG agonist treatment, splenocytes changed from a pro-inflammatory towards an anti-inflammatory phenotype. In this case, the beneficial, anti-inflammatory CD4⁺ T helper (TH) 2 subset was significantly induced by PPARG agonist treatment (**Figure 26 A**). In contrast, no significant changes were observed within the pro-inflammatory CD4⁺ TH1 and TH17 subset (**Figure 26 B, C**).

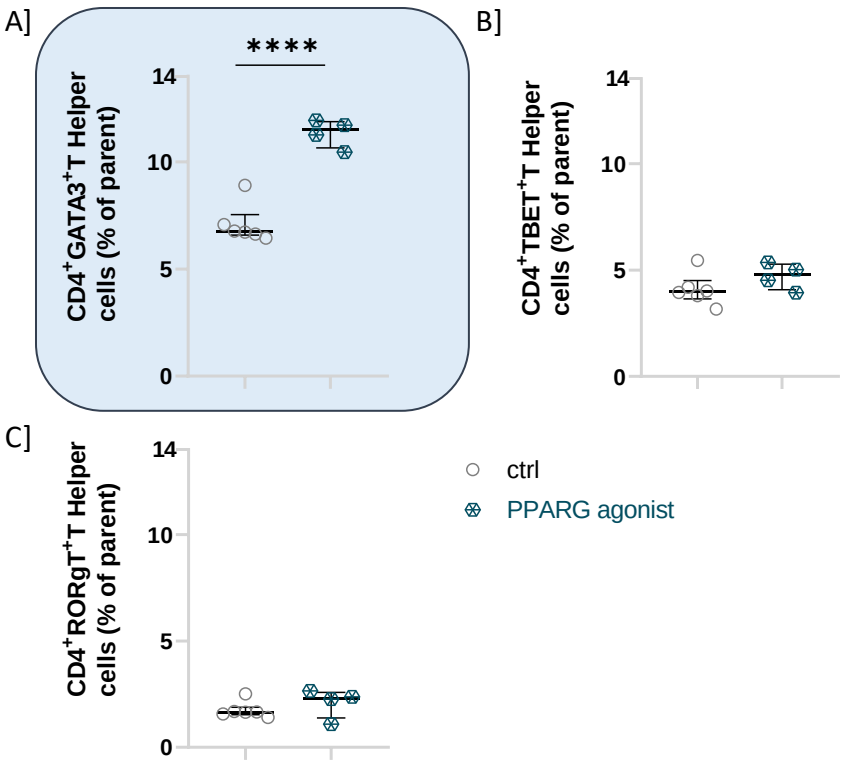

Figure 26: Treatment with PPARG agonist rosiglitazone steers anti-inflammatory CD4⁺ T helper 2 subset polarization in mouse splenocytes and has no systemic effect on the pro-inflammatory CD4⁺ TH17 and TH1 subsets

Relative expression of RORgT (%) as transcriptional marker for the CD4⁺ TH17 subset, TBET (%) as transcriptional marker for the CD4⁺ TH1 subset and GATA3 (%) as transcriptional marker for the CD4⁺ TH2 subset is shown, pre-gated on Livedead+ CD45⁺CD3⁺CD4⁺ T cells of murine splenocytes A] B] No significant influence of PPARG stimulation is shown in the subset polarization of CD4⁺ TH17 cells as well as no change is observed in the subset of CD4⁺ TH1 cells during the curse of fracture healing C] Prominent changes are depicted for the CD4⁺ TH2 cells by significant increase in the splenocyte compartment of mice under PPARG agonist treatment during bone regeneration (unpaired t-test with Welch's correction $p<0.0001$, n=4-5)

In summary, beneficial aspects of PPARG agonist treatment during in vivo fracture healing of mice can be appreciated. Beneficial effects in terms of bone parameter improvement as well as a broad anti-inflammatory effect on the immune cell compartment were shown. To further specify the pro-regenerative/pro-osteogenic effects, in depth in vitro characterization was done for human patient derived hBMSCs. The goal was to mirror the murine data in the human setting. The in vitro effects of PPARG agonist treatment are described in detail in the following chapter.

3.3. In vitro characterization of PPARG related effects in human bone marrow MSCs (hBMSCs)

3.3.1. PPARG as driving force of enhanced osteogenic capacity and increased matrix mineralization of hBMSCs

Since PPARG agonist treatment showed a beneficial bridging of bone in our in vivo mouse model, the underlying factors needed to be investigated. For that we studied PPARG agonist induced, pro-osteogenic effects during in vitro osteogenic differentiation of hBMSCs. In concordance to the beneficial effects of PPARG activation on bone healing, the osteogenic differentiation of hBMSCs was significantly increased by treatment with a PPARG agonist. This was shown by early osteogenic markers such as ALP activity measurement on day 4 and day 7, where an increased pNPP consumption was achieved in PPARG agonist treated hBMSCs compared to the untreated controls. By further addition of insulin during the osteogenic differentiation the effect of PPARG agonist induced osteogenic potential was fortified (**Figure 27 A**). It is important to note, that the level of calcification induced by PPARG treatment is highly dependent on the patient specific osteogenic potential of hBMSCs (**Figure 27 B**). The osteogenic potential was defined by the osteogenic control displaying diverse basal ALP and calcification levels when comparing different patient derived hBMSCs (shown in the appendix, **Figure 63)**. Interestingly, patient hBMSCs showed an individual increase in early osteogenic differentiation potential by PPARG agonist treatment, some displayed only moderately increased effects and others showed a high increase in early pNNP consumption (shown in the appendix, **Figure 64**). PPARG agonist treatment highly increased calcification in the later osteogenic stages in almost all patient derived hBMSCs. Furthermore, hBMSCs from patients with only moderately different levels of early ALP activity, were rescued in the late osteogenic stages by enhanced calcification promoted through PPARG agonist stimulation (shown in the appendix, **Figure 64**).

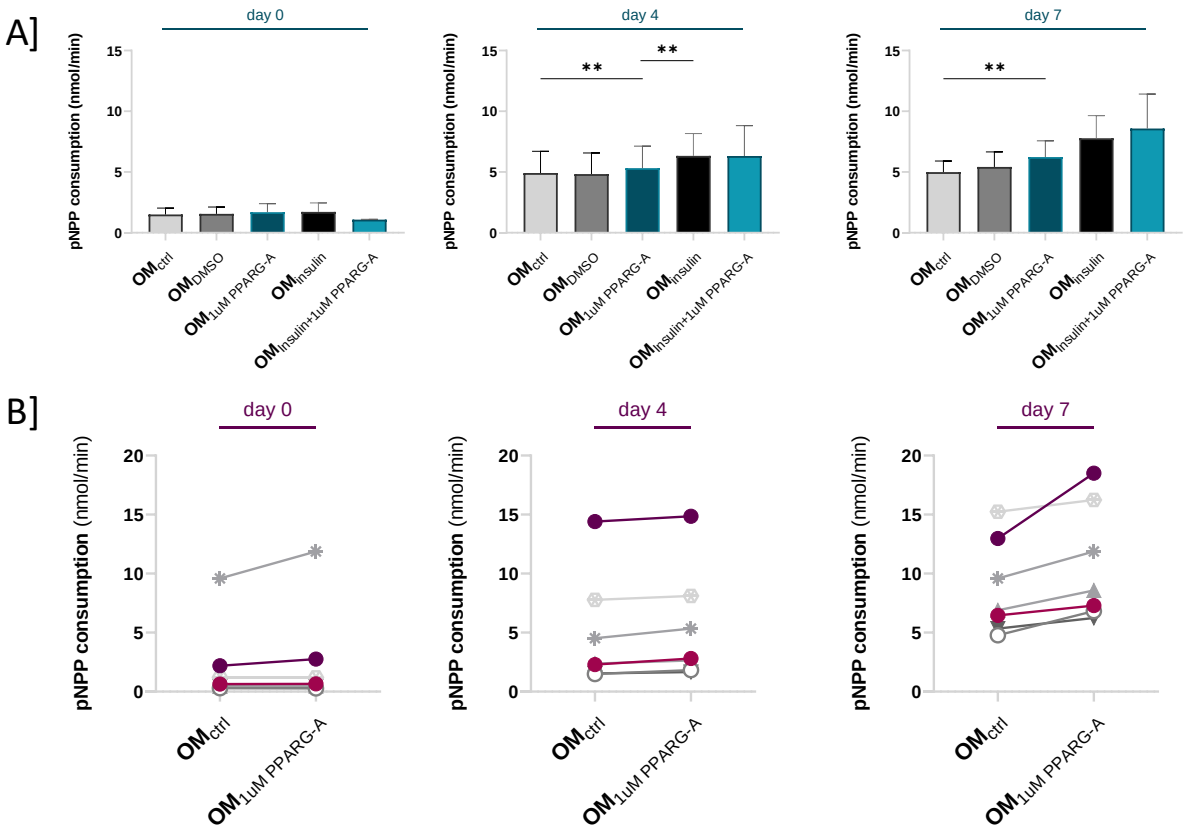

Figure 27: Treatment with PPARG agonist rosiglitazone enhances the potential of hBMSCs to differentiate into the osteogenic lineage shown by the increase of early osteogenic ALP activity and pNNP consumption ALP activity of hBMSCs under PPARG agonist treatment is shown by the consumption of pNNP on three days including day 0, day 4 and day 7 of osteogenic differentiation (OM) **A]** Values presented in the three plots are baseline corrected for the expansion control (EM), the consumption of pNNP is significantly increased by treatment with PPARG agonist rosiglitazone on day 4 and day 7 (ratio paired t-test p=0.0052 and p=0.0024, n=7). In addition, the supplementation of insulin significantly fortified the pNNP consumption rate on day 4 by increasing insulin availability in culture to be metabolized by hBMSCs with increased insulin sensitivity driven by treatment with PPARG agonist rosiglitazone (ratio paired t-test p=0.0067, n=7). On day 7 the significant effect of PPARG agonist treatment is maintained but no significant increase is depicted for the additional supplementation of insulin to the culture (OMinsulin+1uM PPARG-A n=3) **B]** Individual values are presented without baseline correction for the expansion control (EM). Individual patient derived hBMSCs are shown to react to the PPARG treatment harboring significantly increased pNPP consumption, differences in stimulation of individual patient hBMSCs are shown and result from varying ability of osteogenic potential as well as sensitivity towards the PPARG agonist treatment

Since PPARG agonist treatment is widely known for its insulin sensitization effects on cells, one key question was whether higher insulin uptake in osteogenic differentiating cells was the driving force for increased calcification. To test specific effects of insulin during the osteogenic differentiation, insulin was included as positive control in our experimental setup. In addition to the early osteogenic induction provided by PPARG activation, the calcification of osteogenic differentiated hBMSCs was significantly increased by PPARG agonist treatment and further enhanced by supplementation of insulin (**Figure 28**).

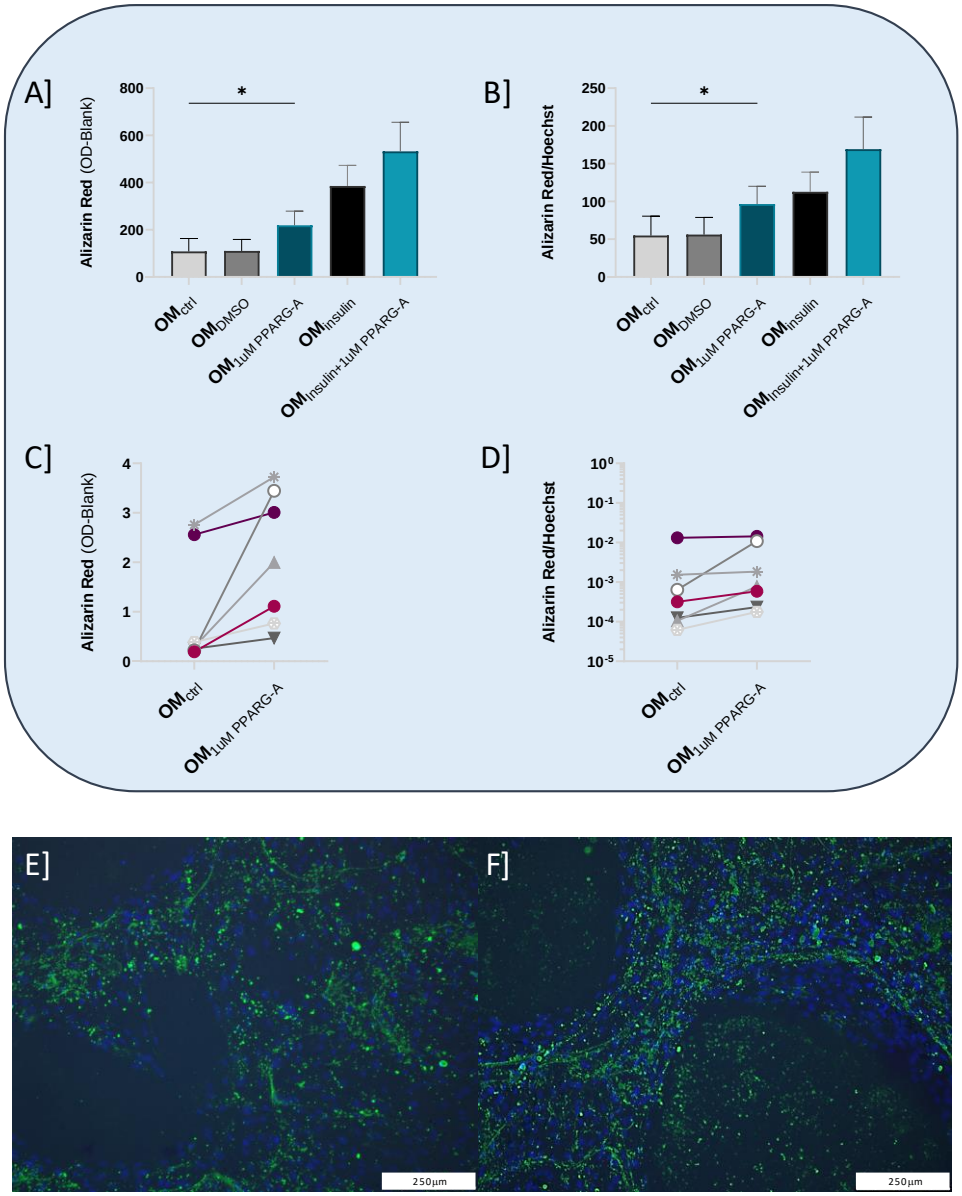

Figure 28: Treatment with PPARG agonist rosiglitazone enhances the calcification levels of hBMSCs in late osteogenic stages

Late osteogenic differentiation potential and calcification driven by PPARG agonist stimulation is shown in bar plots as baseline corrected effect (normalized on expansion control) of all seven patient derived hBMSCs and as line plot of individual uncorrected values displaying donor variability A] Alizarin red staining of hBMSCs is shown for different conditions such as osteogenic control, osteogenic differentiation with DMSO as solvent control, osteogenic differentiation with rosiglitazone, insulin and insulin in combination with rosiglitazone. A significant increase of matrix mineralization is shown for the PPARG treated condition in comparison to the osteogenic control/solvent control (ratio paired t-test p=0.0195, n=7). The supplementation of insulin is shown to mirror the effect of increased mineralization during PPARG treatment (ratio paired t-test p=0.0203, n=7). The PPARG agonist driven effect is increased by additional supplementation of insulin (ratio paired t-test p=0.0993, n=3) B] Similar effects of PPARG agonist driven increase of osteogenic differentiation and matrix mineralization are shown by normalization on the cell number using Hoechst staining for DNA content (ratio paired t-test comparing OM ctrl/DMSO with OM 1 µM rosiglitazone p=0.0325, n=7). No significant increase of matrix mineralization is shown for the supplementation of insulin during osteogenic differentiation compared to the control (ratio paired t-test p=0.0521, n=7) whereas the combination of PPARG agonist stimulation with insulin supplementation enhanced the effects of PPARG agonist only (ratio paired t-test p=0.1441, n=3) C] D] Individual matrix mineralization effects of patient hBMSCs are displayed by increased alizarin red values as well as under normalized conditions both representing the significant increase of osteogenic differentiation and mineralization by PPARG treatment E] Representative staining of calcification in the osteogenic differentiation control condition using the OsteoImage mineralization assay F]

Representative staining of calcification in the osteogenic differentiation with PPARG agonist stimulation using the OsteoImage mineralization assay

Matrix mineralization during PPARG agonist and insulin stimulated osteogenic differentiation of hBMSCs was shown to steer distinct patterns of mineral deposition, more precise calcium phosphate deposition visualized by alizarin red stainings (**Figure 29**). PPARG agonist treatment resulted in a focused calcium deposition, whereas insulin treatment resulted in a large-scale calcium deposits.

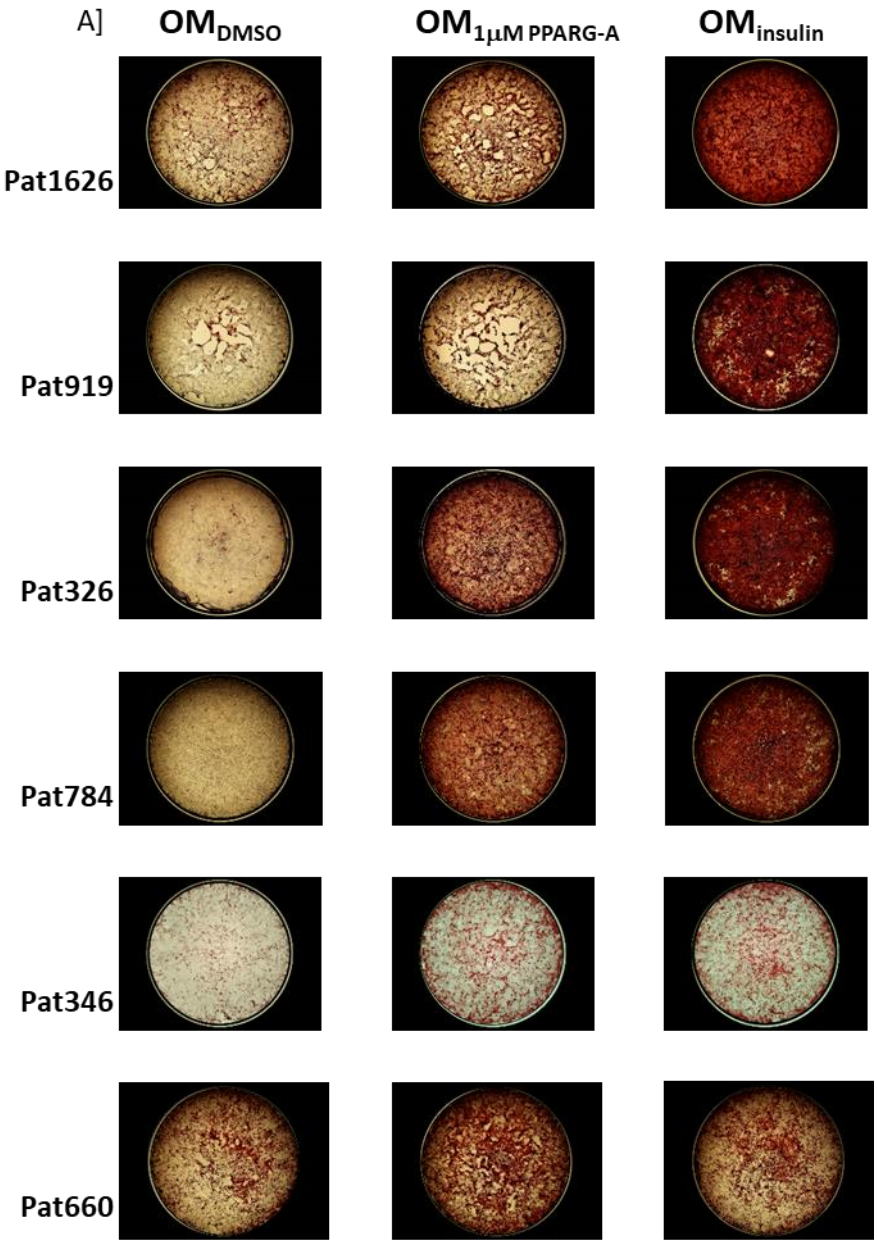

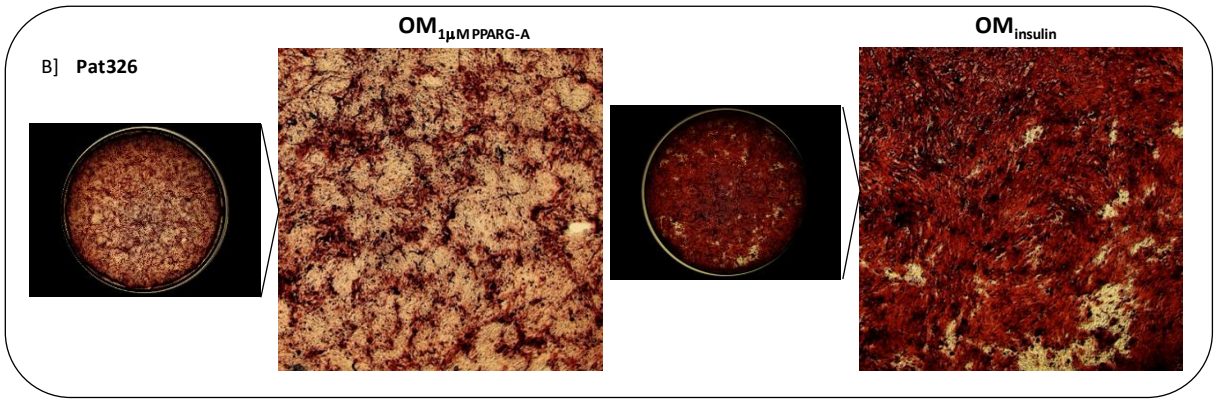

Figure 29: Treatment with PPARG agonist rosiglitazone and supplementation of insulin induces a distinct pattern of matrix mineralization and significantly increases the calcification during osteogenic differentiation
A] The figure visualizes the significantly enhanced osteogenic mineralization and calcification of hBMSCs on day 14 – day 21 of all patients treated with PPARG agonist rosiglitazone. Differences in patient sensitivity towards insulin supplementation are depicted, where high insulin sensitivity is displayed by Pat1626, Pat919, Pat326 and Pat784 and low insulin sensitivity is shown in Pat346 and Pat660. Patients with low osteogenic differentiation capacity were shown to be rescued by the induction of PPARG e.g. Pat784 and Pat326 **B]** Insulin Treatment leads to large-scale calcium deposits when compared to the PPARG agonist treated conditions showing focused calcium deposits exemplarily depicted for Pat326

3.3.1.1. Unique effects of PPARG activation and insulin availability on proliferation

PPARG agonist treatment and insulin supplementation represented different calcification patterns during osteogenic differentiation of hBMSCs. However, both insulin and PPARG agonist treatment resulted in higher calcification. Now it should be investigated whether insulin and PPARG agonist treatment induces differences in proliferation during osteogenic culture of hBMSCs. To differentiate the PPARG agonist driven pro-osteogenic effect from the proliferation capacity, proliferation of hBMSCs was determined under PPARG agonist mediated expansion as wells as during osteogenic differentiation. The proliferation capacity in expanded hBMSCs was shown to be rather reduced by PPARG agonist stimulation compared to the control expansion (**Figure 30 A, Figure 31 C**). Moreover, no significant impact on the proliferation capacity was shown during the osteogenic differentiation stimulated by PPARG agonist treatment. In contrast, the supplementation of insulin during osteogenic differentiation was represented with a significant increase in the proliferation rate of hBMSCs on day 7 of osteogenic differentiation (**Figure 30 B**).

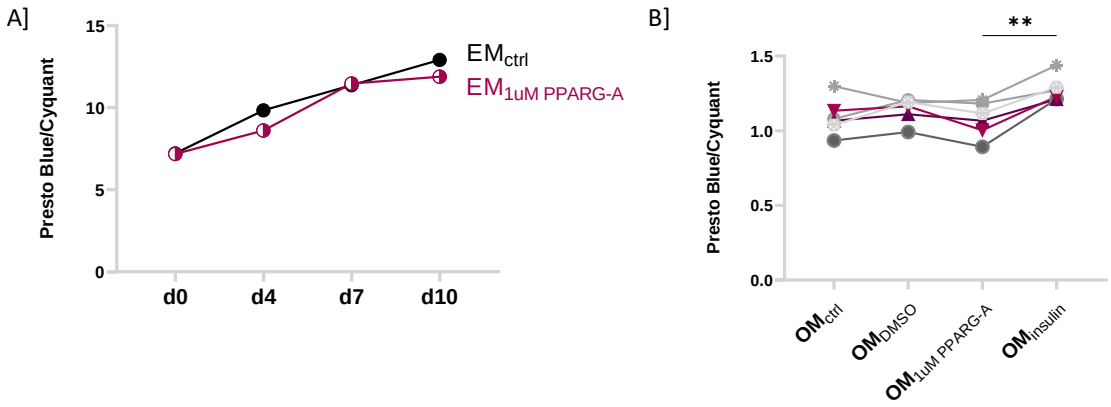

Figure 30: Proliferative capacity of hBMSCs is markedly increased by stimulation with insulin compared to the treatment with PPARG agonist rosiglitazone during osteogenic differentiation
A] Treatment with the PPARG agonist rosiglitazone shows no significant difference on the proliferative potential of hBMSCs during the expansion period shown by normalizing metabolic activity on cell number measured in a kinetic experiment with four time points including day 0, day 4, day 7 and day 10 B] Under osteogenic differentiation the impact of PPARG agonist stimulation on proliferation is not present but with supplementation of insulin the proliferation of hBMSCs is significantly increased on day 7 of osteogenic differentiation (ratio paired t-test p=0.0031, n=6)

Insulin supplementation was shown to increase the proliferation of hBMSCs only under osteogenic differentiation (**Figure 31 D**). This increase could not be shown for expanded hBMSCs. In addition, the supplementation of insulin during osteogenic differentiation or expansion markedly increased the metabolic capacity of hBMSCs (**Figure 31 A, B**). No metabolic or proliferative effects were demonstrated for PPARG agonist treated osteogenic cells, suggesting that PPARG agonist treatment has a specific pro-osteogenic effect rather than proliferative potential.

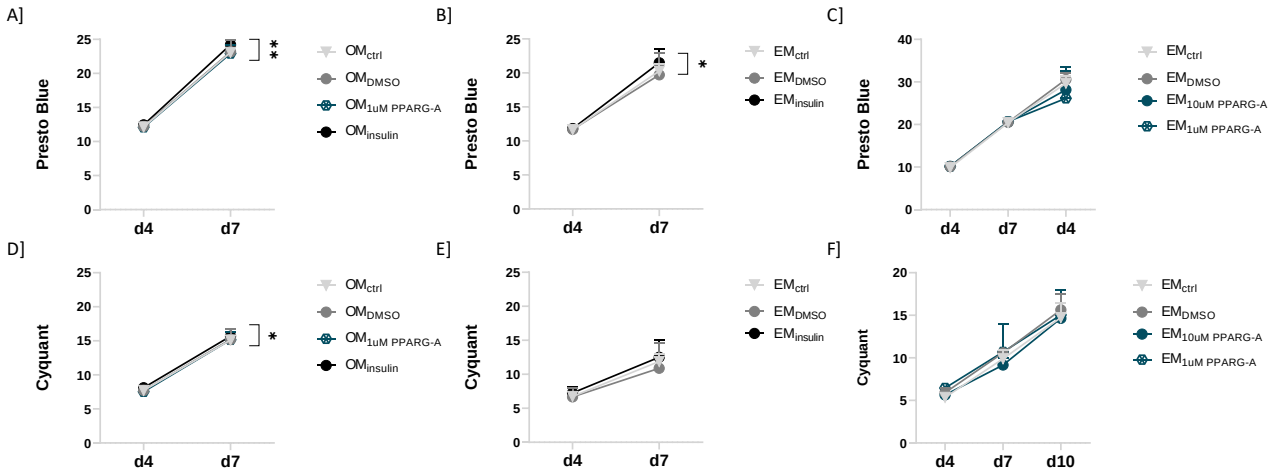

Figure 31: Insulin supplementation is shown to significantly upregulate metabolic activity and proliferation during osteogenic differentiation whereas no effects can be shown in the PPARG agonist treated group
Presto Blue describes the metabolic activity of the hBMSCs under osteogenic differentiation and cyquant describes the cell number/proliferation. Metabolic activity and proliferation are shown as population doublings calculated by Log2 (difference between culture days). The following conditions such as osteogenic control (light grey), osteogenic solvent control (moderate grey), osteogenic differentiation with PPARG agonist (dark cyan) and osteogenic differentiation with insulin supplementation (black) are shown **A]** Insulin driven osteogenic differentiation is marked

by a significantly higher metabolic activity compared to the other conditions (ratio paired t-test p=0.0023, n=6) **B]** insulin likewise increases the metabolic activity of expanded control hBMSCs (ratio paired t-test p=0.0173, n=5-6) **C] F]** PPARG agonist treatment neither increases the metabolic activity nor the proliferation of hBMSCs (n=2-6) **D] E]** The proliferation rate is only enhanced during osteogenic differentiation with insulin, whereas in expanded hBMSCs no effect on the proliferation could be shown (ratio paired t-test p=0.0247, n=5-6)

3.3.1.2. **Unique effects of PPARG activation on co-induction of adipocytes and bone**

The accumulation of adipocytes is rather unusual during osteogenic culture with specific osteogenic inducers. To analyze the effects of PPARG activation not only on bone formation, e.g. osteogenic differentiation, but also on adipose tissue accumulation, e.g. adipocyte induction, we screened for adipocytes in the osteogenic culture system. Interestingly, next to the enhanced matrix mineralization, PPARG agonist treatment was shown to co-induce adipocytes and osteogenic cells during later time points of osteogenic differentiation in all patient derived hBMSCs (**Figure 33,** Figure **33**). With that, our in vitro culture system could mirror the appreciated in vivo adipocyte accumulation next to new bone formation. Adipocytes were formed starting on day 7 – day 10 and accumulated further until day 21 of osteogenic differentiation. It is important to mention, that adipocytes appeared prior to initial calcium deposition and matrix mineralization starting around day 7 – day 10 depending on the individual differentiation potential of each patient derived set of hBMSCs. With this result, I found it necessary to define a term for the PPARG-agonist induced adipocytes during osteogenic differentiation. From now on, osteo-adipocytes are defined as the adipocytes co-induced with osteogenic cells, whereas fat forming adipocytes define the standard adipocytes accumulating during adipogenic differentiation.

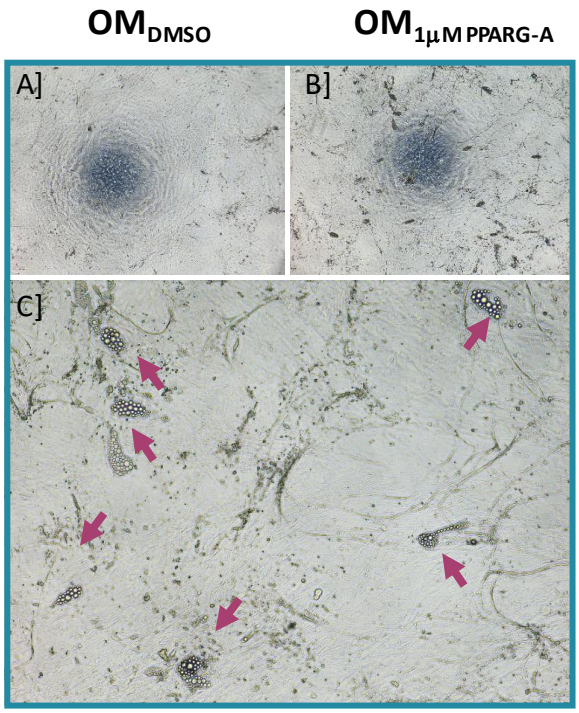

Figure 32: PPARG agonist treatment induces a bilateral differentiation potential in hBMSCs with the accumulation of adipocytes during osteogenic differentiation
Visualization of adipocyte accumulation in PPARG agonist treated Pat326 derived hBMSCs on day 21 of osteogenic differentiation **A]** Osteogenic differentiation with solvent control shows no accumulation of adipocytes during the differentiation process and is marked by its slower matrix mineralization **B]** PPARG agonist treatment induces the accumulation of adipocytes concurrent with enhanced mineralization potential of hBMSCs **C]** Purple arrows depict the adipocytes formed with proximity to the calcium depots during osteogenic differentiation here visualized by 10 fold magnification

Adipocytes were localized in close proximity to the calcium depots (**Figure 33**). A significant accumulation of adipocytes was shown in PPARG treated groups (**Figure 34 C, D**), which was even more enhanced when combining the PPARG treatment with insulin. Interestingly, while only supplementing insulin during osteogenic differentiation this adipocyte co-induction could not be shown (**Figure 33**).

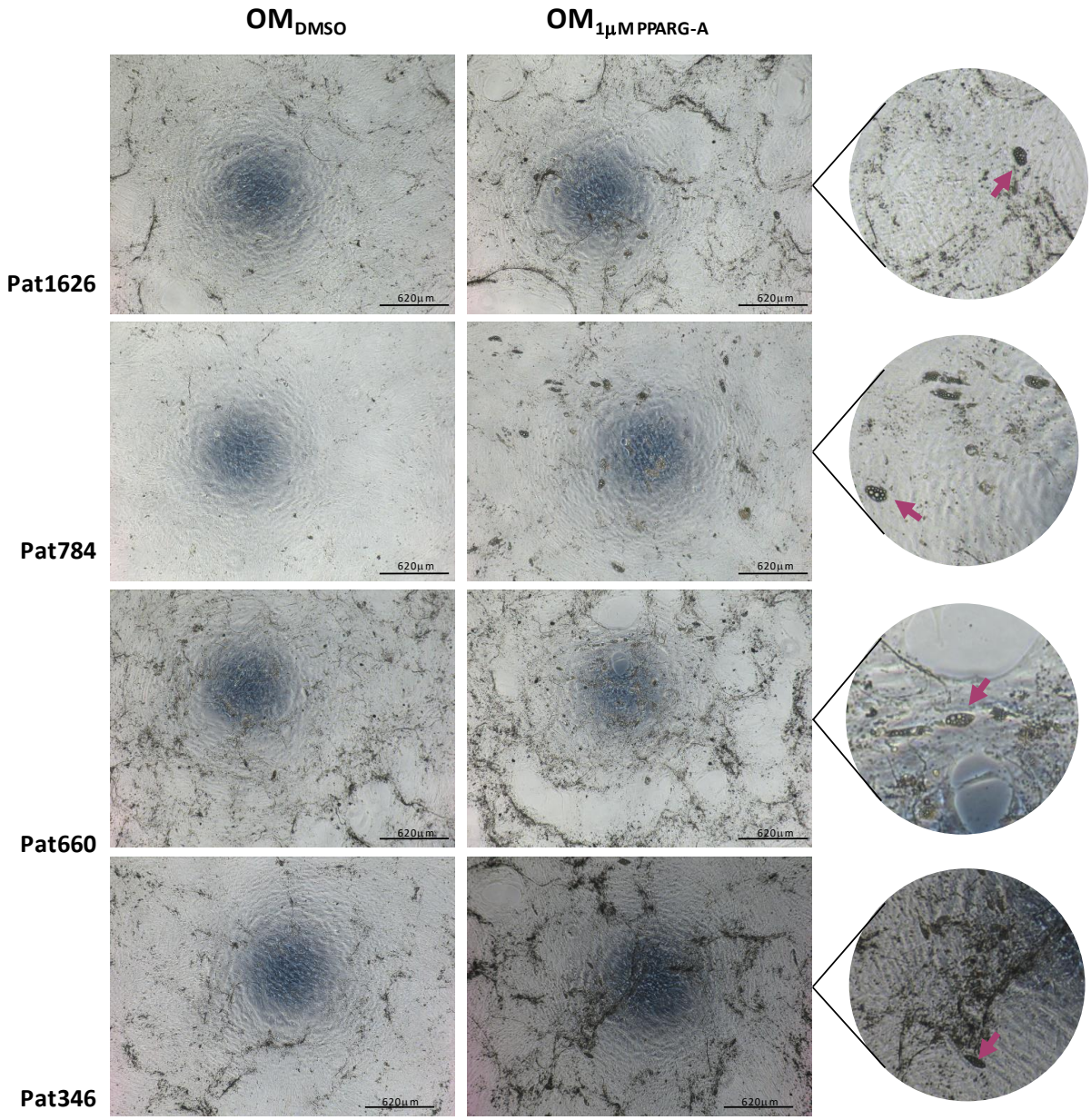

Figure 33: Visualization of individual, patient specific adipocyte accumulation during osteogenic mineralization of hBMSCs with PPARG agonist treatment

PPARG agonist treatment of individual patients steers adipocyte accumulation in proximity to calcium depots exemplarily shown for Pat1626 and Pat784 with low osteogenic differentiation potential as well as for Pat660 and Pat346 with high osteogenic differentiation potential on day 14 – day 21 of differentiation. The figure depicts the osteogenic differentiation with solvent control compared to the PPARG agonist treated osteogenic differentiation with significantly upregulated adipocyte accumulation. Adipocytes of each individual patient are highlighted by purple arrows

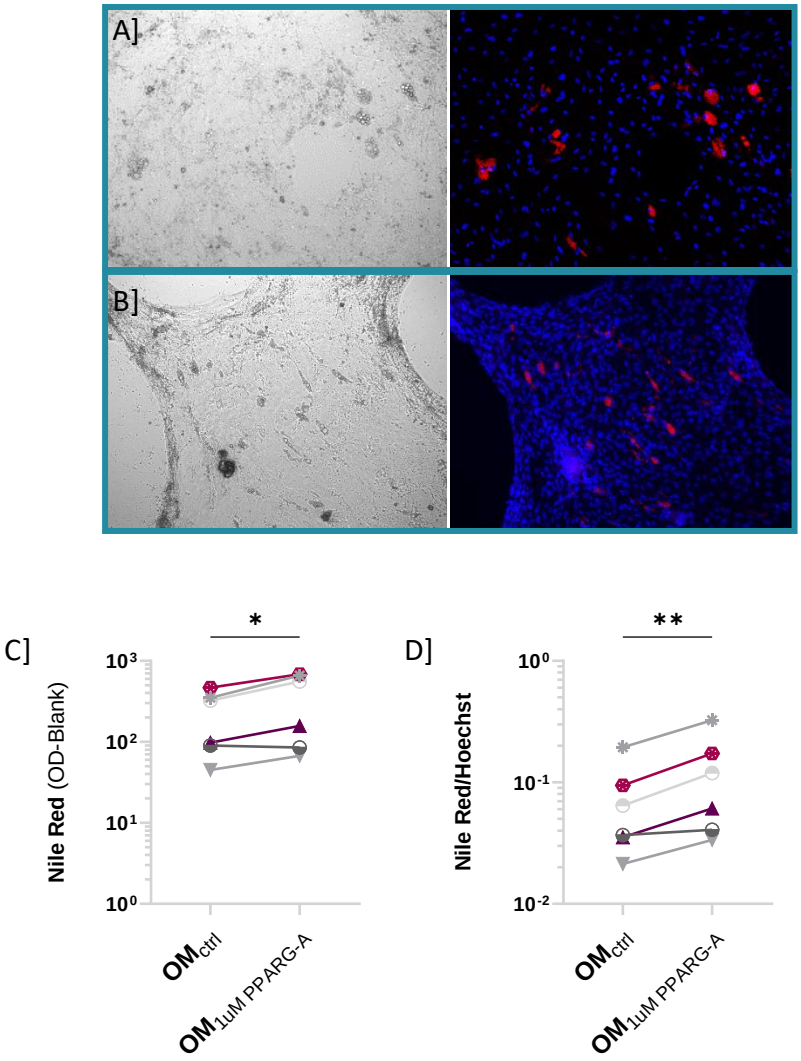

Figure 34: PPARG agonist treatment induces a significant accumulation of adipocytes during osteogenic differentiation visualized by fluorescence staining of lipids and DNA
Adipocytes and cell nuclei of hBMSCs are visualized by NileRed and Hoechst staining on day 14 – day 21 as well as quantified by NileRed/Hoechst value normalization **A]** Adipocyte accumulation in osteogenic differentiated hBMSC of Pat660 is shown by NileRed (red) and nuclei staining using Hoechst (blue) on day 21 with a 10 fold magnification **B]** Visualization of adipocytes by NileRed staining (red) during osteogenic differentiation of Pat819 captured on day 14 of differentiation is shown with a 10 fold magnification **C]** A significant accumulation of adipocytes during osteogenic differentiation is shown by NileRed staining for all patients (ratio paired t-test p=0.0103, n=6) **D]** Quantification of NileRed stained adipocytes using Hoechst DNA staining determines a significant increase of adipocytes during PPARG agonist treatment for all patients (ratio paired t-test p=0.0018, n=6)

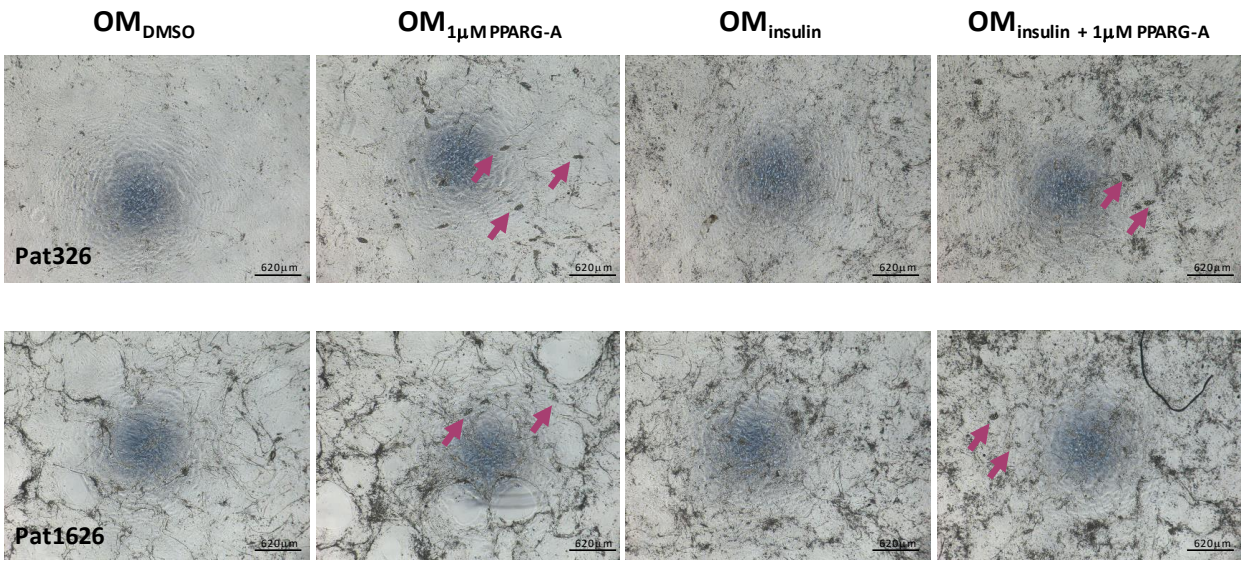

Figure 35: PPARG agonist treatment results in adipocytes accumulation and highest calcium deposition independent of the insulin driven increase in calcification
Pat326 and Pat1626 derived hBMSCs are shown for their distinct mineralization pattern induced by insulin and PPARG agonist treatment. Pat326 shows a low osteogenic differentiation potential whereas Pat1626 is marked by a high osteogenic differentiation potential, both mirroring the mineralization differences in insulin and PPARG treated groups. OM DMSO = solvent control, OM 1 µM rosiglitazone = OM with PPARG agonist treatment, OM insulin = OM with insulin supplementation, OM insulin 1 µM rosiglitazone = OM with PPARG agonist and insulin supplementation. Osteogenic differentiation with the solvent control displays the lowest mineralization compared to all other groups. Treatment with PPARG agonist induces adipocyte accumulation paired with highest calcium deposition. Insulin treatment does not induce adipocyte formation and is marked by a lower osteogenic potential. Combining PPARG treatment with additional insulin supplementation results in an increase of osteogenic potential and combined adipocyte formation.

No morphological difference could be detected between the adipocytes induced during osteogenic differentiation compared to those differentiated in the standard adipogenic differentiation (**Figure 36**).

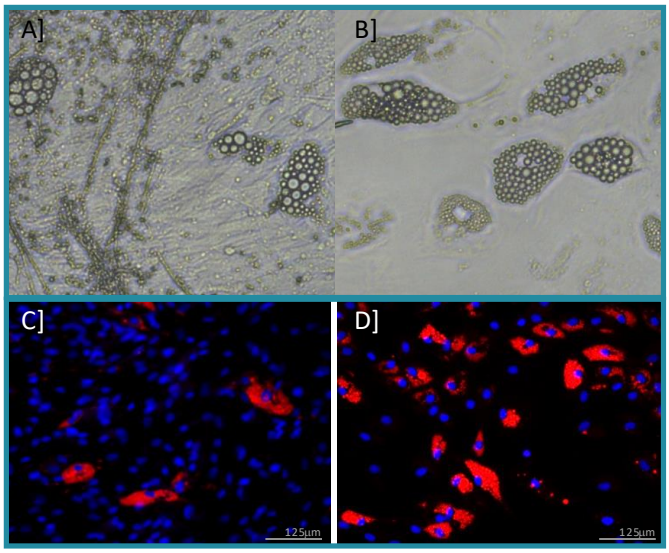

Figure 36: PPARG agonist treatment forms morphological similar adipocytes during osteogenic differentiation as compared to the standard adipogenic differentiation

Adipocytes are determined to be equal in morphology visualized by microscopic images using 10 fold magnification **A]** Adipocytes co-localized during osteogenic differentiation are shown **B]** Adipocytes of standard adipogenic differentiation are shown **C]** Osteo-adipocytes are stained with NileRed (red) for lipids and Hoechst (blue) for cell nuclei **D]** Standard adipocytes are stained with NileRed (red) for lipids and Hoechst (blue) for cell nuclei indication no differences in adipocyte morphology

HBMSCs during adipogenic differentiation showed no enhanced differentiation capacity towards the adipogenic lineage when stimulated with the PPARG agonist rosiglitazone compared to the adipogenic differentiation control (**Figure 37**).

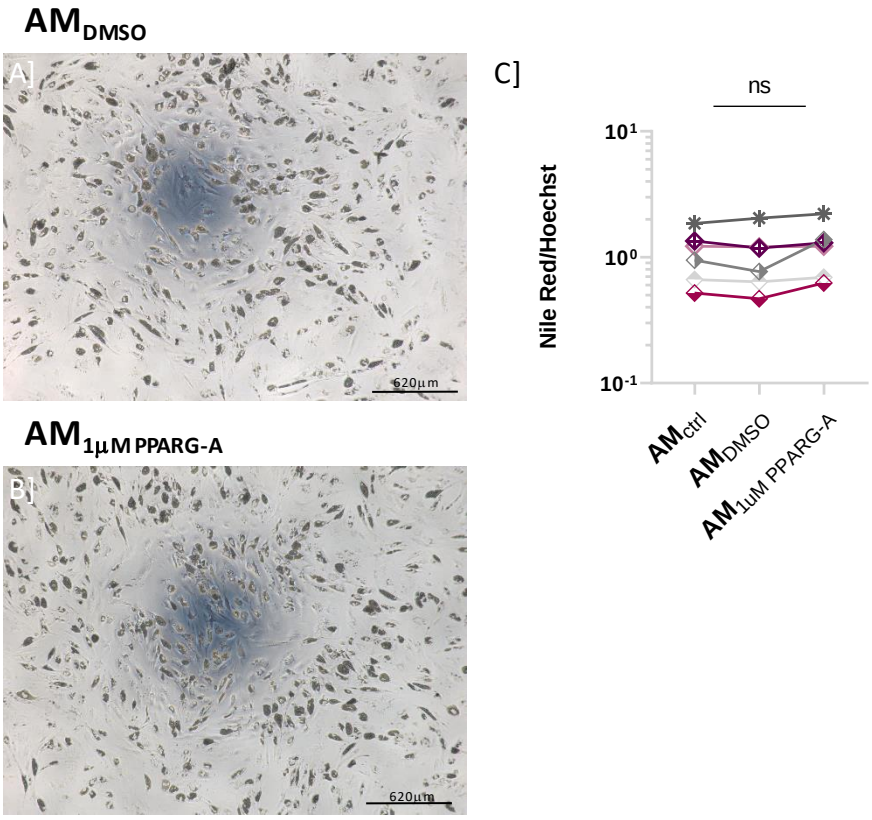

Figure 37: Adipogenic differentiation with and without PPARG agonist stimulation results in equal amounts of adipocytes and no increase in adipogenic differentiation is shown using PPARG agonist treatment
A] Adipogenic differentiation with solvent control is shown visualizing the amount of adipocytes differentiated after 14 days of adipogenic differentiation **B]** PPARG agonist treatment has no significant effect on the adipogenic differentiation potential as well as the adipocyte amount that is formed **C]** Quantification of lipid formation stained with NileRed using Hoechst DNA staining presents no significant difference between PPARG agonist treated hBMSCs compared to the control during adipogenic differentiation

3.3.1.3. Unique secretory effects of PPARG activation on the osteogenic differentiation

Since the adipocytes accumulating in response to PPARG agonist treatment were shown to induce osteogenic differentiation and matrix mineralization of hBMSCs, the question remained on how the adipocytes could be in interaction with bone forming cells. To that purpose, the paracrine characteristics of adipocytes formed during osteogenic differentiation by PPARG

agonist treatment were compared to standard fat forming adipocytes and their secretory profile under PPARG agonist stimulation. It was shown, that osteo-adipocytes secrete significantly higher levels of the well-known adipokine adiponectin compared to fat forming adipocytes (**Figure 38 A, Figure 39 A**). It is important to note, that accumulated adipokines secreted by fat forming adipocytes had to be collected in expansion media to minimize adipogenic supplement driven background in the following experimental procedures. The collection of adipokines in expansion media resulted in generally lower concentration of adipokines compared to the levels measured for osteo-adipocytes. However, this aligned the level of adipokine secretion in fat forming adipocytes to the adipokine secretion levels of osteo-adipocytes. Highlighting the fact that osteo-adipocytes were represented to a lesser extend during osteogenic differentiation in comparison to the amounts of adipocytes appreciated during standard adipogenic differentiation.

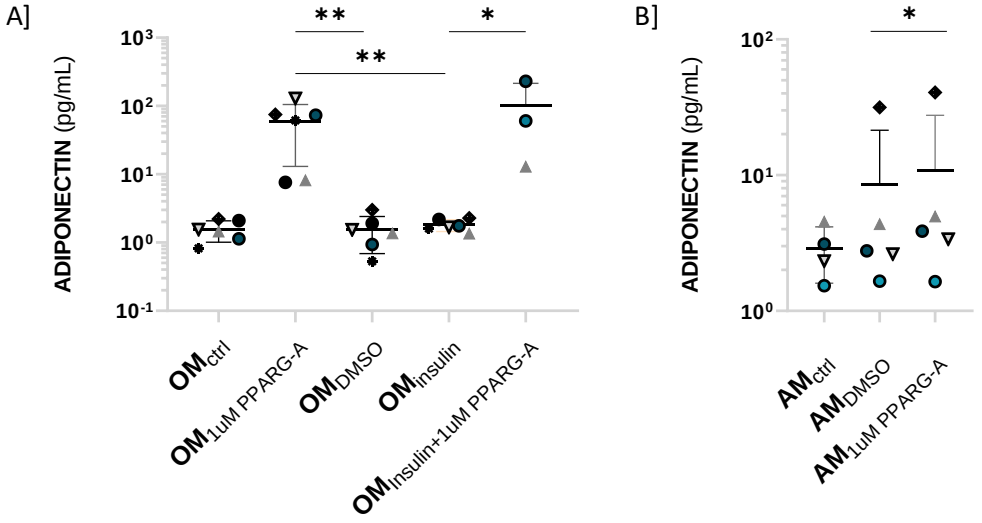

Figure 38: PPARG agonist treatment significantly increases adiponectin secretion during osteogenic differentiation and adipogenic differentiation
Data on adiponectin secretion is depicted as log10 scaled and baseline corrected values (normalized on the expansion control of each patient). Conditions shown include the OM (osteogenic differentiation), OM with PPARG agonist treatment, OM with solvent control, OM with insulin supplementation and OM with combined PPARG agonist and insulin treatment. Adipogenic conditions include the AM (adipogenic differentiation), AM with solvent control and AM with PPARG agonist treatment. **A]** Adiponectin levels significantly increase in the PPARG agonist treated osteogenic differentiation compared to the controls (ratio paired t-test p=0.0025, n=6). A significant decrease of adiponectin production is shown for the insulin treated osteogenic hBMSCs compared to the PPARG agonist treated ones (ratio paired t-test p=0.0017, n=6). The adiponectin production is further enhanced by stimulating with both PPARG agonist and insulin during osteogenic differentiation (mann whitney test p=0.0238, n=3-6) **B]** During adipogenic differentiation a smaller increase of adiponectin production is shown by PPARG agonist treatment compared to the controls (ratio paired t-test p=0.0319, n=5)

This increase of adiponectin production was particularly shown in PPARG agonist stimulated osteo-adipocytes whereas the PPARG agonist treatment of fat forming adipocytes, likewise increased adiponectin secretion to a lesser extend when compared to the adipogenic solvent control (**Figure 38 B**).

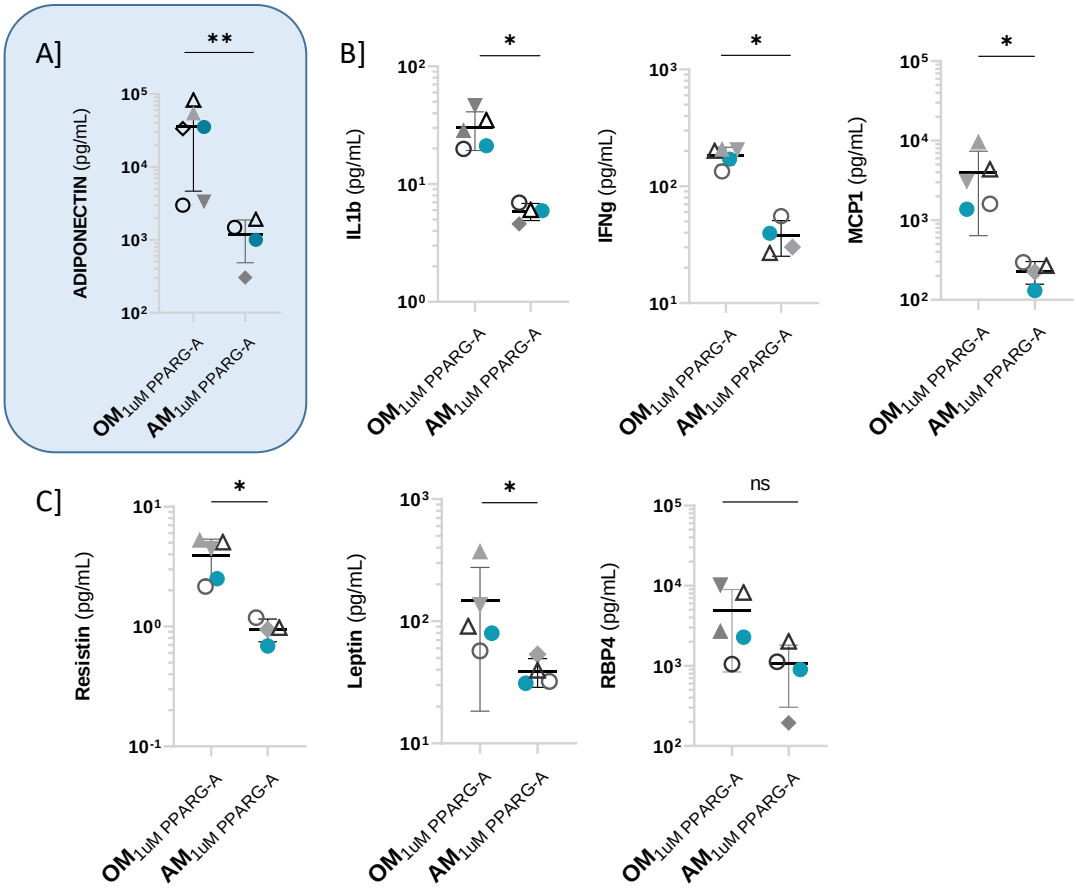

Figure 39: Adipokines markedly increased in the PPARG agonist stimulated osteo-adipocytes compared to the PPARG agonist treated fat forming adipocytes
Osteogenic media conditioned for 3 culture days is compared to adipogenic media conditioned for 24h using baseline expansion media post 14 days of adipogenic differentiation. This is done to normalize the low amount of osteo-adipocytes and their ability to fulfill paracrine purposes in the osteogenic milieu to the milieu of highly secreting fat forming adipocytes. Expansion media is used to generate a conditioned milieu which can be tested on osteogenic cells without having adipogenic differentiation supplements influencing the experimental setup. Here markedly reduced adipokine levels are shown in the fat forming adipocyte milieu. All data plots are shown with log10 axes and in individually colored symbols according to each patient **A]** Adiponectin is significantly increased in osteogenic cultures treated with PPARG agonist rosiglitazone (Mann Whitney p= 0.0095, n=4-6) **B]** Cytokines such as IL1b, IFNg and the chemokine MCP1 are significantly upregulated during osteogenic cultures stimulated by PPARG agonist rosiglitazone (Mann Whitney p=0.0159, n=4-6) **C]** Resistin and leptin are significantly upregulated and the adipokine RBP4 is likewise upregulated in the osteo-adipocyte milieu compared to the fat forming adipocyte milieu (Mann Whitney p=0.0159, n=4-6)

Summarized, the levels of all related adipokines such as interleukin 1 b (IL1b), IFNg and resistin were significantly increased in the milieu of osteo-adipocytes (**Figure 39 B**). Other adipokines such as monocyte chemoattractant protein 1 (MCP1), retinol binding protein 4 (RBP4) and leptin were markedly upregulated in the milieu of osteo-adipocytes (**Figure 39 C**). However, when focusing on the osteogenic compartment. The adiponectin production of the PPARG agonist stimulated osteogenic hBMSCs showed significantly upregulated adiponectin levels compared to the osteogenic control (**Figure 38 A, Figure 40 A**). Most importantly, inflammatory adipokines such as MCP1 and IL1b were significantly downregulated in the

PPARG agonist driven osteogenic milieu while being steady during osteogenic control differentiation (**Figure 40 B**).

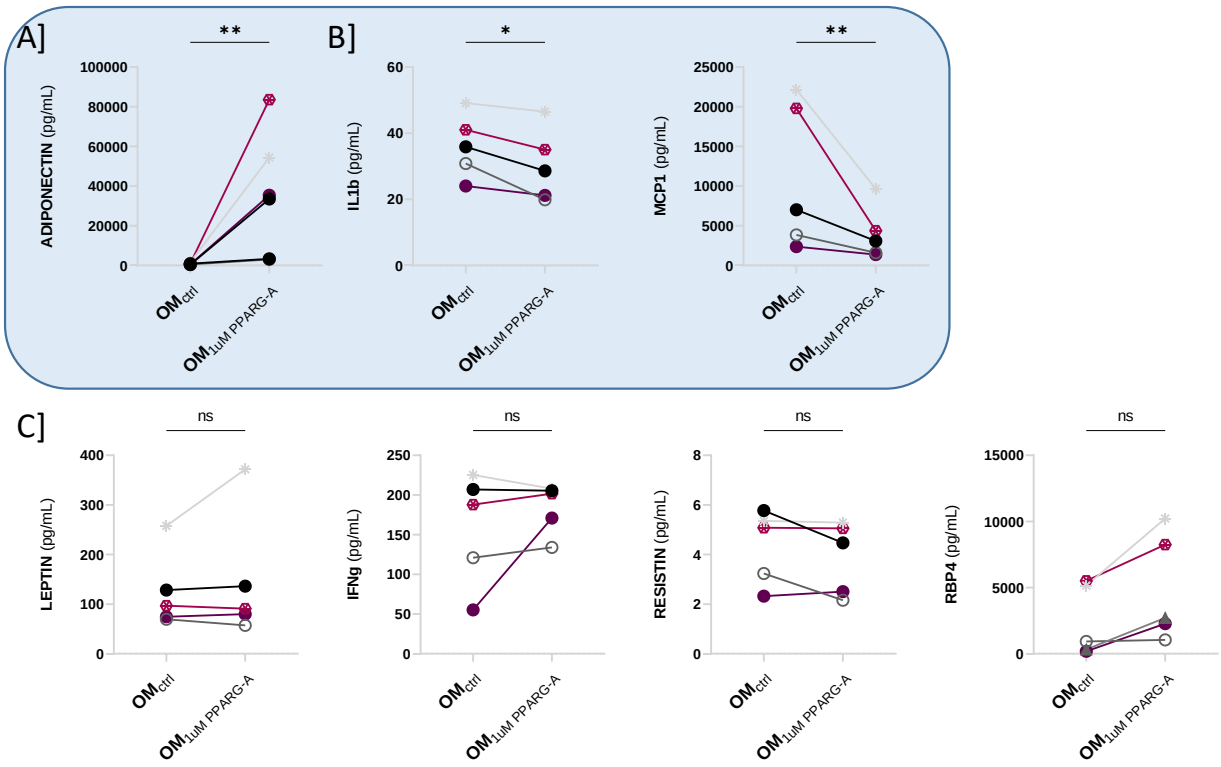

Figure 40: PPARG agonist stimulated osteo-adipocytes have a significantly different paracrine capacity compared to osteogenic differentiated hBMSCs without PPARG agonist induced osteo-adipocytes
Osteogenic medium conditioned for 3 culture days is compared to osteogenic media containing PPARG agonist stimulated osteo-adipocytes. A differential pattern of adipokine secretion can be shown in the PPARG treated osteogenic condition. **A]** A significant induction of adiponectin secretion is shown in the PPARG agonist stimulated osteo-adipocytes (ratio paired t-test p=0.0023, n=6) **B]** The pro-inflammatory cytokine IL1b and the chemokine MCP1 are significantly downregulated in the PPARG agonist treated osteo-adipocyte milieu compared to the osteogenic control (ratio paired t-test p=0.0376 and p=0.0045, n=6) **C]** Other adipokines such as leptin, IFNg, resistin and RBP4 were unaffected by the PPARG agonist stimulation during osteogenic differentiation and the resulting osteo-adipocyte accumulation

This was not the case when supplementing the osteogenic culture with insulin. In detail, the adiponectin levels were not induced in the insulin treated osteogenic conditions and inflammatory adipokines such as MCP1 and IL1b were significantly upregulated (**Figure 38 A, Figure 41**). This was highlighted as further delineate of the PPARG agonistic effects from the insulin driven effects during osteogenic differentiation.

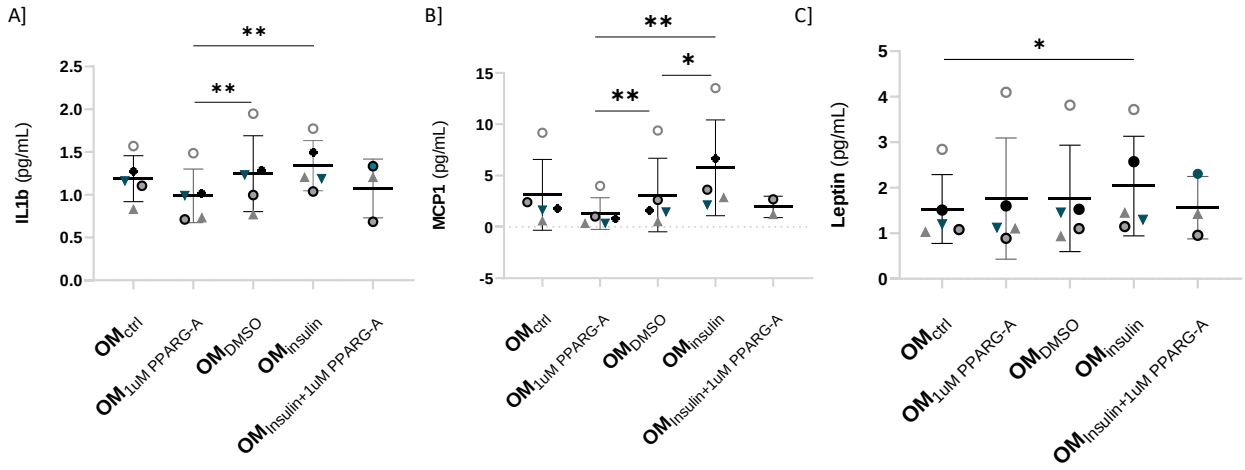

Figure 41: PPARG agonist treatment during osteogenic differentiation results in opposing adipokine secretion when compared to insulin supplemented osteogenic differentiation
IL1b and MCP1 are shown as significantly different regulated adipokines when comparing insulin and PPARG agonist driven osteogenic induction. Osteogenic differentiation is shown for the control, PPARG agonist stimulation, solvent control, insulin supplementation and both PPARG agonist stimulation and insulin supplemented condition. All data plots are normalized on the expansion media control and shown with log10 axes individually colored according to patient specific effects **A]** IL1b is significantly downregulated in the PPARG agonist treated osteogenic differentiation whereas an upregulation by supplementing osteogenic cultures with insulin is shown (ratio paired t-test p $OM_{PPARG-A}$ + OM_{DMSO} =0.0098 and p $OM_{PPARG-Ai}$ + $OM_{insulin}$=0.0066, n=5) **B]** The chemokine MCP1 is significantly downregulated by PPARG agonist treatment and significantly upregulated by insulin treatment during osteogenic differentiation (ratio paired t-test p=0.0062 and p=0.0488, n=5) **C]** Leptin is significantly increased in insulin driven osteogenic differentiation whereas no significant change is observed in the PPARG agonist treatment during osteogenic differentiation (ratio paired t-test p=0.0426, n=5)

3.3.1.4. **Unique secretory effects of fat forming adipocytes on the osteogenic differentiation**

As described in the previous chapter, the secretory impact of osteo-adipocytes is a crucial partaker in the induction of enhanced osteogenic differentiation. However, it is important to distinguish between osteo-adipocytic secretome, which characterizes the bone environment, and fat forming adipocytic secretome, which represents the fat environment. When changing the focus to the PPARG agonist treated fat forming adipocytes the adipokine secretion pattern differs from the pattern of osteo-adipocytes. Initially, PPARG agonist treated fat forming adipocytes secreted significantly more adiponectin compared to the control when analyzing single patient driven secretion. The amounts of secreted adiponectin after 14 days of adipogenic differentiation were markedly lower compared to the levels in the PPARG agonist treated osteogenic differentiated hBMSCs. It has to be taken into account, that the reduced levels were steered by the prior change of adipogenic media to expansion media, resulting in the necessary depletion of adipogenic supplements for the further usage of this conditioned media during the osteogenic differentiation. Nevertheless, no significant decrease of IL1b and MCP1 could be detected in the PPARG agonist treated fat forming adipocyte milieu. It is important to mention, that PPARG agonist treatment of fat forming adipocytes significantly

increased obesity associated RBP4 levels whereas no change in the amount of this adipokine could be shown in the osteo-adipocyte milieu. Summarized, the fat forming adipocytes are marked by a pro-inflammatory secretory milieu. Pro-inflammatory, obesity associated secretion marks the secretory profile of fat forming adipocytes with rather detrimental effects.

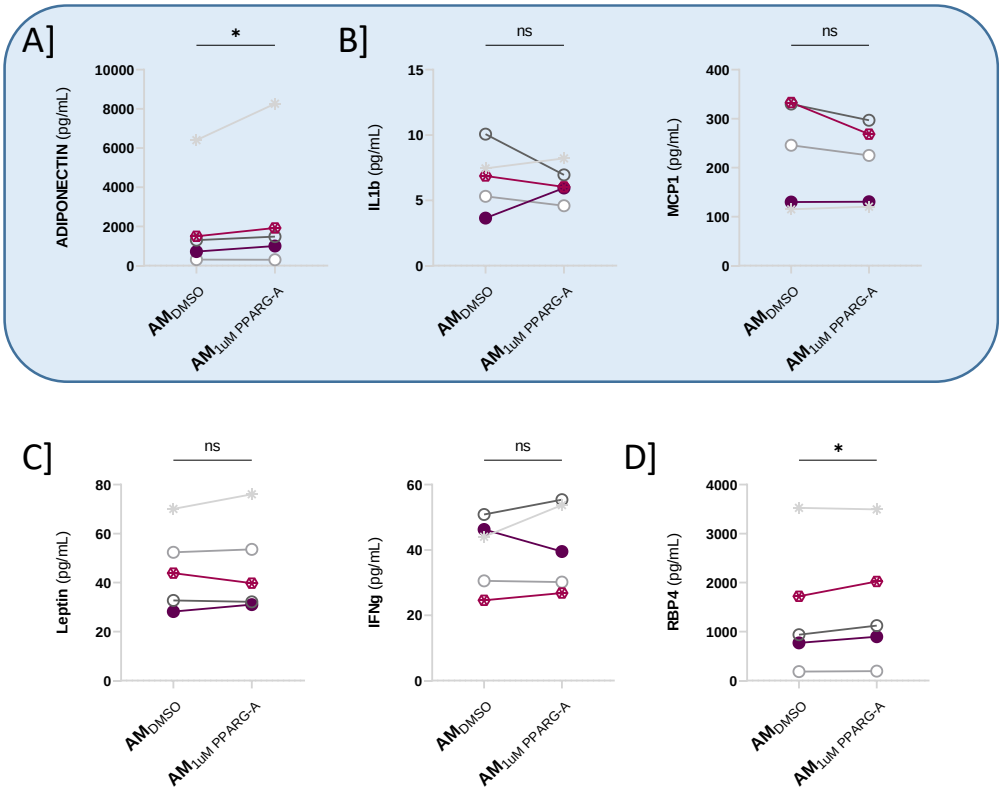

Figure 42: PPARG agonist treatment of fat forming adipocytes results in the increase of adiponectin and RBP4 without influencing the secretion of pro-inflammatory cytokines such as IL1b and MCP1
Conditioned media from fat forming adipocytes differentiated for 14 days with and without PPARG agonist treatment have been harvested after 24h of adipokine accumulation in expansion media. This results in generally lower adipokine concentrations compared to the levels secreted by osteo-adipocytes. Adipokine levels of individual patient hBMSCs are shown for the adipogenic solvent control and PPARG agonist treated fat forming adipogenic media. The solvent control is shown in order to represent the impact of DMSO on the adipogenic differentiation **A]** PPARG agonist treatment of fat forming adipocytes results in a marginal but similar adiponectin increase as compared to the one shown in osteo-adipocytes (ratio paired t-test p=0.023, n=5) **B]** No significant change is depicted for the pro-inflammatory cytokine IL1b and chemokine MCP1 when stimulating fat forming adipocytes with PPARG agonist rosiglitazone (ratio paired t-test p=0.9 and p=0.19, n=5) **C]** No significant regulation of leptin and IFNg secretion by fat forming adipocytes is identified when stimulating with PPARG agonist rosiglitazone (ratio paired t-test p=0.65 and p=53, n=5) **D]** RBP4 secretion is significantly upregulated by PPARG agonist treatment of fat forming adipocytes (ratio paired t-test p=0.04, n=5)

The lower levels of adiponectin secretion of fat forming adipocytes, the steady levels of IL1b and MCP1 as well as the increased RBP4 levels were shown to not influence an increased osteogenic differentiation and mineralization of hBMSCs, when fat forming adipogenic media was supplemented during differentiation. It was identified, that fat forming adipogenic media in general has an effect on osteogenic processes resulting in a faster mineralization of individual patient derived hBMSCs (**Figure 43**).

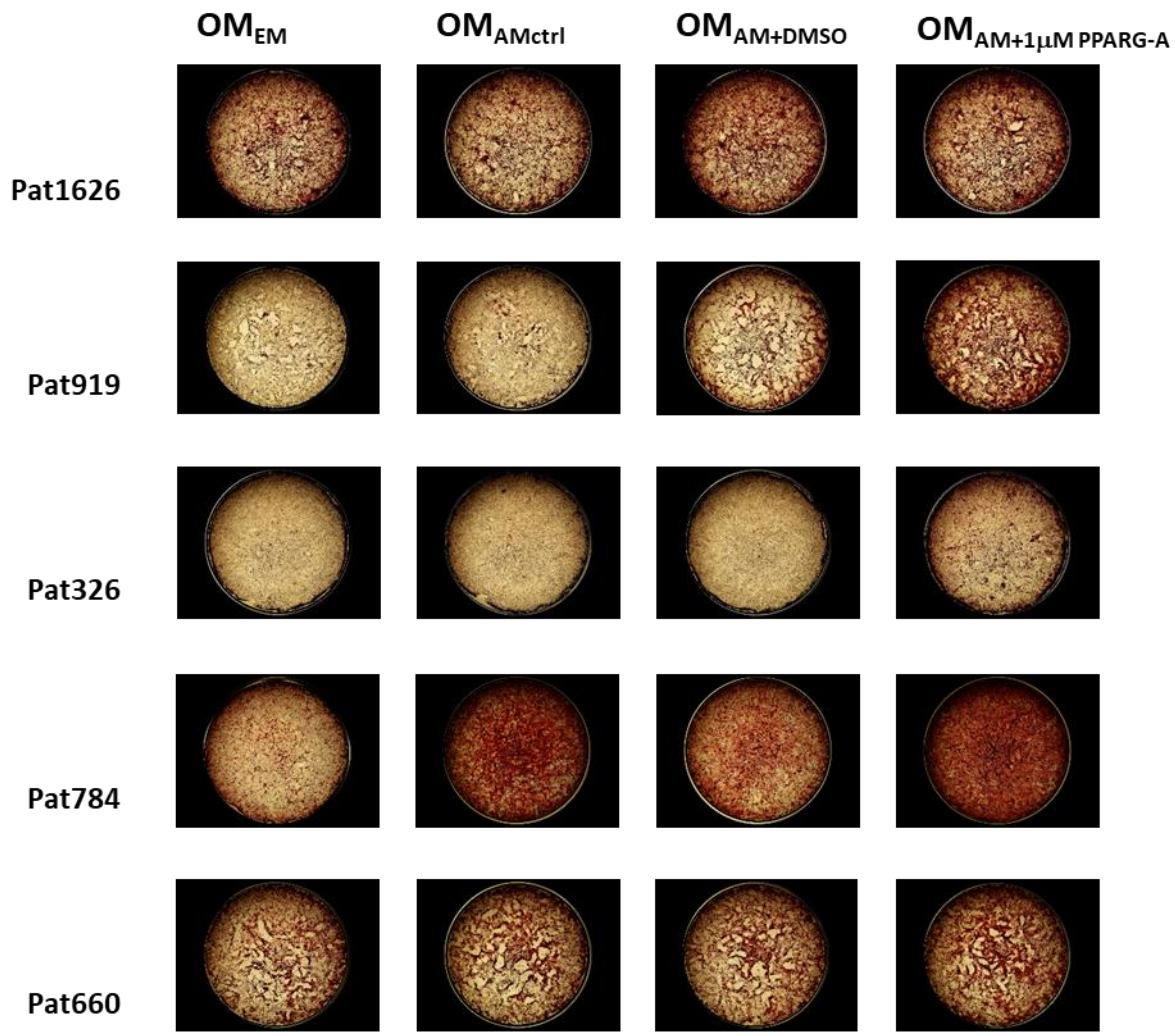

Figure 43: Individual patient specific effects are presented and show a steady increase of mineralization in hBMSC differentiated into the osteogenic lineage while supplementing adipogenic media
Osteogenic differentiation and mineralization capacity of hBMSCs under adipogenic media stimulus is depicted and individual patient specific effects are shown on day 14 and day 21. The stimulation with adipogenic media steers a higher mineralization and calcification of hBMSCs but no specific increase is shown for the supplementation of adipogenic media of prior PPARG agonist stimulated adipogenic hBMSCs. Pat1626 and Pat660 show no significant increase of mineralization by adipogenic media stimulation. Pat784, Pat919 and Pat326 show an elevated calcification during osteogenic differentiation with pre-conditioned adipogenic media. Adipogenic media is shown to harbor no detrimental influence on the osteogenic differentiation capacity of hBMSCs

Osteogenic differentiation and mineralization was shown to be steadily ongoing in all conditions and was not diminished by using fat forming adipogenic media during a differentiation period of 21 days.

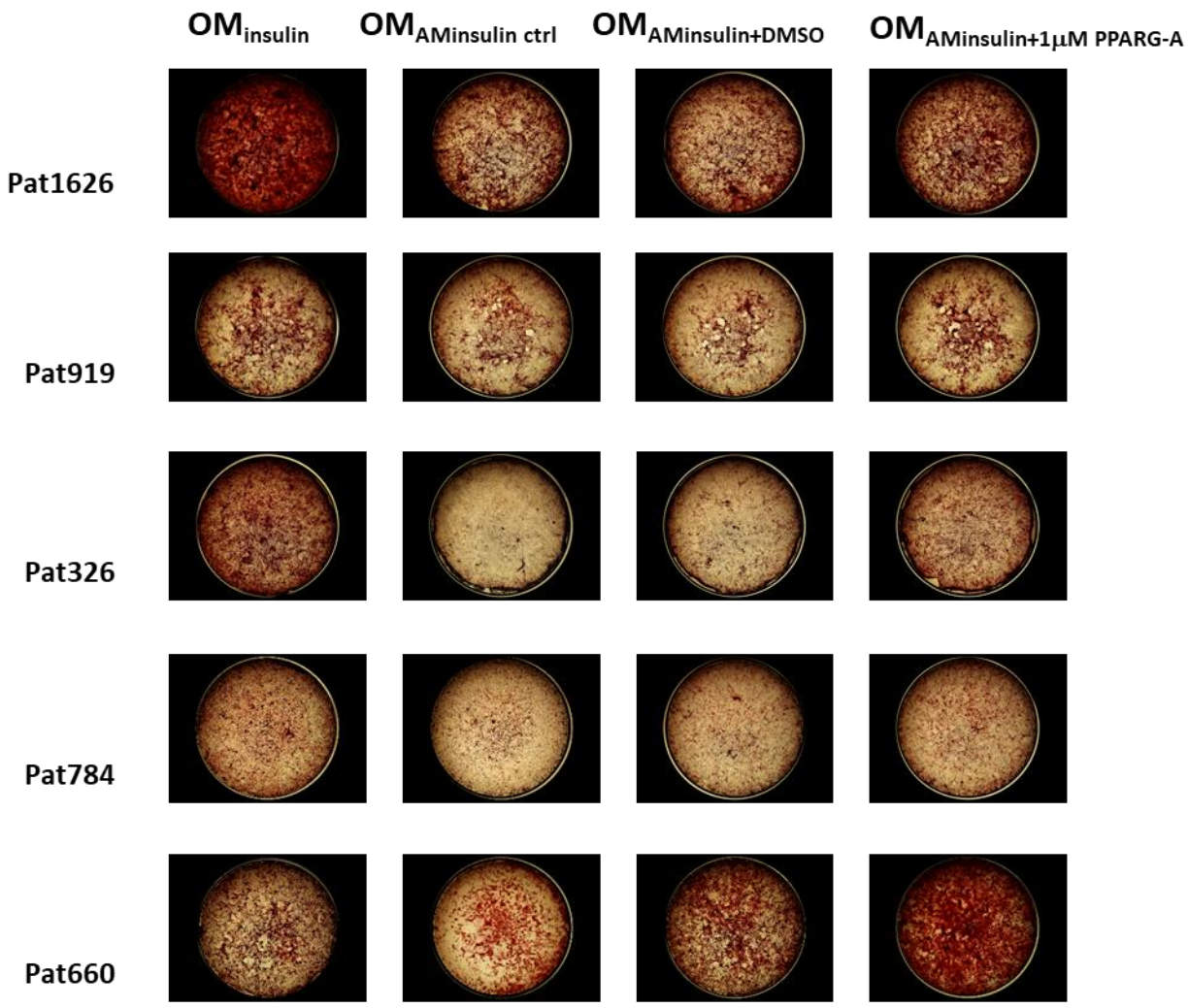

Figure 44: Insulin driven increase of osteogenic mineralization is reduced by additional adipogenic media but PPARG agonist pre-conditioned media shows a steadily increase of mineralization potential
Osteogenic potential is depicted by visualizing the mineralized matrix of individual patient hBMSCs on day 14 and day 21 of differentiation. The highest increase of mineralization capacity is shown by the standard osteogenic differentiation under insulin supplementation. An exception is described by Pat660 showing a high increase of mineralization during osteogenic differentiation with the PPARG agonist pre-stimulated adipogenic media. The other patients are characterized by an increase of mineralization under osteogenic differentiation with PPARG agonist pre-stimulated adipogenic media. Individual patient specific differentiation capacity is likewise depicted by varying mineralization of the osteogenic matrix

The same effect was shown by further supplementing insulin in combination with fat forming adipogenic media with and without PPARG agonist pre-stimulation. The effect of insulin driven osteogenic mineralization was rather decreased by the additional supplementation of fat forming adipogenic media during differentiation. No significant change in the osteogenic potential could be shown by the supplementation of fat forming adipogenic media in all conditions when normalized on cell number (**Figure 45 A, B, C, D**). Thus, suggesting the presence of osteo-adipocytes and their secretome to harbor pronounced pro-osteogenic effects compared to the secretome of fat-forming adipocytes.

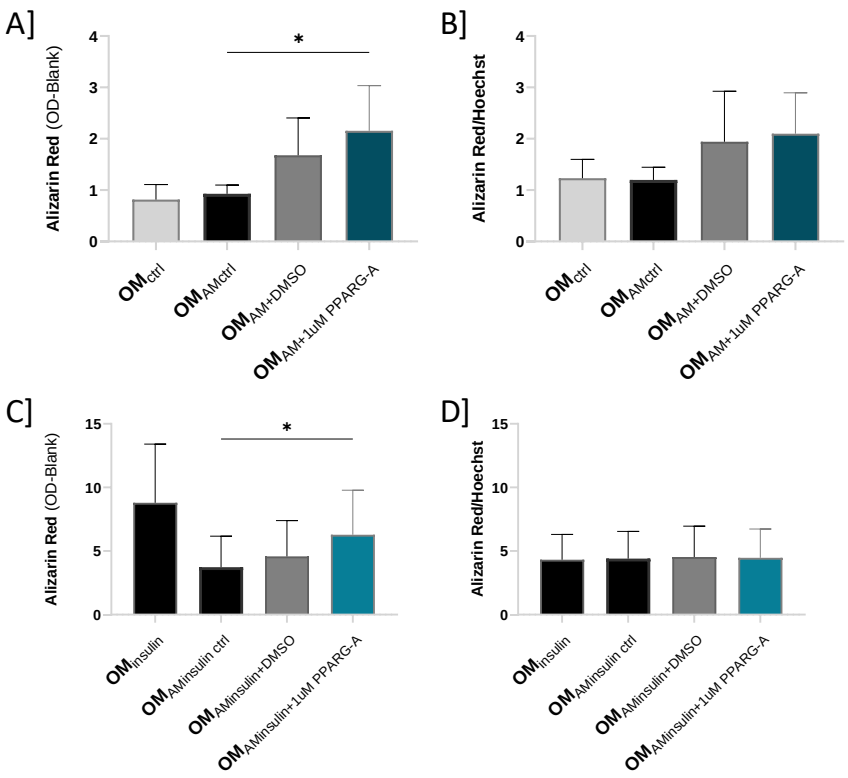

Figure 45: Fat forming adipogenic media has no significant impact on the osteogenic differentiation capacity of hBMSCs regardless of PPARG agonist treatment
Osteogenic differentiation potential and mineralization of hBMSCs under a 1:2 ratio of osteogenic and adipogenic media with and without PPARG agonist stimulation is depicted by alizarin red staining on day 14 and day 21. The calcification is shown as normalized value on cell number (Hoechst DNA staining). Different conditions are compared such as osteogenic differentiation with and without insulin as positive control, osteogenic differentiation using adipogenic media without any supplementation and osteogenic differentiation using adipogenic media with solvent or PPARG agonist stimulation. All conditions are highlighted again with additional supplementation of insulin. All values are baseline corrected on osteogenic differentiation media in a 1:2 ratio with expansion media as control **A]** A steady mineralization potential of osteogenic differentiated hBMSCs is shown even under 1:2 supplementation with adipogenic control medium with a significant increase of mineralization when supplementing with PPARG agonist stimulated adipogenic media (ratio paired t-test p=0.0462, n=6). This mineralization effect is redundant when comparing PPARG treated adipogenic media and solvent control (ratio paired t-test p=0.128, n=6) **B]** When normalizing the calcification on day 14/day 21 on the cell number, no significant change is depicted for the supplementation of osteogenic media with fat forming adipogenic derived media **C]** A similar effect of adipogenic media supplementation is shown for insulin steered osteogenic differentiation. Here a significant increase of mineralization is shown for the supplementation of PPARG agonist treated adipogenic media compared to the adipogenic control media (ratio paired t-test p=0.0457, n=6) whereas this effect is reduced when comparing PPARG agonist treatment with the solvent control **D]** The enhanced mineralization by adipocyte conditioned media is negligible under normalized conditions

3.3.2. PPARG as driving force of metabolic changes in osteogenic hBMSCs

As shown in the previous chapters (**3.3.1.2, 3.3.1.3**), PPARG activation is the key factor to induce adipocytes during osteogenic differentiation. To investigate the effects of those osteo-adipocytes regarding metabolic regulation and energy homeostasis, osteogenic differentiated hBMSCs were analyzed for their mitochondrial function. As a first step, mitochondrial function for different time points of osteogenic control differentiation was assessed, defining the baseline profile of energy metabolism. Osteogenic differentiation has been shown to coincide with the induction of oxidative phosphorylation. In this study, it was highlighted that hBMSCs

change from a high glycolytic activity towards higher oxidative respiration when osteogenic differentiation is initiated. Hereby, the oxidative consumption/extracellular acidification rate (OCR/ECAR) ratio of hBMSCs driven towards the osteogenic phenotype increases depending on the progress of differentiation. It is important to note, that on day 5 of osteogenic induction and differentiation a significant increase of the OCR/ECAR ratio was depicted (**Figure 46 A, B**). In addition, when solely investigating the OCR and ECAR levels a significant increase in the oxidative consumption rate was shown already on day 2 of differentiation (**Figure 47 A**). This increased OCR/ECAR ratio repealed on day 10 of osteogenic differentiation (**Figure 46 C, Figure 47 C**).

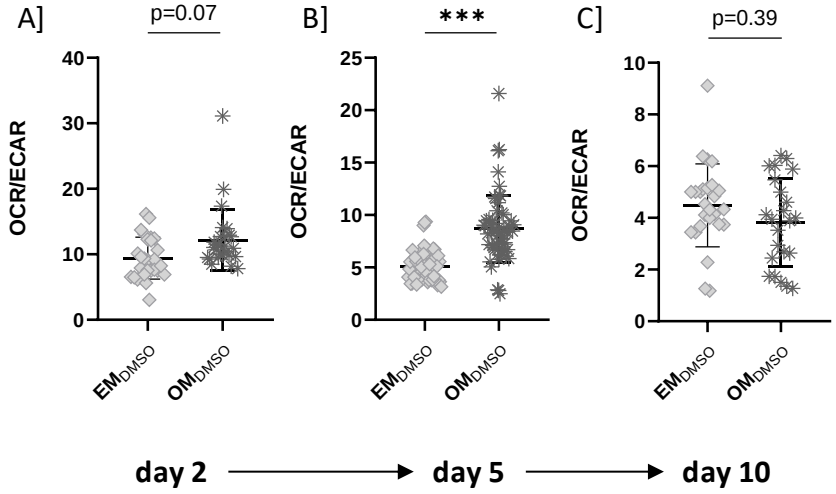

Figure 46: hBMSC undergoing osteogenic differentiation represent increasing OCR/ECAR ratios on day 5 and enhanced oxidative phosphorylation in early stages of osteogenic differentiation
An increase in oxidative consumption and a decrease of extracellular acidification is depicted for early differentiation time points describing a higher oxidative phosphorylation capacity of hBMSCs during the initiation of osteogenic differentiation. Data graphs represent the hBMSCs under expansion with solvent control supplementation (light grey) compared to the osteogenic differentiated hBMSCs under solvent supplementation (dark grey). Patient related effects and technical replicates of importance while using the seahorse analyzer are highlighted by including all data points into the figure. For statistical significance testing, the mean of all replicates of each patient is taken into account **A]** An increasing trend showing higher OCR/ECAR ratios is already depicted on day 2 after the initial induction of osteogenic differentiation (ratio paired t-test p=0.077, n=3) **B]** A significant peak of the OCR/ECAR ratio is shown on day 5 of early osteogenic differentiation compared to the expansion control (ratio paired t-test p=0.0002, n=6) **C]** The osteogenic driven increase of the OCR/ECAR ratio repeals on day 10 when mineralization and calcium deposition starts (ratio paired t-test p=0.39, n=3)

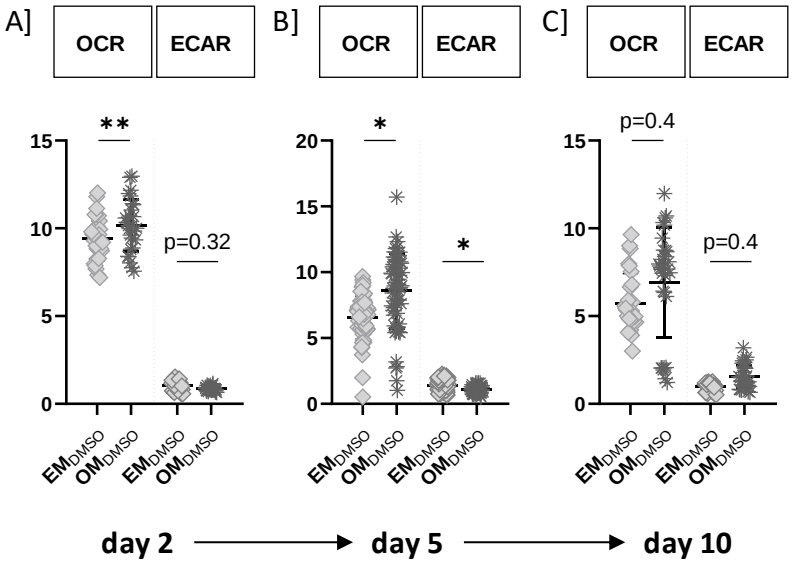

Figure 47: hBMSC undergoing osteogenic differentiation show an early increase of OCR but no decrease of ECAR on day 2 after osteogenic induction

In addition to the OCR/ECAR ratios, the specific effects on each parameter of mitochondrial respiration is depicted for day 2, day 5 and day 10 comparing expansion control (light grey) with osteogenic differentiation under solvent supplementation (dark grey). Data is shown including technical replicates, tested for statistical significance using the replicate mean of each patient **A]** HBMSC show a significantly increased OCR on day 2 after initial osteogenic induction paired with no significant change in the extracellular acidification (ratio paired t-test p=0.0013, n=3) **B]** On day 5 a significant increase in OCR and decrease in ECAR is shown for all patients (ratio paired t-test p=0.0426 and p=0.0023, n=6) **C]** Later osteogenic time-points such as day 10 where calcification and matrix mineralization starts represent trends of higher OCR and ECAR (ratio paired t-test p=0.47 and p=0.42, n=3)

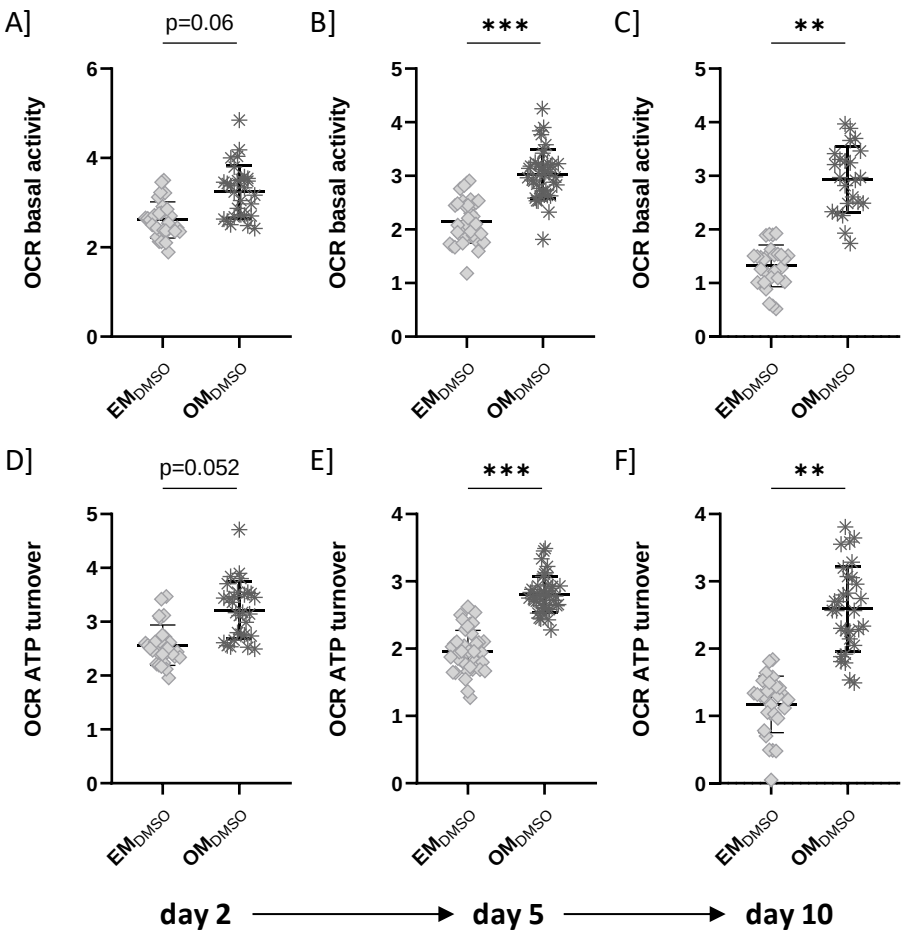

Figure 48: A steadily increasing oxygen consumption favoring cellular ATP demand and a higher ATP production by mitochondria is shown for hBMSCs under osteogenic differentiation
The OCR basal activity is represented as the oxygen consumption needed for cellular ATP demand and ATP turnover is displayed as mitochondrial produced ATP required for the activity of hBMSCs during osteogenic differentiation. Data is shown including technical replicates, tested for statistical significance using the mean of all replicates of each patient. **A] D]** OCR on day 2 after initial osteogenic induction represents a trend of increased basal activity and ATP turnover (ratio paired t-test p=0.061 and p=0.052, n=3) **B] E]** A significant increase in cellular ATP demand and mitochondrial production is depicted for day 5 of early osteogenic differentiation (ratio paired t-test p=0.0001 and p=0.0002, n=6) **C] F]** On day 10 of osteogenic differentiation the effect of day 5 is mirrored and a significant increase basal activity and ATP turnover is shown (ratio paired t-test p=0.0017 and p=0.0016, n=3)

In addition, a significant increase of basal respiration was shown presenting a higher energy demand of the cell under baseline osteogenic conditions especially on day 5 and day 10 of differentiation (**Figure 48 B, C**). Further, a higher ATP turnover was identified for osteogenic differentiated hBMSCs ascending until day 10 of differentiation (**Figure 48 E, F**). The higher amount of ATP production by mitochondria to fulfill the cells needs during osteogenic differentiation was depicted. In detail, day 0 was defined as initial induction of the osteogenic transcription machinery and the time frame between day 7 and day 10 was described as early osteogenic time-points were the first calcium depots started to form. In the latter, a significant increase of oxidative spare capacity was determined underlining the increased flexibility and

capacity of hBMSCs to respond to the high energy demand during osteogenic differentiation (**Figure 49**).

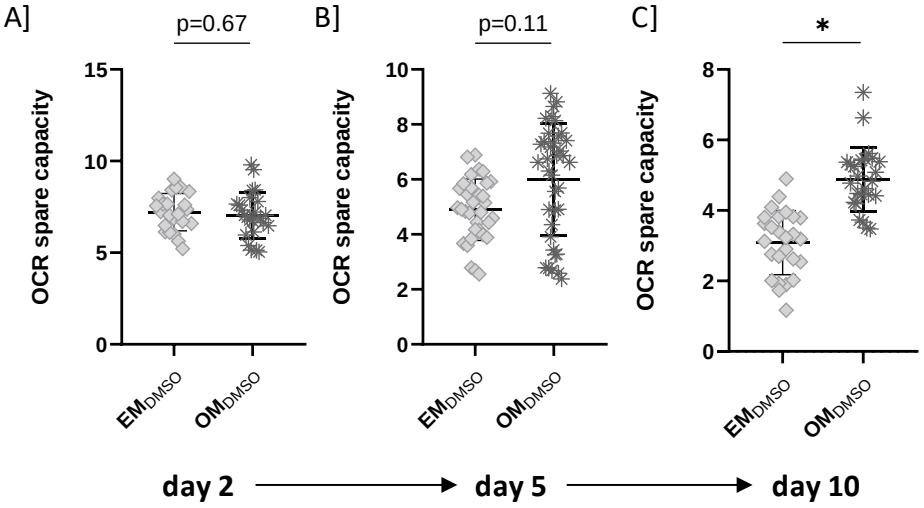

Figure 49: Later osteogenic differentiation time-points where mineralization and calcium deposition starts are accompanied by a higher oxidative spare capacity
OCR spare capacity is shown as the cells ability to act under a high energetic demand such as rebuilding bone and is representing the fitness of hBMSCs under osteogenic differentiation. Data is shown including technical replicates, tested for statistical significance using the replicate mean of each patient. **A] B]** No change in oxidative spare capacity is shown on day 2 and day 5 of early osteogenic differentiation (ratio paired t-test p=0.679 and p=0.113, n=3-6) **C]** A significant increase of OCR spare capacity is show for day 10 of osteogenic differentiation representing the capacity of hBMSCs during high energetic demand such as osteogenic mineralization (ratio paired t-test p=0.0386, n=3)

3.3.2.1. **Unique effects of PPARG activation on the oxidative respiration capacity (OCR)**

The question remained, if PPARG activation could enhance oxidative phosphorylation and other features e.g. OCR spare capacity, enabling an improved energetic supply for osteogenic differentiation. PPARG agonist treatment during osteogenic differentiation was shown to elevate the high OCR/ECAR ratios starting from day 10 of osteogenic differentiation (**Figure 50**). It is notable, that PPARG agonist treatment in early days of differentiation, on day 2 and day 5 respectively, resulted in trending reduction to steady state of the OCR/ECAR ratio compared to the osteogenic differentiation control. Hereby, suggesting an additional coinciding increase of glycolysis and OXPHOS. The singular effects of the PPARG agonist treatment on the OCR and ECAR levels did not show any significant changes (not shown).

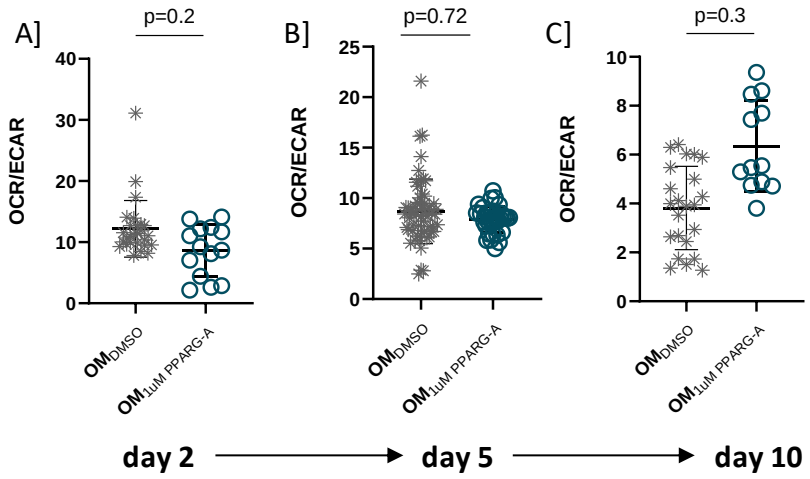

Figure 50: PPARG agonist treatment of hBMSCs positively impacts the OCR/ECAR ratio during osteogenic differentiation
The OCR/ECAR ratio is depicted for the osteogenic differentiation with solvent control (dark grey) compared to the PPARG agonist stimulated osteogenic differentiation (cyan). Data is shown including technical replicates, tested for statistical significance using the replicate mean of each patient. **A] B]** On day 2 after osteogenic initiation the PPARG agonist treated hBMSCs show a decrease in the OCR/ECAR ratio which is outbalanced on day 5 of osteogenic differentiation (ratio paired t-test p=0.21 and p=0.72, n=3-6) **C]** On day 10, a patient specific elevation of the OCR/ECAR ratio is shown for osteogenic differentiated hBMSCs when treated with PPARG agonist rosiglitazone (ratio paired t-test p=0.36, n=3) The displayed effects are driven by increased OCR values rather than ECAR values, which are shown to maintain stable (OCR increase shown in supplementary figure, ratio paired t-test p=0.23, n=3)

Interestingly, when evaluating the PPARG agonist treatment and its influence in the expansion media control a stable OCR/ECAR ratio was shown on day 2 and day 5 of culture with no significant change induced by PPARG agonist treatment. On day 10 of expansion, PPARG agonist treatment induced a significant increase in the OCR/ECAR ratio of expanded hBMSCs compared to osteogenic differentiated hBMSCs (**Figure 51**). When comparing the singular effects on the OCR and ECAR levels no significant change between separately analyzed oxidative consumption was shown for the expanded hBMSCs treated with PPARG agonist rosiglitazone (**Figure 52**).

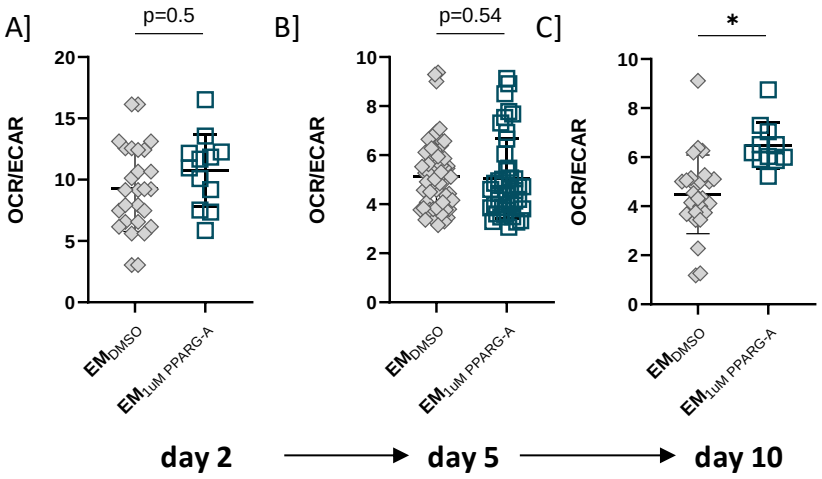

Figure 51: PPARG agonist treatment of hBMSCs during expansion results in a significant increase of the OCR/ECAR ratio on day 10 of expansion
The OCR/ECAR ratio is shown for PPARG agonist treated hBMSC under expansion (cyan) compared to the expansion with solvent control (light grey). Data is shown including technical replicates, tested for statistical significance using the replicate mean of each patient. A] B] On day 2 and day 5 of hBMSCs expansion no significant change is depicted for PPARG agonist stimulated hBMSCs (ratio paired t-test p=0.53 and p=0.54, n=3-6) C] A significant upregulation of the OCR/ECAR ratio is shown on day 10 of expansion when comparing PPARG agonist stimulated hBMSCs with hBMSCs expanded under the influence of the solvent control (ratio paired t-test p=0.02, n=3)

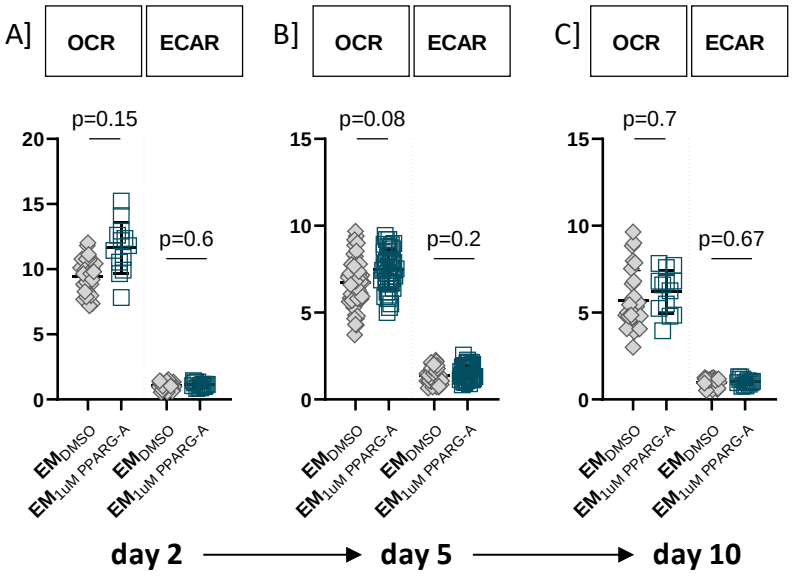

Figure 52: PPARG agonist treatment of expanded hBMSCs shows increasing OCR but no impact on ECAR
The individual OCR and ECAR values are shown for PPARG agonist treated hBMSCs under expansion (cyan) compared to expanded hBMSCs under solvent control (light grey). Data is shown including technical replicates, tested for statistical significance using the replicate mean of each patient. **A]** On day 2, an upregulation of the OCR value and no impact on the extracellular acidification is shown when stimulating with PPARG agonist rosiglitazone (ratio paired t-test p=0.15 and p=0.65, n=3) **B]** The PPARG agonist driven changes in the OCR and ECAR values on day 2 are mirrored on day 5, where an increased OCR is shown for PPARG agonist stimulated hBMSCs (ratio paired t-test p=0.08 and p=0.21, n=6) **C]** On day 10 of expansion the individual PPARG agonist driven effects on the OCR value decrease (ratio paired t-test p=0.71 and p=0.67, n=3)

It is of importance, that the elevated OCR/ECAR ratio in PPARG agonist treated hBMSCs of osteogenic cultures was accompanied by an increased oxidative spare capacity identified on day 10 of osteogenic differentiation (**Figure 53**). It was striking to show that especially hBMSCs of patients harboring a diminished capacity to differentiate into the osteogenic lineage could be rescued by the PPARG agonist driven effect of enhancing the OCR/ECAR ratio as well as the oxidative spare capacity (**Figure 54 C, D**).

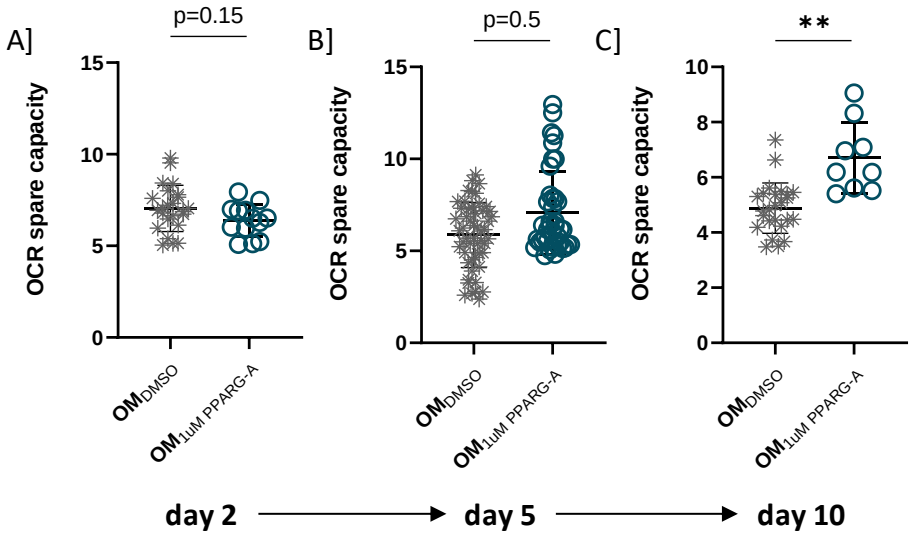

Figure 53: PPARG agonist treatment results in a significant elevation of oxidative spare capacity and with that a higher energetic fitness is shown at later osteogenic stages
The capacity of hBMSCs to respond to a high energetic demand while differentiating towards the osteogenic lineage is depicted to significantly increase in hBMSCs under PPARG agonist treatment (cyan) when compared to the osteogenic differentiation using a solvent control (dark grey). Data is shown including technical replicates, tested for statistical significance using the replicate mean of each patient. **A]** HBMSCs on day 2 of osteogenic differentiation initially show a decrease of oxidative spare capacity when compared to the control (ratio paired t-test p=0.15, n=3) **B] C]** On day 5 of early osteogenic differentiation, the spare capacity is depicted to increase by PPARG agonist treatment until day 10, where a significantly increased oxidative spare capacity is displayed while the first mineralization and calcium deposition takes place (ratio paired t-test p=0.50 and p=0.0016, n=3-6)

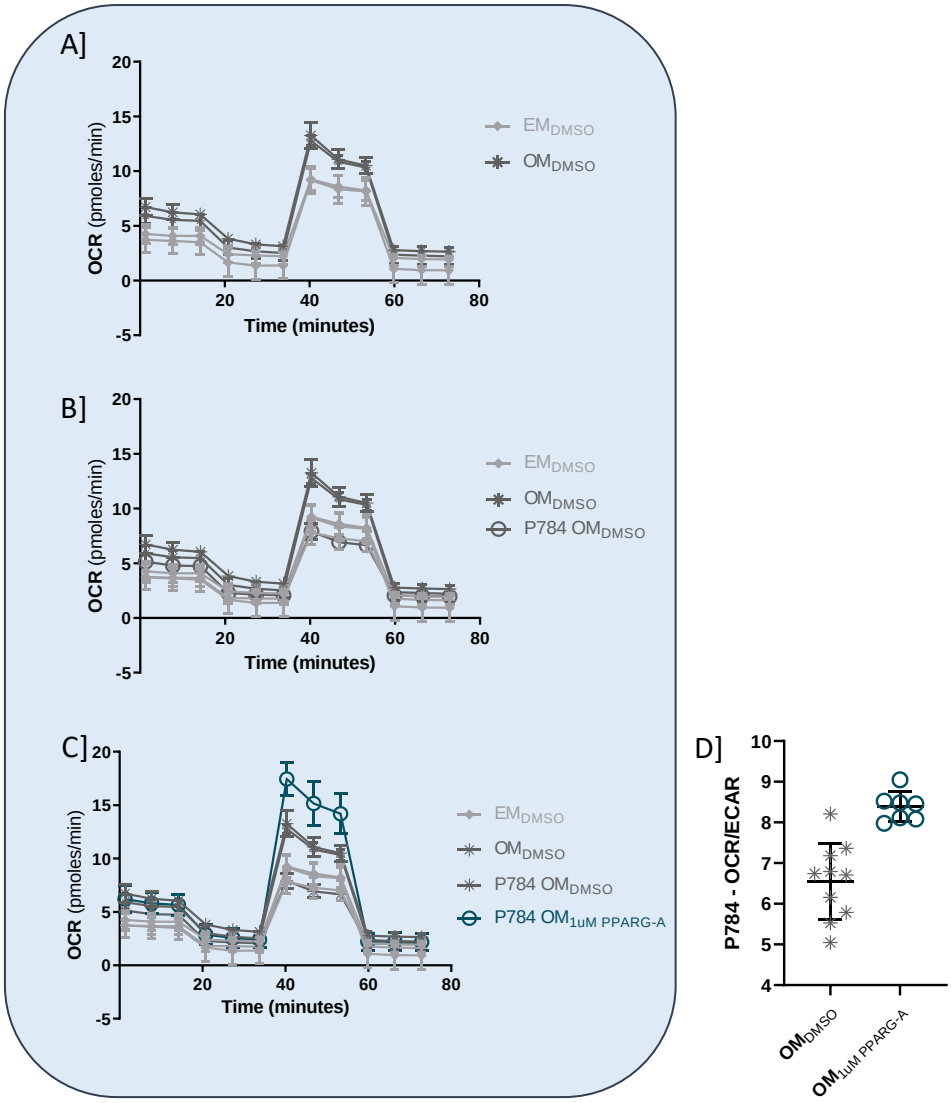

Figure 54: PPARG agonist treatment enables the induction of a beneficial metabolic OCR increase in patients with poor osteogenic differentiation capacity
Three patients are depicted for their individual oxidative capacity measurements throughout the mitochondrial stress test: The first three data points represent the basal activity of each patient, followed by three measurements of ATP synthase inhibition using oligomycin, three measurements of mitochondrial membrane disruption using FCCP and three measurements of the collapsed mitochondrial respiration by using complex I and III inhibitors rotenone and antimycin A. The basal activity is an important measurement combined with the oligomycin driven calculation of ATP linked respiration, the FCCP determined maximal respiration and spare capacity as well as the rotenone/antimycin A analyzed non-mitochondrial respiration. Data points are shown as normalized OCR values per µg DNA. HBMSCs on day 5 of expansion (light grey) as well as osteogenic differentiation are shown (dark grey), highlighting the PPARG agonist treated patient Pat784 and its OCR during osteogenic differentiation (cyan). **A]** During osteogenic differentiation elevated levels of OCR are displayed for patient Pat660 and Pat346 compared to the expansion control **B]** Osteogenic differentiated hBMSCs of patient Pat784 are shown as non-responsive while maintaining low OCR levels **C]** When stimulating hBMSCs of Pat784 with PPARG agonist rosiglitazone, the OCR is increased in comparison to the osteogenic control differentiation. PPARG agonist treatment steers a similar increased OCR in Pat784 as for the other two patients Pat660 and Pat346 during standard osteogenic differentiation **D]** The OCR/ECAR ratio of Pat784 on day 5 of osteogenic differentiation is likewise increased by PPARG agonist treatment highlighting a rescue for osteogenic differentiation driven by PPARG agonist stimulation

Since PPARG agonist treatment induces insulin sensitivity in hBMSCs and insulin is known as an important signaling molecule in energy metabolism, the impact of insulin and the combination of insulin/PPARG agonist on the mitochondrial function was assessed. In contrast

to the sole PPARG agonist treatment, the impact of insulin on the oxidative respiration during osteogenic differentiation was shown to maintain steady OCR/ECAR ratio in hBMSCs. On day 2, the OCR/ECAR ratio was significantly decreased by insulin treatment (**Figure 55 A**). A significant increase of the oxidative consumption rate was shown for day 5 of osteogenic differentiation with supplementation of insulin and insulin in combination with PPARG agonist treatment (**Figure 55 B**). On day 10, insulin supplementation induced a decreased OCR/ECAR ratio when compared to the PPARG agonist treatment. It is of importance, that the reduced OCR/ECAR ratio was again increased compared to the osteogenic control by a combined treatment with insulin and PPARG agonist (**Figure 55 C**).

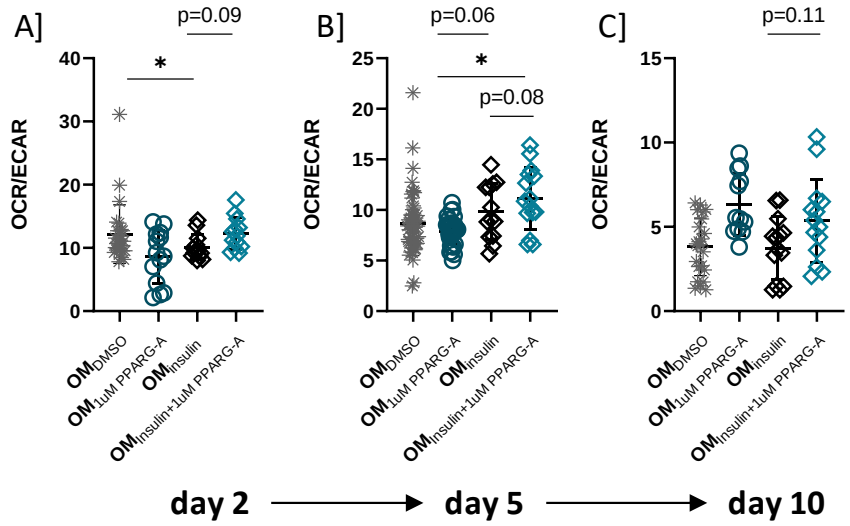

Figure 55: Insulin treatment of hBMSCs during osteogenic differentiation maintains the OCR/ECAR ratio at a constant level, whereas combined PPARG agonist and insulin treatment elevates the OCR/ECAR ratio
Different conditions such as osteogenic differentiation with solvent control (dark grey), osteogenic differentiation with PPARG agonist treatment (cyan), osteogenic differentiation with insulin (black) and osteogenic differentiation with a combination of insulin and PPARG agonist treatment (light cyan) are shown. Data is visualized including technical replicates, tested for statistical significance using the replicate mean of each patient. **A]** On day 2 of osteogenic differentiation a significant decrease of OCR/ECAR ratio is shown for the insulin treated condition compared to the osteogenic differentiation control (ratio paired t-test p=0.0346, n=3) and no significant increase by the combined treatment with PPARG agonist and insulin is depicted (ratio paired t-test p=0.0986, n=3) **B]** A significant increase of OCR/ECAR ratio is shown for the combined treatment with PPARG agonist and insulin during osteogenic differentiation (ratio paired t-test p=0.022, n=3-6), whereas no significant increase is shown for the insulin treated group (ratio paired t-test PPARG agonist/insulin p=0.065 and ratio paired t-test insulin/insulin+PPARG agonist p=0.083, n=3-6) **C]** On day 10 an elevation of the OCR/ECAR ratio is displayed for all PPARG agonist treated groups

The basal activity for insulin supplied hBMSCs was shown to be higher on day 2 with a significant upregulation on day 5 in hBMSCs under the combined insulin/PPARG agonist treatment in comparison to sole insulin stimulation (**Figure 56 B**). This effect was inverted on day 10, where insulin conditioned hBMSCs showed a strongly reduced basal activity compared to the PPARG agonist treatment (**Figure 56 C**). The ATP consumption of hBMSCs under insulin and insulin/PPARG agonist treatment likewise showed a strong decrease. Especially

the combined treatment of osteogenic hBMSCs with insulin and PPARG agonist rosiglitazone significantly induced the ATP turnover when compared to PPARG agonist or insulin only (**Figure 56 A, B**). This significant increased ATP turnover on day 2 and day 5, further lead to a significant reduction of ATP turnover during later stages of osteogenic differentiation under insulin dependent conditions whereas in conditions with sole PPARG agonist treatment this reduction was not shown (**Figure 56 C**). Summarized, this could suggest an insulin driven detrimental effect on mitochondrial function.

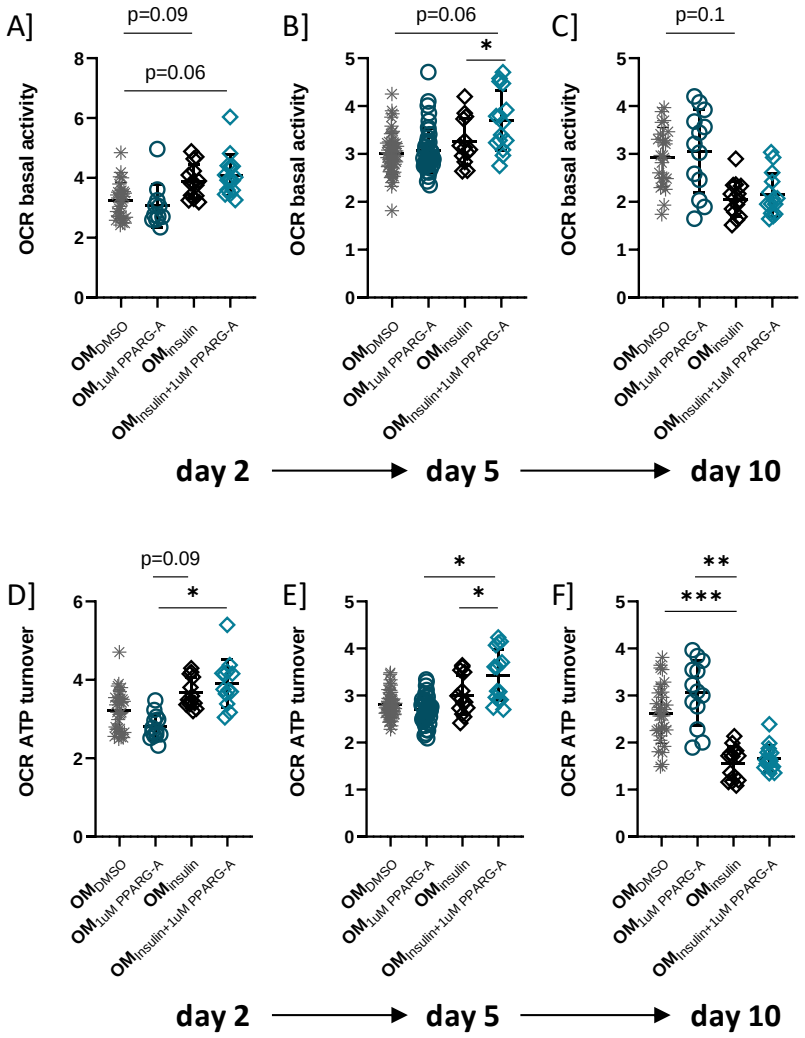

Figure 56: Insulin and PPARG agonist treatment steers a significant increase of basal activity and ATP turnover on day 5 but leads to a significant downregulation of both on day 10 of osteogenic differentiation
This figure shows different conditions of osteogenic differentiation either with solvent control (dark grey), osteogenic differentiation with PPARG agonist treatment (cyan), osteogenic differentiation with insulin (black) and osteogenic differentiation with a combination of insulin and PPARG agonist treatment (light cyan) are shown. Data is visualized including technical replicates, tested for statistical significance using the replicate mean of each patient. The oxidative basal activity of hBMSCs under osteogenic differentiation with insulin/PPARG agonist treatment is shown in combination with the mitochondrial ATP production. **A]** On day 2 an elevation of the basal activity is shown for insulin and insulin+PPARG agonist treatment (ratio paired t-test p=093 and p=0.063, n=3) **B]** PPARG agonist treatment in combination with insulin results in a significant increase of basal activity on day 5 of osteogenic differentiation (ratio paired t-test p=0.0236, n=3-6) **C]** A decrease in basal activity is shown for all insulin stimulated osteogenic conditions on day 10 of differentiation (ratio paired t-test p=0.17, n=3) **D]** Increased basal activity for insulin treated osteogenic conditions is paired with a significant increase of ATP turnover, especially in the PPARG

agonist+insulin treated group (ratio paired t-test p=0.099 and p=0.0496, n=3) **E]** Mitochondrial ATP production is significantly increased in insulin treated conditions, especially in the PPARG agonist+insulin treated group (ratio paired t-test p=0.0442 and p=0.0304, n=3-6) **F]** On day 10 of osteogenic differentiation, the decrease basal activity is combines with a significant downregulation of mitochondrial ATP production in all insulin treated groups compared to the osteogenic control and the PPARG agonist treated osteogenic condition (ratio paired t-test p=0.0002 and p=0.0066, n=3)

The detrimental effect of insulin on the metabolic capacity was further shown by a significant reduction of oxidative spare capacity and a significant increased proton leak of hBMSCs under insulin supplementation compared to the PPARG agonist treatment in later stages of osteogenic differentiation (**Figure 57**). In detail, the spare capacity of hBMSCs under insulin dependent treatment increased on day 2. However, starting from day 5 sole insulin stimulation was shown to negatively affect the spare capacity in comparison to PPARG agonist dependent conditions (**Figure 57 B, C**). Interestingly, the negative effect of insulin on the oxidative spare capacity during late osteogenic stages could be rescued by additional treatment of hBMSCs with a PPARG agonist. Further, a significantly increased OCR proton leak in insulin dependent conditions could be highlighted starting from day 5 when compared to the PPARG agonist treated condition (**Figure 57 E, F**). Indeed, PPARG agonist treatment prevented all osteogenic conditions from a significantly increased proton leak (**Figure 57 F**).

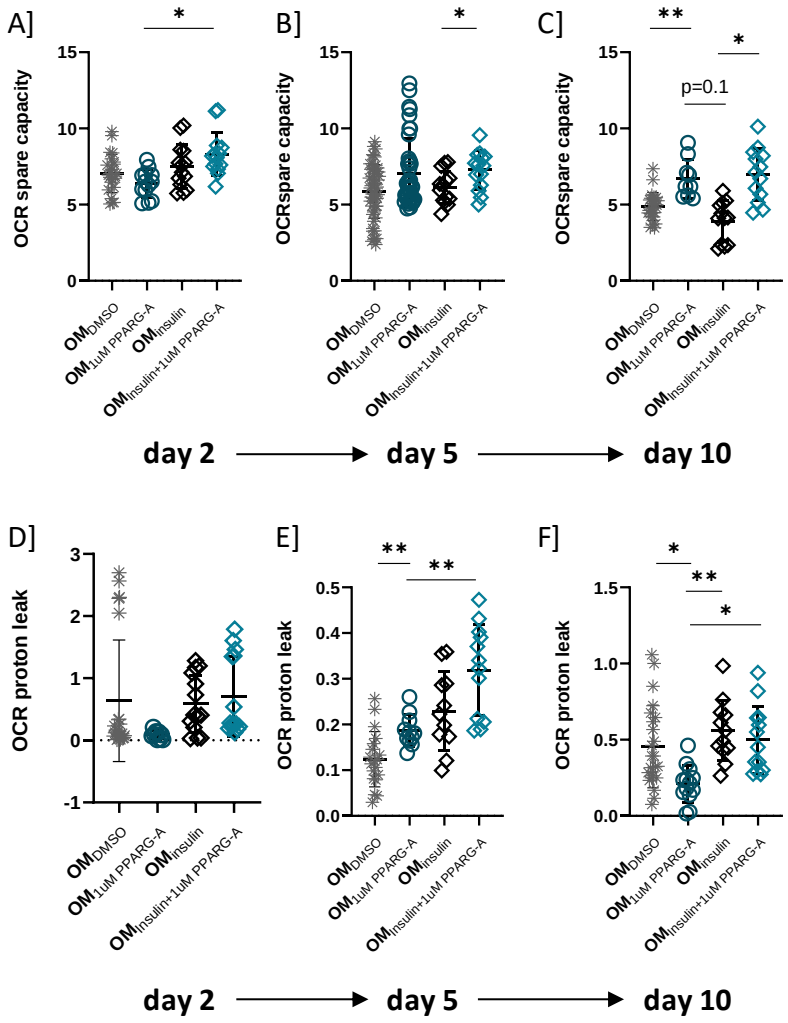

Figure 57: Oxidative spare capacity is uniquely upregulated by PPARG agonist treatment independent of insulin, whereas insulin treatment steers a significant increase of proton leak during osteogenic differentiation

The osteogenic differentiation is shown for conditions with solvent control (dark grey), with PPARG agonist treatment (cyan), with insulin (black) and with a combination of insulin and PPARG agonist treatment (light cyan). Data is visualized including technical replicates, tested for statistical significance using the replicate mean of each patient. The oxidative spare capacity of hBMSCs under distinct osteogenic conditions represents the ability of cells to cope with a high energetic demand and the oxidative proton leak can either be used for detecting mitochondrial damage/or as regulatory mechanism for ATP production of mitochondria. A] D] A significant increase of spare capacity as well as an increased proton leak is shown by the combined treatment with PPARG agonist and insulin on day 2 in comparison to the sole PPARG agonist treatment (ratio paired t-test p=0.0195, n=3) B] On day 5 insulin as well as PPARG agonist treatment steers an increased oxidative spare capacity during osteogenic differentiation, especially in the combined PPARG agonist and insulin treatment (ratio paired t-test p=0.031, n=3-6) E] Increased oxidative spare capacity is accompanied by a significant increase of proton leak in PPARG as well as insulin stimulated conditions (ratio paired t-test PPARG agonist p=0.0061 and PPARG agonist+insuin p=0.0015, n=3-6) E] F] On day 10, a significant increase in oxidative spare capacity is only shown in PPARG agonist treated conditions (ratio paired t-test PPARG agonist p=0.0016 and PPARG agonist+insulin p=0.029, n=3), whereas a significant upregulation of proton leak is only shown in insulin treated conditions and especially PPARG agonist treatment markedly downregulates the proton leak (ratio paired t-test PPARG agonist p=0.043 and insulin p=0.01 and PPARG agonist+insulin p=0.0239, n=3)

3.3.2.2. Unique effects of PPARG activation on the glucose uptake capacity

PPARG agonist treatment affected not only the OCR ratio but also the glycolytic activity of PPARG agonist treated hBMSCs. Therefore, we further investigated the glucose uptake of

osteogenic hBMSCs under PPARG agonist activation. Indeed, PPARG agonist treatment of hBMSCs was demonstrated to significantly increase glucose uptake on day 6 and day 10 of osteogenic differentiation (**Figure 58 A, B**). This glucose uptake elevation was not shown while supplementing insulin to osteogenic hBMSC cultures. Interestingly, the diminished effect in the insulin treated osteogenic hBMSCs could be rescued by the combined treatment with the PPARG agonist rosiglitazone resulting in a significant increase of glucose uptake in these conditions at both time-points.

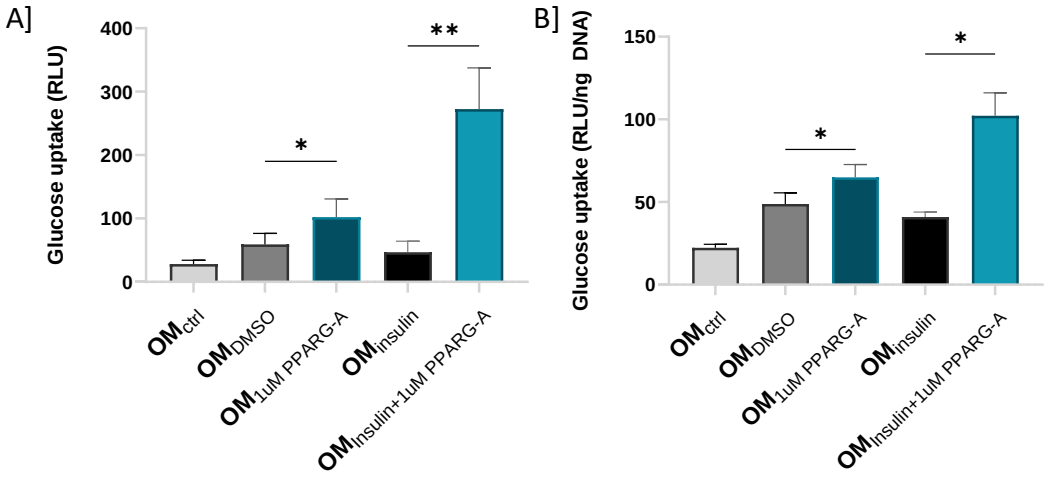

Figure 58: PPARG agonist treatment remarkably upregulates glucose uptake during osteogenic differentiation especially in combination with insulin treatment
Glucose uptake is shown for different osteogenic treatment conditions such as osteogenic control, solvent control, PPARG agonist treatment, insulin treatment as well as the combination of both PPARG agonist+insulin treatment. Glucose uptake in hBMSCs is determined in the form of relative light units (RLU) for two time points, the early osteogenic time-point on day 6 and the late osteogenic time-point on day 10. On day 10 the glucose uptake is shown as normalized values with RLU per ng DNA. A] A significant increase in glucose uptake capacity is shown for PPARG agonist treatment and the combined PPARG agonist and insulin treatment on day 6 of osteogenic differentiation (ratio paired t-test PPARG agonist/DMSO p=0.0436 and PPARG agonist+insulin/insulin p=0.008, n=3) B] A similar pattern of glucose uptake increase is shown for PPARG agonist treated hBMSCs on day 10 of osteogenic differentiation (ratio paired t-test PPARG agonist/DMSO p=0.022 and PPARG agonist+insulin/insulin p=0.0296, n=3)

3.3.3. PPARG driven osteo-adipocytes trigger metabolic changes by a unique gene expression pattern

The discovery of the PPARG agonist driven osteo-adipocytes and their effect on osteogenic differentiation led to two broad questions. First of all, the question remained which kind of adipocyte type was induced within the osteogenic milieu. In this sense, we attempted to pin down characteristics of BAT, WAT or brite adipocytes to the PPARG agonist induced osteo-adipocytes. Second, we asked whether direct effects of osteo-adipocytes drive osteogenic differentiation through specific signaling cascades. Both questions, were investigated by analyzing gene expression patterns and underlying signaling cascades in PPARG agonist stimulated osteogenic differentiation at early (day 7) as well as late osteogenic stage (day 14)

in comparison to the osteogenic control. In order to get a first insight, hBMSC of three different patients were analyzed using the RNA sequencing method.

Indeed, KEGG pathway analysis showed significantly upregulated signaling cascades such as Pi3K/AKT (padj=0.001), AMPK (padj=0.002) and MAPK (padj=0.0005) in the PPARG agonist treatment group already in early stages. In addition, genes underlying the insulin signaling pathway were significantly increased (padj=0.0015). At late osteogenic stage, PPARG agonist treatment resulted in significantly increased PPARG signaling (padj=0.01) in combination with the upregulation of associated genes of the AMPK pathway (padj=0.03) as well as adipocytokine signaling (padj=0.05) defined by KEGG pathway analysis (**Figure 59 C**). To identify differences in specific genes of interest, the PPARG agonist stimulated osteogenic differentiation was clustered against the osteogenic control for the late osteogenic time point (day 14). It was shown that a total of 1.373 genes (p-value cut off 0.1) was differentially regulated within the PPARG agonist treated osteogenic hBMSCs compared to the control. The most prominent finding was the significant upregulation of adiponectin ADIPOQ (padj=0.0000, Log2FC 9.516) in the PPARG agonist treated osteogenic differentiation (**Figure 59 A, B**). This was accompanied by the upregulation of several brite adipocyte associated genes e.g. CIDEA (padj=0.0000, Log2FC 7.666), KLF11 (padj=0.0311, Log2FC 2.328), FABP3 (padj=0.0000, Log2FC 2.729), PPARG (padj=0.0964, Log2FC 1.616) [195]. Further, pathways found in the molecular signature database (MSigDb) such as adipogenesis (padj=0.01), fatty acid metabolism (padj=0.0005), hedgehog signaling (padj=0.01) were shown to be significantly enhanced by PPARG agonist treatment. In addition, genes associated with increased metabolic fitness were changed in expression. Exemplarily, genes such as CD36 (padj=0.0000, Log2FC 4.214) and PGC1b (padj=0.0001, Log2FC 3.170) contributing to mitochondrial fatty acid beta oxidation, PGC1a (padj=0.0003, Log2FC 2.401) involved in mitochondrial activation and AQP11 (padj=0.0000, Log2FC 1.545) as ‘super aquaporin’ regulating oxidative stress were upregulated within the PPARG agonist treated osteogenic hBMSCs [278]. Adiopocyte hallmark genes such as fatty acid binding protein 4 FABP4 (padj=0.0000, Log2FC 9.908), perilipins PLIN1 (padj=0.0000, Log2FC 6.670) and PLIN5 (padj=0.0000, Log2FC 4.368) as well as aquaporins such as the glycerol transporter AQP7 (padj=0.0000, Log2FC 7.912) were show to be enhanced by the treatment with PPARG agonist rosiglitazone [279]. Insulin signaling pathway (**Figure 59 C**) and common associated genes (**Figure 59 A**) were enhanced e.g. LPL (padj=0.0000, Log2FC 5.579), PiK3R1 (padj=0.019, Log2FC 1) and AQP3 (padj=0.0000, Log2FC 2.913), the latter known to contribute to the modulation of Pi3K/Akt insulin signaling [280]. Of most interest, characteristic genes of cBMAT were shown to be significantly upregulated in the PPARG agonist induced osteo-adipocytes. The following cBMAT genes can be summarized as significantly upregulated

via PPARG agonist treatment: SCD-1 (padj=0.0000, Log2FC 2.287), CEBPA (padj=0.0008, Log2FC 2.774), SREBF1 (padj=0.0197, Log2FC 0.985). In response to the first question, this study showed that the osteo-adipocytes cannot be classified as one of the three main adipocyte types e.g. WAT, BAT, brite adipocytes. Osteo-adipocytes have been marked with adipocyte hallmark genes, with the focus on an increase of cBMAT as well as brite associated genes. To address the second question, this study suggests that osteo-adipocytes highly upregulate insulin associated metabolic pathways such as Pi3K/AKT and adipocytokine signaling with the focus on e.g. adiponectin, as already described in the secretome analysis in the previous chapter (**3.3.1.3**) and (**Figure 59 B, C**). According to the gene expression analysis, osteo-adipocytes are further represented as adipocytes with a large gene repertoire of genes associated with high mitochondrial activity and metabolic fitness.

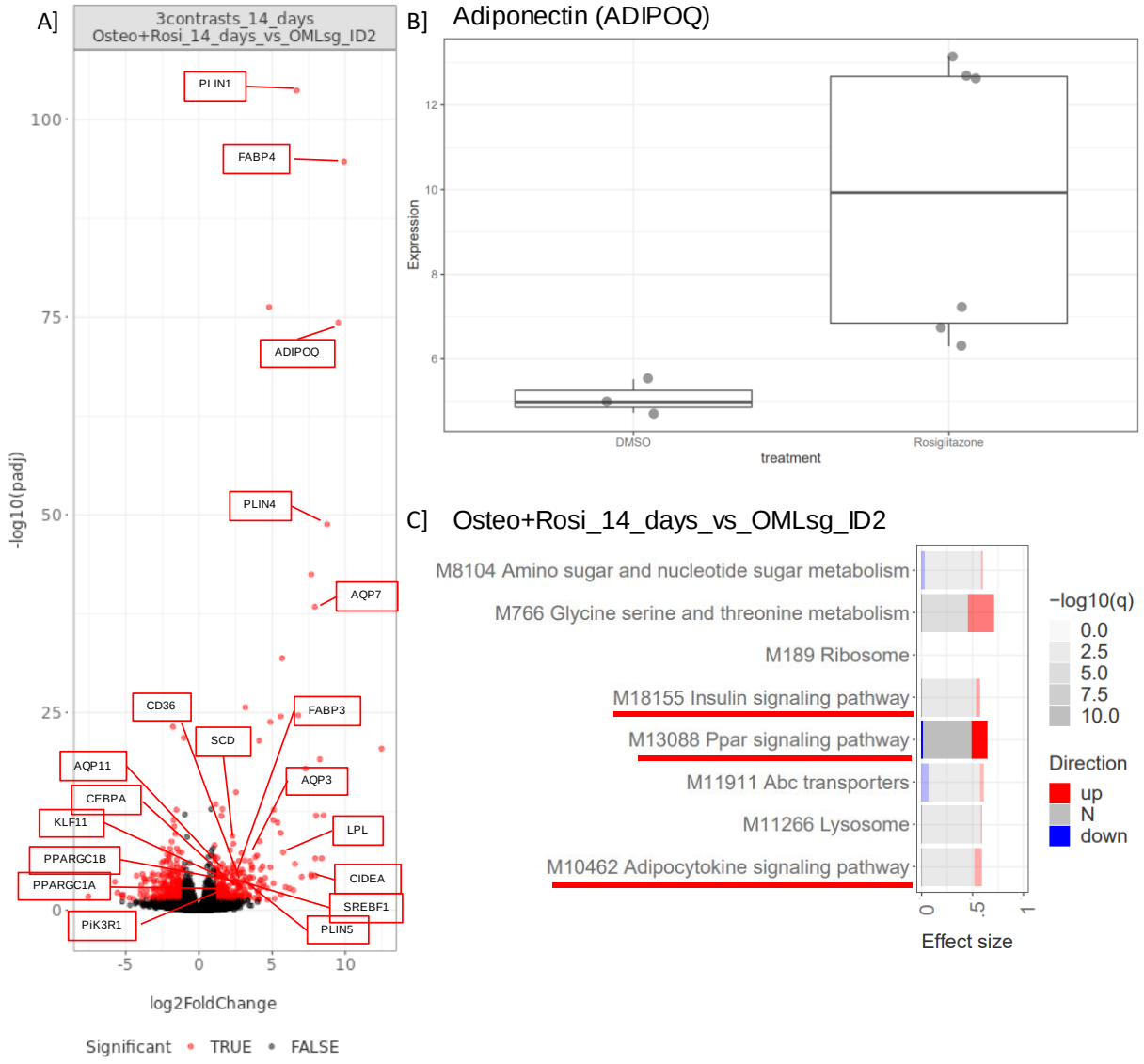

Figure 59: Specific genes and signaling can be identified in PPARG agonist stimulated osteogenic hBMSCs

RNA sequencing data of PPARG agonist stimulated osteogenic hBMSCs in comparison to the osteogenic control is visualized in three different ways: A] Volcano plot of significantly upregulated genes is shown for the PPARG agonist stimulated condition (Osteo+Rosi) in comparison to the osteogenic control (OMLsg) on day 14, this is visualized by plotting the adjusted p-value and Log2FC with a threshold of padj=0.05 and Log2FC of 1 B] Significantly increased expression of adiponectin (ADIPOQ) in the PPARG agonist stimulated osteogenic condition (Rosiglitazone) in comparison to the osteogenic control (DMSO) is shown as boxplot C] KEGG pathway analysis of differentially regulated signaling pathways including insulin signaling, PPAR signaling and adipocytokine signaling is shown for the PPARG agonist treated osteogenic condition (Osteo+Rosi) on day 14, red marks upregulated pathways, blue marks downregulated pathways by concurrent visualization of the effect size, further thresholding was done using padj=0.05, Log2FC of 1 and AUC of 0.5 (Analysis and statistical evaluation performed by Dr. Andranik Ivanov)

4. Discussion

In the following discussion, I will elaborate on the beneficial impact of PPARG agonist treatment during the regeneration of bone. First, the crucial importance of adipocyte and bone interaction during regeneration and inflammation is explored. Second, the detrimental as well as supporting role of PPARG agonist primed BMAs during bone healing will be highlighted. In this context, the broad spectrum of pro-regenerative BMAs e.g. adipokine secretion, metabolic fitness induction, and alterations of insulin and glucose metabolism during osteogenic differentiation of hBMSCs will be discussed. With this discussion, I want to emphasize that there is no black and white when it comes to BMA driven effects especially in the unique environment of the bone marrow.

4.1. Studying bone regeneration under explorative immune activation

4.1.1. BMAs as connecting piece between regeneration and anti-inflammation

In this first part of my thesis, it could be demonstrated that the systemic neutralization of pro-inflammatory cytokines such as TNFa and IFNg during early and late regeneration phases resulted in a significant upregulation of anti-inflammatory $CD4^+$ T helper 2 cells (TH2) during in vivo fracture healing. In the literature, this polarization of T helper cells into TH2 cells is known to steer an anti-inflammatory milieu by secreted cytokines such as IL4 and is known to promote beneficial fracture regeneration [252][134][136]. However, limited amount of research has been done on the presence of CD4+ TH2 cells in the compartment of adipose tissue. In the literature, CD4+ TH2 cells are proposed to alleviate systemic inflammation and metabolic dysfunction e.g. insulin resistance [137][138][139]. In connection to the beneficial impact of anti-inflammation on bone, various publications showed that the neutralization of TNFa and IFNg reduced detrimental effects on bone [281][43]. In contrast, systemic anti-TNFa treatment was likewise shown to result in disturbed fracture healing and low dose TNFa was shown to steer positive effects on bone in early phases of regeneration. This is going in line with the fact, that pro-inflammation is needed in the early fracture repair [98]. The cytokine IFNg is described with ambiguous effects on osteoblasts. It is well-known, that overexpression of IFNg is connected to the induction of pro-inflammatory CD4+ TH1 cells impairing bone regeneration. This detrimental shift in immune activation can likewise be induced in CD4+ T cells by e.g. depletion of PPARG, the main candidate transcription factor of this thesis [105]. In fact, PPARG ligands activating PPARG, known as the main transcription factor of adipogenic differentiation are inducing anti-inflammatory effects by directly inhibiting IFNg by repressing IFNg promotor constructs [282]. In line with that, PPARG is defined with an essential role in controlling TH2

effector function and is involved in the resolution of inflammation in different cell types [116][283][131][284].

In our setup, the systemic neutralization of both pro-inflammatory TNFa and IFNg did not improve bone structure parameters. However, we could highlight that systemically blocking pro-inflammatory cytokines is accompanied by the induction of an overall anti-inflammatory state. In addition to the anti-inflammatory milieu, an unexpected accumulation of bone marrow adipocytes next to the fracture site was identified. This exciting result can be delineated to the fact, that IFNg neutralization is known to steer bone marrow adipocyte differentiation by activating the signaling through PPARG [102]. This could serve as explanation for the occuring accumulation of bone marrow adipocytes in our experiments after neutralization of TNFa and IFNg. This result changed the perspective of solely determining immunological effects on bone towards including adipose tissues located within the bone marrow in proximity to bone forming cells and immune cells at the injury site. Underlining that, no detrimental effects of the accumulating bone marrow adipose tissue on the bone parameters could have been shown during our study. This improvement goes against the common view of the community indicating adipocytes as detrimental during the regeneration of bone. Indeed, the beneficial effects could be explained by the induction of a systemic anti-inflammatory milieu by neutralization of TNFa and IFNg in the whole body as well as within adipose tissue. Up to now, adipose tissue has been described to exert pro-inflammatory signaling in various chronic diseases and is shown to harbor high levels of TNFa and IL6, rather steering detrimental effects on regeneration [208]. However, the common view on bone marrow adipocytes in regeneration is currently re-thought and I intend to fortify this re-thinking by the means of my research. Most recently, the energy supply from bone marrow adipocytes was shown to be indispensable for the adaptations of MSCs and immune cells to dramatic stress situation such as injury [285]. Supply of nutrients and energy from bone marrow adipose tissue to other cells during bone regeneration upon fracture is proposed as rescue mechanism [169].

Since, we intended to induce an anti-inflammatory fracture adjacent adipose tissue and CD4+ TH2 cell priming, I shifted the focus from only neutralization of IFNg towards the specific induction of anti-inflammatory adipocytes using the PPARG agonist rosiglitazone. While using PPARG as main transcription factor for adipogenic differentiation, I could show an anti-inflammatory shift correlating with a significant accumulation of bone marrow adipocytes during our in vivo bone regeneration experiments. Hereby reproducing the already shown effects resulting from the neutralization of pro-inflammatory cues such as IFNg and TNFa. Above all, PPARG activation and the resulting adipogenic differentiation within bone, was shown to steer significantly improved bone parameters during our bone healing experiments. Indeed, I could show a significant increase in CD4+ TH2 cells by PPARG agonist treatment during our in vivo

experiments. Whereas, the remaining pro-inflammatory subsets of the CD4+ compartment such as TH1 cells and TH17 cells were not affected by the PPARG agonist treatment. In the literature, important anti-diabetic drugs such as PPARG agonists are known to steer CD4+ TH2 polarization. Both, the development of CD4+ TH2 cells and their fatty acid metabolism is dependent on PPARG signaling. [134][136] Hereby connecting the induction of PPARG agonist driven adipocytes and the TH2 cell polarization with beneficial effects on skeletal parameters during bone regeneration. In our model, the exposition of young mice to physiological pathogens during regeneration enabled the development and accumulation of environmentally primed, PPARG agonist induced BMAT, identified as pro-regenerative, anti-inflammatory key component during fracture healing. In summary, linking bone marrow adipocytes to anti-inflammatory features steering beneficial regeneration.

4.1.2. PPARG agonist primed BMAs combine site specific pro-regenerative effects on bone

The treatment with the PPARG agonist rosiglitazone resulted in a high accumulation of adipocytes first in the distal part at the growth plate of the unfractured as well as the fractured bone in comparison to the control without PPARG agonist stimulation. The localization of adipocyte accumulation suggested the adipocytes to be cBMAT. Indeed, PPARG agonist treatment markedly increased the bone volume and tissue volume in concurrence with significantly enhanced trabecular thickness and the ability of bone to endure torsional forces. Furthermore, the bridging of bone was significantly increased by the PPARG agonist treatment compared to control bones. We further intended to link this beneficial bone structure and healing process to the accumulating adipocytes within the marrow investigating the amount and location of cBMAT in the different experimental treatment and control groups.

On the one hand, our work showed that even without treatment with a PPARG agonist, the cBMAT accumulation was induced by the sole fracture incidence. Hereby, we are the first to show a correlation between fracture induction and healing with the physiological response of adipocyte development. On the other hand, PPARG agonist treated bones were shown to also induce adipocyte accumulation independently of the fracture incidence. The highest amount of cBMAT accumulation happened in the PPARG agonist treated fractured bones. It has to be highlighted, that especially in unfractured bones, a strong delta of cBMAT upregulation next to the distal growth plate was induced by PPARG agonist treatment. In the literature, a positive correlation of marrow adiposity and bone mineral content has been described especially in young animals [286][287]. This goes in line with our results, since our osteotomy model was likewise using young, healthy animals. It is a fact, that cBMAT has been described to initially develop from more transient and primitive progenitor stromal cells, whereas rBMAT was proposed to differentiate from definite adult progenitors [288]. It is still questionable if there is

a steady cBMAT source nourishing the development of adipocytes towards a pro-regenerative phenotype during bone turnover and healing. Our experiments showed, that adipocytes induced by PPARG treatment were marked by a larger adipocyte size compared to those induced in the control condition. In our research no accumulation of rBMAT could be identified in any of the PPARG agonist treated or control bones. This was not surprising since rBMAT only accumulates in aged individuals [22]. In the literature, contradictory opinions on the PPARG agonist activation and adipose tissue accumulation are postulated either stating the specific induction of cBMAT or rBMAT [286][72]. However, it is important to note that cBMAT is proposed to have the ability of taking the role of rBMAT e.g. in supporting hematopoiesis especially in the young, while the phenotypic fate is still plastic [203][204].

We could further show that PPARG agonist treatment resulted in a significant upregulation of the omega-6 to omega-3 fatty acid ratio in proximal regions of femoral control bones, where rBMAT is usually located. Whereas, no increase was shown for the distal region of femoral control bone, comprising cBMAT. In the literature, omega-6 polyunsaturated fatty acids (PUFAs) are known as biochemical sources of pro-inflammatory prostaglandins and have been controversially discussed for their concentration dependent, detrimental influence on bone health [34]. Low doses of e.g. prostaglandin E2 have been described to induce bone formation compared to high concentrations which harbor detrimental effects in inhibiting proliferation by cAMP signaling [289][290]. The recent finding of the prostaglandin 15d-PGJ2 as important endogenous ligand for PPARG, linked the induction of anti-inflammatory features and pro-inflammatory cytokine inhibition to the increase of omega-6. Indeed, prostaglandin production by omega-6 and omega-3 PUFAs and their ability to activate PPARG is well described in the literature [86]. In addition to that, iloprost a widely known prostacyclin analog is shown to harbor immunomodulatory features steering a pro-regenerative fracture healing milieu comprising downregulated pro-inflammatory immune cells and enhanced mineralization of osteogenic hMSCs [291]. This draw the line towards explaining the upregulation of omega-6 PUFAs in concordance with PPARG agonist treatment [35]. In regards to the omega-3 PUFAs, no significant change was shown in the femoral bones of PPARG agonist treated mice. This is unfortunate, since apart from the controversial impact of omega-6 PUFAs on bone, omega-3 PUFAs are described with beneficial effects on bone mineral density (BMD) by e.g. increasing bone collagen synthesis.

Next to the fatty acid composition in PPARG agonist driven BMAT, the most important finding of this study was that we were able to identify a new, pro-regenerative cBMAT aligned in the distal part of the bone in near proximity to the fracture site. This cBMAT was shown only in PPARG agonist treated fractured bones, whereas in fractured control bones no adipocytes could be determined. The enhancement of this pro-reg cBMAT was associated with an

increased bone volume in all PPARG agonist treated mice. Moreover, an increase of SCD-1 in all BMAT regions could be shown in PPARG agonist treated mice, which was specifically enhanced only in the pro-reg cBMAT region in comparison to the control. The in vivo SCD-1 increase is depicted as ratio of palmitoleic acid to palmitic acid. This goes in line with the in the literature described higher amounts of unsaturated fatty acids e.g. palmitoleate and oleate in cBMAT, that markedly distinguishes it from other adipose tissue types [286][73]. Further, an increase in SCD-1 is likewise determined for cBMAT enabling the formation of monounsaturated fatty acids. Interestingly, SCD-1 has been shown to prevent lipotoxicity and palmitic acid induced ER stress and inflammation in hMSCs [292]. Interestingly, we could reproduce the increase of SCD-1 in vivo by a significant increase of SCD-1 gene expression during beneficial in vitro osteogenic differentiation under PPARG agonist stimulation. This goes in line with current literature on the overexpression of SCD-1 being shown to promote osteogenic differentiation in mesenchymal stromal cells [293]. The fracture aligned pro-reg cBMAT is proposed to act as a potential supplier or storage hub for metabolites, cytokines and proteins inducing a rescue mechanism for cells under high energetic demand such as during fracture injury [294].

4.2. Changing the adipocyte focus to bone - Mirroring beneficial PPARG activation in osteogenic cultures

I could show, that the in vivo induced enhancement of bone formation and healing by the means of PPARG agonist treatment can be reproduced in osteogenic cultures using hBMSCs. Indeed, early osteogenic differentiation markers e.g. ALP activity was significantly increased by PPARG agonist treatment in comparison to the control. Further, osteogenic differentiation at later time-points defined by the amount of mineralized matrix was likewise shown to be significantly enhanced by PPARG agonist treatment. These are important results, since osteogenic differentiation is the hallmark of good bone regeneration, driving bone formation and fracture bridging. There is scarce evidence in the literature of PPARG agonist driven, enhanced mineralization under standard osteogenic differentiation [87][295]. However, literature showed that PPARG agonist treatment leads to a coinciding induction of adipogenic- as well as osteogenic differentiation, while osteogenic differentiation was shown to be further accelerated under the same conditions [296]. In fact, PPARG inhibition and the resulting blockage of BMAT expansion has been shown to steer bone loss in e.g. type 2 diabetic patients [297]. Underlining that, the knock-down of PPARG during osteogenic differentiation with BMP2 has been shown to result in impaired osteogenic differentiation, migration, proliferation and non-union of critical size bone defects [219]. In summary, the in vivo appreciated beneficial impact of PPARG agonist stimulation on bone was reproduced during in vitro osteogenic differentiation. Eventually, the impact of systemic anti-inflammation and the induction of pro-

regenerative cBMAT finally resulted in an enhanced beneficial bone structure. An important side note is that PPARG agonist treatment was shown to be a specific driver of osteogenic differentiation without influencing the proliferative capacity of hBMSCs.

4.2.1. PPARG agonist driven insulin sensitization and insulin supplementation differs in osteogenic cultures

Interestingly, I could show that a morphological distinct pattern of matrix mineralization was steered during osteogenic differentiation with high insulin concentrations compared to the one induced by PPARG agonist treatment. In detail, insulin driven mineralization showed large-scale calcium deposits, whereas PPARG agonist driven mineralization was displayed as more focused calcium deposits. Since, PPARG agonist treatment is marked by the sensitization of cells towards insulin, we intended to define if the enhanced osteogenic potential was specifically resulting from insulin driven signaling. This question is underlined by the fact that bone formation itself has been shown to be depend on insulin signaling [225][226]. PPARG agonist treatment was shown to induce specific pro-osteogenic effects without influencing the proliferation of hBMSC, it was surprising to show that insulin treatment resulted in broader effects. In summary, high insulin concentrations were marked by enhanced osteogenic mineralization, proliferation under osteogenic stimuli as well as an increased overall metabolic capacity of expanded as well as osteogenic differentiated hBMSCs. In the literature, insulin is described as inducer of proliferation as well as inducer of osteogenic mineralization in tendon derived progenitor cells [298]. Interestingly, the increased mineralization in tendon progenitor cells, which was steered by insulin was likewise shown to be mitigated by inhibiting the IGF-1 receptor [298][299]. High levels of insulin e.g. during hyperinsulinemia have been shown to be rather pro-proliferative, whereas high glucose levels e.g. hyperglycemia has been shown to decrease proliferation. However, in the above described publication, both conditions were shown in to enhance mineralization of tendon derived progenitors. The authors even described the insulin and glucose overstimulation as hypermetabolism. It is still questionable if such hypermetabolic states could be associated with a rather pathological ossification state, which could be likewise presented in our experiments on insulin driven mineralization [298]. On the contrary, PPARG agonist treatment has been proposed to inhibit cell proliferation by lowering circulating insulin and hereby beneficially affecting the insulin/IGF axis. In line with that, PPARG agonists could be of potential use as preventive for hypermetabolic states/hyperinsulinemia by outbalancing the overactivated insulin/IGF axis [227]. In summary, compared to insulin stimulation, the PPARG agonist induced effects were specifically pro-osteogenic and resulted in a physiological and beneficial impact during osteogenic differentiation of hBMSCs. These effects will be delineated in detail in the next chapters.

4.2.2. PPARG agonist treatment highlights adipocyte and bone co-induction

Of most interest during this study, was the unique effect of PPARG activation on the co-induction of adipocytes next to the enhanced matrix mineralization during later stages of osteogenic differentiation. Osteo-adipocyte accumulation localized in close proximity to calcium depots mirrored the already described effects of PPARG agonist treatment during in vivo fracture healing, where pro-regenerative cBMAT accumulation was correlated with an improved bone structure. In the literature, skeletal muscle fibro/adipogenic progenitors have been shown to expand in response to injury and were shown to provide important signals of pro-differentiation for myogenic progenitors [206]. In addition, the accumulation of adipocytes has been shown to correlate with muscle degeneration, but the effects of these adipocytes have been found to be secondary to muscle degeneration rather than the cause of it [300]. In our experiments, the co-induced adipocytes highlighted as osteo-adipocytes were formed starting from day 7 of osteogenic differentiation prior to the initial calcium deposition/mineralization. This goes in line with the proposition of adipocyte accumulation secondary to bone injury being involved in improving the healing outcome. To further argument on that, research regarding patients treated with IL6 and BMP2 showed the co-formation of adipose tissue in bone resulting in a beneficial fracture healing [215]. Surprisingly, adipocytes were even shown to enhance regeneration of critical-size bone defects when implemented in a decellularized human adipose tissue hydrogel [207]. The regenerative effect in the above described setting was further increased by the incorporation of adipose-derived stromal cells which had been pre-conditioned with osteogenic media [207]. Concomitant induction of adipocytes in bone highlight a necessary interconnectivity of both cell types during healthy and physiological regeneration. Indeed, literature on intracellular lipid droplet formation supporting osteoblastogenesis as well as the recent evidence that osteogenic cells rely on fatty acid utilization further strengthens the positive impact of fatty acids and lipids to combat high energetic demands during differentiation [169]. In line with that, research has been done on the lipid repertoire in cell membranes of mesenchymal stromal cells and its ability to enhance osteogenic differentiation directed by omega-3 PUFAs [301]. A comparable beneficial impact was shown for spontaneous adipocyte accumulation during chondrogenic differentiation [210].

In my experiments, the combined treatment of PPARG agonist rosiglitazone and high insulin concentrations further enhanced the osteo-adipocyte induced mineralization. This could be due to the PPARG agonist driven sensitization of hBMSCs towards insulin and the resulting insulin metabolism as well as osteogenic induction. It is widely known, that PPARG activation induces genes involved in insulin signaling knowingly improving insulin sensitivity and enhancing glucose and lipid metabolism [236]. Further, PPARG activation is known to influence phosphorylation events of insulin receptor substrate (IRS-1 and IRS-2) proteins, the

activation of phosphatidylinositol-3-kinase (PI3-kinase) and protein kinase B (Akt) signaling. Indeed, PI3k/Akt signaling has been shown to promote fracture healing by the interaction with the Wnt/b-catenin pathway. The PI3k/Akt/b-catenin axis as well as Wnt3a is described for the partaking and induction of osteoblast proliferation, differentiation as well as mineralization [302]. This is again underlining my results, showing improved osteogenic mineralization due to the combined PPARG agonist and insulin treatment. However, solely supplementing high insulin concentrations during osteogenic differentiation showed no osteo-adipocyte accumulation in any of the tested patient derived hBMSCs. In the literature, it is known that insulin has a pro-proliferative and pro-developmental effect on pre-adipocytes. These insulin responses are mediated by signaling through IRS-1 and IRS-2 [303][234]. However, IRS-1 has been shown to negatively regulate adipogenesis in bone marrow stromal cells by downregulation of e.g. PPARG in comparison to IRS-2, which was associated with the upregulation of adipogenesis [233][234]. This could mean, that the insulin driven effect in our experimental setup is resulting from signaling via IRS-1 rather than IRS-2. Another reason could be that high insulin concentrations are known to tackle IGF-1, while IGF-1 is associated with a decline in BMAT. Underlining the loss of adipocytes in concurrence with an enhancement of osteogenic differentiation, our experimental insulin condition could resemble a high insulinemic state. [304][305] This high insulinemic milieu could be the cause of a detrimental hypermetabolic state, while still inducing increased mineralization of osteogenic hBMSCs associated with detrimental effects such as low bone turnover, high bone mass and cellular senescence [232]. Insulin lowering agents such as PPARG agonists have been shown to downregulate IGF signaling and by that could be important regulators of a rescue mechanism improving hyperinsulinemic states [265][264].

In my experiments, osteo-adipocytes showed a strong morphological resemblance to common adipogenic differentiated hBMSCs cultivated without the influence of osteogenic triggers. This is according to the literature, since the morphological similarity of BMAT and WAT was described in various studies. However, both adipose tissue types were represented as functionally different. [306][197] Conversely, while performing control differentiations steering the common fat forming adipocyte lineage under PPARG agonist treatment, no increase in adipocyte number could be shown in comparison to the differentiation without the PPARG agonist. This goes in line with my in vivo results showing a steady weigh of mice under PPARG agonist treatment compared to the control group. The common understanding of PPARG activation has been marked by the fact that PPARG is known to steer adipogenic differentiation [43]. However, within the bone marrow, research on lineage decision into adipogenic or osteogenic committed mesenchymal stromal cells is described as a decision making at the expense of one or the other [307]. Two phases have been described for adipogenesis namely

the determination and terminal differentiation phase [308]. On the one hand, the determination phase is known as adipocyte lineage commitment phase, where other differentiation processes are inhibited. On the other hand, the terminal phase defines the phase where pre-adipocytes are converted into mature adipocytes. Underlining that, it could well be that my results on adipocyte development in cultured and already primed lineage driven adipogenic cells is no longer dependent on further PPARG agonist stimulation at least not with respect to the enhancement of adipocytes accumulation. Accordingly, there is additional evidence in the literature that PPARG activation can positively regulate both adipocyte as well as osteoblast differentiation of mesenchymal stromal cells from marrow [309]. The osteo-adipocytes appearing during our experimental osteogenic cultures were further characterized by gene expression analysis. Results showed, a significant upregulation of brite specific genes in PPARG agonist stimulated osteogenic hBMSCs e.g. CIDEA, KLF11, FABP3 and PPARG itself. However, a concurrent upregulation of common adipocyte genes as well as genes specific for cBMAT induction was shown in PPARG agonist primed osteogenic cultures. It is of importance to say, that the limitation of our experimental setup was shown to be the co-culture of our osteo-adipocytes with osteogenic cells, resulting in the fact that I could not strictly differentiate the gene expression changes between both cell types. However, when focusing on the osteo-adipocyte characterization: A recent publication has identified a specific role of PPARG agonist rosiglitazone in steering a functional change from white to brown adipocytes, namely brown-in-white (brite) adipocytes [195]. This induction of browning and the resulting accumulation of brite adipocytes is associated with an increased upregulation of brite-selective genes and mitochondrial oxidative capacity. Hereby, highlighting the development of a metabolically active and beneficial adipocyte type. It is still to be elucidated what kind of bone marrow adipocyte type was introduced by treating osteogenic cultures with PPARG agonist albeit evidence is clear that PPARG activation and resulting adipocyte formation enhanced mineralization by steering PPARG signaling during osteogenesis.

4.2.3. PPARG stimulated osteo-adipocytes present specific characteristics improving bone regeneration

In my experiments, PPARG induced osteo-adipocytes were shown to exert specific paracrine effects when accumulating during osteogenic differentiation. The secretory profile of PPARG agonist primed osteo-adipocytes comprised significantly higher levels of adiponectin, a well-known adipokine when compared to common fat forming adipocytes. Indeed, this secretory profile was confirmed on the gene expression level were PPARG agonist primed osteogenic hBMSCs showed significantly increased levels of ADIPOQ in comparison to the control differentiation at early (day 7) and late (day 14) osteogenic time points. In the literature, AdipoR1 overexpression is associated with increased bone volume and enhanced trabecular

number [310]. Next to that, adiponectin has been shown to increase the expression of osteoblastic genes by that increasing the mineralization capacity of cells during osteogenic differentiation [261][311][312]. Remarkably, adiponectin secretion from adipocytes has been described to directly inhibit adipogenic differentiation and promote osteogenic differentiation of BMSCs [313]. This is further implying a concurrent induction of both differentiation pathways harboring beneficial effects on bone formation. Adiponectin is further shown to induce a balance towards anti-inflammation [256]. This makes adiponectin, a prominent target to reduce pro-inflammation in bone. In the literature, the influence of adiponectin was shown to mirror the influence of Th2 cytokine secretion, especially IL4 and adiponectin has been suggested to share similar mechanistic pathways as TH2 cells in steering M2 macrophage polarization [314][118]. Hereby, our in vivo data on cBMAT accumulation and TH2 cell induction by PPARG agonist treatment could be interlinked by the increased adiponectin levels. It is still questionable, which secretory profile can be pinned down to each BMAT type e.g. cBMAT and rBMAT. However, adiponectin production has been shown to be higher in cBMAT compared to rBMAT [315][316]. These results from the literature, again can be connected to our in vivo generated data on the PPARG agonist induced adipocyte accumulation in the distal part of the bone e.g. cBMAT locality, which should strongly resemble the in vitro cultured PPARG agonist induced osteo-adipocytes [204].

Additional anti-inflammatory features could be shown in our experiments, since PPARG agonist primed osteo-adipocytes profoundly downregulated pro-inflammatory adipocytokines such as MCP1 and IL1b. These effects were underlined by various studies characterizing adiponectin as adipokine able to improve e.g. diet-induced inflammation especially by suppression of TNFa induced MCP1 expression [317]. The predominant results, showed anti-inflammatory and anti-apoptotic features of adiponectin [318][319]. In concurrence, research showed that the treatment of human adipose tissue with IL1b has reverse effects on adiponectin, specifically reducing adiponectin mRNA levels and production [320]. Current literature on the effects of IL1b can be summarized to cause insulin resistance and the reduction of PPARG signaling [321]. Regarding bone, the detrimental, prolonged early inflammatory phase of bone regeneration is enrolled by enhanced production of pro-inflammatory cytokines and chemokines such as MCP1, TNFa, IL1b and IL6 [18][252]. This further leads to a prolonged recruitment and accumulation of inflammatory cells towards the fracture inhibiting adaptive homeostasis as well as the anti-inflammatory switch needed for regeneration [16][322]. However, controversial data exist for MCP1, which has been described with pro- and anti-inflammatory features in relation to bone [323]. MCP1 is associated with bone remodeling as well as pathological bone conditions. Indeed, MCP-1 is important for macrophage recruitment in early phases of bone healing where it has important regulatory

features in the recruitment and activation of bone cells needed for skeletal fracture repair and bone remodeling [324][325]. However, increasing levels of MCP1 are likewise known to drive osteoclast formation [326]. Higher MCP1 levels are likewise associated with a decreased BMD and are positively associated with inflammatory markers such as TNFa and IL6 [327]. Therefore, the induction of MCP1 in early fracture healing phases might possess beneficial features but when overproduced during the later stages, when the change towards anti-inflammation is indispensable, it harbors detrimental effects [18][252]. Antagonism of MCP1 has been described to improve metabolic control by restoring the balance between adipogenesis and hematopoiesis in bone marrow of patients with type 2 diabetes [328]. The antagonism of MCP1 by PPARG agonist treatment could be of beneficial impact also in bone regeneration. In line with that, reduced bone marrow adipogenesis and increased osteocyte density has been characterized for MCP1 antagonism [328]. Chronic inflammatory states have been shown to have detrimental effects on bone regeneration because of the steady upregulation of TNFa and the NFkB signaling pathways which by implication lead to the activation of osteoclasts [252][329][330]. In the literature, PPARG agonists have been described with prominent therapeutic features for inflammatory bone diseases because PPARG signaling downregulates TNFa mediated osteoclast differentiation in part by the suppression of MCP1 activity [331]. All in all, representing the PPARG agonist treatment, the concurrent osteo-adipocyte induction and the change into anti-inflammatory adipokine secretion was shown as beneficially during osteogenic differentiation.

In my experiments, osteogenic cultures stimulated with high insulin concentrations could not be associated with the previously described anti-inflammatory change in adipokine secretion. Indeed, high insulin concentrations during osteogenic cultures changed the secretion of adipokines and adipocytokines towards a pro-inflammatory profile with significantly increased secretion of MCP1 and IL1b as well as higher leptin levels compared to the osteogenic control. No increase of anti-inflammatory adiponectin could be shown during high insulin supplementation in osteogenic differentiating hBMSCs. With that, only pro-inflammatory adipokines could be highlighted in this condition. In addition, no osteo-adipocyte accumulation could be shown in our experiments while supplementing high insulin concentrations. In the literature, hyperinsulinemia and increased insulin-signaling is partially interconnected with the increase of cell senescence [332]. The described adipokine pattern goes in line with the known inhibition of adiponectin by pro-inflammatory cytokines such as TNFa, IL6, IL1b [149][333][334]. In addition, MCP1 is described as enhancer of adipose tissue inflammation by macrophage infiltration associated with a detrimental metabolic phenotype and insulin resistance [335]. In the literature, insulin responsiveness in hBMSCs is depicted as rescue mechanism allowing fat storage in bone marrow without manifesting disturbed insulin signaling

[235]. However, in this case of high insulin concentration, no fat storage e.g. osteo-adipocyte induction could be shown. By that, suggesting a rather manifested, dysregulated insulin signaling. This goes in line with the proposition that high insulin concentrations steer a hypermetabolic osteogenic differentiation of a rather detrimental type. In that case, osteogenic differentiation is enhanced and hBMSCs are driven towards cellular senescence because of increased metabolic activity [232]. This connects to the previously described strong proliferative impact of insulin during osteogenic differentiation which could result in exhaustion of osteoblasts [336]. In the literature, oxidative stress as described during fracture healing has been shown to likewise induce cellular senescence. Hereby, highlighting the important decision making between either healthy and active or senescent osteogenic differentiation by characterizing the microenvironment. A detrimental microenvironment is represented by senescence-associated secretory phenotype (SASP) comprising specific adipokines and adipocytokines [336]. Clear evidence for the promotion of senescence has been shown in the prior induction of inflammatory cytokines, chemokines as well as adipokines [337]. In detail, the adipokine leptin is widely described for its involvement in inflammation by increasing IL6 and IL8 levels and is proposed to induce bone as well as cartilage erosion [338][339][340]. Furthermore, high levels of leptin as well as IL1b have been observed in osteoarthritic osteoblasts [341][255]. In concurrence with that, IL1b, MCP1 as well as IGF-binding proteins have been defined as senescence induced adipocytokine [342][343][344][345]. Similarly, leptin, resistin as well as adiponectin were defined as SASP [346]. In our study, MCP1. IL1b and leptin were shown to be induced by hyperinsulinemic states, whereas a strong decrease in adiponectin was determined. However, in the literature, leptin production is enhanced under hypoxic conditions, such as in fractures and is described with beneficial effects as in the induction of ALP and other markers of osteogenic differentiation [347][348]. Hereby, highlighting the dual effect of senescence with strong osteogenic mineralization patterns, likewise shown in our experimental setup. Further characterization of this experimentally induced hyperinsulinemia and concurrent mineralization is of importance, since the balance between healthy and harmful mineralization could not be elucidated within this thesis.

We further investigated and compared the secretory effects of co-induced, PPARG-driven osteo-adipocytes with secretory effects of the common PPARG agonist pre-stimulated, fat forming adipocyte on osteogenic differentiation. My research showed, that the control fat forming adipocytes and their secretory features have no detrimental influence on the mineralization of osteogenic cells for a period of 21 days of osteogenic culture. Above all, a steady increase in matrix mineralization of osteogenic cells and constant beneficial effect of diverse fat forming adipogenic media was appreciated during osteogenic differentiation. Along with that, fat forming adipogenic media in combination with high insulin concentrations resulted

in a steady mineralization of all conditions. When characterizing the common fat forming adipocytes and their secretory pattern, it was highlighted, that PPARG pre-conditioning of the fat forming adipocytes had no effect on the pro-inflammatory MCP1 and IL1b in comparison to common fat forming adipocytes. In recent literature, the secretome of BMAT has been compared to the common adipocyte compartment e.g. WAT, underlining BMATs function related to bone formation and hematopoiesis [73]. Many proteins secreted by both compartments have been shown to influence surrounding cells [294]. Adipokines secreted by WAT have been shown to differ from the secretion profile of BMAT. Exemplarily, leptin was shown to be rather expressed by large vacuoles of WAT compared to smaller non-hypertrophic BMAT vacuoles [349]. In fact, pro-inflammatory MCP1 expression in WAT has been shown to contribute to the enhanced chemotaxis of M1 macrophages into adipocytes resulting in increased insulin resistance during pathological states e.g. obesity [335][350]. Further, steady levels of pro-inflammatory IL1b and a high glycolytic and insulinemic environment induces a rather pathological adipocyte phenotype [216]. This might also be indicated in our culture system, since common adipogenic media are loaded with high amounts of insulin and glucose. The overload of nutrients in common adipocyte media further linked the effects of increased proliferation capacity of hBMSCs with the omitted insulin sensitivity during osteogenic differentiation [351]. When focusing on the anti-inflammatory adiponectin levels of PPARG agonist pre-stimulated, common adipocytes, a significant increase of adiponectin could be shown as already described for PPARG agonist primed osteo-adipocytes. However, the levels of adiponectin in common adipocytes were markedly reduced compared to the ones secreted by osteo-adipocytes. This is in line, with the literature describing elevated secretion of adiponectin from BMAT in comparison to WAT [352]. Of interest was that a significant increase of RBP4 secretion could be shown in PPARG agonist primed fat forming adipocytes, whereas no change could be shown for this adipokine in osteo-adipocytes. In fact, RBP4 increases in obesity induced pathologies and is tightly linked with RBP4 induced insulin resistance and upregulation of pro-inflammatory cytokines such as TNFa and MCP1 [176]. Further, RBP4 has been shown to downregulate PPARG expression and signaling and with that inducing adipose tissue inflammation [353][176]. The detrimental impact of RBP4 has been described in various research however, a recent report showed that RBP4 signaling is especially harmful under glucolipotoxicity steering pro-inflammation and insulin resistance [354]. Underlining that, my results showed that the resulting effects of PPARG agonist treatment are strongly depending on the environment, which is built up by the connecting adipocyte and bone cells. The PPARG agonist treatment of common fat forming adipocytes is highly different and less effective in comparison to PPARG agonist treatment inducing the de-novo differentiation of osteo-adipocytes next to osteogenic cells. Hereby, characterizing osteo-adipocytes with a unique

PPARG agonist stimulated phenotype with broad effects on inflammation, insulin sensitivity and in having a pro-osteogenic adipokine pattern.

4.2.4. PPARG stimulates a high metabolic fitness supporting osteogenic differentiation

4.2.4.1. Metabolic adaptation in osteogenic and adipogenic differentiation of hBMSCs

In this thesis, I was able to underline that hBMSCs undergoing osteogenic lineage commitment rely on a significant increase of OCR, as a measurement of OXPHOS and decrease of ECAR, as a measurement of glycolysis in early stages of osteogenic differentiation [153]. This goes in line with various studies describing an increased mitochondrial activity and associated OXPHOS at the expense of glycolysis during osteogenic differentiation [355][356][357][358]. However, others controversially described an enhanced mitochondrial OXPHOS while glycolysis was maintained at the basic level of undifferentiated cells [359]. In our work, the induction of mitochondrial OXPHOS was followed by a combined increase of ECAR in later stages, where matrix mineralization starts to form. In the literature, it has been shown that the omitted increase of OXPHOS can be balanced by an increase in glycolysis [356]. These results were mirrored by prominent changes of OCR in early osteogenic time-points, whereas in later mineralization stages, an equal increase of OCR and ECAR was shown. Other research showed, that lipid droplets within osteoblasts itself can support osteogenic differentiation of bone marrow MSCs. Those lipid droplets were marked by fatty acids providing energy in the form of ATP to MSCs in early stages of osteogenic differentiation. In fact, blockage of mitochondrial fatty acid uptake in these cells resulted in a reduction of OCR in early osteogenic time-points without influencing glycolysis levels, whereas the OCR levels of mature osteoblasts were not changed by inhibiting fatty acid metabolism [169]. In the following, the Warburg effect is highlighted as alternative process where increased OXPHOS activity can likewise be followed by a rise in glycolytic activity in cells [360]. Of importance, the Warburg effect has been show to arise under challenging conditions with high energetic demand, where cells have the ability to use the aerobic glycolysis while downregulating laborious OXPHOS. This was shown to enable rapid energy production despite a reduced oxygen availability during hypoxic conditions such as fractures [162][3]. Our experiments showed that the early increase of OCR/ECAR ratio was accompanied by a significant increase of basal activity starting from day 5 of early osteogenic differentiation continuing further until day 10 when initial mineralization takes place. Both osteogenic time points were additionally marked by a favored ATP demand next to a higher capacity of ATP production by mitochondria. In the literature, both basal and ATP-linked mitochondrial activity have been shown to increase during osteogenic differentiation [359]. Indeed, MSCs with high capacity for oxidative metabolism and a

decreased reliance on glycolysis harbor protective effects when transplanted into glucose- and oxygen deprived environments [361]. Exemplarily, bone marrow derived MSC with high OXPHOS capacity have been used as ‘superhealers’ in the environment of infarcted hearts. In contrast, hBMSCs under a pro-inflammatory trigger e.g. TNFa, have been marked with detrimental bone healing caused by a reduced osteogenic lineage differentiation ability. TNFa stimulation of hBMSCs is further associated with a reduced OXPHOS capacity and low metabolic fitness [362]. Our research could elucidate, that the initial matrix mineralization and calcium deposition is associated with a simultaneously enhanced oxidative spare capacity. Hereby, linking the strong energetic demand during osteogenic mineralization with the increase of hBMSCs fitness. Others showed, that higher levels of respiratory spare capacity have been associated with the adaptation of cells to elevated energetic demand, cellular survival and function [363]. In addition, literature associated the higher spare capacity of cells with a lower ROS generation and with that marked cells harboring a higher OCR spare capacity with a lesser susceptibility to stress, cell death and senescence.

With this and within the following chapter, we want to highlight, that adipocytes are metabolic sensor cells harboring the capacity to modulate the fracture environment, when under stimulation of the right target e.g. PPARG. Apart from the sole adipocyte impact, we would like to highlight a beneficial metabolic crosstalk between osteo-adipocytes and osteogenic hBMSCs during regeneration [187]. Underlining that, PPARG agonist treatment of adipocytes has been described to steer adipocyte hyperplasia comprising de novo differentiation of small adipocytes improving insulin sensitivity, enlarged energy storage capacity and control favorable metabolic effects by e.g. adipokines, among others. [188].

4.2.4.2. **PPARG agonist driven metabolic changes in osteogenic differentiation**

The main results of this study include the metabolic changes induced by PPARG agonist treatment during osteogenic differentiation. Hereby, PPARG agonist treatment was highlighted to significantly increase the OCR/ECAR ratio during the expansion of hBMSCs especially in later time points such as day 10 of expansion. However, the ECAR levels remained unchanged under PPARG agonist treatment. In concordance with that, the OCR/ECAR ratio during osteogenic differentiation was positively influenced by PPARG treatment in the phase were initial calcium deposits and mineralization were formed. However, in early stages of osteogenic differentiation the balance of glycolysis and OXPHOS was shown to rely more on the glycolytic ability of hBMSCs. In the literature, other members of the PPAR family e.g. PPARB/PPARD have been shown to steer the metabolic capability of MSC by switching from glycolysis towards OXPHOS. For PPARG, those effects have not yet been evaluated in detail. In the literature, only the PPAR-gamma coactivator a (PGC1a) was shown to steer mitochondrial activation

[364][365]. At least, PPARG activity was associated with fatty acid synthesis, carbohydrate and lipid metabolism, sequestration of fats and reducing plasma glucose levels as well as oxidative stress [366][367][368].

In our setup, PPARG agonist treatment and its induction of osteo-adipocytes was shown to enhance adiponectin secretion, while adiponectin was described in the literature with a strong impact on supporting osteogenic differentiation [369]. The involvement of PPARG in reducing oxidative stress has been likewise shown [370]. In fact, the expression of adiponectin receptors has been correlated with the increase of mitochondrial respiration capacity and upregulation of ATP production [371]. Hereby, steering osteoanabolic functions during bone formation via increased AMPK phosphorylation, and PGC1a expression. This again highlights the impact of our results, since we could show an increased adiponectin production, a higher mitochondrial flexibility as well as an enhanced osteogenic differentiation steered by PPARG agonist stimulation. In addition, our KEGG pathway analysis of PPARG agonist stimulated osteogenic cultures resulted in significant upregulated signaling via AMPK in late osteogenic time points (day 14). Underlining that, other genes involved in mitochondrial activation such as PGC1a were shown to be significantly upregulated under PPARG stimulation within the osteogenic setting. We are the first to describe the effect of enhanced spare capacity during osteogenic differentiation with the known adipocyte inducer and agonist for PPARG. This increase was not shown for the hBMSCs under standard expansion culture. Interestingly, research on mitochondrial dysfunction has been described for pathological, metabolic settings e.g. T2DM and with that underline the importance of the OXPHOS/glycolysis balance in adipogenic differentiation. In concordance with the osteogenic differentiation, adipocyte differentiation is likewise known to rely on the induction of mitochondrial OXPHOS in dependence of PGC1a [372]. In fact, PPARG agonist activity even has been shown to induce broader effects such as browning of adipocytes while simultaneously enhancing mitochondrial oxidative capacity [195]. Indeed, mature adipocytes described in the former publication were shown to rapidly adapt to metabolic changes by a 6-fold increase of respiratory spare capacity allowing energy dissipation and the maintenance of homeostasis under hypoglycemic conditions [372]. However, the independence of PPARG agonist rosiglitazone on PGC1a enabling the induction of mitochondrial biogenesis in adipose tissue has been controversially discussed [373].

In this thesis, even patient derived hBMSCs marked with a very low osteogenic differentiation capacity and a low oxidative consumption were shown to be rescued by PPARG agonist treatment. PPARG agonist treatment and the resulting osteo-adipocytes were shown to influence the induction of a metabolic hBMSC phenotype suitable and indispensable for osteogenic differentiation and mineralization. Research on tissue protection and regeneration showed that the balance of cell growth and differentiation is essential and that PPARs have

gained more and more attention as drivers of injury protection and healing [374]. In concordance, early and late skin and wound healing phases have been described to rely on PPARG, PPARA and PPARB signaling [375][376]. Hereby, PPARs are identified as important players in building the metabolic foundation for the lineage differentiation of hBMSCs. Recent data has established a link between higher mitochondrial biogenesis and the induction of PPARG signaling [377]. When comparing a PPARG knock-out condition with a control prostate cancer cell line, a significant diminishment of maximal respiratory capacity, basal respiration, ATP production, and OCR spare capacity was identified with the loss of PPARG [377]. All in all, the described effects of a significant induction of oxidative spare capacity in cells and its beneficial effects during metabolic challenging conditions highlight the positive relation of the in our experimental setup induced osteo-adipocytes on the osteogenic differentiation. This goes in line with the recently described direct effect of PPARG agonist treatment on the induction of metabolically active brite adipocytes harboring a strongly enhanced mitochondrial respiratory capacity [195].

4.2.5. Hyperinsulinemia: PPARG agonist treatment as rescue mechanism?

Our data highlighted a beneficial effect of PPARG agonist treatment on the metabolic capacity of osteogenic hBMSCs in comparison to high insulin driven effects. Those were shown to rather induce negative effects on the mitochondrial respiration during late osteogenic differentiation. PPARs on the other hand have been determined to enable regeneration of tissues even in unideal healing situations such as under a persistent, chronic inflammatory and hypermetabolic diabetic milieu [374][378][376]. The high insulin concentrations supplemented in our experiments were suggested to mirror a detrimental metabolic phenotype by presenting a hyperinsulinemic/metabolic bone environment with increased inflammatory cytokine production and a significant upregulation of leptin levels [379]. However, in early osteogenic time points, those negative effects of high insulin concentrations were not yet sophisticated. Indeed, both insulin as well as PPARG agonist treatments were shown to partially increase the OCR/ECAR ratio, basal activity and ATP turnover especially when a combination of both treatments was investigated. This goes in line with recent research on enhanced insulin signaling of obese hBMSCs driving a hypermetabolic phenotype marked by a strong increase of oxygen consumption (OCR) and production of reactive oxygen species (ROS) [380]. In addition, the overexpression of insulin receptors (IRs) and leptin receptors (LEPR) have been shown to steer enhanced proliferation, differentiation and mineralization of hBMSCs driving cellular senescence [232].

In fact, cell stress driven insulin resistance is shown to result in an increase of proton leak, which can be associated with our experimental data. Consistent with this, the significant reduction in proton leak by the PPARG agonist treatment during our osteogenic culture setting

could be explained by the insulin-sensitizing properties of PPARG. In our experiments sole insulin primed conditions were not shown to form co-localized osteo-adipocytes nor to produce adiponectin during differentiation. However, a similar osteogenic induction with diverse mineralization pattern and increased leptin/pro-inflammatory cytokine levels could be shown. In the literature, the induction of osteogenic differentiation and metabolic respiration have been shown to correlate in obese hBMSCs in the same manner as in physiological metabolically balanced conditions [232]. Similar to healthy patients with insulin resistance, morbidly obese patients have been characterized with a strong increase in mitochondrial respiration including basal respiration, maximal respiration, ATP turnover and spare capacity [381]. However, research showed a concurrent increase of proton leak, which was depicted in morbidly obese patients when comparing to the insulin resistant patients. To explain the above described characteristics, the authors discussed a compensatory effect of cells in a metabolically compromised/inflexible physiological system. Hereby, re-balancing the energy metabolism with an increased mitochondrial activity to deal with the high amounts of fuel. Further, protecting the surrounding environment and cells from spillover of excess nutrients and lipids [382][381]. PPARG agonist stimulation and its metabolic re-balancing effects, were shown in our gene expression data, where PPARG agonist stimulated osteogenic hBMSCs were marked by a significant increase of AQP11, a known regulator of oxidative stress [278]. In fact, combined PPARG agonist and insulin treatment induced a significantly increased oxidative spare capacity, while a concomitant increase of proton leak could be identified. Sole insulin treatment steered a steady OCR/ECAR ratio, while a rather detrimental reduction in the OCR basal activity and ATP turnover was shown during late osteogenic time points and calcium deposition. In contrast, PPARG agonist treatment only as well as combined PPARG agonist treatment with insulin resulted in a rescue dynamic aligning the OCR/ECAR ratio and significantly enhancing spare capacity. Furthermore, a re-balancing of the increased proton leak induced in insulin conditions when simultaneously treating them with our PPARG agonist at late osteogenic time points. However, the insulin driven reduction of basal oxidative activity and ATP turnover could not be improved by additional PPARG agonist treatment.

There is the possibility, that PPARG agonist treatment has the ability to re-balance the detrimental insulinemic phenotype of osteogenic cells. This goes in line with described research on systemic PPARG depletion, which has been shown to induce acute metabolic inflexibility, hyperinsulinemia and hyperglycemia [383]. In our research, common genes of insulin signaling cascades such as LPL, PiK3C2b and AQP3, with the latter being important during insulin signaling via the Pi3K/Akt pathway, were significantly upregulated in PPARG agonist stimulated osteogenic cultures [280]. Indeed, research elucidating the mechanism behind the PPRAG agonist treatment and its improvement of metabolic pathologies can be

traced back to insulin-stimulated glucose uptake by increasing PI3K signaling [384]. Of importance, during osteogenic differentiation the expression of Glut4 has been shown to increase up to five-fold in dependence of insulin whereas other glucose transporters were shown to remain unchanged. Hereby highlighting the impact of glucose uptake during osteogenic differentiation to provide energy for the differentiation process and the limiting effects of insulin resistance during this process [385]. The literature has highlighted a strong association between insulin resistance and decreased mitochondrial function [386][387]. Our data showed, a significant upregulation of genes associated with mitochondrial fatty acid beta oxidation e.g. CD36 and PGC1b was shown in our gene expression data of PPARG agonist stimulated osteogenic differentiated hBMSCs. Hereby, a re-balancing of obese conditions and nutrient overload could be explained. Further, PPARG coactivator 1b (PGC1b) in interaction with other cofactors has been described to control the energy balance by increased expression of enzymes steering mitochondrial b-oxidation under high energy expenditure [173]. In addition, our data highlighted, that sole PPARG agonist treatment leads to a significant reduction of proton-leak in comparison to all insulin supplemented conditions independent of PPARG agonist co-treatment. By that underlining, that no re-balancing of osteogenic conditions with PPARG agonist stimulated metabolic features was needed as a balanced and beneficial osteogenic differentiation was already ongoing. Further, PPARG agonist driven activation of the transcriptional coactivators PGC1a as well as PGC1b during PPAR signaling is known to promote mitochondrial biogenesis [388][389][373]. Hereby, connecting our results on the PPARG agonist mediated reshaping of the mitochondrial biogenesis, which could present a new strategy for metabolic flexibility of hBMSCs.

4.2.6. And what about hyperglycemia?

In fact, PPARG agonist treatment was shown to induce significantly higher levels of glucose uptake during the course of osteogenic differentiation and especially in late time points when critical energy is needed for calcium deposition and matrix mineralization. In contrast to that, supplementation of osteogenic cultures with insulin did not steer any beneficial increase of glucose uptake in comparison to the control differentiation. Of most importance is that PPARG agonist treatment in combination to the insulin supplementation rescued the glucose metabolism in insulin treated groups and significantly enhanced the glucose uptake during the course of osteogenic differentiation. This goes in line with the published effects of PPARG signaling on glucose as well as insulin parameters in patients suffering from metabolic disorders. PPARG and its activation has been well known for its ability to control the energy balance and glucose homeostasis [236][390].

In line with that, our experimental KEGG pathway analysis showed a significant upregulation of Pi3K/Akt signaling in the PPARG agonist treated osteogenic cultures. In the literature, it is

known that PPARG is involved in the signaling cascade of insulin driven glucose uptake by engaging PI3K and with that regulating glucose uptake, lipid metabolism and cell differentiation [391]. Recently, PPARG signaling has been linked to glycolysis and gluconeogenesis in liver and muscle and the suppression of PPARG was shown to reduce insulin driven glucose uptake and transport by GLUT1 and GLUT4 in adipocytes [392][393]. When directing the focus towards PI3K signaling and its association with PPARG agonist stimulation, various authors have described a beneficial impact of PI3K/AKT signaling in proliferation, and differentiation of osteogenic cells comprising ALP activation and calcium deposition for further bone formation [394][395]. However, others have described an inverse relationship of PI3K/AKT signaling, the pro-osteogenic WNT/b catenin pathway and PPARG activity in dependence of the surrounding environment [366][396][397]. In addition, our research highlighted a significant upregulation of fatty acid metabolism and hedgehog signaling in PPARG agonist stimulated osteogenic cultures. The widely known Warburg effect induced by e.g. hedgehog signaling has been previously shown to provide essential energy for physiological osteogenic differentiation and bone formation as well as under dramatic injury. Exemplarily, in muscle and adipocytes, this activation of the cilium-dependent Smo/Ca2+/AMPK axis in form of a rapid Warburg-like metabolic program has been described, relying on a strong glucose intake with independence of insulin signaling [398]. With that, underlining the beneficial association of PPARG agonist treatment during injury driven metabolism.

In the literature, some adipokines have been shown to harbor direct as well as indirect effects on glucose and lipid metabolism [399]. Exemplarily, high amounts of secreted adiponectin, such as by our defined osteo-adipocytes, have been shown to result in insulin sensitivity by the reduction of surrounding glucose levels as well as by the increase of fatty acid combustion [260]. In addition, PPARG ablation was recently described to be associated with a shift from oxidative fatty acid metabolism towards glucose utilization/glycolysis [400]. In line with that, PPARG knockout has been shown to induce hyperglycemia/hypertriglyceridemia, hyperinsulinemia and insulin resistance, with all processes being directly linked to PPARG action as shown exemplarily in the muscle [401]. Adipo-cytokines such as MCP1 and IL1b were downregulated in our experimental PPARG agonist treatment during osteogenic differentiation and could present detrimental partakers in glucose uptake regulation. This is due to the fact, that more and more adipo-cytokines can be associated with insulin resistance and reduced glucose uptake. In the literature, pro-inflammatory IL1b and MCP1 are both associated with high glucose concentrations and glucose production [335]. Further, IL1b has been shown to inhibit GLUT4 translocation to the plasma membrane [402]. Indeed, our experimental insulin treatment resulted in a strong upregulation of these pro-inflammatory

cytokines during osteogenic differentiation and this detrimental surrounding could be improved by PPARG agonist treatment, further enhancing glucose uptake as a rescue mechanism.

5. Limitations and outlook

First, as both an advantage and a limitation, I want to highlight the co-culture of two cell types induced by activation of the transcription factor PPARG. This resulted in the exciting formation of a bone adipocyte milieu. However, due to the resulting, unclear delineation of the effects of both the osteogenic compartment and the adipogenic compartment, the interpretation of specific effects of either lineage was difficult. Second, the number of patients analyzed in this study was very low, emphasizing the patient heterogeneity. However, the tested number of patients was high enough to get a first insight into the workings of PPARG agonist treatment on bone, which would gain immense potential when studied further. In line with that, the comparison of specific cohorts of patients with different backgrounds e.g. high risk patients suffering from specific metabolic or regenerative disorders as well as patients under chronic diabetic treatment could be of interest in deepening the read-out. Third, a clear definition of the osteo-adipocyte phenotype and classification of its features was not possible with the current experimental setup. This is a very important limitation that is well known in the community, since the different BMAT types are mainly defined only by their locality in bone and prominently using animal models. Nevertheless, we stepped forward and referred to the bone healing supporting BMAT as regenerative BMAT.

Our readout presents the short term treatment of bone regeneration with PPARG agonists as a suitable option to enhance the healing capacity. This is due to the fact that it combines the induction of anti-inflammation, metabolic fitness and most importantly beneficial osteogenic differentiation. Of importance is that PPARs are already used systemically in metabolic disorders and could be re-purposed to improve the outcome of tissue and bone regeneration. This drug class could even be administered locally into the bone marrow to fulfill its purpose. When going away from the clinical application of this treatment and back to the basic science, the activation of PPARG as a transcription factor opens a new era of experimental applications, since its activation is a natural inducer of the co-culture of two cell types. It could be of interest to find other transcription factors that enable the co-induction of various other cell types and by that improving static culture system to a more sophisticated and physiological system.

6. Conclusion

Until now, research concerning tissue specific adipocytes e.g. the ones residing within the bone microenvironment, highlighted detrimental features of these cells and a worsening impact on bone regeneration. One could say, that studies on BMAT were mainly focusing on the black and not the white. Metabolic disease, aging and chronic inflammation resulting in BMA accumulation were taken as showcase example of BMAs generating detrimental tissue regeneration. Surely, such pathological situations especially the ones associated with metabolic or inflammatory stressors represent strong drivers of adverse bone healing. However, in my work I could pioneer in highlighting the other side of the coin, where healthy and pro-regenerative BMAs are gatekeepers for a beneficial bone-adipocyte milieu during fracture healing. I could show that those BMAs naturally developed at the distal part of the bone fracture coinciding with injury healing. Additional PPARG agonist treatment fortified the adipocyte accumulation and their anti-inflammatory phenotype resulting in improved bone formation as well as a beneficial anti-inflammatory TH2 cell switch in vivo. Reproducibility of the in vivo results was shown using PPARG agonist driven in vitro osteogenic cultures, where osteo-adipocytes appeared prior to the formation of calcium deposits by that resulting in an increased osteogenic potential of hBMSCs. It was appreciated, that PPARG agonist driven BMAs act as crucial regulators of metabolic and inflammatory cues during osteogenic differentiation. On the one hand, increased gene-expression and secretion of the anti-inflammatory adipokine adiponectin was appreciated and on the other hand, a decreased secretion of pro-inflammatory cues such as MCP1 and IL1b was induced. Pro-regenerative, PPARG agonist primed BMAs enabled an outstanding metabolic capacity of osteogenic hBMSCs marked by the increased oxidative capacity and ATP production as well as higher insulin sensitivity and enhanced insulin-driven glucose uptake. The summarized features of PPARG agonist primed BMAs represent them as crucial for the management of metabolic and inflammatory emergency situations such as a fracture incident (**Figure 60**). With this thesis, I want to emphasize the beneficial pro-regenerative impact of BMAs during the bone fracture healing process and their preferential induction by PPARG agonist treatment, which leads to a pro-metabolic and anti-inflammatory shift in osteogenic hBMSCs. The further investigation of PPARG agonist primed adipocytes in reliance to positive regeneration outcomes will lead to a change of perspective in our current research community.

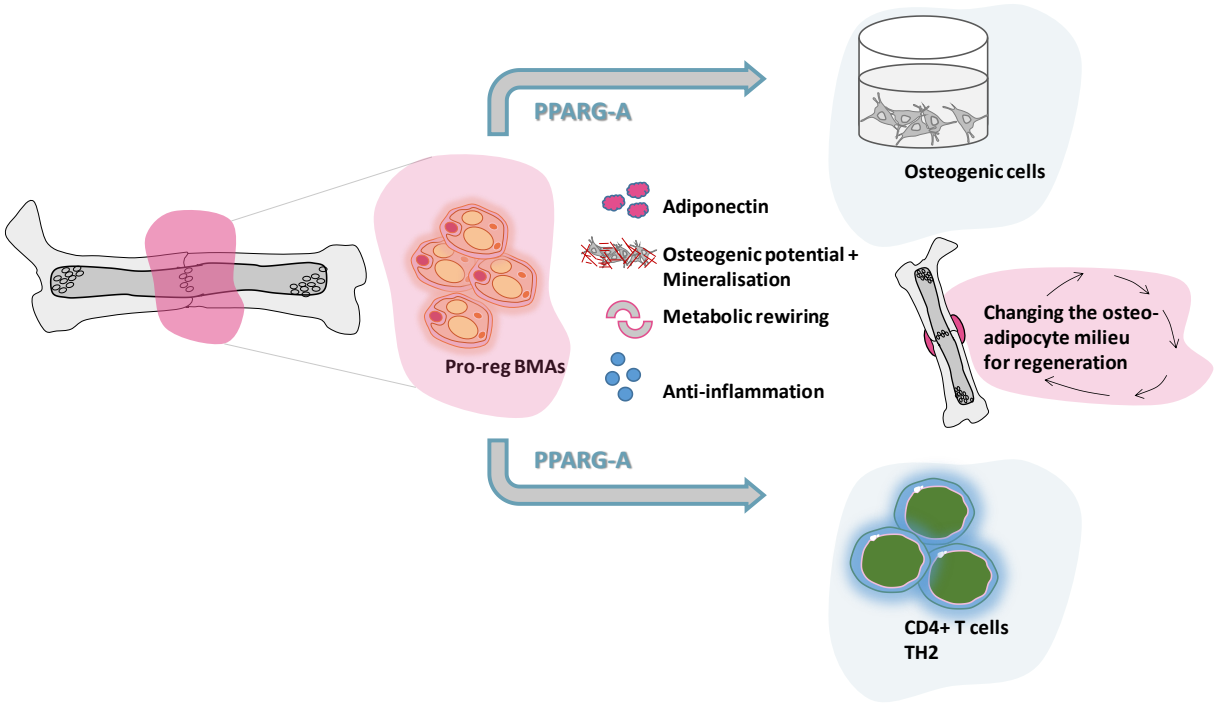

Figure 60: Changing the osteo-adipocyte milieu for regeneration
PPARG agonist priming of BMAs leads to the induction of a pro-regenerative BMA type that has potential beneficial effects during the regeneration of bone fractures. PPARG agonist treatment steers the secretion of anti-inflammatory adiponectin, enhances the potential of osteogenic differentiation and mineralization of hBMSCs and enables increased metabolic activity and oxidative capacity in vitro. All of this creates an anti-inflammatory environment and goes in line with the polarization of anti-inflammatory immune cells such as CD4+ TH2 cells in vivo.

Bibliography

[1] K. Schmidt-Bleek, A. Petersen, A. Dienelt, C. Schwarz, and G. N. Duda, “Initiation and early control of tissue regeneration-bone healing as a model system for tissue regeneration,” *Expert Opinion on Biological Therapy*, vol. 14, no. 2. pp. 247–259, 2014. doi: 10.1517/14712598.2014.857653.

[2] P. Kolar *et al.*, “The early fracture hematoma and its potential role in fracture healing,” *Tissue Engineering - Part B: Reviews*. 2010. doi: 10.1089/ten.teb.2009.0687.

[3] J. Loeffler, G. N. Duda, F. A. Sass, and A. Dienelt, “The Metabolic Microenvironment Steers Bone Tissue Regeneration,” *Trends in Endocrinology and Metabolism*, vol. 29, no. 2. pp. 99–110, 2018. doi: 10.1016/j.tem.2017.11.008.

[4] J. Lienau, H. Schell, G. N. Duda, P. Seebeck, S. Muchow, and H. J. Bail, “Initial vascularization and tissue differentiation are influenced by fixation stability,” *J. Orthop. Res.*, 2005, doi: 10.1016/j.orthres.2004.09.006.

[5] G. Karsenty and F. Oury, “The central regulation of bone mass, the first link between bone remodeling and energy metabolism,” *Journal of Clinical Endocrinology and Metabolism*. 2010. doi: 10.1210/jc.2010-1030.

[6] P. Ducy *et al.*, “Leptin inhibits bone formation through a hypothalamic relay: A central control of bone mass,” *Cell*, 2000, doi: 10.1016/S0092-8674(00)81558-5.

[7] W. E. G. Müller, E. Tolba, H. C. Schröder, and X. Wang, “Polyphosphate: A Morphogenetically Active Implant Material Serving as Metabolic Fuel for Bone Regeneration,” *Macromolecular Bioscience*. 2015. doi: 10.1002/mabi.201500100.

[8] J. Taubmann *et al.*, “Metabolic reprogramming of osteoclasts represents a therapeutic target during the treatment of osteoporosis,” *Sci. Rep.*, 2020, doi: 10.1038/s41598-020-77892-4.

[9] T. B. Sigmarsdottir *et al.*, “Metabolic and transcriptional changes across osteogenic differentiation of mesenchymal stromal cells,” *Bioengineering*, 2021, doi: 10.3390/bioengineering8120208.

[10] J. Blum, R. Epstein, S. Watts, and A. Thalacker-Mercer, “Importance of Nutrient Availability and Metabolism for Skeletal Muscle Regeneration,” *Frontiers in Physiology*. 2021. doi: 10.3389/fphys.2021.696018.

[11] K. Ito and T. Suda, “Metabolic requirements for the maintenance of self-renewing stem cells,” *Nature Reviews Molecular Cell Biology*. 2014. doi: 10.1038/nrm3772.

[12] P. Hoff *et al.*, “Human immune cells’ behavior and survival under bioenergetically restricted conditions in an in vitro fracture hematoma model,” *Cell. Mol. Immunol.*, 2013, doi: 10.1038/cmi.2012.56.

[13] D. R. Epari, J. Lienau, H. Schell, F. Witt, and G. N. Duda, “Pressure, oxygen tension and temperature in the periosteal callus during bone healing-An in vivo study in sheep,” *Bone*, 2008, doi: 10.1016/j.bone.2008.06.007.

[14] J. R. Sheen and V. V. Garla, *Fracture Healing Overview*. 2019.

[15] F. Loi, L. A. Córdova, J. Pajarinen, T. hua Lin, Z. Yao, and S. B. Goodman, “Inflammation, fracture and bone repair,” *Bone*. 2016. doi: 10.1016/j.bone.2016.02.020.

[16] J. N. Fullerton and D. W. Gilroy, “Resolution of inflammation: A new therapeutic frontier,” *Nature Reviews Drug Discovery*. 2016. doi: 10.1038/nrd.2016.39.

[17] M. Gury-BenAri *et al.*, “The Spectrum and Regulatory Landscape of Intestinal Innate Lymphoid Cells Are Shaped by the Microbiome,” *Cell*, 2016, doi: 10.1016/j.cell.2016.07.043.

[18] J. Pajarinen *et al.*, “Mesenchymal stem cell-macrophage crosstalk and bone healing,” *Biomaterials*, 2019, doi: 10.1016/j.biomaterials.2017.12.025.

[19] P. Hoff *et al.*, “Immunological characterization of the early human fracture hematoma,” *Immunol. Res.*, 2016, doi: 10.1007/s12026-016-8868-9.

[20] C. Schlundt *et al.*, “Macrophages in bone fracture healing: Their essential role in endochondral ossification,” *Bone*, 2018, doi: 10.1016/j.bone.2015.10.019.

[21] C. N. Serhan, N. Chiang, and T. E. Van Dyke, “Resolving inflammation: Dual anti-inflammatory and pro-resolution lipid mediators,” *Nature Reviews Immunology*. 2008. doi: 10.1038/nri2294.

[22] J. J. El-Jawhari, E. Jones, and P. V. Giannoudis, “The roles of immune cells in bone healing; what we know, do not know and future perspectives,” *Injury*. 2016. doi: 10.1016/j.injury.2016.10.008.

[23] K. Schmidt-Bleek *et al.*, “Initial immune reaction and angiogenesis in bone healing,” *J.*

Tissue Eng. Regen. Med., 2014, doi: 10.1002/term.1505.

[24] K. Schmidt-Bleek, B. J. Kwee, D. J. Mooney, and G. N. Duda, “Boon and Bane of Inflammation in Bone Tissue Regeneration and Its Link with Angiogenesis,” *Tissue Engineering - Part B: Reviews*. 2015. doi: 10.1089/ten.teb.2014.0677.

[25] K. Schmidt-Bleek *et al.*, “Inflammatory phase of bone healing initiates the regenerative healing cascade,” *Cell Tissue Res.*, vol. 347, no. 3, pp. 567–573, 2012, doi: 10.1007/s00441-011-1205-7.

[26] G. Juban, “Transcriptional control of macrophage inflammatory shift during skeletal muscle regeneration,” *Seminars in Cell and Developmental Biology*. 2021. doi: 10.1016/j.semcdb.2021.06.011.

[27] J. Scheller, A. Chalaris, C. Garbers, and S. Rose-John, “ADAM17: A molecular switch to control inflammation and tissue regeneration,” *Trends in Immunology*. 2011. doi: 10.1016/j.it.2011.05.005.

[28] K. Schmidt-Bleek, R. Marcucio, and G. Duda, “Future Treatment Strategies for Delayed Bone Healing: An Osteoimmunologic Approach,” *Journal of the American Academy of Orthopaedic Surgeons*. 2016. doi: 10.5435/JAAOS-D-16-00513.

[29] M. M. Matzelle *et al.*, “Resolution of inflammation induces osteoblast function and regulates the Wnt signaling pathway,” *Arthritis Rheum.*, 2012, doi: 10.1002/art.33504.

[30] J. Lee, H. Byun, S. K. Madhurakkat Perikamana, S. Lee, and H. Shin, “Current Advances in Immunomodulatory Biomaterials for Bone Regeneration,” *Advanced Healthcare Materials*. 2019. doi: 10.1002/adhm.201801106.

[31] D. M. Mosser and J. P. Edwards, “Exploring the full spectrum of macrophage activation,” *Nature Reviews Immunology*. 2008. doi: 10.1038/nri2448.

[32] O. Delarosa *et al.*, “Requirement of IFN-γ-mediated indoleamine 2,3-dioxygenase expression in the modulation of lymphocyte proliferation by human adipose-derived stem cells,” *Tissue Eng. - Part A*, 2009, doi: 10.1089/ten.tea.2008.0630.

[33] M. S. Von Bergwelt-Baildon *et al.*, “CD25 and indoleamine 2,3-dioxygenase are up-regulated by prostaglandin E2 and expressed by tumor-associated dendritic cells in vivo: Additional mechanisms of T-cell inhibition,” *Blood*, 2006, doi: 10.1182/blood-2005-08-3507.

[34] M. Bao *et al.*, “Therapeutic potentials and modulatory mechanisms of fatty acids in bone,” *Cell Proliferation*. 2020. doi: 10.1111/cpr.12735.

[35] J. U. Scher and M. H. Pillinger, “15d-PGJ2: The anti-inflammatory prostaglandin?,” *Clinical Immunology*, vol. 114, no. 2. pp. 100–109, 2005. doi: 10.1016/j.clim.2004.09.008.

[36] A. Bigham-Sadegh and A. Oryan, “Basic concepts regarding fracture healing and the current options and future directions in managing bone fractures,” *International Wound Journal*. 2015. doi: 10.1111/iwj.12231.

[37] L. C. Gerstenfeld *et al.*, “Three-dimensional reconstruction of fracture callus morphogenesis,” *J. Histochem. Cytochem.*, 2006, doi: 10.1369/jhc.6A6959.2006.

[38] C. Colnot, “Skeletal cell fate decisions within periosteum and bone marrow during bone regeneration,” *J. Bone Miner. Res.*, 2009, doi: 10.1359/jbmr.081003.

[39] M. H. ROSS, J. O. ELY, and J. G. ARCHER, “Alkaline phosphatase activity and pH optima.,” *J. Biol. Chem.*, 1951, doi: 10.1016/s0021-9258(19)77778-3.

[40] K. B. S. Paiva and J. M. Granjeiro, “Matrix Metalloproteinases in Bone Resorption, Remodeling, and Repair,” in *Progress in Molecular Biology and Translational Science*, 2017. doi: 10.1016/bs.pmbts.2017.05.001.

[41] J. C. Berkmann *et al.*, “In vivo validation of spray-dried mesoporous bioactive glass microspheres acting as prolonged local release systems for bmp-2 to support bone regeneration,” *Pharmaceutics*, 2020, doi: 10.3390/pharmaceutics12090823.

[42] K. Schmidt-Bleek, B. M. Willie, P. Schwabe, P. Seemann, and G. N. Duda, “BMPs in bone regeneration: Less is more effective, a paradigm-shift,” *Cytokine and Growth Factor Reviews*, vol. 27. pp. 141–148, 2016. doi: 10.1016/j.cytogfr.2015.11.006.

[43] T. H. Ambrosi *et al.*, “Adipocyte Accumulation in the Bone Marrow during Obesity and Aging Impairs Stem Cell-Based Hematopoietic and Bone Regeneration,” *Cell Stem Cell*, 2017, doi: 10.1016/j.stem.2017.02.009.

[44] P. J. Marie and M. Kassem, “Extrinsic mechanisms involved in age-related defective bone formation,” *Journal of Clinical Endocrinology and Metabolism*. 2011. doi: 10.1210/jc.2010-2113.

[45] U. T. Iwaniec and R. T. Turner, “Failure to generate bone marrow adipocytes does not

protect mice from ovariectomy-induced osteopenia," *Bone*, 2013, doi: 10.1016/j.bone.2012.11.034.

[46] S. A. Shapses and D. Sukumar, "Bone metabolism in obesity and weight loss," *Annual Review of Nutrition*. 2012. doi: 10.1146/annurev.nutr.012809.104655.

[47] J. Y. Huh, Y. J. Park, M. Ham, and J. B. Kim, "Crosstalk between adipocytes and immune cells in adipose tissue inflammation and metabolic dysregulation in obesity," *Molecules and Cells*. 2014. doi: 10.14348/molcells.2014.0074.

[48] N. Ouchi, J. L. Parker, J. J. Lugus, and K. Walsh, "Adipokines in inflammation and metabolic disease," *Nature Reviews Immunology*. 2011. doi: 10.1038/nri2921.

[49] M. Maruyama *et al.*, "Modulation of the Inflammatory Response and Bone Healing," *Frontiers in Endocrinology*, vol. 11. 2020. doi: 10.3389/fendo.2020.00386.

[50] M. W. Lee, M. Lee, and K. J. Oh, "Adipose tissue-derived signatures for obesity and type 2 diabetes: Adipokines, batokines and microRNAs," *Journal of Clinical Medicine*. 2019. doi: 10.3390/jcm8060854.

[51] N. Katsiki and E. Ferrannini, "Anti-inflammatory properties of antidiabetic drugs: A 'promised land' in the COVID-19 era?," *Journal of Diabetes and its Complications*. 2020. doi: 10.1016/j.jdiacomp.2020.107723.

[52] V. Kothari, J. A. Galdo, and S. T. Mathews, "Hypoglycemic agents and potential anti-inflammatory activity," *Journal of Inflammation Research*. 2016. doi: 10.2147/JIR.S86917.

[53] S. E. Kahn *et al.*, "Rosiglitazone-associated fractures in type 2 diabetes," *Diabetes Care*, vol. 31, no. 5, pp. 845–851, 2008, doi: 10.2337/dc07-2270.

[54] M. R. Cowie and M. Fisher, "SGLT2 inhibitors: mechanisms of cardiovascular benefit beyond glycaemic control," *Nature Reviews Cardiology*. 2020. doi: 10.1038/s41569-020-0406-8.

[55] A. Ammazzalorso, C. Maccallini, P. Amoia, and R. Amoroso, "Multitarget PPARγ agonists as innovative modulators of the metabolic syndrome," *European Journal of Medicinal Chemistry*. 2019. doi: 10.1016/j.ejmech.2019.04.030.

[56] M. C. Thomas and D. Z. I. Cherney, "The actions of SGLT2 inhibitors on metabolism, renal function and blood pressure," *Diabetologia*. 2018. doi: 10.1007/s00125-018-4669-

0.

[57] A. Guilherme, J. V. Virbasius, V. Puri, and M. P. Czech, “Adipocyte dysfunctions linking obesity to insulin resistance and type 2 diabetes,” *Nature Reviews Molecular Cell Biology*. 2008. doi: 10.1038/nrm2391.

[58] D. M. Muoio and C. B. Newgard, “Mechanisms of disease: Molecular and metabolic mechanisms of insulin resistance and β-cell failure in type 2 diabetes,” *Nature Reviews Molecular Cell Biology*. 2008. doi: 10.1038/nrm2327.

[59] P. Tontonoz and B. M. Spiegelman, “Fat and Beyond: The Diverse Biology of PPARγ,” *Annu. Rev. Biochem.*, 2008, doi: 10.1146/annurev.biochem.77.061307.091829.

[60] M. Qatanani and M. A. Lazar, “Mechanisms of obesity-associated insulin resistance: Many choices on the menu,” *Genes and Development*. 2007. doi: 10.1101/gad.1550907.

[61] D. Cipolletta *et al.*, “PPAR-γ is a major driver of the accumulation and phenotype of adipose tissue T reg cells,” *Nature*, vol. 486, no. 7404, pp. 549–553, 2012, doi: 10.1038/nature11132.

[62] R. Siersbæk, R. Nielsen, and S. Mandrup, “PPARγ in adipocyte differentiation and metabolism - Novel insights from genome-wide studies,” *FEBS Letters*. 2010. doi: 10.1016/j.febslet.2010.06.010.

[63] S. K. Hegazy, “Evaluation of the anti-osteoporotic effects of metformin and sitagliptin in postmenopausal diabetic women,” *J. Bone Miner. Metab.*, vol. 33, no. 2, pp. 207–212, 2015, doi: 10.1007/s00774-014-0581-y.

[64] R. K. Semple, V. K. K. Chatterjee, and S. O’Rahilly, “PPAR gamma and human metabolic disease.,” *J. Clin. Invest.*, 2006.

[65] A. R. Nawrocki *et al.*, “Mice lacking adiponectin show decreased hepatic insulin sensitivity and reduced responsiveness to peroxisome proliferator-activated receptor γ agonists,” *J. Biol. Chem.*, 2006, doi: 10.1074/jbc.M505311200.

[66] C. K. H. Wong *et al.*, “Intensification with dipeptidyl peptidase-4 inhibitor, insulin, or thiazolidinediones and risks of all-cause mortality, cardiovascular diseases, and severe hypoglycemia in patients on metformin-sulfonylurea dual therapy: A retrospective cohort study,” *PLoS Med.*, 2019, doi: 10.1371/journal.pmed.1002999.

[67] B. M. Y. Cheung, “Behind the rosiglitazone controversy,” *Expert Review of Clinical Pharmacology*. 2010. doi: 10.1586/ecp.10.126.

[68] H. Maegawa *et al.*, “Short-term low-dosage pioglitazone treatment improves vascular dysfunction in patients with type 2 diabetes,” *Endocr. J.*, 2007, doi: 10.1507/endocrj.K06-203.

[69] A. Okuno *et al.*, “Troglitazone increases the number of small adipocytes without the change of white adipose tissue mass in obese Zucker rats,” *J. Clin. Invest.*, 1998, doi: 10.1172/JCI1235.

[70] N. Petrovic, T. B. Walden, I. G. Shabalina, J. A. Timmons, B. Cannon, and J. Nedergaard, “Chronic peroxisome proliferator-activated receptor γ (PPARγ) activation of epididymally derived white adipocyte cultures reveals a population of thermogenically competent, UCP1-containing adipocytes molecularly distinct from classic brown adipocytes,” *J. Biol. Chem.*, 2010, doi: 10.1074/jbc.M109.053942.

[71] K. J. Suchacki *et al.*, “Bone marrow adipose tissue is a unique adipose subtype with distinct roles in glucose homeostasis,” *Nat. Commun.*, vol. 11, no. 1, 2020, doi: 10.1038/s41467-020-16878-2.

[72] C. L. Ackert-Bicknell, K. R. Shockley, L. G. Horton, B. Lecka-Czernik, G. A. Churchill, and C. J. Rosen, “Strain-specific effects of rosiglitazone on bone mass, body composition, and serum insulin-like growth factor-I,” *Endocrinology*, vol. 150, no. 3, pp. 1330–1340, 2009, doi: 10.1210/en.2008-0936.

[73] Z. Li, J. Hardij, D. P. Bagchi, E. L. Scheller, and O. A. MacDougald, “Development, regulation, metabolism and function of bone marrow adipose tissues,” *Bone*, 2018, doi: 10.1016/j.bone.2018.01.008.

[74] M. C. Horowitz *et al.*, “Bone marrow adipocytes,” *Adipocyte*. 2017. doi: 10.1080/21623945.2017.1367881.

[75] R. M. Evans, G. D. Barish, and Y. X. Wang, “PPARs and the complex journey to obesity,” *Nature Medicine*. 2004. doi: 10.1038/nm1025.

[76] J. Auwerx *et al.*, “A unified nomenclature system for the nuclear receptor superfamily,” *Cell*. 1999. doi: 10.1016/S0092-8674(00)80726-6.

[77] R. Stienstra, C. Duval, M. Müller, and S. Kersten, “PPARs, obesity, and inflammation,”

PPAR Research. 2007. doi: 10.1155/2007/95974.

[78] G. D. Barish, V. A. Narkar, and R. M. Evans, “PPARδ: A dagger in the heart of the metabolic syndrome,” *Journal of Clinical Investigation*. 2006. doi: 10.1172/JCI27955.

[79] M. Ahmadian *et al.*, “Pparγ signaling and metabolism: The good, the bad and the future,” *Nat. Med.*, 2013, doi: 10.1038/nm.3159.

[80] V. Bocher, I. Pineda-Torra, J. C. Fruchart, and B. Staels, “PPARS: Transcription factors controlling lipid and lipoprotein metabolism,” 2002. doi: 10.1111/j.1749-6632.2002.tb04258.x.

[81] J. Berger and D. E. Moller, “The mechanisms of action of PPARs,” *Annual Review of Medicine*. 2002. doi: 10.1146/annurev.med.53.082901.104018.

[82] A. Christofides, E. Konstantinidou, C. Jani, and V. A. Boussiotis, “The role of peroxisome proliferator-activated receptors (PPAR) in immune responses,” *Metabolism: Clinical and Experimental*. 2021. doi: 10.1016/j.metabol.2020.154338.

[83] L. Széles, D. Töröcsik, and L. Nagy, “PPARγ in immunity and inflammation: cell types and diseases,” *Biochimica et Biophysica Acta - Molecular and Cell Biology of Lipids*. 2007. doi: 10.1016/j.bbalip.2007.02.005.

[84] M. Hernandez-Quiles, M. F. Broekema, and E. Kalkhoven, “PPARgamma in Metabolism, Immunity, and Cancer: Unified and Diverse Mechanisms of Action,” *Frontiers in Endocrinology*. 2021. doi: 10.3389/fendo.2021.624112.

[85] C. L. Varley *et al.*, “Role of PPARγ and EGFR signalling in the urothelial terminal differentiation programme,” *J. Cell Sci.*, 2004, doi: 10.1242/jcs.01042.

[86] T. Varga, Z. Czimmerer, and L. Nagy, “PPARs are a unique set of fatty acid regulated transcription factors controlling both lipid metabolism and inflammation,” *Biochimica et Biophysica Acta - Molecular Basis of Disease*. 2011. doi: 10.1016/j.bbadis.2011.02.014.

[87] G. R. Beck *et al.*, “The effects of thiazolidinediones on human bone marrow stromal cell differentiation in vitro and in thiazolidinedione-treated patients with type 2 diabetes,” *Transl. Res.*, 2013, doi: 10.1016/j.trsl.2012.08.006.

[88] D. Holmes, “Non-union bone fracture: A quicker fix,” *Nature*. 2017. doi: 10.1038/550S193a.

[89] D. J. Hak *et al.*, “Delayed union and nonunions: Epidemiology, clinical issues, and financial aspects,” *Injury*, 2014, doi: 10.1016/j.injury.2014.04.002.

[90] T. Histing *et al.*, “Small animal bone healing models: Standards, tips, and pitfalls results of a consensus meeting,” *Bone*. 2011. doi: 10.1016/j.bone.2011.07.007.

[91] A. Cheng *et al.*, “Early systemic immune biomarkers predict bone regeneration after trauma,” *Proc. Natl. Acad. Sci. U. S. A.*, 2021, doi: 10.1073/pnas.2017889118.

[92] C. H. Bucher *et al.*, “Experience in the adaptive immunity impacts bone homeostasis, remodeling, and healing,” *Front. Immunol.*, 2019, doi: 10.3389/fimmu.2019.00797.

[93] D. Nam *et al.*, “T-lymphocytes enable osteoblast maturation via IL-17F during the early phase of fracture repair,” *PLoS One*, 2012, doi: 10.1371/journal.pone.0040044.

[94] D. Toben *et al.*, “Fracture healing is accelerated in the absence of the adaptive immune system,” *J. Bone Miner. Res.*, 2011, doi: 10.1002/jbmr.185.

[95] D. C. Lacey, P. J. Simmons, S. E. Graves, and J. A. Hamilton, “Proinflammatory cytokines inhibit osteogenic differentiation from stem cells: implications for bone repair during inflammation,” *Osteoarthr. Cartil.*, 2009, doi: 10.1016/j.joca.2008.11.011.

[96] Y. Liu *et al.*, “Mesenchymal stem cell-based tissue regeneration is governed by recipient T lymphocytes via IFN-γ and TNF-α,” *Nat. Med.*, 2011, doi: 10.1038/nm.2542.

[97] X. Li, B. Shang, Y. N. Li, Y. Shi, and C. Shao, “IFNγ and TNFα synergistically induce apoptosis of mesenchymal stem/stromal cells via the induction of nitric oxide,” *Stem Cell Res. Ther.*, 2019, doi: 10.1186/s13287-018-1102-z.

[98] J. K. Chan *et al.*, “ Low-dose TNF augments fracture healing in normal and osteoporotic bone by up-regulating the innate immune response ,” *EMBO Mol. Med.*, 2015, doi: 10.15252/emmm.201404487.

[99] H. Marotte and P. Miossec, “Prevention of bone mineral density loss in patients with rheumatoid arthritis treated with anti-TNFα therapy,” *Biologics: Targets and Therapy*. 2008. doi: 10.2147/btt.s2338.

[100] L. Gilbert, “Inhibition of Osteoblast Differentiation by Tumor Necrosis Factor- ,” *Endocrinology*, 2000, doi: 10.1210/en.141.11.3956.

[101] C. Ruiz, E. Pérez, O. García-Martínez, L. Díaz-Rodríguez, M. Arroyo-Morales, and C.

Reyes-Botella, “Expression of cytokines IL-4, IL-12, IL-15, IL-18, and IFNγ and modulation by different growth factors in cultured human osteoblast-like cells,” *J. Bone Miner. Metab.*, 2007, doi: 10.1007/s00774-007-0767-7.

[102] C. Vidal, S. Bermeo, W. Li, D. Huang, R. Kremer, and G. Duque, “Interferon gamma inhibits adipogenesis in vitro and prevents marrow fat infiltration in oophorectomized mice,” *Stem Cells*, 2012, doi: 10.1002/stem.1063.

[103] G. Duque *et al.*, “EMBRYONIC STEM CELLS/INDUCED PLURIPOTENT STEM CELLS Autocrine Regulation of Interferon c in Mesenchymal Stem Cells Plays a Role in Early Osteoblastogenesis,” *Stem Cells*, 2009.

[104] S. Reinke *et al.*, “Terminally differentiated CD8+ T cells negatively affect bone regeneration in humans,” *Sci. Transl. Med.*, 2013, doi: 10.1126/scitranslmed.3004754.

[105] R. M., L. A.C., W. T.M., K. C.J., and G. C.K., “The peroxisome proliferator-activated receptor-γ is a negative regulator of macrophage activation,” *Nature*, 1998.

[106] K. A. Alexander *et al.*, “Osteal macrophages promote in vivo intramembranous bone healing in a mouse tibial injury model,” *J. Bone Miner. Res.*, 2011, doi: 10.1002/jbmr.354.

[107] S. M. Abdelmagid, M. F. Barbe, and F. F. Safadi, “Role of inflammation in the aging bones,” *Life Sciences*. 2015. doi: 10.1016/j.lfs.2014.11.011.

[108] Q. Gu, H. Yang, and Q. Shi, “Macrophages and bone inflammation,” *Journal of Orthopaedic Translation*. 2017. doi: 10.1016/j.jot.2017.05.002.

[109] P. J. Murray, “Macrophage Polarization,” *Annual Review of Physiology*. 2017. doi: 10.1146/annurev-physiol-022516-034339.

[110] R. J. Sulston and W. P. Cawthorn, “Bone marrow adipose tissue as an endocrine organ: Close to the bone?,” *Horm. Mol. Biol. Clin. Investig.*, vol. 28, no. 1, pp. 21–38, 2016, doi: 10.1515/hmbci-2016-0012.

[111] A. Georgiadi and S. Kersten, “Mechanisms of gene regulation by fatty acids,” *Advances in Nutrition*, vol. 3, no. 2. pp. 127–134, 2012. doi: 10.3945/an.111.001602.

[112] A. L. Hevener *et al.*, “Macrophage PPARγ is required for normal skeletal muscle and hepatic insulin sensitivity and full antidiabetic effects of thiazolidinediones,” *J. Clin. Invest.*, vol. 117, no. 6, pp. 1658–1669, 2007, doi: 10.1172/JCI31561.

[113] Y. Zhang, T. Böse, R. E. Unger, J. A. Jansen, C. J. Kirkpatrick, and J. J. J. P. van den Beucken, “Macrophage type modulates osteogenic differentiation of adipose tissue MSCs,” *Cell Tissue Res.*, 2017, doi: 10.1007/s00441-017-2598-8.

[114] P. J. Murray and T. A. Wynn, “Protective and pathogenic functions of macrophage subsets,” *Nature Reviews Immunology*. 2011. doi: 10.1038/nri3073.

[115] W. Ying, P. S. Cheruku, F. W. Bazer, S. H. Safe, and B. Zhou, “Investigation of macrophage polarization using bone marrow derived macrophages,” *J. Vis. Exp.*, 2013, doi: 10.3791/50323.

[116] G. Le Menn and J. G. Neels, “Regulation of Immune Cell Function by PPARs and the Connection with Metabolic and Neurodegenerative Diseases,” no. II, 2018, doi: 10.3390/ijms19061575.

[117] J. I. Odegaard *et al.*, “Alternative M2 Activation of Kupffer Cells by PPARδ Ameliorates Obesity-Induced Insulin Resistance,” *Cell Metab.*, 2008, doi: 10.1016/j.cmet.2008.04.003.

[118] K. Kang *et al.*, “Adipocyte-Derived Th2 Cytokines and Myeloid PPARδ Regulate Macrophage Polarization and Insulin Sensitivity,” *Cell Metab.*, 2008, doi: 10.1016/j.cmet.2008.04.002.

[119] S. M. van den Berg, A. D. van Dam, P. C. N. Rensen, M. P. J. de Winther, and E. Lutgens, “Immune modulation of brown(ing) adipose tissue in obesity,” *Endocrine Reviews*. 2017. doi: 10.1210/er.2016-1066.

[120] J. R. Brestoff and D. Artis, “Immune regulation of metabolic homeostasis in health and disease,” *Cell*. 2015. doi: 10.1016/j.cell.2015.02.022.

[121] X. Hui *et al.*, “Adiponectin Enhances Cold-Induced Browning of Subcutaneous Adipose Tissue via Promoting M2 Macrophage Proliferation,” *Cell Metab.*, 2015, doi: 10.1016/j.cmet.2015.06.004.

[122] F. Lovren *et al.*, “Adiponectin primes human monocytes into alternative anti-inflammatory M2 macrophages,” *Am. J. Physiol. - Hear. Circ. Physiol.*, 2010, doi: 10.1152/ajpheart.00115.2010.

[123] K. M. Murphy and S. L. Reiner, “The lineage decisions of helper T cells,” *Nature Reviews Immunology*. 2002. doi: 10.1038/nri954.

[124] J. Zhu and W. E. Paul, “CD4 T cells: Fates, functions, and faults,” *Blood*, 2008, doi: 10.1182/blood-2008-05-078154.

[125] H. Takayanagi *et al.*, “T-cell-mediated regulation of osteoclastogenesis by signalling cross-talk between RANKL and IFN-γ,” *Nature*, 2000, doi: 10.1038/35046102.

[126] K. Sato *et al.*, “Th17 functions as an osteoclastogenic helper T cell subset that links T cell activation and bone destruction,” *J. Exp. Med.*, 2006, doi: 10.1084/jem.20061775.

[127] E. Bettelli, T. Korn, M. Oukka, and V. K. Kuchroo, “Induction and effector functions of TH17 cells,” *Nature*. 2008. doi: 10.1038/nature07036.

[128] R. D. Britt, M. A. Thompson, S. Sasse, C. M. Pabelick, A. N. Gerber, and Y. S. Prakash, “Th1 cytokines tnf-α and ifn-γ promote corticosteroid resistance in developing human airway smooth muscle,” *Am. J. Physiol. - Lung Cell. Mol. Physiol.*, 2019, doi: 10.1152/ajplung.00547.2017.

[129] A. M. Miller, “Role of IL-33 in inflammation and disease,” *Journal of Inflammation*. 2011. doi: 10.1186/1476-9255-8-22.

[130] V. P. Marques *et al.*, “Influence of TH1/TH2 switched immune response on renal ischemia-reperfusion injury,” *Nephron - Experimental Nephrology*. 2006. doi: 10.1159/000093676.

[131] S. Saidi *et al.*, “IL-33 is expressed in human osteoblasts, but has no direct effect on bone remodeling,” *Cytokine*, vol. 53, no. 3, pp. 347–354, 2011, doi: 10.1016/j.cyto.2010.11.021.

[132] D. G. Alleva, E. B. Johnson, F. M. Lio, S. A. Boehme, P. J. Conlon, and P. D. Crowe, “Regulation of murine macrophage proinflammatory and anti-inflammatory cytokines by ligands for peroxisome proliferator-activated receptor-gamma: counter-regulatory activity by IFN-gamma.,” *J. Leukoc. Biol.*, 2002.

[133] R. Cunard *et al.*, “Regulation of Cytokine Expression by Ligands of Peroxisome Proliferator Activated Receptors,” *J. Immunol.*, 2002, doi: 10.4049/jimmunol.168.6.2795.

[134] C. Miggitsch *et al.*, “Human bone marrow adipocytes display distinct immune regulatory properties,” *EBioMedicine*, 2019, doi: 10.1016/j.ebiom.2019.07.023.

[135] W. M. Awara, A. E. El-Sisi, M. El-Refaei, M. M. El-Naa, and K. El-Desoky, “Insulinotropic

and Anti-Inflammatory Effects of Rosiglitazone in Experimental Autoimmune Diabetes," *Rev. Diabet. Stud.*, 2005, doi: 10.1900/rds.2005.2.146.

[136] M. Angela *et al.*, "Fatty acid metabolic reprogramming via mTOR-mediated inductions of PPARγ directs early activation of T cells," *Nat. Commun.*, 2016, doi: 10.1038/ncomms13683.

[137] T. McLaughlin *et al.*, "T-cell profile in adipose tissue is associated with insulin resistance and systemic inflammation in humans," *Arterioscler. Thromb. Vasc. Biol.*, 2014, doi: 10.1161/ATVBAHA.114.304636.

[138] M. Zeyda, J. Huber, G. Prager, and T. M. Stulnig, "Inflammation correlates with markers of T-cell subsets including regulatory T cells in adipose tissue from obese patients," *Obesity*, 2011, doi: 10.1038/oby.2010.123.

[139] S. Winer *et al.*, "Normalization of obesity-associated insulin resistance through immunotherapy," *Nat. Med.*, 2009, doi: 10.1038/nm.2001.

[140] S. P. Nobs *et al.*, "PPARγ in dendritic cells and T cells drives pathogenic type-2 effector responses in lung inflammation," *J. Exp. Med.*, vol. 214, no. 10, pp. 3015–3035, 2017, doi: 10.1084/jem.20162069.

[141] G. N. Chae and S. J. Kwak, "NF-κB is involved in the TNF-α induced inhibition of the differentiation of 3T3-L1 cells by reducing PPARγ expression," *Exp. Mol. Med.*, 2003, doi: 10.1038/emm.2003.56.

[142] J. Ye, "Regulation of PPARγ function by TNF-α," *Biochemical and Biophysical Research Communications*. 2008. doi: 10.1016/j.bbrc.2008.07.068.

[143] M. S. Kim *et al.*, "Tumor necrosis factor and interleukin 1 decrease RXRα, PPARα, PPARγ, LXRα, and the coactivators SRC-1, PGC-1α, and PGC-1β in liver cells," *Metabolism.*, 2007, doi: 10.1016/j.metabol.2006.10.007.

[144] R. R. Ricardo-Gonzalez *et al.*, "IL-4/STAT6 immune axis regulates peripheral nutrient metabolism and insulin sensitivity," *Proc. Natl. Acad. Sci. U. S. A.*, 2010, doi: 10.1073/pnas.1009152108.

[145] K. Smitka and D. Marešová, "Adipose Tissue as an Endocrine Organ: An Update on Pro-inflammatory and Anti-inflammatory Microenvironment," *Prague medical report*. 2015. doi: 10.14712/23362936.2015.49.

[146] D. Cipolletta, “Adipose tissue-resident regulatory T cells: Phenotypic specialization, functions and therapeutic potential,” *Immunology*, 2014, doi: 10.1111/imm.12262.

[147] A. Chawla, K. D. Nguyen, and Y. P. S. Goh, “Macrophage-mediated inflammation in metabolic disease,” *Nature Reviews Immunology*. 2011. doi: 10.1038/nri3071.

[148] V. Z. Rocha *et al.*, “Interferon-γ, a Th1 Cytokine, Regulates Fat Inflammation,” *Circ. Res.*, 2008, doi: 10.1161/circresaha.108.177105.

[149] N. Ouchi, S. Kihara, T. Funahashi, Y. Matsuzawa, and K. Walsh, “Obesity, adiponectin and vascular inflammatory disease,” *Current Opinion in Lipidology*. 2003. doi: 10.1097/00041433-200312000-00003.

[150] P. Mancuso, “The role of adipokines in chronic inflammation,” *ImmunoTargets and Therapy*. 2016. doi: 10.2147/ITT.S73223.

[151] H. Mori *et al.*, “Secreted frizzled-related protein 5 suppresses adipocyte mitochondrial metabolism through WNT inhibition,” *J. Clin. Invest.*, 2012, doi: 10.1172/JCI63604.

[152] A. Chandra, P. Kaur, S. K. Sahu, and A. Mittal, “A new insight into the treatment of diabetes by means of pan PPAR agonists,” *Chemical Biology and Drug Design*. 2022. doi: 10.1111/cbdd.14020.

[153] N. Romero, G. Rogers, A. Neilson, and B. P. Dranka, “Quantifying Cellular ATP Production Rate Using Agilent Seahorse XF Technology,” *Agil. Technol.*, 2018.

[154] D. Nolfi-Donegan, A. Braganza, and S. Shiva, “Mitochondrial electron transport chain: Oxidative phosphorylation, oxidant production, and methods of measurement,” *Redox Biology*. 2020. doi: 10.1016/j.redox.2020.101674.

[155] E. L. Pearce and E. J. Pearce, “Metabolic pathways in immune cell activation and quiescence,” *Immunity*. 2013. doi: 10.1016/j.immuni.2013.04.005.

[156] I. Martínez-Reyes and N. S. Chandel, “Mitochondrial TCA cycle metabolites control physiology and disease,” *Nature Communications*. 2020. doi: 10.1038/s41467-019-13668-3.

[157] R. Z. Zhao, S. Jiang, L. Zhang, and Z. Bin Yu, “Mitochondrial electron transport chain, ROS generation and uncoupling (Review),” *International Journal of Molecular Medicine*. 2019. doi: 10.3892/ijmm.2019.4188.

[158] Agilent Technologies, “Agilent Seahorse XF Cell Mito Stress Test Kit User Guide - Kit 103015-100,” 2019.

[159] L. A. J. O’Neill, R. J. Kishton, and J. Rathmell, “A guide to immunometabolism for immunologists,” *Nature Reviews Immunology*. 2016. doi: 10.1038/nri.2016.70.

[160] D. Fang and E. N. Maldonado, “VDAC Regulation: A Mitochondrial Target to Stop Cell Proliferation,” in *Advances in Cancer Research*, 2018. doi: 10.1016/bs.acr.2018.02.002.

[161] B. Yetkin-Arik *et al.*, “The role of glycolysis and mitochondrial respiration in the formation and functioning of endothelial tip cells during angiogenesis,” *Sci. Rep.*, 2019, doi: 10.1038/s41598-019-48676-2.

[162] C. J. de Saedeleer, T. Copetti, P. E. Porporato, J. Verrax, O. Feron, and P. Sonveaux, “Lactate Activates HIF-1 in Oxidative but Not in Warburg-Phenotype Human Tumor Cells,” *PLoS One*, 2012, doi: 10.1371/journal.pone.0046571.

[163] S. W. S. Leung and Y. Shi, “The glycolytic process in endothelial cells and its implications,” *Acta Pharmacologica Sinica*. 2022. doi: 10.1038/s41401-021-00647-y.

[164] P. Kushwaha, M. J. Wolfgang, and R. C. Riddle, “Fatty acid metabolism by the osteoblast,” *Bone*, 2018, doi: 10.1016/j.bone.2017.08.024.

[165] G. Adamek, R. Felix, H. L. Guenther, and H. Fleisch, “Fatty acid oxidation in bone tissue and bone cells in culture. Characterization and hormonal influences.,” *Biochem. J.*, 1987, doi: 10.1042/bj2480129.

[166] J. L. Frey *et al.*, “Wnt-Lrp5 Signaling Regulates Fatty Acid Metabolism in the Osteoblast,” *Mol. Cell. Biol.*, 2015, doi: 10.1128/mcb.01343-14.

[167] C. Beermann, J. Jelinek, T. Reinecker, A. Hauenschild, G. Boehm, and H. U. Klör, “Short term effects of dietary medium-chain fatty acids and n-3 long-chain polyunsaturated fatty acids on the fat metabolism of healthy volunteers,” *Lipids Health Dis.*, 2003, doi: 10.1186/1476-511X-2-1.

[168] S. C. Lim *et al.*, “Loss of the Mitochondrial Fatty Acid β-Oxidation Protein Medium-Chain Acyl-Coenzyme A Dehydrogenase Disrupts Oxidative Phosphorylation Protein Complex Stability and Function,” *Sci. Rep.*, 2018, doi: 10.1038/s41598-017-18530-4.

[169] E. Rendina-Ruedy, A. R. Guntur, and C. J. Rosen, “Intracellular lipid droplets support osteoblast function,” *Adipocyte*, 2017, doi: 10.1080/21623945.2017.1356505.

[170] M. Rydén *et al.*, “Mapping of early signaling events in tumor necrosis factor-α-mediated lipolysis in human fat cells,” *J. Biol. Chem.*, 2002, doi: 10.1074/jbc.M109498200.

[171] J. A. Maassen, J. A. Romijn, and R. J. Heine, “Fatty acid-induced mitochondrial uncoupling in adipocytes as a key protective factor against insulin resistance and beta cell dysfunction: A new concept in the pathogenesis of obesity-associated type 2 diabetes mellitus,” *Diabetologia*. 2007. doi: 10.1007/s00125-007-0776-z.

[172] R. Walczak and P. Tontonoz, “Setting fat on fire,” *Nature Medicine*. 2003. doi: 10.1038/nm1103-1348.

[173] Y. Kamei *et al.*, “PPARγ coactivator 1β/ERR ligand 1 is an ERR protein ligand, whose expression induces a high-energy expenditure and antagonizes obesity,” *Proc. Natl. Acad. Sci. U. S. A.*, 2003, doi: 10.1073/pnas.2135217100.

[174] H. Von Bank, M. Hurtado-Thiele, N. Oshimura, and J. Simcox, “Mitochondrial lipid signaling and adaptive thermogenesis,” *Metabolites*. 2021. doi: 10.3390/metabo11020124.

[175] M. Di Paola and M. Lorusso, “Interaction of free fatty acids with mitochondria: Coupling, uncoupling and permeability transition,” *Biochimica et Biophysica Acta - Bioenergetics*. 2006. doi: 10.1016/j.bbabio.2006.03.024.

[176] J. Norseen *et al.*, “Retinol-Binding Protein 4 Inhibits Insulin Signaling in Adipocytes by Inducing Proinflammatory Cytokines in Macrophages through a c-Jun N-Terminal Kinase- and Toll-Like Receptor 4-Dependent and Retinol-Independent Mechanism,” *Mol. Cell. Biol.*, 2012, doi: 10.1128/mcb.06193-11.

[177] A. K. Jha *et al.*, “Network integration of parallel metabolic and transcriptional data reveals metabolic modules that regulate macrophage polarization,” *Immunity*, 2015, doi: 10.1016/j.immuni.2015.02.005.

[178] H. Z. Imtiyaz and M. C. Simon, “Hypoxia-inducible factors as essential regulators of inflammation,” *Curr. Top. Microbiol. Immunol.*, 2010, doi: 10.1007/82-2010-74.

[179] L. A. J. O’Neill and D. Grahame Hardie, “Metabolism of inflammation limited by AMPK and pseudo-starvation,” *Nature*. 2013. doi: 10.1038/nature11862.

[180] E. L. Mills *et al.*, “Succinate Dehydrogenase Supports Metabolic Repurposing of Mitochondria to Drive Inflammatory Macrophages,” *Cell*, 2016, doi:

10.1016/j.cell.2016.08.064.

[181] M. D. Buck, D. O'Sullivan, and E. L. Pearce, "T cell metabolism drives immunity," *Journal of Experimental Medicine*. 2015. doi: 10.1084/jem.20151159.

[182] K. Hoenderdos *et al.*, "Hypoxia upregulates neutrophil degranulation and potential for tissue injury," *Thorax*, 2016, doi: 10.1136/thoraxjnl-2015-207604.

[183] P. Sadiku and S. R. Walmsley, "Hypoxia and the regulation of myeloid cell metabolic imprinting: consequences for the inflammatory response," *EMBO Rep.*, 2019, doi: 10.15252/embr.201847388.

[184] V. M. Stoecklein, A. Osuka, and J. A. Lederer, "Trauma equals danger--damage control by the immune system," *J. Leukoc. Biol.*, 2012, doi: 10.1189/jlb.0212072.

[185] C. A. Tibbitt *et al.*, "Single-Cell RNA Sequencing of the T Helper Cell Response to House Dust Mites Defines a Distinct Gene Expression Signature in Airway Th2 Cells," *Immunity*, 2019, doi: 10.1016/j.immuni.2019.05.014.

[186] M. Yin and M. Pacifici, "Vascular regression is required for mesenchymal condensation and chondrogenesis in the developing limb," *Dev. Dyn.*, 2001, doi: 10.1002/dvdy.1212.

[187] C. Saillan-Barreau, B. Cousin, M. André, P. Villena, L. Casteilla, and L. Pénicaud, "Human adipose cells as candidates in defense and tissue remodeling phenomena," *Biochem. Biophys. Res. Commun.*, 2003, doi: 10.1016/j.bbrc.2003.08.034.

[188] H. Kwon and J. E. Pessin, "Adipokines mediate inflammation and insulin resistance," *Frontiers in Endocrinology*. 2013. doi: 10.3389/fendo.2013.00071.

[189] M. J. Cipolla, N. Bishop, R. S. Vinke, and J. A. Godfrey, "PPARγ activation prevents hypertensive remodeling of cerebral arteries and improves vascular function in female rats," *Stroke*, 2010, doi: 10.1161/STROKEAHA.109.576942.

[190] A. Uccelli, L. Moretta, and V. Pistoia, "Mesenchymal stem cells in health and disease," *Nature Reviews Immunology*. 2008. doi: 10.1038/nri2395.

[191] B. Bjørndal, L. Burri, V. Staalesen, J. Skorve, and R. K. Berge, "Different adipose depots: Their role in the development of metabolic syndrome and mitochondrial response to hypolipidemic agents," *Journal of Obesity*. 2011. doi: 10.1155/2011/490650.

[192] J. Sanchez-Gurmaches, C. M. Hung, and D. A. Guertin, “Emerging Complexities in Adipocyte Origins and Identity,” *Trends in Cell Biology*. 2016. doi: 10.1016/j.tcb.2016.01.004.

[193] D. T. Chu and B. Gawronska-Kozak, “Brown and brite adipocytes: Same function, but different origin and response,” *Biochimie*. 2017. doi: 10.1016/j.biochi.2017.04.017.

[194] K. I. Stanford, R. J. W. Middelbeek, and L. J. Goodyear, “Exercise effects on white adipose tissue: Beiging and metabolic adaptations,” *Diabetes*, 2015, doi: 10.2337/db15-0227.

[195] A. Loft *et al.*, “Browning of human adipocytes requires KLF11 and reprogramming of PPARγ superenhancers,” *Genes Dev.*, 2015, doi: 10.1101/gad.250829.114.

[196] B. Lecka-Czernik, “Marrow fat metabolism is linked to the systemic energy metabolism,” *Bone*, 2012, doi: 10.1016/j.bone.2011.06.032.

[197] Y. Li, Y. Meng, and X. Yu, “The unique metabolic characteristics of bone marrow adipose tissue,” *Frontiers in Endocrinology*. 2019. doi: 10.3389/fendo.2019.00069.

[198] L. Zhong, L. Yao, P. Seale, and L. Qin, “Marrow adipogenic lineage precursor: A new cellular component of marrow adipose tissue,” *Best Practice and Research: Clinical Endocrinology and Metabolism*. 2021. doi: 10.1016/j.beem.2021.101518.

[199] J. Chen, Y. Shi, J. Regan, K. Karuppaiah, D. M. Ornitz, and F. Long, “Osx-Cre targets multiple cell types besides osteoblast lineage in postnatal mice,” *PLoS One*, 2014, doi: 10.1371/journal.pone.0085161.

[200] Y. Liu *et al.*, “Osterix-Cre Labeled Progenitor Cells Contribute to the Formation and Maintenance of the Bone Marrow Stroma,” *PLoS One*, 2013, doi: 10.1371/journal.pone.0071318.

[201] T. H. Ambrosi, M. T. Longaker, and C. K. F. Chan, “A Revised Perspective of Skeletal Stem Cell Biology,” *Frontiers in Cell and Developmental Biology*. 2019. doi: 10.3389/fcell.2019.00189.

[202] K. J. Suchacki and W. P. Cawthorn, “Molecular Interaction of Bone Marrow Adipose Tissue with Energy Metabolism,” *Curr. Mol. Biol. Reports*, vol. 4, no. 2, pp. 41–49, 2018, doi: 10.1007/s40610-018-0096-8.

[203] C. L. Bigelow and M. Tavassoli, “Studies on conversion of yellow marrow to red marrow

by using ectopic bone marrow implants," *Exp. Hematol.*, 1984.

[204] C. S. Craft, Z. Li, O. A. MacDougald, and E. L. Scheller, "Molecular Differences Between Subtypes of Bone Marrow Adipocytes," *Curr. Mol. Biol. Reports*, 2018, doi: 10.1007/s40610-018-0087-9.

[205] E. L. Scheller *et al.*, "Region-specific variation in the properties of skeletal adipocytes reveals regulated and constitutive marrow adipose tissues," *Nat. Commun.*, 2015, doi: 10.1038/ncomms8808.

[206] A. W. B. Joe *et al.*, "Muscle injury activates resident fibro/adipogenic progenitors that facilitate myogenesis," *Nat. Cell Biol.*, 2010, doi: 10.1038/ncb2015.

[207] O. A. Mohiuddin *et al.*, "Decellularized Adipose Tissue Hydrogel Promotes Bone Regeneration in Critical-Sized Mouse Femoral Defect Model," *Front. Bioeng. Biotechnol.*, 2019, doi: 10.3389/fbioe.2019.00211.

[208] T. H. Ambrosi and T. J. Schulz, "The emerging role of bone marrow adipose tissue in bone health and dysfunction," *Journal of Molecular Medicine*, vol. 95, no. 12. pp. 1291–1301, 2017. doi: 10.1007/s00109-017-1604-7.

[209] J. W. Lewis, J. R. Edwards, A. J. Naylor, and H. M. McGettrick, "Adiponectin signalling in bone homeostasis, with age and in disease," *Bone Research*. 2021. doi: 10.1038/s41413-020-00122-0.

[210] H.-K. Bae, B.-D. Jung, S. Lee, C.-K. Park, B.-K. Yang, and H.-T. Cheong, "Chondrogenic Differentiation of Porcine Skin-Derived Stem Cells with Different Characteristics of Spontaneous Adipocyte Formation," *J. Anim. Reprod. Biotechnol.*, 2017, doi: 10.12750/jet.2017.32.3.193.

[211] E. D. Rosen and B. M. Spiegelman, "Adipocytes as regulators of energy balance and glucose homeostasis," *Nature*. 2006. doi: 10.1038/nature05483.

[212] L. Luo and M. Liu, "Adipose tissue in control of metabolism," *Journal of Endocrinology*. 2016. doi: 10.1530/JOE-16-0211.

[213] H. Zhuang *et al.*, "Molecular Mechanisms of PPAR-γ; Governing MSC Osteogenic and Adipogenic Differentiation," *Curr. Stem Cell Res. Ther.*, 2016, doi: 10.2174/1574888x10666150531173309.

[214] I. Takada, A. P. Kouzmenko, and S. Kato, "Wnt and PPARγ signaling in

osteoblastogenesis and adipogenesis," *Nature Reviews Rheumatology*. 2009. doi: 10.1038/nrrheum.2009.137.

[215] R. L. Huang *et al.*, "IL-6 potentiates BMP-2-induced osteogenesis and adipogenesis via two different BMPR1A-mediated pathways article," *Cell Death Dis.*, 2018, doi: 10.1038/s41419-017-0126-0.

[216] M. Sharma *et al.*, "Enhanced glycolysis and HIF-1α activation in adipose tissue macrophages sustains local and systemic interleukin-1β production in obesity," *Sci. Rep.*, 2020, doi: 10.1038/s41598-020-62272-9.

[217] S. I. Anghel and W. Wahli, "Fat poetry: A kingdom for PPARγ," *Cell Research*. 2007. doi: 10.1038/cr.2007.48.

[218] G. Pascual *et al.*, "A sumoylation-dependent pathway mediating transrepression of inflammatory response genes by PPARγ NIH Public Access," 2005.

[219] C. Wang *et al.*, "Peroxisome Proliferator-Activated Receptor-γ Knockdown Impairs Bone Morphogenetic Protein-2–Induced Critical-Size Bone Defect Repair," *Am. J. Pathol.*, 2019, doi: 10.1016/j.ajpath.2018.11.019.

[220] G. Wilcox, "Insulin and Insulin," *Clin. Biochem. Rev.*, 2005.

[221] C. M. Taniguchi, B. Emanuelli, and C. R. Kahn, "Critical nodes in signalling pathways: Insights into insulin action," *Nature Reviews Molecular Cell Biology*. 2006. doi: 10.1038/nrm1837.

[222] W. Zhang *et al.*, "Effects of insulin and insulin-like growth factor 1 on osteoblast proliferation and differentiation: Differential signalling via Akt and ERK," *Cell Biochem. Funct.*, 2012, doi: 10.1002/cbf.2801.

[223] K. Fulzele, D. J. DiGirolamo, Z. Liu, J. Xu, J. L. Messina, and T. L. Clemens, "Disruption of the insulin-like growth factor type 1 receptor in osteoblasts enhances insulin signaling and action," *J. Biol. Chem.*, 2007, doi: 10.1074/jbc.M700651200.

[224] O. T. Hardy, M. P. Czech, and S. Corvera, "What causes the insulin resistance underlying obesity?," *Current Opinion in Endocrinology, Diabetes and Obesity*. 2012. doi: 10.1097/MED.0b013e3283514e13.

[225] R. Rubin and R. Baserga, "Insulin-like growth factor-I receptor: Its role in cell proliferation, apoptosis, and tumorigenicity," *Laboratory Investigation*. 1995.

[226] C. Kuhn, S. A. Hurwitz, M. G. Kumar, J. Cotton, and D. F. Spandau, “Activation of the insulin-like growth factor-1 receptor promotes the survival of human keratinocytes following ultraviolet B irradiation,” *Int. J. Cancer*, 1999, doi: 10.1002/(SICI)1097-0215(19990129)80:3<431::AID-IJC16>3.0.CO;2-5.

[227] V. Vella, M. L. Nicolosi, S. Giuliano, M. Bellomo, A. Belfiore, and R. Malaguarnera, “PPAR-γ agonists as antineoplastic agents in cancers with dysregulated IGF axis,” *Frontiers in Endocrinology*. 2017. doi: 10.3389/fendo.2017.00031.

[228] Y. F. Zhao *et al.*, “Osteogenic potential of bone marrow stromal cells derived from streptozotocin-induced diabetic rats,” *Int. J. Mol. Med.*, 2013, doi: 10.3892/ijmm.2013.1227.

[229] C. Contaldo *et al.*, “Expression levels of insulin receptor substrate-1 modulate the osteoblastic differentiation of mesenchymal stem cells and osteosarcoma cells,” *Growth Factors*, 2014, doi: 10.3109/08977194.2013.870168.

[230] M. Janghorbani, R. M. Van Dam, W. C. Willett, and F. B. Hu, “Systematic review of type 1 and type 2 diabetes mellitus and risk of fracture,” *American Journal of Epidemiology*. 2007. doi: 10.1093/aje/kwm106.

[231] M. Retzepi and N. Donos, “The effect of diabetes mellitus on osseous healing,” *Clinical Oral Implants Research*. 2010. doi: 10.1111/j.1600-0501.2010.01923.x.

[232] M. Tencerova *et al.*, “Obesity-Associated Hypermetabolism and Accelerated Senescence of Bone Marrow Stromal Stem Cells Suggest a Potential Mechanism for Bone Fragility,” *Cell Rep.*, 2019, doi: 10.1016/j.celrep.2019.04.066.

[233] N. Wang *et al.*, “IRS-1 targets TAZ to inhibit adipogenesis of rat bone marrow mesenchymal stem cells through PI3K-Akt and MEK-ERK pathways,” *Eur. J. Pharmacol.*, 2019, doi: 10.1016/j.ejphar.2019.01.064.

[234] Y. Wang *et al.*, “MiR-431 inhibits adipogenic differentiation of human bone marrow-derived mesenchymal stem cells via targeting insulin receptor substance 2,” *Stem Cell Res. Ther.*, 2018, doi: 10.1186/s13287-018-0980-4.

[235] M. Tencerova, M. Okla, and M. Kassem, “Insulin Signaling in Bone Marrow Adipocytes,” *Current Osteoporosis Reports*. 2019. doi: 10.1007/s11914-019-00552-8.

[236] F. Giorgino, A. Leonardini, L. Laviola, S. Perrini, and A. Natalicchio, “Cross-Talk

between PPARγ and insulin signaling and modulation of Insulin Sensitivity," *PPAR Research*. 2009. doi: 10.1155/2009/818945.

[237] J. Wei *et al.*, "Glucose Uptake and Runx2 Synergize to Orchestrate Osteoblast Differentiation and Bone Formation," *Cell*, 2015, doi: 10.1016/j.cell.2015.05.029.

[238] M. Beeson *et al.*, "Activation of protein kinase C-ζ by insulin and phosphatidylinositol-3,4,5-(PO4)3 is defective in muscle in type 2 diabetes and impaired glucose tolerance: Amelioration by rosiglitazone and exercise," *Diabetes*, 2003, doi: 10.2337/diabetes.52.8.1926.

[239] X. Zhou *et al.*, "The Activation of Peroxisome Proliferator-activated Receptor γ Enhances Insulin Signaling Pathways Via Up-regulating Chemerin Expression in High Glucose Treated HTR-8/SVneo Cells," *Matern. Med.*, 2020, doi: 10.1097/FM9.0000000000000044.

[240] D. Y. Guan *et al.*, "Rosiglitazone promotes glucose metabolism of GIFT tilapia based on the PI3K/Akt signaling pathway," *Physiol. Rep.*, 2021, doi: 10.14814/phy2.14765.

[241] K. J. Oh, D. S. Lee, W. K. Kim, B. S. Han, S. C. Lee, and K. H. Bae, "Metabolic adaptation in obesity and type ii diabetes: Myokines, adipokines and hepatokines," *Int. J. Mol. Sci.*, 2017, doi: 10.3390/ijms18010008.

[242] G. D. Roodman, "Genes associate with abnormal bone cell activity in bone metastasis," *Cancer Metastasis Rev.*, 2012, doi: 10.1007/s10555-012-9372-x.

[243] E. Shin and J. S. Koo, "The role of adipokines and bone marrow adipocytes in breast cancer bone metastasis," *International Journal of Molecular Sciences*. 2020. doi: 10.3390/ijms21144967.

[244] L. F. Liu, W. J. Shen, M. Ueno, S. Patel, and F. B. Kraemer, "Characterization of age-related gene expression profiling in bone marrow and epididymal adipocytes," *BMC Genomics*, 2011, doi: 10.1186/1471-2164-12-212.

[245] S. Rahman, Y. Lu, P. J. Czernik, C. J. Rosen, S. Enerback, and B. Lecka-Czernik, "Inducible brown adipose tissue, or beige fat, is anabolic for the skeleton," *Endocrinology*, 2013, doi: 10.1210/en.2012-2162.

[246] C. Xie and Q. Chen, "Adipokines: New Therapeutic Target for Osteoarthritis?," *Current Rheumatology Reports*. 2019. doi: 10.1007/s11926-019-0868-z.

[247] J. M. Bruun, A. S. Lihn, S. B. Pedersen, and B. Richelsen, “Monocyte chemoattractant protein-1 release is higher in visceral than subcutaneous human adipose tissue (AT): Implication of macrophages resident in the AT,” *J. Clin. Endocrinol. Metab.*, 2005, doi: 10.1210/jc.2004-1696.

[248] R. Terkeltaub, W. A. Boisvert, and L. K. Curtiss, “Chemokines and atherosclerosis,” *Current Opinion in Lipidology*. 1998. doi: 10.1097/00041433-199810000-00003.

[249] K. Takahashi *et al.*, “Adiposity Elevates Plasma MCP-1 Levels Leading to the Increased CD11b-positive Monocytes in Mice,” *J. Biol. Chem.*, 2003, doi: 10.1074/jbc.M309895200.

[250] P. Sartipy and D. J. Loskutoff, “Monocyte chemoattractant protein 1 in obesity and insulin resistance,” *Proc. Natl. Acad. Sci. U. S. A.*, 2003, doi: 10.1073/pnas.1133870100.

[251] H. Takaishi, T. Taniguchi, A. Takahashi, Y. Ishikawa, and M. Yokoyama, “High glucose accelerates MCP-1 production via p38 MAPK in vascular endothelial cells,” *Biochem. Biophys. Res. Commun.*, 2003, doi: 10.1016/S0006-291X(03)00712-5.

[252] C. Schlundt *et al.*, “Individual effector/regulator T cell ratios impact bone regeneration,” *Front. Immunol.*, 2019, doi: 10.3389/fimmu.2019.01954.

[253] L. Flower, R. Gray, J. Pinkney, and V. Mohamed-Ali, “Stimulation of interleukin-6 release by interleukin-1β from isolated human adipocytes,” *Cytokine*, 2003, doi: 10.1016/S1043-4666(02)00495-7.

[254] E. Somm *et al.*, “Interleukin-1 receptor antagonist is upregulated during diet-induced obesity and regulates insulin sensitivity in rodents,” *Diabetologia*, 2006, doi: 10.1007/s00125-005-0046-x.

[255] T. Simopoulou *et al.*, “Differential expression of leptin and leptin’s receptor isoform (Ob-Rb) mRNA between advanced and minimally affected osteoarthritic cartilage; effect on cartilage metabolism,” *Osteoarthr. Cartil.*, 2007, doi: 10.1016/j.joca.2007.01.018.

[256] N. Kamio, S. Akifusa, N. Yamaguchi, K. Nonaka, and Y. Yamashita, “Anti-inflammatory activity of a globular adiponectin function on RAW 264 cells stimulated by lipopolysaccharide from Aggregatibacter actinomycetemcomitans,” *FEMS Immunol. Med. Microbiol.*, 2009, doi: 10.1111/j.1574-695X.2009.00573.x.

[257] W. P. Cawthorn *et al.*, “Bone marrow adipose tissue is an endocrine organ that contributes to increased circulating adiponectin during caloric restriction,” *Cell Metab.*, 2014, doi: 10.1016/j.cmet.2014.06.003.

[258] A. Booth, A. Magnuson, J. Fouts, and M. Foster, “Adipose tissue, obesity and adipokines: Role in cancer promotion,” *Horm. Mol. Biol. Clin. Investig.*, 2015, doi: 10.1515/hmbci-2014-0037.

[259] T. Yamauchi *et al.*, “Targeted disruption of AdipoR1 and AdipoR2 causes abrogation of adiponectin binding and metabolic actions,” *Nat. Med.*, 2007, doi: 10.1038/nm1557.

[260] J. Fruebis, “Proteolytic cleavage product of 30-kDa adipocyte complement-related protein increases fatty acid oxidation in muscle and causes weight loss in mice,” *Proc. Natl. Acad. Sci.*, 2001, doi: 10.1073/pnas.041591798.

[261] I. Kanazawa, T. Yamaguchi, S. Yano, M. Yamauchi, M. Yamamoto, and T. Sugimoto, “Adiponectin and AMP kinase activator stimulate proliferation, differentiation, and mineralization of osteoblastic MC3T3-E1 cells,” *BMC Cell Biol.*, 2007, doi: 10.1186/1471-2121-8-51.

[262] R. Lago *et al.*, “A new player in cartilage homeostasis: adiponectin induces nitric oxide synthase type II and pro-inflammatory cytokines in chondrocytes,” *Osteoarthr. Cartil.*, 2008, doi: 10.1016/j.joca.2007.12.008.

[263] Y. Shinoda *et al.*, “Regulation of bone formation by adiponectin through autocrine/paracrine and endocrine pathways,” *J. Cell. Biochem.*, 2006, doi: 10.1002/jcb.20890.

[264] S. THEOCHARIS, “Peroxisome proliferator-activated receptor-$gamma; ligands as cell-cycle modulators,” *Cancer Treat. Rev.*, 2004, doi: 10.1016/s0305-7372(04)00079-9.

[265] C. Freudlsperger, I. Moll, U. Schumacher, and A. Thies, “Anti-proliferative effect of peroxisome proliferator-activated receptor γ agonists on human malignant melanoma cells in vitro,” *Anticancer. Drugs*, 2006, doi: 10.1097/00001813-200603000-00011.

[266] M. Tavallaie *et al.*, “Moderation of mitochondrial respiration mitigates metabolic syndrome of aging,” *Proc. Natl. Acad. Sci. U. S. A.*, 2020, doi: 10.1073/pnas.1917948117.

[267] A. A. Eissa Ahmed, N. M. Al-Rasheed, and N. M. Al-Rasheed, “Antidepressant-like

effects of rosiglitazone, a PPARγ agonist, in the rat forced swim and mouse tail suspension tests," *Behav. Pharmacol.*, 2009, doi: 10.1097/FBP.0b013e328331b9bf.

[268] T. Takazawa *et al.*, "Peroxisome proliferator-activated receptor γ agonist rosiglitazone increases expression of very low density lipoprotein receptor gene in adipocytes," *J. Biol. Chem.*, 2009, doi: 10.1074/jbc.M109.047993.

[269] N. Yuan *et al.*, "BADGE, a synthetic antagonist for PPARγ, prevents steroid-related osteonecrosis in a rabbit model," *BMC Musculoskelet. Disord.*, 2018, doi: 10.1186/s12891-018-2050-6.

[270] K. Sato *et al.*, "PPARγ antagonist attenuates mouse immunemediated bone marrow failure by inhibition of T cell function," *Haematologica*, 2015, doi: 10.3324/haematol.2014.121632.

[271] J. Appelt *et al.*, "The neuropeptide calcitonin gene-related peptide alpha is essential for bone healing," *EBioMedicine*, 2020, doi: 10.1016/j.ebiom.2020.102970.

[272] Bruker, "Bone mineral density (BMD) and tissue mineral density (TMD) calibration and measurement by micro-CT using Bruker-MicroCT," *Bruker Method Note*, 2010.

[273] M. Dominici *et al.*, "Minimal criteria for defining multipotent mesenchymal stromal cells. The International Society for Cellular Therapy position statement," *Cytotherapy*, 2006, doi: 10.1080/14653240600855905.

[274] A. Peister, J. A. Mellad, B. L. Larson, B. M. Hall, L. F. Gibson, and D. J. Prockop, "Adult stem cells from bone marrow (MSCs) isolated from different strains of inbred mice vary in surface epitopes, rates of proliferation, and differentiation potential," *Blood*, 2004, doi: 10.1182/blood-2003-09-3070.

[275] Y. Hu *et al.*, "Comparative study on in vitro culture of mouse bone marrow mesenchymal stem cells," *Stem Cells Int.*, 2018, doi: 10.1155/2018/6704583.

[276] I. Sekiya, B. L. Larson, J. T. Vuoristo, J. G. Cui, and D. J. Prockop, "Adipogenic Differentiation of Human Adult Stem Cells from Bone Marrow Stroma (MSCs)," *J. Bone Miner. Res.*, 2004, doi: 10.1359/JBMR.0301220.

[277] D. Bishop-Bailey, T. Hla, and T. D. Warner, "Bisphenol A diglycidyl ether (BADGE) is a PPARγ agonist in an ECV304 cell line," *Br. J. Pharmacol.*, 2000, doi: 10.1038/sj.bjp.0703628.

[278] S. Bestetti *et al.*, “Human aquaporin-11 guarantees efficient transport of H2O2 across the endoplasmic reticulum membrane,” *Redox Biol.*, 2020, doi: 10.1016/j.redox.2019.101326.

[279] M. Galli, A. Hameed, A. Żbikowski, and P. Zabielski, “Aquaporins in insulin resistance and diabetes: More than channels!,” *Redox Biology*. 2021. doi: 10.1016/j.redox.2021.102027.

[280] X. Wu, K. Chen, and K. J. Williams, “An oxide transport chain essential for balanced insulin action,” *Atherosclerosis*, 2020, doi: 10.1016/j.atherosclerosis.2020.02.006.

[281] S. Reinke *et al.*, “Terminally differentiated CD8+ T cells negatively affect bone regeneration in humans,” *Sci. Transl. Med.*, vol. 5, no. 177, 2013, doi: 10.1126/scitranslmed.3004754.

[282] R. Cunard, Y. Eto, J. T. Muljadi, C. K. Glass, C. J. Kelly, and M. Ricote, “Repression of IFN-γ Expression by Peroxisome Proliferator-Activated Receptor γ,” *J. Immunol.*, 2004, doi: 10.4049/jimmunol.172.12.7530.

[283] C. E. Juge-Aubry *et al.*, “Adipose tissue is a major source of interleukin-1 receptor antagonist: Upregulation in obesity and inflammation,” *Diabetes*, 2003, doi: 10.2337/diabetes.52.5.1104.

[284] A. Hyong *et al.*, “Rosiglitazone, a PPAR gamma agonist, attenuates inflammation after surgical brain injury in rodents,” *Brain Res.*, 2008, doi: 10.1016/j.brainres.2008.04.025.

[285] Z. Li *et al.*, “Lipolysis of bone marrow adipocytes is required to fuel bone and the marrow niche during energy deficits,” *Elife*, vol. 11, pp. 50–70, 2022, doi: 10.7554/elife.78496.

[286] E. L. Scheller *et al.*, “Region-specific variation in the properties of skeletal adipocytes reveals regulated and constitutive marrow adipose tissues,” *Nat. Commun.*, vol. 6, 2015, doi: 10.1038/ncomms8808.

[287] A. L Newton, L. J Hanks, M. Davis, and K. Casazza, “The relationships among total body fat, bone mineral content and bone marrow adipose tissue in early-pubertal girls,” *Bonekey Rep.*, vol. 2, no. 4, 2013, doi: 10.1038/bonekey.2013.49.

[288] T. Mizoguchi *et al.*, “Osterix marks distinct waves of primitive and definitive stromal progenitors during bone marrow development,” *Dev. Cell*, 2014, doi: 10.1016/j.devcel.2014.03.013.

[289] T. M. Baylink, S. Mohan, R. J. Fitzsimmons, and D. J. Baylink, “Evaluation of signal transduction mechanisms for the mitogenic effects of prostaglandin E2 in normal human bone cells in vitro,” *J. Bone Miner. Res.*, 1996, doi: 10.1002/jbmr.5650111007.

[290] Y. F. Ma, H. Z. Ke, and W. S. S. Jee, “Prostaglaridin E2 adds bone to a cancellous bone site with a closed growth plate and low bone turnover in ovariectomized rats,” *Bone*, 1994, doi: 10.1016/8756-3282(94)90700-5.

[291] S. Wendler *et al.*, “Immune modulation to enhance bone healing-a new concept to induce bone using prostacyclin to locally modulate immunity,” *Front. Immunol.*, 2019, doi: 10.3389/fimmu.2019.00713.

[292] A. Dalla Valle *et al.*, “Induction of Stearoyl-CoA 9-Desaturase 1 Protects Human Mesenchymal Stromal Cells Against Palmitic Acid-Induced Lipotoxicity and Inflammation,” *Front. Endocrinol. (Lausanne).*, 2019, doi: 10.3389/fendo.2019.00726.

[293] Z. Zhou, Y. Lu, Y. Wang, L. Du, Y. Zhang, and J. Tao, “Let-7c regulates proliferation and osteodifferentiation of human adipose-derived mesenchymal stem cells under oxidative stress by targeting SCD-1,” *Am. J. Physiol. - Cell Physiol.*, 2019, doi: 10.1152/ajpcell.00211.2018.

[294] B. O. Zhou *et al.*, “Bone marrow adipocytes promote the regeneration of stem cells and haematopoiesis by secreting SCF,” *Nat. Cell Biol.*, vol. 19, no. 8, pp. 891–903, 2017, doi: 10.1038/ncb3570.

[295] H. K. Pillai *et al.*, “Ligand binding and activation of PPARγ by firemaster® 550: Effects on adipogenesis and osteogenesis in vitro,” *Environ. Health Perspect.*, vol. 122, no. 11, pp. 1225–1232, 2014, doi: 10.1289/ehp.1408111.

[296] M. van de Vyver, E. Andrag, I. L. Cockburn, and W. F. Ferris, “Thiazolidinedione-induced lipid droplet formation during osteogenic differentiation,” *J. Endocrinol.*, vol. 223, no. 2, pp. 119–132, 2014, doi: 10.1530/JOE-14-0425.

[297] S. Botolin and L. R. McCabe, “Inhibition of PPARγ prevents type I diabetic bone marrow adiposity but not bone loss,” *J. Cell. Physiol.*, 2006, doi: 10.1002/jcp.20804.

[298] S. S. Durgam, N. N. Altmann, H. E. Coughlin, A. Rollins, and L. D. Hostnik, “Insulin enhances the in vitro osteogenic capacity of flexor tendon-derived progenitor cells,” *Stem Cells Int.*, 2019, doi: 10.1155/2019/1602751.

[299] P. Xue *et al.*, “IGF1 promotes osteogenic differentiation of mesenchymal stem cells derived from rat bone marrow by increasing TAZ expression,” *Biochem. Biophys. Res. Commun.*, 2013, doi: 10.1016/j.bbrc.2013.02.088.

[300] T. Hosoyama, N. Ishiguro, K. Yamanouchi, and M. Nishihara, “Degenerative muscle fiber accelerates adipogenesis of intramuscular cells via RhoA signaling pathway,” *Differentiation*, 2009, doi: 10.1016/j.diff.2008.11.001.

[301] K. R. Levental *et al.*, “w-3 polyunsaturated fatty acids direct differentiation of the membrane phenotype in mesenchymal stem cells to potentiate osteogenesis,” *Sci. Adv.*, 2017, doi: 10.1126/sciadv.aao1193.

[302] J. Dong, X. Xu, Q. Zhang, Z. Yuan, and B. Tan, “The PI3K/AKT pathway promotes fracture healing through its crosstalk with Wnt/β-catenin,” *Exp. Cell Res.*, 2020, doi: 10.1016/j.yexcr.2020.112137.

[303] M. A. Scott, V. T. Nguyen, B. Levi, and A. W. James, “Current methods of adipogenic differentiation of mesenchymal stem cells,” *Stem Cells Dev.*, 2011, doi: 10.1089/scd.2011.0040.

[304] M. A. Bredella *et al.*, “Vertebral bone marrow fat is positively associated with visceral fat and inversely associated with IGF-1 in obese women,” *Obesity*, 2011, doi: 10.1038/oby.2010.106.

[305] K. E. Govoni, J. E. Wergedal, L. Florin, P. Angel, D. J. Baylink, and S. Mohan, “Conditional deletion of insulin-like growth factor-I in collagen type 1α2-expressing cells results in postnatal lethality and a dramatic reduction in bone accretion,” *Endocrinology*, 2007, doi: 10.1210/en.2007-0608.

[306] E. L. Scheller, W. P. Cawthorn, A. A. Burr, M. C. Horowitz, and O. A. MacDougald, “Marrow Adipose Tissue: Trimming the Fat,” *Trends in Endocrinology and Metabolism*. 2016. doi: 10.1016/j.tem.2016.03.016.

[307] J. N. Beresford, J. H. Bennett, C. Devlin, P. S. Leboy, and M. E. Owen, “Evidence for an inverse relationship between the differentiation of adipocytic and osteogenic cells in rat marrow stromal cell cultures,” *J. Cell Sci.*, 1992, doi: 10.1242/jcs.102.2.341.

[308] E. D. Rosen and O. A. MacDougald, “Adipocyte differentiation from the inside out,” *Nature Reviews Molecular Cell Biology*. 2006. doi: 10.1038/nrm2066.

[309] Q. Kang *et al.*, “A Comprehensive analysis of the dual roles of BMPs in regulating adipogenic and osteogenic differentiation of mesenchymal progenitor cells,” *Stem Cells Dev.*, 2009, doi: 10.1089/scd.2008.0130.

[310] Y. Y. Lin *et al.*, “Adiponectin receptor 1 regulates bone formation and osteoblast differentiation by GSK-3β/β-Catenin signaling in mice,” *Bone*, 2014, doi: 10.1016/j.bone.2014.03.051.

[311] T. Chen, Y. W. Wu, H. Lu, Y. Guo, and Z. H. Tang, “Adiponectin enhances osteogenic differentiation in human adipose-derived stem cells by activating the APPL1-AMPK signaling pathway,” *Biochem. Biophys. Res. Commun.*, 2015, doi: 10.1016/j.bbrc.2015.03.168.

[312] K. Uchihashi *et al.*, “Organotypic culture of human bone marrow adipose tissue,” *Pathol. Int.*, 2010, doi: 10.1111/j.1440-1827.2010.02511.x.

[313] S. Yang, H. Liu, Y. Liu, L. Liu, W. Zhang, and E. Luo, “Effect of adiponectin secreted from adipose-derived stem cells on bone-fat balance and bone defect healing,” *J. Tissue Eng. Regen. Med.*, 2019, doi: 10.1002/term.2915.

[314] J. I. Odegaard and A. Chawla, “Alternative macrophage activation and metabolism,” *Annu. Rev. Pathol. Mech. Dis.*, 2011, doi: 10.1146/annurev-pathol-011110-130138.

[315] E. L. Scheller *et al.*, “Bone marrow adipocytes resist lipolysis and remodeling in response to β-adrenergic stimulation,” *Bone*, 2019, doi: 10.1016/j.bone.2018.01.016.

[316] E. L. Scheller, A. A. Burr, O. A. MacDougald, and W. P. Cawthorn, “Inside out: Bone marrow adipose tissue as a source of circulating adiponectin,” *Adipocyte*. 2016. doi: 10.1080/21623945.2016.1149269.

[317] J. Ryu *et al.*, “Adiponectin Alleviates Diet-Induced Inflammation in the Liver by Suppressing MCP-1 Expression and Macrophage Infiltration,” *Diabetes*, 2021, doi: 10.2337/db20-1073.

[318] E. Rojas *et al.*, “The role of adiponectin in endothelial dysfunction and hypertension,” *Curr. Hypertens. Rep.*, 2014, doi: 10.1007/s11906-014-0463-7.

[319] G. Deng, Y. Long, Y. R. Yu, and M. R. Li, “Adiponectin directly improves endothelial dysfunction in obese rats through the AMPK-eNOS Pathway,” *Int. J. Obes.*, 2010, doi: 10.1038/ijo.2009.205.

[320] A. S. Lihn, J. M. Bruun, G. He, S. B. Pedersen, P. F. Jensen, and B. Richelsen, “Lower expression of adiponectin mRNA in visceral adipose tissue in lean and obese subjects,” *Mol. Cell. Endocrinol.*, 2004, doi: 10.1016/j.mce.2004.03.002.

[321] C. Lagathu *et al.*, “Long-term treatment with interleukin-1β induces insulin resistance in murine and human adipocytes,” *Diabetologia*, 2006, doi: 10.1007/s00125-006-0335-z.

[322] T. H. Lin *et al.*, “Chronic inflammation in biomaterial-induced periprosthetic osteolysis: NF-κB as a therapeutic target,” *Acta Biomaterialia*. 2014. doi: 10.1016/j.actbio.2013.09.034.

[323] S. L. Deshmane, S. Kremlev, S. Amini, and B. E. Sawaya, “Monocyte chemoattractant protein-1 (MCP-1): An overview,” *Journal of Interferon and Cytokine Research*. 2009. doi: 10.1089/jir.2008.0027.

[324] A. C. Wu, N. A. Morrison, W. L. Kelly, and M. R. Forwood, “MCP-1 expression is specifically regulated during activation of skeletal repair and remodeling,” *Calcif. Tissue Int.*, 2013, doi: 10.1007/s00223-013-9718-6.

[325] M. Ishikawa *et al.*, “MCP/CCR2 signaling is essential for recruitment of mesenchymal progenitor cells during the early phase of fracture healing,” *PLoS One*, 2014, doi: 10.1371/journal.pone.0104954.

[326] N. A. Morrison, C. J. Day, and G. C. Nicholson, “Dominant negative MCP-1 blocks human osteoclast differentiation,” *J. Cell. Biochem.*, 2014, doi: 10.1002/jcb.24663.

[327] X. W. Yang *et al.*, “Elevated CCL2/MCP-1 levels are related to disease severity in postmenopausal osteoporotic patients,” *Clin. Lab.*, 2016, doi: 10.7754/Clin.Lab.2016.160408.

[328] D. Ferland-McCollough, D. Maselli, G. Spinetti, and P. Madeddu, “Chemokine MCP-1 feedback loop between adipocytes and mesenchymal stromal cells causes unremitting fat accumulation and contributes to osteocyte and hematopoietic stem cell rarefaction in the bone marrow of diabetic patients,” *Cytotherapy*, 2018, doi: 10.1016/j.jcyt.2018.02.091.

[329] Y. Kadoya, P. A. Revell, N. Al-Saffar, A. Kobayashi, G. Scott, and M. A. R. Freeman, “Bone formation and bone resorption in failed total joint arthroplasties: Histomorphometric analysis with histochemical and immunohistochemical technique,” *J. Orthop. Res.*, 1996, doi: 10.1002/jor.1100140318.

[330] M. K. Chang *et al.*, “Osteal Tissue Macrophages Are Intercalated throughout Human and Mouse Bone Lining Tissues and Regulate Osteoblast Function In Vitro and In Vivo,” *J. Immunol.*, 2008, doi: 10.4049/jimmunol.181.2.1232.

[331] H. Hounoki *et al.*, “Activation of peroxisome proliferator-activated receptor γ inhibits TNF-α-mediated osteoclast differentiation in human peripheral monocytes in part via suppression of monocyte chemoattractant protein-1 expression,” *Bone*, 2008, doi: 10.1016/j.bone.2007.11.016.

[332] V. N. Anisimov, “Insulin/IGF-1 signaling pathway driving aging and cancer as a target for pharmacological intervention,” *Exp. Gerontol.*, 2003, doi: 10.1016/S0531-5565(03)00169-4.

[333] A. H. Berg and P. E. Scherer, “Adipose tissue, inflammation, and cardiovascular disease,” *Circulation Research*. 2005. doi: 10.1161/01.RES.0000163635.62927.34.

[334] K. Ohashi, N. Ouchi, and Y. Matsuzawa, “Anti-inflammatory and anti-atherogenic properties of adiponectin,” *Biochimie*. 2012. doi: 10.1016/j.biochi.2012.06.008.

[335] H. Kanda *et al.*, “MCP-1 contributes to macrophage infiltration into adipose tissue, insulin resistance, and hepatic steatosis in obesity,” *J. Clin. Invest.*, 2006, doi: 10.1172/JCI26498.

[336] C. Beauséjour, “Bone marrow-derived cells: The influence of aging and cellular senescence,” *Handb. Exp. Pharmacol.*, 2007, doi: 10.1007/978-3-540-68976-8_4.

[337] J. P. Coppé, P. Y. Desprez, A. Krtolica, and J. Campisi, “The senescence-associated secretory phenotype: The dark side of tumor suppression,” *Annual Review of Pathology: Mechanisms of Disease*. 2010. doi: 10.1146/annurev-pathol-121808-102144.

[338] V. Cirmanová, M. Bayer, L. Stárka, and K. Zajíčková, “The effect of leptin on bone - An evolving concept of action,” *Physiological Research*. 2008. doi: 10.33549/physiolres.931499.

[339] S. Muraoka, N. Kusunoki, H. Takahashi, K. Tsuchiya, and S. Kawai, “Leptin stimulates interleukin-6 production via janus kinase 2/signal transducer and activator of transcription 3 in rheumatoid synovial fibroblasts,” *Clin. Exp. Rheumatol.*, 2013.

[340] J. Conde *et al.*, “Adiponectin and Leptin Induce VCAM-1 Expression in Human and Murine Chondrocytes,” *PLoS One*, 2012, doi: 10.1371/journal.pone.0052533.

[341] M. S. Mutabaruka, M. Aoulad Aissa, A. Delalandre, M. Lavigne, and D. Lajeunesse, “Local leptin production in osteoarthritis subchondral osteoblasts may be responsible for their abnormal phenotypic expression,” *Arthritis Res. Ther.*, 2010, doi: 10.1186/ar2925.

[342] R. Aquino-Martinez *et al.*, “Senescent cells exacerbate chronic inflammation and contribute to periodontal disease progression in old mice,” *J. Periodontol.*, 2021, doi: 10.1002/JPER.20-0529.

[343] J. P. Coppé *et al.*, “Senescence-associated secretory phenotypes reveal cell-nonautonomous functions of oncogenic RAS and the p53 tumor suppressor.,” *PLoS Biol.*, 2008, doi: 10.1371/journal.pbio.0060301.

[344] S. Kumar, A. J. T. Millis, and C. Baguoni, “Expression of interleukin 1-inducible genes and production of interleukin 1 by aging human fibroblasts,” *Proc. Natl. Acad. Sci. U. S. A.*, 1992, doi: 10.1073/pnas.89.10.4683.

[345] S. Wang, E. J. Moerman, R. A. Jones, R. Thweatt, and S. Goldstein, “Characterization of IGFBP-3, PAI-1 and SPARC mRNA expression in senescent fibroblasts,” *Mech. Ageing Dev.*, 1996, doi: 10.1016/S0047-6374(96)01814-3.

[346] L. Xu, Y. Wang, J. Wang, J. Zhai, L. Ren, and G. Zhu, “Radiation-induced osteocyte senescence alters bone marrow mesenchymal stem cell differentiation potential via paracrine signaling,” *Int. J. Mol. Sci.*, 2021, doi: 10.3390/ijms22179323.

[347] G. Y. Liu *et al.*, “Leptin promotes the osteoblastic differentiation of vascular smooth muscle cells from female mice by increasing RANKL expression,” *Endocrinology*, 2014, doi: 10.1210/en.2013-1298.

[348] C. Hellmich, J. A. Moore, K. M. Bowles, and S. A. Rushworth, “Bone Marrow Senescence and the Microenvironment of Hematological Malignancies,” *Frontiers in Oncology*. 2020. doi: 10.3389/fonc.2020.00230.

[349] Y. Zhang, K. Y. Guo, P. A. Diaz, M. Heo, and R. L. Leibel, “Determinants of leptin gene expression in fat depots of lean mice,” *Am. J. Physiol. - Regul. Integr. Comp. Physiol.*, 2002, doi: 10.1152/ajpregu.00392.2001.

[350] J. L. Kaplan *et al.*, “Adipocyte progenitor cells initiate monocyte chemoattractant protein-1-mediated macrophage accumulation in visceral adipose tissue,” *Mol. Metab.*, 2015, doi: 10.1016/j.molmet.2015.07.010.

[351] C. Goossens, S. Vander Perre, G. Van den Berghe, and L. Langouche, “Proliferation and differentiation of adipose tissue in prolonged lean and obese critically ill patients,” *Intensive Care Med. Exp.*, 2017, doi: 10.1186/s40635-017-0128-3.

[352] W. P. Cawthorn *et al.*, “Bone marrow adipose tissue is an endocrine organ that contributes to increased circulating adiponectin during caloric restriction,” *Cell Metab.*, vol. 20, no. 2, pp. 368–375, 2014, doi: 10.1016/j.cmet.2014.06.003.

[353] G. S. Harmon, M. T. Lam, and C. K. Glass, “PPARs and lipid ligands in inflammation and metabolism,” *Chemical Reviews*. 2011. doi: 10.1021/cr2001355.

[354] K. Gokulakrishnan *et al.*, “Augmentation of RBP4/STRA6 signaling leads to insulin resistance and inflammation and the plausible therapeutic role of vildagliptin and metformin,” *Mol. Biol. Rep.*, 2021, doi: 10.1007/s11033-021-06420-y.

[355] C. O. Smith and R. A. Eliseev, “Energy Metabolism During Osteogenic Differentiation: The Role of Akt,” *Stem Cells Dev.*, 2021, doi: 10.1089/scd.2020.0141.

[356] B. H. Shares, M. Busch, N. White, L. Shum, and R. A. Eliseev, “Active mitochondria support osteogenic differentiation by stimulating-Catenin acetylation,” *J. Biol. Chem.*, 2018, doi: 10.1074/jbc.RA118.004102.

[357] Y. Hu *et al.*, “OXPHOS-dependent metabolic reprogramming prompts metastatic potential of breast cancer cells under osteogenic differentiation,” *Br. J. Cancer*, 2020, doi: 10.1038/s41416-020-01040-y.

[358] E. B. Tahara, F. D. T. Navarete, and A. J. Kowaltowski, “Tissue-, substrate-, and site-specific characteristics of mitochondrial reactive oxygen species generation,” *Free Radic. Biol. Med.*, 2009, doi: 10.1016/j.freeradbiomed.2009.02.008.

[359] L. C. Shum, N. S. White, B. N. Mills, K. L. De Mesy Bentley, and R. A. Eliseev, “Energy Metabolism in Mesenchymal Stem Cells during Osteogenic Differentiation,” *Stem Cells Dev.*, 2016, doi: 10.1089/scd.2015.0193.

[360] A. J. C. de Groof *et al.*, “Increased OXPHOS activity precedes rise in glycolytic rate in H-RasV12/ E1A transformed fibroblasts that develop a Warburg phenotype,” *Mol. Cancer*, 2009, doi: 10.1186/1476-4598-8-54.

[361] C. C. Hughey *et al.*, “Increased oxygen consumption and OXPHOS potential in superhealer mesenchymal stem cells,” *Cell Regen.*, 2012, doi: 10.1186/2045-9769-1-3.

[362] Y. Hao, M. Wu, and J. Wang, “Fibroblast growth factor-2 ameliorates tumor necrosis factor-alpha-induced osteogenic damage of human bone mesenchymal stem cells by improving oxidative phosphorylation,” *Mol. Cell. Probes*, 2020, doi: 10.1016/j.mcp.2020.101538.

[363] O. K. Mancini *et al.*, “Mitochondrial oxidative stress reduces the immunopotency of mesenchymal stromal cells in adults with coronary artery disease,” *Circ. Res.*, 2018, doi: 10.1161/CIRCRESAHA.117.311400.

[364] P. S. Chowdhury, K. Chamoto, A. Kumar, and T. Honjo, “PPAR-induced fatty acid oxidation in T cells increases the number of tumor-reactive CD8 + T cells and facilitates anti–PD-1 therapy,” *Cancer Immunol. Res.*, vol. 6, no. 11, pp. 1375–1387, 2018, doi: 10.1158/2326-6066.CIR-18-0095.

[365] K. Chamoto *et al.*, “Mitochondrial activation chemicals synergize with surface receptor PD-1 blockade for T cell-dependent antitumor activity,” *Proc. Natl. Acad. Sci. U. S. A.*, 2017, doi: 10.1073/pnas.1620433114.

[366] A. Vallée and Y. Lecarpentier, “Crosstalk between peroxisome proliferator-activated receptor gamma and the canonical WNT/β-catenin pathway in chronic inflammation and oxidative stress during carcinogenesis,” *Frontiers in Immunology*. 2018. doi: 10.3389/fimmu.2018.00745.

[367] L. D. Roberts, A. J. Murray, D. Menassa, T. Ashmore, A. W. Nicholls, and J. L. Griffin, “The contrasting roles of PPARδ and PPARγ in regulating the metabolic switch between oxidation and storage of fats in white adipose tissue,” *Genome Biol.*, 2011, doi: 10.1186/gb-2011-12-8-r75.

[368] J. C. Corona and M. R. Duchen, “PPARγ as a therapeutic target to rescue mitochondrial function in neurological disease,” *Free Radical Biology and Medicine*. 2016. doi: 10.1016/j.freeradbiomed.2016.06.023.

[369] Y. Wang, X. Zhang, J. Shao, H. Liu, X. Liu, and E. Luo, “Adiponectin regulates BMSC osteogenic differentiation and osteogenesis through the Wnt/β-catenin pathway,” *Sci. Rep.*, 2017, doi: 10.1038/s41598-017-03899-z.

[370] S. Polvani, M. Tarocchi, and A. Galli, “PPAR and oxidative stress: Con(β) catenating NRF2 and FOXO,” *PPAR Research*. 2012. doi: 10.1155/2012/641087.

[371] S. Pal *et al.*, “Adiponectin receptors by increasing mitochondrial biogenesis and

respiration promote osteoblast differentiation: Discovery of isovitexin as a new class of small molecule adiponectin receptor modulator with potential osteoanabolic function," *Eur. J. Pharmacol.*, 2021, doi: 10.1016/j.ejphar.2021.174634.

[372] M. Keuper *et al.*, "Spare mitochondrial respiratory capacity permits human adipocytes to maintain ATP homeostasis under hypoglycemic conditions," *FASEB J.*, 2014, doi: 10.1096/fj.13-238725.

[373] R. Pardo, N. Enguix, J. Lasheras, J. E. Feliu, A. Kralli, and J. A. Villena, "Rosiglitazone-induced mitochondrial biogenesis in white adipose tissue is independent of peroxisome proliferator-activated receptor γ coactivator-1α," *PLoS One*, 2011, doi: 10.1371/journal.pone.0026989.

[374] L. Michalik and W. Wahli, "Involvement of PPAR nuclear receptors in tissue injury and wound repair," *Journal of Clinical Investigation*. 2006. doi: 10.1172/JCI27958.

[375] L. Michalik *et al.*, "Impaired skin wound healing in peroxisome proliferator-activated receptor (PPAR)α and PPARβ mutant mice," *J. Cell Biol.*, 2001, doi: 10.1083/jcb.200011148.

[376] T. Yu *et al.*, "Insulin promotes macrophage phenotype transition through PI3K/Akt and PPAR-γ signaling during diabetic wound healing," *J. Cell. Physiol.*, 2019, doi: 10.1002/jcp.27185.

[377] L. C. A. Galbraith *et al.*, "PPAR-gamma induced AKT3 expression increases levels of mitochondrial biogenesis driving prostate cancer," *Oncogene*, 2021, doi: 10.1038/s41388-021-01707-7.

[378] B. H. Chung *et al.*, "Protective effect of peroxisome proliferator activated receptor gamma agonists on diabetic and non-diabetic renal diseases," 2005. doi: 10.1111/j.1440-1797.2005.00456.x.

[379] M. P. Czech, M. Tencerova, D. J. Pedersen, and M. Aouadi, "Insulin signalling mechanisms for triacylglycerol storage," *Diabetologia*. 2013. doi: 10.1007/s00125-013-2869-1.

[380] S. C. Manolagas, "From estrogen-centric to aging and oxidative stress: A revised perspective of the pathogenesis of osteoporosis," *Endocrine Reviews*. 2010. doi: 10.1210/er.2009-0024.

[381] A. Böhm *et al.*, “Increased mitochondrial respiration of adipocytes from metabolically unhealthy obese compared to healthy obese individuals,” *Sci. Rep.*, 2020, doi: 10.1038/s41598-020-69016-9.

[382] V. Raje *et al.*, “Adipocyte lipolysis drives acute stress-induced insulin resistance,” *Sci. Rep.*, 2020, doi: 10.1038/s41598-020-75321-0.

[383] F. Gilardi *et al.*, “Systemic PPARγ deletion in mice provokes lipoatrophy, organomegaly, severe type 2 diabetes and metabolic inflexibility,” *Metabolism.*, 2019, doi: 10.1016/j.metabol.2019.03.003.

[384] K. F. Petersen, M. Krssak, S. Inzucchi, G. W. Cline, S. Dufour, and G. I. Shulman, “Mechanism of troglitazone action in type 2 diabetes,” *Diabetes*, 2000, doi: 10.2337/diabetes.49.5.827.

[385] K. F. Petersen and G. I. Shulman, “Etiology of insulin resistance,” *Am. J. Med.*, 2006, doi: 10.1016/j.amjmed.2006.01.009.

[386] K. F. Petersen *et al.*, “Mitochondrial dysfunction in the elderly: Possible role in insulin resistance,” *Science (80-.).*, 2003, doi: 10.1126/science.1082889.

[387] K. F. Petersen, S. Dufour, D. Befroy, R. Garcia, and G. I. Shulman, “Impaired Mitochondrial Activity in the Insulin-Resistant Offspring of Patients with Type 2 Diabetes,” *N. Engl. J. Med.*, 2004, doi: 10.1056/nejmoa031314.

[388] L. Sun *et al.*, “Pioglitazone improves mitochondrial function in the remnant kidney and protects against Renal fibrosis in 5/6 nephrectomized rats,” *Front. Pharmacol.*, 2017, doi: 10.3389/fphar.2017.00545.

[389] T. Wenz, F. Diaz, B. M. Spiegelman, and C. T. Moraes, “Activation of the PPAR/PGC-1α Pathway Prevents a Bioenergetic Deficit and Effectively Improves a Mitochondrial Myopathy Phenotype,” *Cell Metabolism*. 2008. doi: 10.1016/j.cmet.2008.07.006.

[390] A. Zieleniak, M. Wójcik, and L. A. Woźniak, “Structure and physiological functions of the human peroxisome proliferator-activated receptor γ,” *Archivum Immunologiae et Therapiae Experimentalis*. 2008. doi: 10.1007/s00005-008-0037-y.

[391] Y. B. Kim *et al.*, “Troglitazone but not metformin restores insulin-stimulated phosphoinositide 3-kinase activity and increases p110β protein levels in skeletal muscle of type 2 diabetic subjects,” *Diabetes*, 2002, doi: 10.2337/diabetes.51.2.443.

[392] R. Egami *et al.*, “Trans-omic analysis reveals obesity-associated dysregulation of inter-organ metabolic cycles between the liver and skeletal muscle,” *iScience*, 2021, doi: 10.1016/j.isci.2021.102217.

[393] W. Liao *et al.*, “Suppression of PPAR-γ attenuates insulin-stimulated glucose uptake by affecting both GLUT1 and GLUT4 in 3T3-L1 adipocytes,” *Am. J. Physiol. - Endocrinol. Metab.*, 2007, doi: 10.1152/ajpendo.00695.2006.

[394] J. C. Xi *et al.*, “The PI3K/AKT cell signaling pathway is involved in regulation of osteoporosis,” *J. Recept. Signal Transduct.*, 2015, doi: 10.3109/10799893.2015.1041647.

[395] H. Li, C. Yang, M. Lan, X. Liao, and Z. Tang, “Arctigenin promotes bone formation involving PI3K/Akt/PPARγ signaling pathway,” *Chem. Biol. Drug Des.*, 2020, doi: 10.1111/cbdd.13659.

[396] C. C. Chia, S. Y. Rong, S. T. Keh, M. H. Feng, and S. H. Liu, “Hyperglycemia enhances adipogenic induction of lipid accumulation: Involvement of extracellular signal-regulated protein kinase 1/2, phosphoinositide 3-kinase/Akt, and peroxisome proliferator-activated receptor γ signaling,” *Endocrinology*, 2007, doi: 10.1210/en.2007-0179.

[397] E. J. Moerman, K. Teng, D. A. Lipschitz, and B. Lecka-Czernik, “Aging activates adipogenic and suppresses osteogenic programs in mesenchymal marrow stroma/stem cells: The role of PPAR-γ2 transcription factor and TGF-β/BMP signaling pathways,” *Aging Cell*, 2004, doi: 10.1111/j.1474-9728.2004.00127.x.

[398] R. Teperino *et al.*, “Hedgehog partial agonism drives warburg-like metabolism in muscle and brown fat,” *Cell*, 2012, doi: 10.1016/j.cell.2012.09.021.

[399] E. E. Kershaw and J. S. Flier, “Adipose tissue as an endocrine organ,” 2004. doi: 10.1210/jc.2004-0395.

[400] D. Lasar *et al.*, “Peroxisome Proliferator Activated Receptor Gamma Controls Mature Brown Adipocyte Inducibility through Glycerol Kinase,” *Cell Rep.*, 2018, doi: 10.1016/j.celrep.2017.12.067.

[401] A. L. Hevener *et al.*, “Muscle-specific Pparg deletion causes insulin resistance,” *Nat. Med.*, 2003, doi: 10.1038/nm956.

[402] J. Jager, T. Grémeaux, M. Cormont, Y. Le Marchand-Brustel, and J. F. Tanti,

“Interleukin-1β-induced insulin resistance in adipocytes through down-regulation of insulin receptor substrate-1 expression,” *Endocrinology*, 2007, doi: 10.1210/en.2006-0692.

Appendix

A. 1. Materials and methods

Table 11: Consumable materials

Consumable material	Manufacturer
CasyTT cell counter	Schärfe Systems, Reutlingen, Germany
Cell culture flasks - tissue culture	Becton Dickinson, Franklin lakes, New York, US
Cell culture plates - tissue culture (96-well, 48-well and 6-well plates)	Corning Inc., Corning, New York, US
Cell culture safety hood - Herasafe	Thermo Fisher Scientific , Waltham, Massachusetts, US
Cell scraper	TPP AG, Trasadingen, Switzerland
Cell strainer - Falcon (40µM)	Becton Dickinson, Franklin lakes, New York, US
Cell strainer, Falcon	Becton Dickinson, Franklin lakes, New York, US
Centrifuge 5810R	Eppendorf, Hamburg, Germany
Combitips advanced (5mL, 10mL)	Eppendorf, Hamburg, Germany
CoolCell LX	Corning Inc., Corning, New York, US
Countess Automated Cell Counter II FL	Thermo Fisher Scientific , Waltham, Massachusetts, US
Cryo tubes	Thermo Fisher Scientific , Waltham, Massachusetts, US
Cytoflex S system	Beckman Coulter, Krefeld, Germany
Disposable sterile filter	Sigma-Aldrich, St. Louis, MI, US
Eppendorf ep T.I.P.S	Eppendorf, Hamburg, Germany
Falcon tubes (50mL, 15mL)	Becton Dickinson, Franklin lakes, New York, US
Feather disposable scalpel no. 21	FEATHER Safety Razor Co-Ltd, Osaka, Japan
Fine scissors - ThoughCut Straight 9cm	Fine Science Tools GmbH, Heidelberg, Germany
Fixateur MouseExFix external	RISystems AG, Switzerland
Freezer	Liebherr, Bulle, Germany
Fridge	Liebherr, Bulle, Germany
Incubator	Heraeus, Hanau, Germany/ Binder, Tuttlingen, Germany
Inverted microscope	Leica Microsystems, Wetzlar, Germany
LSR Fortessa system	Becton Dickinson, Franklin lakes, New York, US
MicroCT skyscan 1172	BRUKER, Kontich, Belgium
Microscope (cell culture)	Leica Microsystems Nussloch GmbH, Bensheim, Germany
Microscope (histology)	Zeiss, Oberkochen, Germany
Microscopy slides	Marienfeld GmbH & Co KG, Lauda-Königshofen, Germany
Multipette M4	Eppendorf, Hamburg, Germany
Nanodrop ND 1000 spectrometer	Thermo Fisher Scientific , Waltham, Massachusetts, US
Non-CO2 incubator	Agilent, Santa Clara, CA, US
Parafilm - M	Bemis, Neenah, US
Pipettes	Eppendorf, Hamburg, Germany
Plate reade infinite M200 PRO	Tecan Group, Männedorf, Switzerland
Rotary microtome	Leica Microsystems Nussloch GmbH, Bensheim, Germany
Round-bottom tube with cell strainer cap - Falcon	Becton Dickinson, Franklin lakes, New York, US
Safety gloves Vasco nitril long	Braun, Melsungen, Germany
Seahorse 96-well cell calibrant cartridges	Agilent, Santa Clara, CA, US
Seahorse 96-well cell culture microplate	Agilent, Santa Clara, CA, US
Seahorse Xfe 96 analyzer	Agilent, Santa Clara, CA, US
Serological pipettes (5mL, 10mL)	Corning Inc., Corning, New York, US
Sterican - größe 17 (0,55 x 25mm)	Braun, Melsungen, Germany
Syringe plunger - Discardit II	Becton Dickinson, Franklin lakes, New York, US
Syringes	Braun, Melsungen, Germany
Tissue culture dish - Falcon (6mm)	Becton Dickinson, Franklin lakes, New York, US
TPP tissue culture flask (T300 cm^2, T175 cm^2)	TPP AG, Trasadingen, Switzerland
Tweezers and scissors	Medicon, Tuttlingen, Germany
Vacusafe	Integra Biosciences AG, Zizers, Switzerland
Vitro-Clud	Langenbrinck, Emmendingen, Germany
Vortexer Reax Top	Heidolph Instruments, Schwabach, Germany
Waterbath	Memmert GmbH, Schwabach, Germany

Table 12: Chemicals

Chemicals	Manufacturer
3-isobutyl-1-methylxanthine (IBMX)	Sigma-Aldrich, St. Louis, MI, US
4',6-diamidino-2-phenylindole (DAPI)	Sigma-Aldrich, St. Louis, MI, US
4-Nitrophenylphosphate (pNPP)	Sigma-Aldrich, St. Louis, MI, US
Alizarin Red S	Merck, Darmstadt, Germany
Ampuwa	Fresenius, Bad Homburg, Germany
Ascorbic acid 2-phosphate sesquimagnesium salt hydrate	Sigma-Aldrich, St. Louis, MI, US
Bisphenol-A-diglycidylether (BADGE)	Sigma-Aldrich, St. Louis, MI, US
Bovine serum albumin (BSA)	Sigma-Aldrich, St. Louis, MI, US
Cetylpyridinium chloride	Sigma-Aldrich, St. Louis, MI, US
Dexamethasone	Sigma-Aldrich, St. Louis, MI, US
Dimethylsulfoxid cell culture (DMSO)	AppliCHem, Darmstadt, Germany
Dulbecco's Phosphate buffered saline	Gibco, Grand Island, NY, US
Dulbecco's Modified Eagle Medium – high glucose	Gibco, Grand Island, NY, US
Dulbecco's Modified Eagle Medium – low glucose D6646-500ml	Gibco, Grand Island, NY, US
Eosin	Chroma-Waldeck, Münster, Germany
Ethanol for histology	Herbeta, Berlin, Germany
Fetal calve serum Superior	Biochrom AG, Berlin, Germany
Glutamax	Gibco, Grand Island, NY, US
Hematoxylin	Chroma Waldeck, Münster, Germany
Hoechst (bisBenzimide)	Sigma-Aldrich, St. Louis, MI, US
Indomethacin	Sigma-Aldrich, St. Louis, MI, US
Insulin from bovine pancreas	Sigma-Aldrich, St. Louis, MI, US
InVivoMAb anti-mouse IFNg	BioXCell, Lebanon, NH, US
InVivoMAb anti-mouse TNFa	BioXCell, Lebanon, NH, US
Nile Red	Sigma-Aldrich, St. Louis, MI, US
Papanicolaous Lösung 1a Harris Hämatoxylinlösung	Merck, Darmstadt, Germany
paraformaldehyde 16% solution	Electron Microscopy Sciences, Hatfield, US
Paraformaldehyde 20% Solution, EM Grade 15713	Electron Microscopy Sciences, Hatfield, US
Penicillin/Streptomycin	Biochrom AG, Berlin, Germany
PrestoBlue Cell Viability Reagent	Invitrogen, Thermo Fisher Scientific, Waltham, Massachusetts, US
RBC lysis buffer (10X)	BioLegend, San Diego, CA, US
RNAse Zap	Sigma-Aldrich, St. Louis, MI, United Stated
Rosiglitazone diet S8090-P005	Ssniff, Soest, Germany
Sodiumchloride (NaCl)	Merck, Darmstadt, Germany
Sodiumhydroxyde solution (NaOH) 1M	Sigma-Aldrich, St. Louis, MI, US
Trizol	Ambion, Life Technologies, Carlsbad, CA, US
TruStain FcX (anti-mouse CD16/32) blocking solution	BioLegend, San Diego, CA, US
Xylol	J.T. Baker, Avantor Performance Materials, Center Valley, PA, US
β-glycerolphosphate	Sigma-Aldrich, St. Louis, MI, US

Table 13: Kits

Kits	Manufacturer
FluoroFix staining buffer kit	BioLegend, San Diego, CA, US
LiveDead staining kit	Invitrogen, Thermo Fisher Scientific, Waltham, Massachusetts, US
True-Nuclear Transcription Factor Buffer Set	BioLegend, San Diego, CA, US
Direct-zol RNA Miniprep kit	Zymo research, Freiburg, Germany
Seahorse XF Cell Mito Stress test	Agilent, Santa Clara, CA, US
Seahorse Xfe 96 FluxPak mini	Agilent, Santa Clara, CA, US
Glucose Uptake-Glo assay	Promega, Madison, Wisconsin, US
Legendplex Human Adipokine panel (13-plex)	BioLegend, San Diego, CA, US

Table 14: Software

Software	Manufacturer
FlowJo version 10.7.1	Becton Dickinson, Franklin lakes, New York, US
Diva software version 8.0.1	Becton Dickinson, Franklin lakes, New York, US
GraphPad Prism version 8	GraphPad, San Diego, CA, US

Table 15: Animals and cells

Animals and cells	Manufacturer
C57BL/6N mice (female)	Charles River Laboratories, Wilmington, MA, US
Mesenchymal stromal cells (bone)	Charité, Berlin, Germany

A. 2. Results

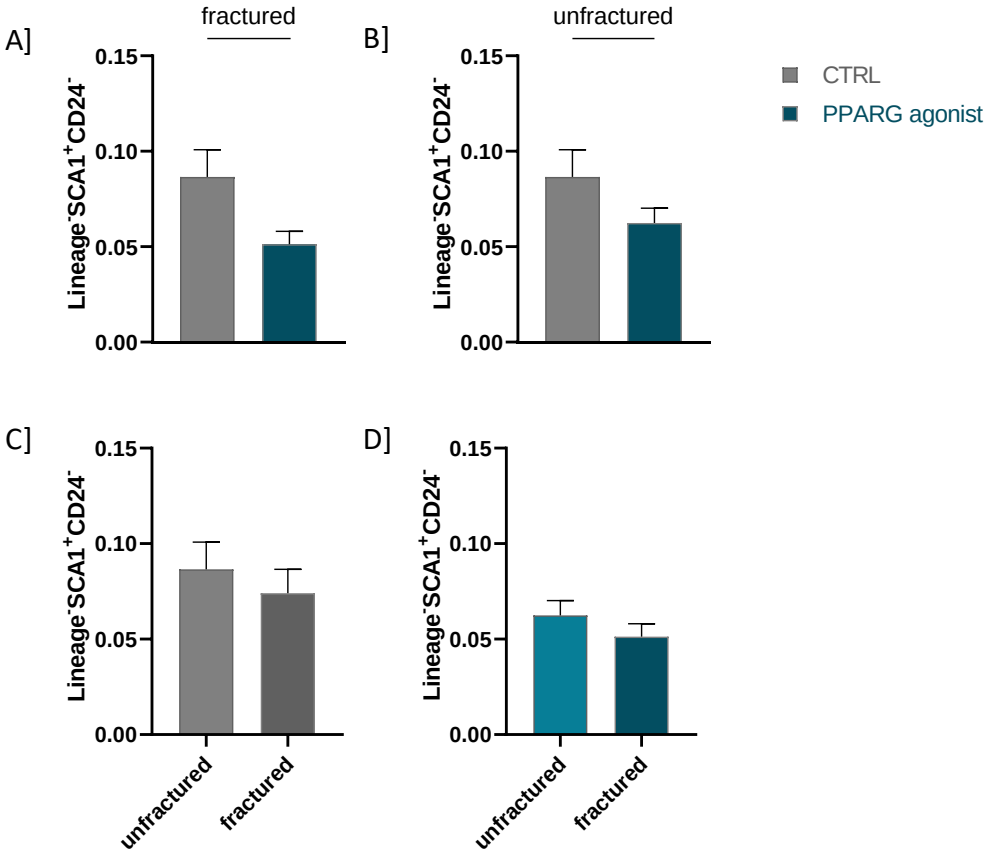

Figure 61: The adipogenic lineage is slightly decreased by the treatment with PPARG agonist rosiglitazone in unfractured and fractured bone marrow
The adipogenic lineage is described as subset of living CD45-CD31- (lineage$^-$) cells marked by Sca1 expression and the loss of CD24. The frequency of the Sca1+CD24- subset is displayed in relation to all living cells. PPARG agonist treatment (cyan) is shown to reduce the adipogenic precursor lineage within the bone marrow compared to the control (dark grey) **A] B]** In the fractured and unfractured bone a slight reduction of adipogenic precursor subset is shown (unpaired t-test with Welch's correction p=0.059 and p=0.177, n=6) **C] D]** When comparing unfractured and fractured bones within the control group as well as within the PPARG agonist treated group no significant change is shown for the adipogenic precursor subset. The PPARG agonist treated group shows a reduced amount of adipogenic precursors in both bones compared to the control (n=6 each)

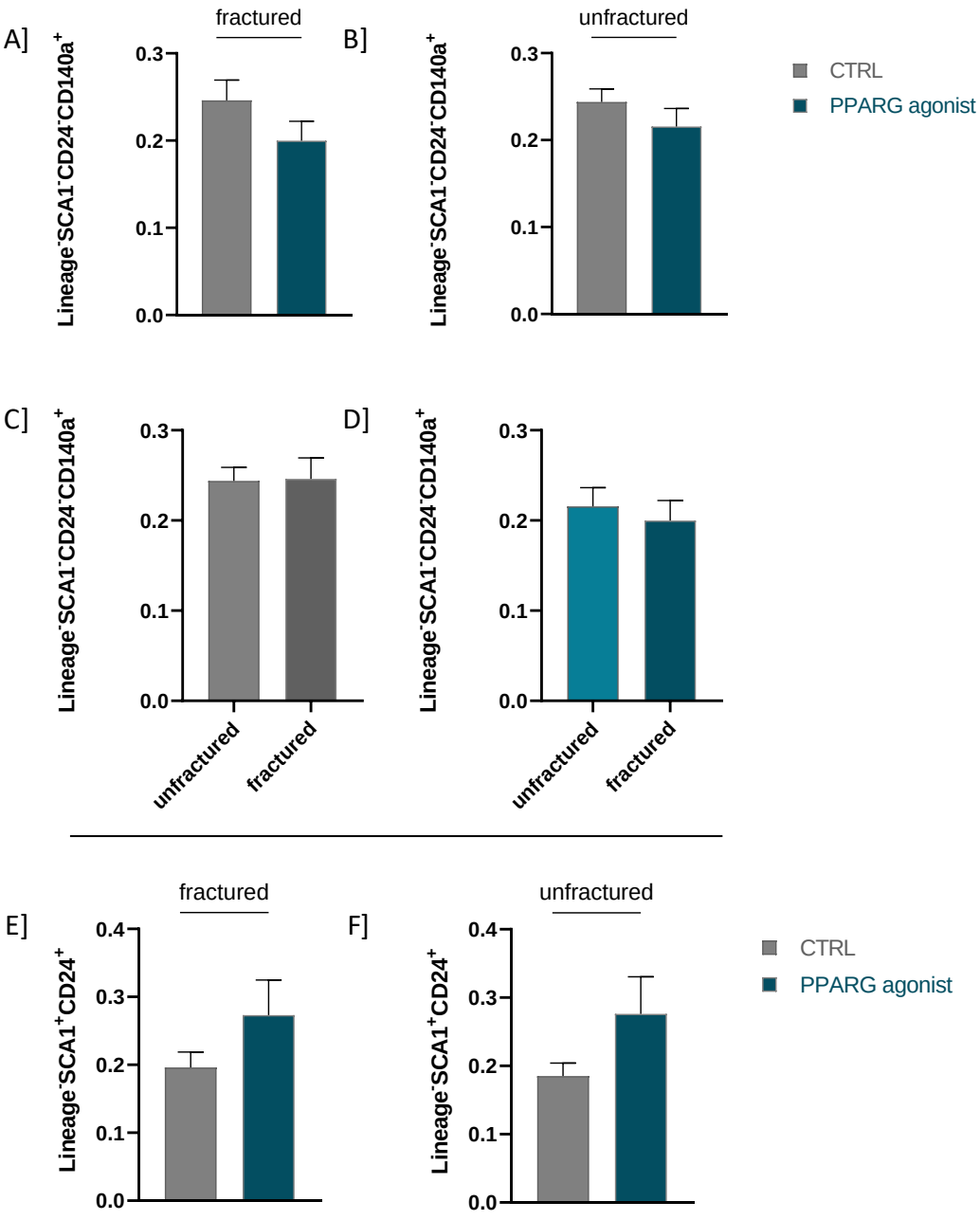

Figure 62: PPARG agonist treatment has no effect on the osteogenic precursor cells but enhances the multipotent precursor subset in the bone marrow
The osteogenic lineage is described as subset of living CD45-CD31- (lineage$^-$) cells marked by the loss of Sca1 and the gain of CD140a expression. The multipotent precursor cells are defined by the expression of Sca1 and CD24. The frequency of both subsets is displayed in relation to all living cells. PPARG agonist treatment (cyan) is shown to not influence the osteogenic precursor lineage within the bone marrow compared to the control (dark grey) but is rather shown to induce the multipotent lineage within bone marrow **A] B]** PPARG agonist treatment is shown to harbor no direct effects on the osteogenic precursor subset in the fracture setting and the unfractured bone (n=6) **C] D]** No changes in the osteogenic compartment are shown while comparing the fractured and unfractured bone in each group, control and PPARG agonist treated bones (=6) **E] F]** Multipotent progenitor cells are enriched under PPARG agonist treatment in fractured and unfractured bones (unpaired t-test with Welch's correction p=0.164 and p=0.214, n=6)

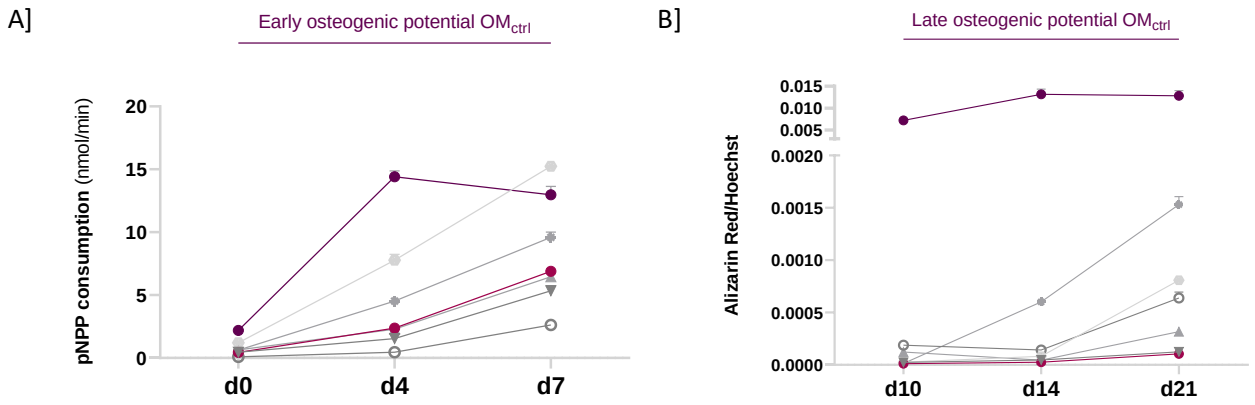

Figure 63: Osteogenic baseline potential of patient hBMSCs differs in ALP activity and calcification rate
Individual patient derived hBMSCs are highlighted in the following color/symbol scheme: Pat374 (dark purple), Pat1626 (light grey), Pat660 (moderate grey), Pat326 (pink), Pat346 (light grey upward pointing triangle), Pat919 (moderate grey downward pointing triangle), Pat784 (grey empty circle) **A]** Early osteogenic potential is displayed as pNPP consumption (ALP activity) for d0, d4 and d7. High ALP activity is shown for patient derived hBMSCs from Pat374, Pat1626, Pat660 and **B]** late osteogenic potential is shown as alizarin staining normalized on cell number for d10, d14 and d21. High calcification rates are shown for Pat374, Pat660 and Pat1626 characterizing them with a higher osteogenic baseline potential

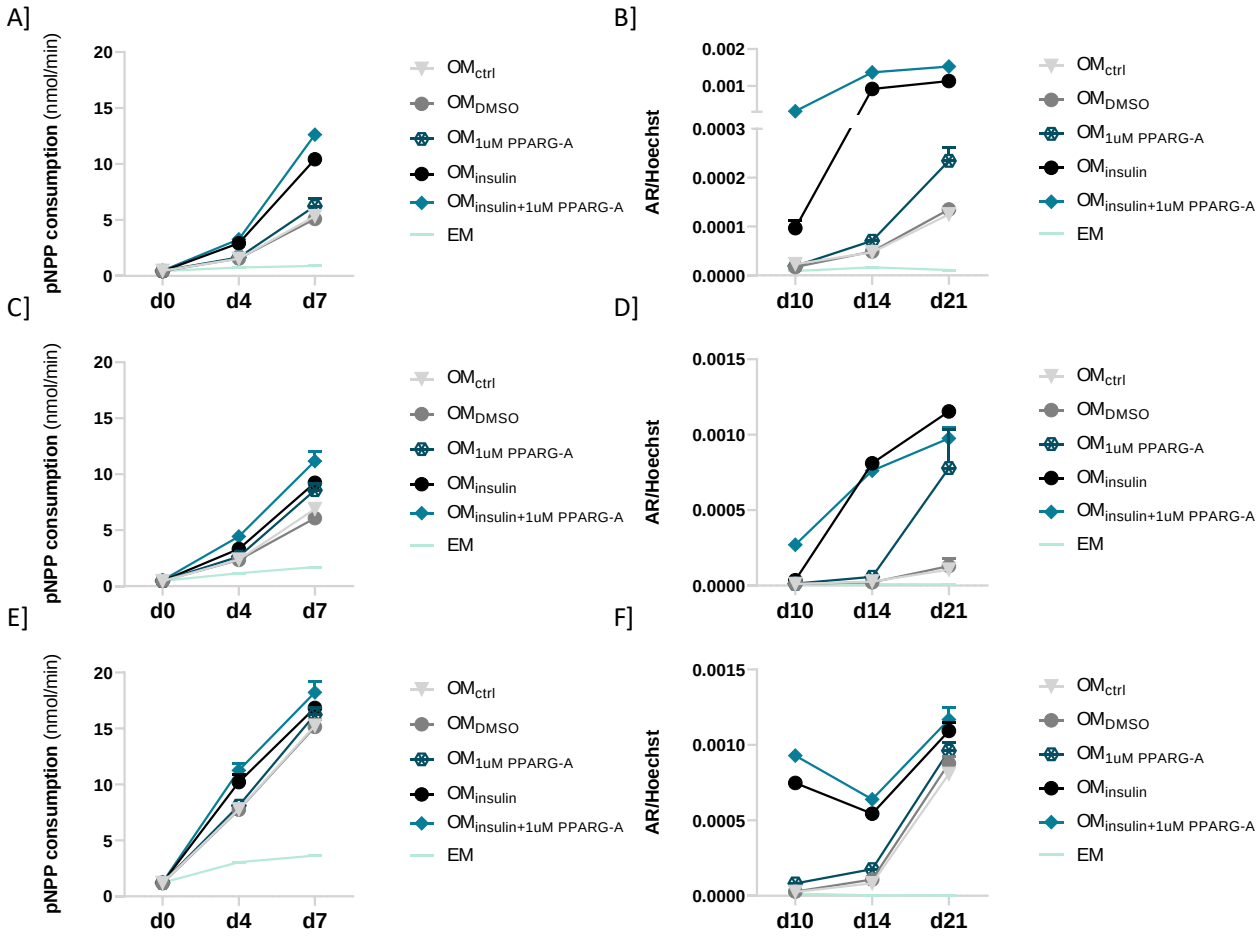

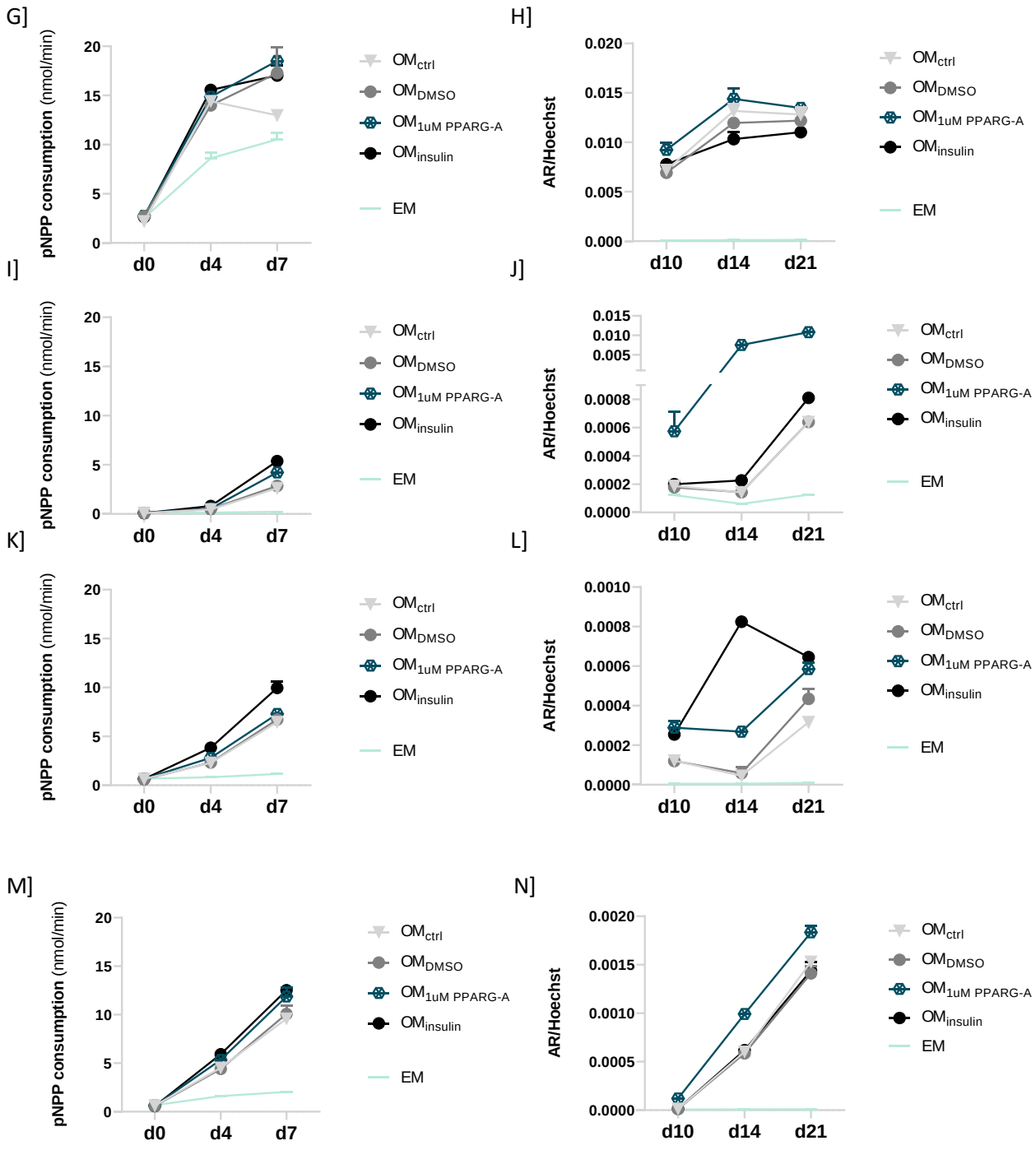

Figure 64: Individual patient specific effects are shown for PPARG agonist and insulin stimulated early and late osteogenic differentiation

ALP activity is depicted as pNPP consumption defining the early osteogenic differentiation potential, whereas alizarin red stained mineralized matrix normalized on cell number is shown as late osteogenic marker. Each patient derived set of hBMSCs is shown for the different culture conditions such as osteogenic control (light grey), osteogenic solvent control (moderate grey), osteogenic differentiation with PPARG agonist treatment (dark cyan), osteogenic differentiation with insulin supplementation (black), osteogenic differentiation with combined PPARG agonist and insulin treatment (light cyan) and expansion media control (light green) **A] B]** Pat919 is characterized by a high insulin dependency and a good response to PPARG agonist treatment especially in the later time points of osteogenic differentiation **C] D]** Pat326 is shown with an increased ALP activity following PPARG agonist stimulation, which is even more pronounced in the later time points of differentiation **E] F]** Pat1626 is displayed with a strong ALP activity in all conditions and a high insulin reactivity already on d10 and d14 of late osteogenic differentiation shown by increased calcification **G] H]** Pat374 displays reduced effects of insulin and PPARG agonist treatment on ALP activity and calcification, whereas the PPARG agonist stimulation still shows the highest impact

on osteogenic differentiation **I] J]** Pat784 harbors increased sensitivity towards PPARG agonist treatment with even higher calcification rates compared to the insulin stimulated condition **K] L]** PPARG agonist treatment does not show a significant enhancement of the ALP activity in Pat346, whereas insulin has a more pronounced impact. PPARG agonist treatment rather steers an increase in calcification during later time points of differentiation **M] N]** Pat660 is sensitive towards PPARG agonist and insulin treatment in the early differentiation time points but PPARG agonist treatment is solely driving the higher calcification rates compared to insulin treatment